Regulation of Cardiac Hypertrophy by the Chromatin Remodeling Factor DPF3a and DNA Methylation Analysis in Congenital Heart Disease

DISSERTATION

zur Erlangung des akademischen Grades des
Doktors der Naturwissenschaften (Dr. rer. nat.)

eingereicht im Fachbereich Biologie, Chemie,
Pharmazie der Freien Universität Berlin

vorgelegt von
Huanhuan Cui
崔欢欢
aus Shaanxi, China

Oktober 2015

Die Arbeit wurde von May 2011 bis Oktober 2015 am Max-Planck-Institut für Molekulare Genetik sowie am Experimental and Clinical Research Center (Charité Universitätsmedizin Berlin & Max-Delbrück-Centrum für Molekulare Medizin) unter der Leitung von Frau Prof. Silke Rickert-Sperling angefertigt.

1. Gutachter: Prof. Dr. Silke Rickert-Sperling
Experimental and Clinical Research Center
Charité Universitätsmedizin Berlin & Max-Delbrück Centrum für Molekulare Medizin
Lindenberger Weg 80, 13125 Berlin
Email: silke.sperling@charite.de

2. Gutachter: Prof. Dr. Ana Pombo
Berlin Institute for Medical Systems Biology
Max-Delbrück-Centrum für Molekulare Medizin
Robert-Rössle-Str. 10, 13125 Berlin
Email: ana.pombo@mdc-berlin.de

Datum der Disputation: 26.04.2016

For my family

献给我的家人

Table of Contents

1 Introduction

1.1 Cardiac development and disease

1.1.1 The human heart

The human heart is a muscular organ containing four chambers; namely, the left atrium, left ventricle, right atrium and right ventricle. The heart pumps blood through the blood vessels of the circulatory system by repeated rhythmic contractions, and the circulation of this blood supplies oxygen and nutrients to the whole body. Deoxygenated blood from the body is returned to the right atrium of the heart via the superior and inferior vena cava, through the tricuspid valve into the right ventricle, before being pumped through the pulmonary artery to the lungs for re-oxygenation and removal of carbon dioxide. Oxygenated blood returns to the left atrium from the lungs through the pulmonary veins, and then passes through the mitral valve to the left ventricle, where it is pumped through the aorta to different organs of the body (Figure 1).

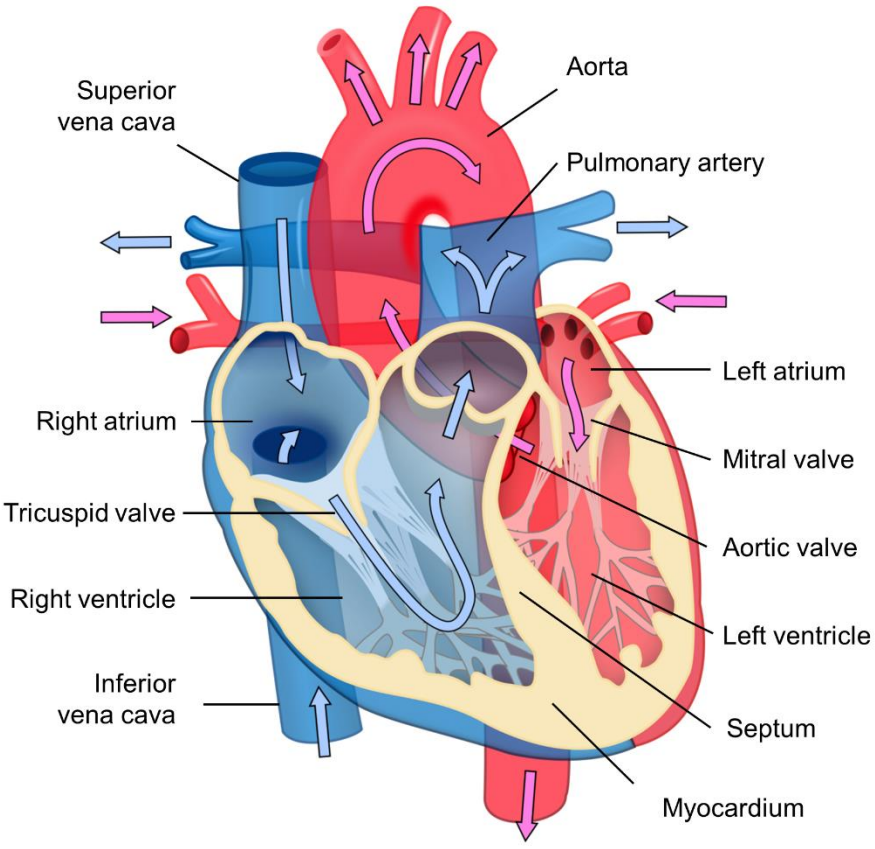

Figure 1. Schematic representation of the mature four-chambered mammalian heart. Figure modified from http://en.wikipedia.org/wiki/File:Heart_diagram_blood_flow_en.svg.

The cardiac conduction system of the heart consists of specialized cells and fibers that send signals to the cardiac muscle causing it to contract. There are five main components of the cardiac conduction system: the sino-atrial node (SAN), the atrio-ventricular node (AVN), the bundle of His, the left and right bundle branches, and the Purkinje fibres. The SAN initiates the electrical impulse by causing the atrial muscles to contract. The signal then travels to the AVN, goes through the bundle of His, down to the bundle branches, and through the Purkinje fibers, finally causing the ventricles to contract (Moorman et al., 1998).

1.1.2 Cardiac development

The four-chambered heart is composed of both cardiomyocytes and non-cardiomyocytes. The latter includes, for example, cardiac fibroblasts, endothelial cells, epicardial cells, and vascular smooth muscle cells. Interestingly, ventricular cardiomyocytes make up only 30–40% of the total cell number, but account for 70–80% of the total mass of the heart (Tirziu et al., 2010). All of these cell types are derived from multipotent progenitors at gastrulation, and contribute to heart formation, structure, and function.

During human embryogenesis, the heart is the first organ to form and to function. Initially, cardiac progenitor cells divide from a common progenitor at gastrulation to form two groups of cells (Bruneau, 2008). At human embryonic day 15, early cardiac progenitor cells in the anterior mesoderm form the cardiac crescent (Harvey, 2002), which is referred to as the first heart field (FHF). The second heart field (SHF) is derived from the pharyngeal mesoderm located medial and anterior to the cardiac crescent (Figure 2). By day 20, cells from the FHF migrate to the midline and form a beating linear heart tube, containing cardiomyocytes and an inner layer of endothelial cells (Srivastava, 2006). The SHF cells migrate to the end of the tube and form the arterial and venous poles. At around day 28, the heart tube undergoes a complex rightward looping and remodeling. Through this looping, the inflow and outflow segments are brought to the anterior pole of the heart, and consequently distinct chambers, including the right and left ventricle as well as the outflow and inflow tract with atria and sinus venosus, begin to appear (Christoffels et al., 2000; Harvey, 2002). Later on, the outflow tract becomes the aorta and pulmonary arteries and the inflow tract turns into the atrioventricular canal. From around day 32, the chambers are separated, and the four-chambered heart structure forms and continues to mature. The FHF further contributes to the left ventricle, and the right and left atria, while the SHF contributes to the right ventricle, the outflow tract, and the right and left atria (Kelly, 2007). The separation of the outflow tract requires the migration of cardiac neural

crest cells from the dorsal neural tube into the arterial pole. At around day 60, morphogenesis of the human heart is complete, with the rate of cell proliferation now significantly reduced and the size of the cardiomyocytes increasing. In fact, it is not until birth that the cardiomyocytes stop proliferating (Leu et al., 2001).

Heart development is a tightly regulated process, which is temporally and spatially coordinated by signaling pathways and networks of transcription factors (Evans et al., 2010). Inductive signaling, including bone morphogenetic protein (Bmp), fibroblast growth factor (Fgf), Wnt, Notch and sonic hedgehog (Shh) activate a core set of evolutionarily conserved transcription factors that are expressed in both the FHF and SHF during embryonic development (Olson, 2006; Rochais et al., 2009). These transcription factors form a network that regulates genes connecting upstream signaling of muscle-specific genes, as well as genes that encode proteins involved in cardiac growth, patterning and contractility (Bruneau, 2008). For example, Gata4 and Nkx2-5 are key transcriptional regulators in both the FHF and SHF. The transcription factor Tbx5 is only expressed in the FHF, whereas Lsl1 and Tbx1 are specifically expressed in the SHF (Kelly et al., 2001; Waldo et al., 2001). These central regulators activate the expression of genes that control cardiac cell fate and morphogenesis of cardiac structures derived from the FHF and SHF, as well as fetal genes encoding muscle-specific proteins such as myosin heavy chain (MHC), cardiac α-actin, atrial natriuretic factor, and brain natriuretic peptide (Moorman and Christoffels, 2003).

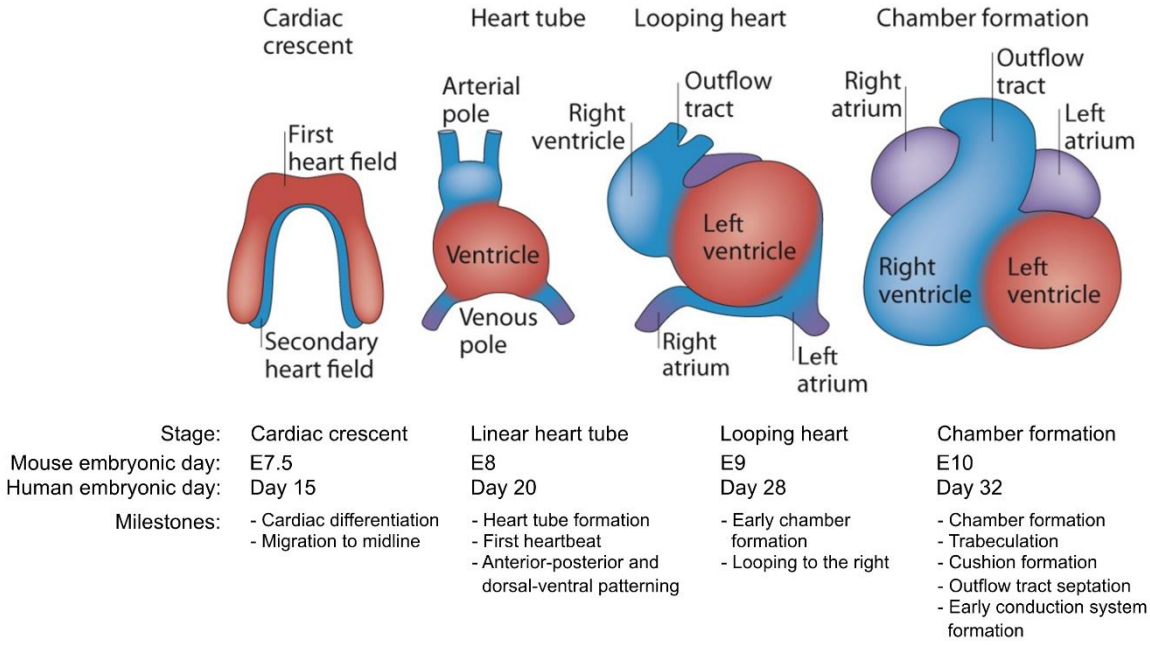

Figure 2. Developmental stages of the mammalian heart. Figure modified from Xin et al., 2013.

1.1.3 Cardiac diseases

Tetralogy of Fallot

Tetralogy of Fallot (TOF) is one of the most common cyanotic congenital heart diseases (CHDs). It affects one in 3,500 newborns and accounts for around 7–10% of all CHDs (Apitz et al., 2009; Hoffman and Kaplan, 2002). TOF is a defect that occurs during heart looping and outflow tract formation, and is characterized by a ventricular septal defect with an overriding aorta, pulmonary stenosis and right ventricular hypertrophy. The ventricular hypertrophy is considered to be a secondary anomaly, resulting from increased right ventricular systolic pressure (Davlouros et al., 2006).

The etiology of TOF is multifactorial. It occurs in a number of syndromes but in the majority of cases it is an isolated defect. Isolated TOF can be caused by various gene mutations, including, for example, *JAG1* (Glaeser et al., 2006), *NKX2-5* (Goldmuntz et al., 2001), *GATA4/6* (Lin et al., 2010; Tomita-Mitchell et al., 2007), *ZFPM2* (De Luca et al., 2011), *GDF1* (Karkera et al., 2007) and *FOXH1* (Roessler et al., 2008). More recently, the polygenic background of isolated TOF was described (Grunert et al., 2014). Here, TOF was shown to be caused by a combination of rare and private variations in neural crest, apoptotic and sarcomeric genes. These genes are associated with disturbances in expression in an interaction regulatory network. Furthermore, TOF cases also occur in the context of syndromic disorders such as DiGeorge and Velocardiofacial syndrome, which are caused by chromosomal 22q11.2 deletions that can be detected in up to 16% of TOF patients (Goldmuntz et al., 1998; Khositseth et al., 2005; Maeda et al., 2000). The cardiac phenotype in these cases is probably caused by hemizygosity of the cardiac transcription factor TBX1 that is located in the region of 22q11.2 (Merscher et al., 2001).

Ventricular septal defect

Ventricular septal defect (VSD), a defect in the septum between the right and left ventricles, is one of the most common CHDs. It presents from birth and occurs in up to 40% of all congenital cardiac malformations (Minkkila and Tikanoja, 1996). VSD does not only occur as a common isolated CHD but also presents as an intrinsic component of several complex malformations, including TOF (Penny and Vick, 2011). There are four types of VSD: perimembranous, supracristal, inlet and muscular.

Epidemiological studies suggest that VSD has a multifactorial background. Genetic mutations such as single nucleotide polymorphism and copy number variation have been shown to be associated with VSD. For example, mutations in *GATA4* and *TBX5*, two

cardiac transcription factors important for normal cardiac septation, have been associated with VSD (Garg et al., 2003; Liu et al., 2009; Zhang et al., 2008). Chromosomal 22q11.2 deletion and 8p23.1 duplication have been identified in patients with VSD (Soemedi et al., 2012; Tomita-Mitchell et al., 2012; Zhao et al., 2013). Furthermore, exposure to environmental factors such as teratogens, maternal stress, phenylketonuria and pregestational diabetes also play an important role in VSD (Jenkins et al., 2007).

Hypertrophic cardiomyopathy

Hypertrophic cardiomyopathy (HCM) is the most common monogenically inherited cardiac disease. It affects one in every 500 individuals in the general population (Marian et al., 1995) and presents increased penetrance with aging (Spirito et al., 2014). This disease is diverse in phenotypic and genetic expression, as well as clinical presentation. Clinically, it is characterized by unexplained thickening of the left ventricular wall (usually asymmetric septal hypertrophy), contractile dysfunction, and potentially fatal arrhythmias. In addition to cardiac hypertrophy, noticeable histological disarray of myofilaments and fibrosis are present in HCM. Most HCM patients are asymptomatic; however, up to 25% develop significant symptoms, including chest pain and/or heart failure, with the most severe cases requiring a heart transplant (Enriquez and Goldman, 2014). Arrhythmias occur in approximately 20% of HCM patients, leading to a poorer prognosis, as these patients have a higher probability of stroke and heart failure (Nishimura and Ommen, 2006).

Genetically, HCM is caused by mutations (1,400 variants) in genes encoding proteins involved in the cardiac sarcomere, Z-disc or intracellular calcium modulators (Force et al., 2010). A disease-causing mutation can be found in 50–60% of HCM patients. The two most common genes are cardiac β-myosin heavy chain (*MYH7*) and cardiac myosin binding protein C (*MYBPC3*); mutations in either of these genes are found in 70% of successfully genotyped patients (Efthimiadis et al., 2014). Many mutations in *MYH7* are missense mutations presented between exons 3 and 23 that encode the myosin ‘head’ and ‘neck’ (Walsh et al., 2010). In *MYBPC3*, most mutations are deletions or insertions that lead to a frameshift, leading to a truncated protein with no function (Marston et al., 2009). These mutations could further result in the dysfunction of myocytes, which may eventually cause hypertrophy. However, the molecular mechanisms that lead to the hypertrophic phenotype in HCM are poorly understood.

Aortic stenosis

Aortic stenosis (AS) is a narrowing of the aortic valve (between the aorta and the left ventricle). This narrowing causes a pressure overload by obstructing blood flow from the heart into the aorta and subsequently to the rest of the body. In response, the left ventricle needs to work harder to pump blood into the aorta, consequently triggering a hypertrophic response that results in an increase in myocyte size, left ventricular wall thickness, and total mass. Depending on the level of the obstruction, aortic stenosis is classified as valvular, sub-valvular or supra-valvular.

Epidemiological studies have shown aortic stenosis and atherosclerosis have similar clinical risk factors. These factors include advance age, gender, smoking, hypertension, lipoprotein cholesterol levels, and diabetes (Boon et al., 1997; Stewart et al., 1997). At the molecular level, chromosome 16q22.1-q22.3 and genetic polymorphisms in the lipoprotein(a) gene have been shown to play causal roles in calcification and stenosis of the aortic valve (Bella et al., 2007; Thanassoulis et al., 2013). Furthermore, polymorphisms in the apolipoprotein E allele and vitamin D receptor gene *BsmI* are associated with the development of aortic stenosis (Novaro et al., 2003; Ortlepp et al., 2001).

1.2 Cardiac hypertrophy

Cardiac hypertrophy refers to the increase in myocardial mass in response to pressure or volume stress, or mutations of sarcomeric proteins (Lips et al., 2003). This state can be further classified as either physiological or pathological hypertrophy. Physiological hypertrophy is the normal response to healthy exercise or pregnancy, whereby cardiac function is enhanced or remains the same while the cardiac muscle mass is increased. The latter, pathological hypertrophy, can be either concentric or eccentric; that is, induced by pressure or volume overload, respectively. This state typically occurs in settings of cardiac disease and is harmful for both cardiac structure and function (Frey et al., 2004). Sustained hypertrophy, which can eventually lead to heart failure, is associated with increased interstitial fibrosis, cell death and contractile dysfunction (Barry et al., 2008; Bernardo et al., 2010). Usually, pathological hypertrophy is considered to be a key risk factor for myocardial infarction, arrhythmia and sudden death. It accompanies nearly all forms of cardiovascular disease (Levy et al., 1990), for example, HCM, TOF, aortic stenosis and hypertension. Therefore, the prevention of pathological hypertrophy would be of great therapeutic interest in the ultimate prevention of cardiovascular disease.

1.2.1 The fetal gene program

The activation of the fetal gene program is one of the most important features of cardiac hypertrophy at the molecular level. Corresponding expression profile analysis has shown that the fetal heart and failing heart have a similar pattern of differentially expressed genes (Thum et al., 2007). Fetal genes are often expressed only in the developing heart and are re-expressed in hypertrophic hearts. These genes, for example *MHC*, atrial natriuretic factor (*Nppa*), and brain natriuretic peptide (*Nppb*), are considered to be hypertrophic markers (Sadoshima and Izumo, 1997) and are tightly controlled by transcriptional regulators and chromatin modifying and remodeling factors. *Nppa* and *Nppb* are highly expressed in the embryonic heart and are notably absent in the healthy adult heart (Gardner, 2003). Upon hypertrophic stimulation, *Nppa* and *Nppb* are directly regulated by the cardiac transcription factor Gata4 (Gardner et al., 2007; Richards, 2007). Moreover, the basic helix-loop-helix (bHLH) transcription factors Hey1 and Hey2 can repress the transcriptional activity of *Nppa* and *Nppb* by direct binding or via interactions with Gata4 and Gata6 (Fischer et al., 2005; Kathiriya et al., 2004). There are two isoforms of *MHC*, namely *α-MHC* and *β-MHC,* in cardiac muscle. The latter accounts for more than 90% of *MHC* in the human adult heart (LeWinter, 2005). Upregulation of *β-MHC* expression, with a concomitant decrease in *α-MHC*, is a sensitive marker of cardiac hypertrophy in the human heart (Lowes et al., 1997; Miyata et al., 2000). In cardiac development and disease, this switch of *MHC* isoforms is tightly regulated by the chromatin remodeling factor Brg1 and its interaction partners, histone deacetylases (HDACs) and poly ADP-ribose polymerases (PARPs) (Hang et al., 2010). In addition, the cardiac transcription factor Gata4 and the histone methyltransferase Ezh2 are also involved in the regulation of *MHC* isoforms (Delgado-Olguin et al., 2012).

1.2.2 Molecular pathways in pathological hypertrophy

At the cellular level, cardiac hypertrophy is characterized by an increase in cardiomyocyte size, with enhanced protein synthesis, and changes to sarcomeric organization (Barry et al., 2008). The development of pathological hypertrophy is directly dependent on the response of cardiomyocytes to systemic stress or genetic abnormalities (Frey and Olson, 2003). In response to pathological insults, several protein kinases, like casein kinase 2 (CK2) and mitogen-activated protein kinases (MAPKs), within the cardiomyocyte form the basis of the mechanotransduction apparatus.

Mitogen-activated protein kinases pathway

The MAPK pathway contains multiple levels of kinases that establish a phosphorylation-based amplification cascade and play an important role in intracellular signal transduction during the development of pathological hypertrophy. MAPKs are dual phosphorylated at the T(E/P/G)Y motif in the kinase domain to become catalytically active (Canagarajah et al., 1997). The typical event leading to this phosphorylation is a well-known conserved three-tiered kinase cascade in which a MAPKKK activates a MAPKK, which in turn activates the MAPK through serial phosphorylation (Figure 3). Based on the terminal kinase in the pathway, MAPKs are divided into four subfamilies, including extracellular signal-regulated kinase (ERK1/2), c-Jun amino-terminal kinase (JNK), p38 kinase, and ERK5 (Rose et al., 2010). These kinases are activated in hypertrophic hearts (e.g. pressure or volume overloaded hearts) (Muslin, 2008), and in cultured cardiomyocytes in response to pathological hypertrophic stimuli (e.g. angiotensin II, endothelin 1, phenylephrine) (Wang and Proud, 2002).

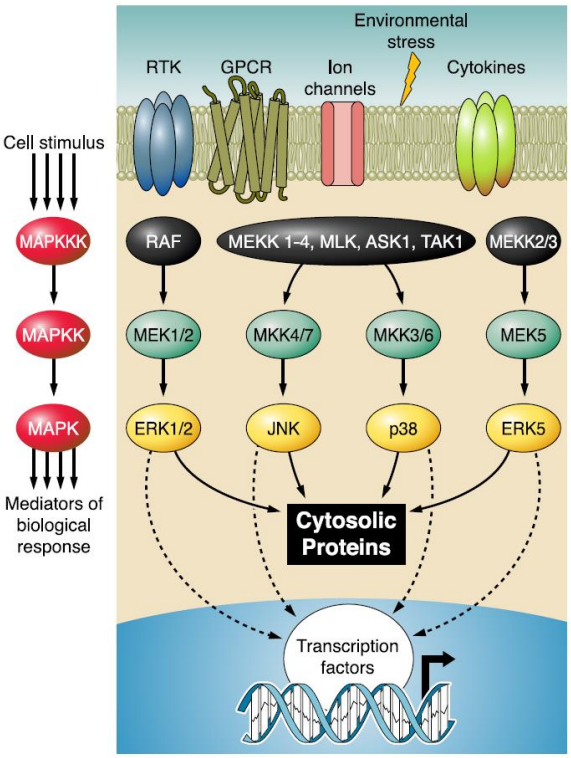

Figure 3. Mitogen-activated protein kinase signaling in cardiac hypertrophy. RTK: tyrosine kinase receptor; GPCR, G-protein coupled receptor; MAPK: mitogen-activated protein kinase; MAPKK: mitogen-activated protein kinase kinase; MAPKKK: mitogen-activated protein kinase kinase kinase. Figure taken from Rose et al., 2010.

Hypertrophic signals activate the tyrosine kinase receptor (RTK) that recruits and activates the MAPKKK RAF at the plasma membrane. Subsequently, RAF phosphorylates and stimulates the MAPKKs, namely MEK1 and MEK2, that serve as dedicated kinases for ERK1 and ERK2 phosphorylation (Shaul and Seger, 2007). Transgenic mice over-expressing constitutively active MEK1 develop hypertrophy via activating ERK1/2 (Bueno et al., 2000). In line with this, reduced hypertrophic response is observed in *in vitro* cardiomyocyte culture by inhibition of the MEK1-ERK1/2 pathway (Bueno and Molkentin, 2002). The downstream molecular mechanisms involved in MEK1-ERK1/2-mediated hypertrophy include transcription factors such as NFATs and GATAs (Liang et al., 2001b; Sanna et al., 2005). In addition, JNK, p38, and ERK5-mediated pathways have also been shown to be activated in pathological hypertrophy (Rose et al., 2010).

Casein kinase 2 pathway

Another signaling molecule postulated to be involved in the hypertrophic response is CK2, a typical serine/threonine kinase consisting of two catalytic subunits (α and α') and a dimer of regulatory β subunits. CK2 targets more than 300 putative substrates on serine, threonine and tyrosine, and has been implicated in regulating many cellular and developmental processes (Litchfield, 2003). CK2-dependent phosphorylation prevents caspase-mediated cleavage of a number of proteins involved in the regulation of cell survival, and the suppression of CK2 decreases cell proliferation and viability (Kang et al., 2009).

The CK2 holoenzyme normally phosphorylates Ser/Thr at a consensus sequence of E/D/X-S/T-D/E/X-E/D/X-E/D-E/D/X. Its subunits play a role in the assembly of the tetrameric CK2 complex, by anchoring substrates and regulating the kinase activity of the catalytic subunits (Litchfield, 2003). Knockout of CK2α in mice leads to structural defects in the heart and somites, with mice dying in mid-gestation (Seldin et al., 2008). In response to hypertrophic stimuli such as the cardiac growth factor angiotensin II, the catalytic subunits CK2α and CK2α' are activated and translocate from the cytoplasm to the nucleus (Figure 4). On one hand, CK2α induces cardiac hypertrophy via activating and phosphorylating histone deacetylase 2 (HDAC2) at serine 394 (Eom et al., 2011). On the other hand, activation of CK2α' results in the phosphorylation of p27, and consequently causes an imbalanced feedback loop between p27 and CK2α' that is crucial for agonist- and stress-induced cardiac hypertrophic growth (Hauck et al., 2008).

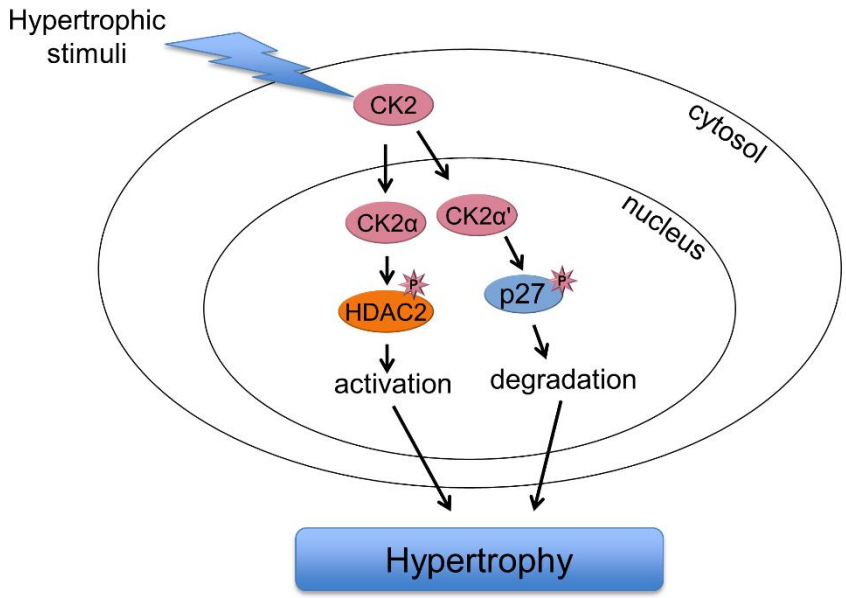

Figure 4. Casein kinase 2 signaling in cardiac hypertrophy. CK2: casein kinase 2; HDAC2: histone deacetylase 2; P: phosphorylation.

1.3 Epigenetic regulation of cardiac development and disease

In higher eukaryotes, the basic repeating unit of chromatin is the nucleosome, a complex of 147 bases of DNA wound around an octamer of histone proteins. The histone octamer contains pairs of histones H2A, H2B, H3, and H4 (Luger et al., 1997). The core histones are tightly packed in globular regions. Their N-terminal tails are rather unstructured and extend from the globular region, making them accessible to histone modifying proteins. Histone H1 binds to a short stretch of linker DNA that connects the nucleosomes. It functions in the compaction of chromatin into higher-order structures, allowing DNA to be tightly packaged and replicated. Chromatin structures or states can be determined by the nucleosome spacing. Euchromatin and heterochromatin are two functional states which are related to transcriptional activation and inactivation, respectively (Campos and Reinberg, 2009; Fedorova and Zink, 2008). Epigenetic mechanisms, including ATP-dependent chromatin remodeling, DNA methylation, histone modification and non-coding RNAs (ncRNAs), cause alterations in gene expression by changing chromatin accessibility or architecture (Figure 5).

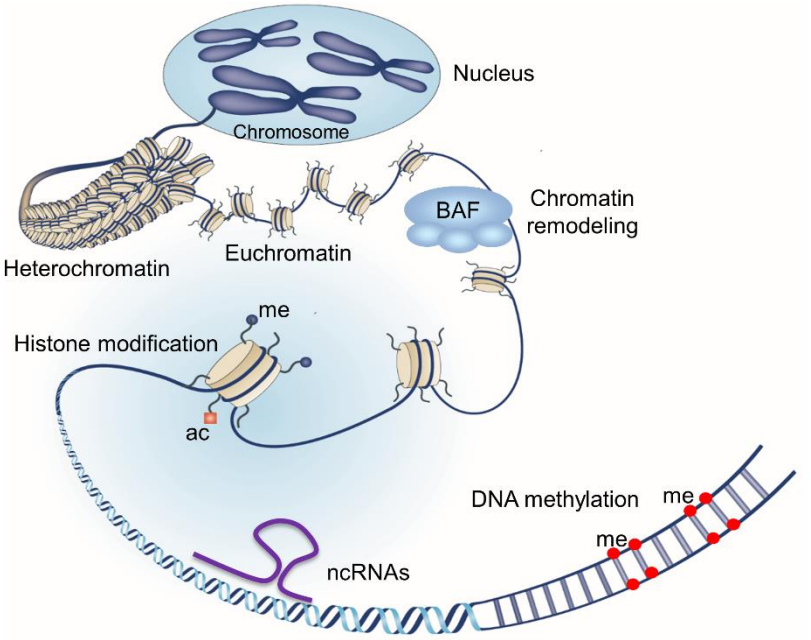

Figure 5. Diagrammatic representation of chromatin and epigenetic modifications. BAF: brahma-associated chromatin remodeling complexes; me: methylation; ac: acetylation; ncRNA: non-coding RNA. Figure modified from Arrowsmith et al., 2012.

1.3.1 The BAF complex

The ATP-dependent chromatin remodeling complexes use free energy derived from ATP hydrolysis to move, eject, release or rearrange the nucleosome (Clapier and Cairns, 2009). All the catalytic members of the ATP-dependent chromatin-remodeling complexes share an evolutionarily conserved SWI-like ATPase catalytic domain, which serves as a motor to regulate histone-DNA interactions for DNA assembly and chromatin restructuring, allowing transcription factors access to DNA. Based on the distinct function of flanking domains, the ATP-dependent chromatin remodeling complexes can be divided into four families: SWI/SNF (switching defective/sucrose non-fermenting), ISWI (imitation switch), CHD (chromodomain helicase DNA binding), and INO80 (inositol requiring 80) (Ho and Crabtree, 2010). These flanking domains recognize specific histone modifications, adjust ATPase activity, directly modify histones, or recruit other DNA-binding transcription factors and thus determine the genomic targeting specificity and biological function of each family. Many studies have shown that chromatin remodeling factors play important roles in heart development and disease by controling and regulating cardiac gene expression in a temporal and tissue specific manner (Bruneau, 2010; Chang and Bruneau, 2012; Han et al., 2011).

In mammals, the SWI/SNF complexes are called brahma-associated factor (BAF) complexes, and contain up to 12 components. The core ATPase component of the BAF complexes is encoded by either *brahma* (*Brm*) or *brahma-related gene 1* (*Brg1*). Animal studies have suggested that *Brm* and *Brg1* have distinct functions during cardiac development. *Brm* knockout mice develop normally, displaying only a slight increase in body weight (Reyes et al., 1998), whereas *Brg1* null embryos die during the peri-implantation stage (Bultman et al., 2000). In mice, the specific deletion of endothelial *Brg1* at ~E10.5 can lead to embryonic lethality and defects in yolk sac vasculogenesis (Griffin et al., 2008; Stankunas et al., 2008). Ablation of *Brg1* in the endocardium causes hypotrabeculation at E9.0 (Stankunas et al., 2008). Further studies have shown that Brg1 directly represses the secreted matrix metalloproteinase *Adamts1*, which promotes myocardial trabeculation. Loss of *Brg1* initiates premature expression of *Adamts1* in the endocardium to degrade the cardiac jelly and prevent excessive trabeculation (Stankunas et al., 2008). In the myocardium, Brg1 functions to regulate gene expression, as well as cardiac growth and differentiation. Deletion of myocardial *Brg1* causes lethality at E11.5 because of a thin, compact myocardium, VSD and reduced cell proliferation (Hang et al., 2010).

Brg1 is essential for the switch between *β-MHC* and *α-MHC* during cardiac development and disease. In embryonic cardiomyocytes, Brg1 represses *α-MHC* via interactions with HDACs, while it forms a complex with PARPs to activate β-MHC (Hang et al., 2010). A lack of Brg1 results in a switch to predominately *α-MHC* expression and loss of *β-MHC*, and leads the cardiomyocytes to exit the fetal state. Although Brg1 is highly expressed in developing hearts, it is turned off in adult hearts and its catalytic fuction is replace by Brm. Under conditions of pressure overload, Brg1 can be reactivated, allowing a pathological switch from *α-MHC* expression to *β-MHC* expression. Moreover, Brg1 is up-regulated in patients with hypertrophic cardiomyopathy. Expression levels of Brg1 correlate with the thickness of interventricular septum and also with the *MHC* isoform switch (Hang et al., 2010). More recently, Brg1 was shown to be bound by the cardiac-specific long non-coding RNA (lncRNA), *Mhrt* (Han et al., 2014). *Mhrt* was found to be down-regulated in the hypertrophic heart of pressure-overloaded mice. The down-regulation of *Mhrt* is dependent on the activation of Brg1. Rescuing Mrht expression inhibited hypertrophy and enhanced cardiac fuction in these mice, indicating the protective role of this lncRNA in pathological cardiac hypertrophy. Mechanistically, *Mhrt* directly binds to the helicase domain of Brg1 and subsequently prevents Brg1 from recognizing its genomic DNA targets, which include the *MHC* genes (Han et al., 2014).

Other BAF subunits, such as Baf60c, Baf180 and Baf45c (Dpf3), also play an important role during cardiac development and morphogenesis. These subunits recruit the BAF complex to numerous genomic target sites by either interacting with DNA-binding transcription factors or recognizing specific histone modifications. *Baf60c* is highly expressed in the developing heart and skeletal muscle. *Baf60c* knockdown embryos die at E10, with severe cardiac and muscle defects, including hypoplastic ventricles with reduced trabeculation and a shortened outflow tract (Lickert et al., 2004). During cardiogenesis, Baf60c interacts with DNA-binding transcription factors such as Tbx5 and Gata4 to regulate cardiac-specific genes. In skeletal muscle, Baf60c is recruited to myogenic genes via interaction with MyoD and Six4, and is thus required for muscle differentiation and maintenance of glycolytic metabolism (Forcales et al., 2012; Meng et al., 2013). Baf180 contains six bromodomains that serve as readers of acetylated histones. In mice, knockout of *Baf180* causes embryonic lethality with trophoblastic placental defects and VSD (Wang et al., 2004). Another histone reader, Baf45c2 (Dpf3b), contains a tandem plant homeodomain (PHD) that specifically recognizes methylated and acetylated histones (Lange et al., 2008). The role of Dpf3 will be discussed in detail in the next section.

1.3.2 The epigenetic factor Dpf3

Dpf3, also known as Baf45c (Brg1/Brm-associated factor 45c) or Cred4, is the third member of d4 protein family, which also includes Dpf1 (Neud4/Baf45b) and Dpf2 (ubi-d4/Baf45d). *Dpf1* has been shown to be strictly neuro-specific and is expressed in differentiated neurons of the post-mitotic zone during embryonic development (Chestkov et al., 1996; Lessard et al., 2007). *Dpf2* is ubiquitously expressed in all embryonic and adult tissues. It has been involved in cell death after deprivation of trophic factors (Gabig et al., 1994; Mertsalov et al., 2000). *Dpf3* was initially identified and cloned from mouse and chicken cDNA libraries (Ninkina et al., 2001). It has been shown to play a role in the transition of neuronal precursors to differentiated neurons (Lessard et al., 2007). In human adult tissue, *DPF3* is specifically expressed in cardiac and skeletal muscle. During development, *Dpf3* shows tissue-specific expression in the heart, somites and neurons of mouse, chicken, and zebrafish (Lange et al., 2008).

The d4 proteins are evolutionary highly conserved and are characterized by an N-terminal 2/3 domain, which is encoded by exons 2 and 3 and is unique to this protein family; a C2H2-Krüppel-like zinc finger, and a tandem plant homeodomain (PHD) at the C-terminus, which was previously called the d4 domain (Chestkov et al., 1996). In human,

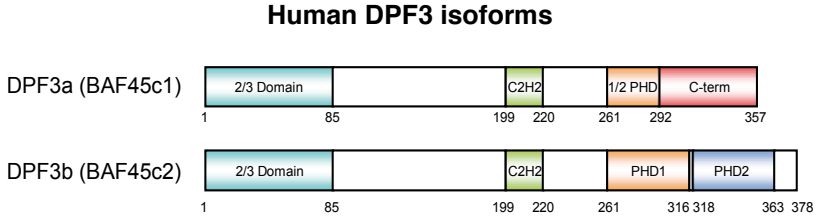

Figure 6. Schematic representation of the human DPF3 isoforms. Note that the splice variant DPF3a contains a half PHD (plant homeodomain) finger and a specific C-terminus (C-term), whereas DPF3b contains a double PHD finger. Teal: 2/3 domain; green: C2H2-Krüppel-like zinc finger; orange: half PHD in DPF3a and PHD1 in DPF3b; red: DPF3a specific C-terminus; blue: PHD2.

mouse and chicken, there are two splice variants of *Dpf3* that result in two isoforms, namely Dpf3a (Baf45c1) and Dpf3b (Baf45c2). Using tandem affinity purification followed by mass spectrometry, our group found that both Dpf3a and Dpf3b are associated with the BAF chromatin remodeling complex (Lange et al., 2008). Dpf3b has full PHD fingers, which bind to methylated and acetylated lysine residues of histone H3 and H4 (Lange et al., 2008). Dpf3a, on the other hand, only has a truncated version of the first PHD finger (half PHD) and a specific C-terminus with unknown function (Zeng et al., 2010) (Figure 6).

In a genome-wide gene expression study of congenital malformed human hearts, our group found that both spliced variants of *DPF3* were significantly up-regulated in the right ventricular myocardium of patients with TOF (Kaynak et al., 2003). Morpholino knockdown of *dpf3* in zebrafish leads to incomplete cardiac looping and severely reduced ventricular contractility, with disassembled muscular fibers caused by transcriptional deregulation of structural and regulatory proteins. siRNA knockdown of *Dpf3* in C2C12 mouse skeletal muscle cells causes myofibrillar disarray, which confirmed the phenotype observed in MO^{dpf3} zebrafish. Promoter analysis identified *Dpf3* as a novel downstream target of Mef2a in HL1 cardiomyocytes (Lange et al., 2008). Furthermore, a recent study found that *Dpf3*, which is up-regulated in patients with chronic lymphocytic leukemia, is positively regulated by the signal transducer and activator Stat5 (Theodorou et al., 2013).

In cardiac and muscle gene regulation, Dpf3b represents a tissue-specific anchor that recognizes modified histones via PHD fingers and recruits the BAF chromatin remodeling complex (Lange et al., 2008). The binding of Dpf3b to histone H3 is promoted by histone H3 lysine 14 acetylation (H3K14ac) and inhibited by histone H3 lysine 4 methylation (H3K4me3). In addition, DPF3b binds to H3K4me1 and H3K4me2, suggesting a gradual interaction of DPF3b with histone H3. Therefore, the interaction between DPF3b and histone H3 modulated by site-specific different modifications is likely to be critical for recruiting the BAF remodeling complex to genomic targets. The tandem PHD fingers of

Dpf3b work as one functional unit, supporting a model in which H3K14ac marks a gene locus and recruits Dpf3b/BAF to pre-initiate gene transcription, while H3K4me3 releases DPF3b/BAF from the locus, thereby enabling the entry of a transcriptional machinery complex to initiate and activate gene transcription (Zeng et al., 2010). Moreover, DPF3 links the heterodimer of the nuclear factor NF-κB, RelA/p50, to the BAF complex via protein-protein interaction, and acts as transcriptional co-activators in BAF complex-dependent activation of the RelA/p50 heterodimer (Ishizaka et al., 2012).

Furthermore, mutations in *DPF3* have been shown to be associated with human diseases. Variants in the 5' region of *DPF3* were found to be associated with increased risk of breast cancer development, lymph node metastases, and tumor size (Hoyal et al., 2005). It is likely that these mutations affect *DPF3* activity by down-regulating *DPF3* transcription levels or by impacting RNA splicing. In addition, polymorphisms in the introngenic region of *DPF3* were found to be associated with sperm morphology and cleft lip/palate with dental anomalies in two large-scale association studies (Kosova et al., 2014; Vieira et al., 2008).

1.3.3 DNA methylation

DNA methylation, the addition of methyl groups to the nucleotides of genomic DNA, is the most common epigenetic modification to the mammalian genome. DNA methylation mainly occurs in a CpG dinucleotide context and is distributed throughout the majority of the genome. The DNA methyltransferases (DNMTs), composed of three proteins, catalyze the transfer of a methyl group from cofactor S-adenosylmethionine to carbon 5 of the cytosine ring to generate 5-mC. The key enzyme DNMT1 is a maintenance methyltransferase and modifies previously hemi-methylated DNA during replication. In contrast, DNMT3a and DNMT3b mediate *de novo* methylation and catalyze methylation of previously unmethylated CpG dinucleotides (Reik and Dean, 2001). More recently, the ten-eleven translocation (TET) family of proteins has been shown to be responsible for the oxidation of 5mC to 5hmC (Branco et al., 2012). Methylated DNA regions can be recognized by four different methyl-CpG binding domain (MBD) proteins: MBD1, 2 and 4, and MECP2 (Buck-Koehntop and Defossez, 2013). The MBD proteins bind to methylated DNA and recruit epigenetic modifiers such as histone deacetylases, polycomb complexes, non-coding RNAs, and ATP-dependent chromatin remodeling factors, to modulate gene expression (Ballestar and Wolffe, 2001; Suzuki and Bird, 2008).

The relationship between methylation and gene expression is complex. In general, high promoter methylation is often associated with low or no gene expression, as promoter

methylation directly interferes with the binding of transcriptional regulators (Wade, 2001). In contrast, methylation in gene bodies is generally associated with high gene expression (Jones, 2012). Studies have shown that DNA methylation patterns have tissue specificity. In cardiac tissue, DNA methylation is correlated with gene expression that is different to other organs such as kidney and liver (Xie et al., 2011). Changes in DNA methylation patterns are highly dynamic, widespread, and tissue-specific during cardiomyocyte development and postnatal maturation (Gilsbach et al., 2014; Liang et al., 2011). In neonatal and adult cardiomyocytes, demethylation is observed in cell type-specific enhancer regions and in gene bodies of cardiomyocyte genes (Gilsbach et al., 2014). In the adult heart, most of the low methylated enhancer regions are enriched by GATA and MEF2 binding sites and are further characterized by p300 and active histone marks (Hon et al., 2013). In addition, DNA methylation plays a role in cardiac disease. For instance, the hypomethylation of gene promoters is correlated with increased gene expression in end-stage failing hearts (Movassagh et al., 2011). Differentially methylated regions are enriched in cardiac regulators such as *NKX2-5* and *HAND1* in TOF patients (Sheng et al., 2014) and these genes are implicated in dilated cardiomyopathy (Haas et al., 2013).

1.4 Experimental technologies

1.4.1 Model systems to study cardiac disease

Cell culture is a powerful *in vitro* model to investigate signaling pathways, molecular mechanisms, as well as metabolic and epigenetic regulations in cardiac development, differentiation and disease. Isolated mouse or rat primary cardiomyocytes are widely used to study cardiac function *in vitro*. In addition, several stable cell lines have been generated for the study of cardiac biology. The HL1 cell line, established from mouse atrial cardiac muscle cells, shows a similar gene expression pattern to adult cardiomyocytes. It can be indefinitely passaged in culture, while maintaining a differentiated cardiomyocyte phenotype and the ability to contract (Claycomb et al., 1998). The H9C2 cell line, derived from rat embryonic cardiac tissue, has the properties of both cardiomyocytes and skeletal muscle (Kimes and Brandt, 1976). In particular, the H9C2 cell line is frequently used to study cardiac hypertrophy, since it shows similar hypertrophic responses *in vitro* to primary neonatal cardiomyocytes (Watkins et al., 2011). The murine myoblast cell line C2C12 has the ability to differentiate into myotubes, and thus it is a useful *in vitro* model to study myogenesis (Yaffe and Saxel, 1977). Furthermore, mouse embryonic stem cells (ESCs) (e.g. P19 cells), human ESCs (e.g. H1 or hES2 cells), and human induced

pluripotent stem cells (iPSCs) offer useful models for studying cardiomyocyte differentiation (McBurney et al., 1982; Moore et al., 2004; Yang et al., 2008).

Several animal models, including fruit fly (Drosophila melanogaster), zebrafish (Danio rerio), mouse (Mus musculus) and rat (Rattus norvegicus), have been used in cardiac disease research. The fruit fly is an invertebrate model organism that is characterized by a simple tube-shaped heart. Many genes involved in cardiac disease are highly conserved between the fruit fly and human (Bier and Bodmer, 2004). Therefore, the fruit fly can be used for genetic screening and to understand the molecular mechanisms of human disease (Wolf and Rockman, 2011). The zebrafish has a two chambered-heart that contains a single atrium and a single ventricle. Because of its small size, fecundity and brief generation time, the zebrafish is frequently used for *in vivo* study of cardiac development, function and regeneration (Major and Poss, 2007; Schoenebeck and Yelon, 2007). The mouse and the rat are two of the most popular mammalian animal models for cardiovascular study. The rat is widely used for pharmaceutical testing as there is a high similarity between the rat and the human cardiovascular system (Gill et al., 1989). In contrast, the mouse is extensively used as a good model for genetic studies of cardiac disease, as it can be easily genetically manipulated (Snider and Conway, 2011).

Finally, patients with cardiac disease and their families provide a unique resource to gain insights into cardiac functional properties and molecular pathways (Sperling, 2011). Cardiac biopsies from patients can be used to study genetic and epigenetic alterations as well as gene expression changes, which provide insights into understanding the phenotype of these patients. Besides directly using materials from patients, the generation of patient-specific iPSCs presents new opportunities to study cardiac diseases (Dambrot et al., 2011), for example, they have been successfully used in the analysis of Long-QT syndrome and familial HCM (Lan et al., 2013; Moretti et al., 2010).

1.4.2 Mass spectrometry

Mass spectrometry (MS) is one of the most widely used technologies in proteomic studies. This approach is based on measuring the molecular weight of a sample or distinguishing molecules by their mass-to-charge ratios. Biochemical enrichment of proteins using immunoprecipitation in combination with MS is often applied to the identification of interacting partners of proteins of interest. When a specific and high affinity antibody is lacking for immunoprecipitation, an alternative method is tag-based protein expression and purification (Abu-Farha et al., 2008). One example is tandem affinity purification (TAP). In this method, a protein of interest fused to a TAP-tag is expressed in cells and

used as a bait to purify protein complexes that assemble on the TAP-tagged protein *in vivo*. Enriched protein complexes are then processed by enzymatic digestion to generate short peptides for MS analysis (Kaiser et al., 2008). More recently, the development of stable isotope labeling by amino acids in cell culture (SILAC) has enabled the generation of relatively quantitative information. Here, two cell populations are cultured in the presence of heavy or light amino acids, respectively, and are further combined in immunoprecipitation and MS analysis (Kirchner and Selbach, 2012).

Post-translational modifications, such as phosphorylation, are important events for the regulation of cellular processes. Phosphorylation involves transient covalent addition of phosphate groups to the serine, threonine, or tyrosine residues of proteins by protein kinases. Efficient analysis of protein phosphorylation by MS requires high enrichment phosphopeptides. Three methods are commonly used to get enriched phosphopeptides, namely immobilized-metal affinity chromatography (IMAC), titanium dioxide (TiO_2) affinity matrix and phosphorylated specific antibodies. IMAC employs a matrix composed of resins (e.g. iminodiacetic acid, nitrilotriacetic acid) and metal ions (e.g. $Fe3^+$, $Ga3^+$). The latter are usually positively charged, and therefore can catch negatively charged phosphate groups (Block et al., 2009). TiO_2 itself has affinity to organic phosphates, and is thus widely used to enrich phosphopeptides (Fila and Honys, 2012). The performance of TiO_2 evaluated by MS showed superior enrichment of phosphopeptides in comparison to IMAC-based methods (Cantin et al., 2007). Phosphorylated specific antibodies are routinely used to selectively immunoprecipitate phosphoproteins. However, the difficulty is generating a specific antibody that has high selectivity for the target phosphopeptides (Zhang and Neubert, 2006).

1.4.3 Chromatin immunoprecipitation

Chromatin immunoprecipitation (ChIP) is a powerful technique to identify interactions between a chromatin-associated protein and its genomic targets. In ChIP, the materials from living cells or tissue samples are fixed with formaldehyde to cross-link proteins to DNA. The cross-linked chromatin is then shared to generate 100 to 500bp DNA fragments, followed by immunoprecipitation with a desired antibody to enrich the DNA fragments bound to the protein of interest. After reverse cross-linking, the specific DNA fragments are isolated, and subsequently applied to microarrays (ChIP-chip) or next generation sequencing (ChIP-seq) to get a genome-wide readout of the specific binding sites (Blecher-Gonen et al., 2013; Johnson et al., 2007). In addition, ChIP-qPCR is

routinely applied to detect known candidate target genes and to validate the binding sites identified by ChIP-chip or ChIP-seq (Mukhopadhyay et al., 2008).

1.4.4 DNA methylation analysis

DNA methylation is an important epigenetic mark that occurs on the cytosine residues in the context of CpG dinucleotides. There are three commonly used approaches to detect genome-wide DNA methylation levels, including chemical conversion, affinity-based enrichment of methylated DNA fragments and digestion of genomic DNA with methyl-sensitive restriction enzymes (Laird, 2010). The choice of the method depends on the resolution and genome coverage needs. Bisulfite sequencing (BS-seq) is a chemical conversion method that determines CpG methylation at base resolution and is considered to be the gold standard for mapping DNA methylation (Krueger et al., 2012). By applying sodium bisulfite treatment to DNA, all non-methylated cytosines are converted to uracil, which will finally be detected as thymine residues, analogous to a C to T mutation by sequencing. Methylation-dependent immunoprecipitation followed by sequencing (MeDIP-seq) and methyl-CpG binding domain protein-enriched genome sequencing (MBD-seq) are based on the isolation of methylated DNA fragments by immunoprecipitation (Down et al., 2008; Serre et al., 2010). The resolution of these two methods is highly dependent on the DNA fragment size, CpG density, and immunoprecipitation quality of the reagent. Methylation-sensitive restriction enzyme digestion followed by sequencing (MRE-seq) can determine CpG methylation at base resolution by digesting genomic DNA with endonuclease. However, the coverage of MRE-seq is usually limited by the cutting frequency of the endonuclease (Rivera and Ren, 2013).

1.5 Aims of the project

Pathological cardiac hypertrophy, which associates with most forms of cardiac disease, leads to remodeling of the ventricular chambers and eventually heart failure. Reports have demonstrated the impact of the protein kinase CK2 (section 1.2.2) and the chromatin remodeling factor BRG1 (section 1.3.1) in the process of cardiac hypertrophy. However, it is so far unclear how the CK2 signals change the chromatin structure and gene transcription that eventually leads to cardiac hypertrophy and how BRG1 is targeted to the fetal genes in this setting. In the present study, the role of the chromatin remodeling factor DPF3a in this pathway was studied by performing *in vivo* and *in vitro* biochemical and molecular assays.

CHDs, such as TOF and VSD have been associated with many genetic factors (section 1.1.3). However, the underlying causes for the majority of patients remain unclear and additional non-genetic factors like epigenetic modifications are likely to impact on the disease etiology. Several studies have already shown DNA methylation changes associated with cardiac defects for selected candidate genes (section 1.3.3). To shift the focus of CHD research from single loci to an unbiased epigenome analysis, we performed MBD-seq on myocardial biopsies of TOF and VSD and examined the impact of genome-wide DNA methylation alterations in correlation with gene expression changes on TOF.

2 Manuscript 1

Phosphorylation of the chromatin remodeling factor DPF3a induces cardiac hypertrophy through releasing HEY repressors from DNA

Huanhuan Cui, Jenny Schlesinger, Sophia Schoenhals, Martje Tönjes, Ilona Dunkel, David Meierhofer, Elena Cano, Kerstin Schulz, Michael F. Berger, Timm Haack, Salim Abdelilah-Seyfried, Martha L. Bulyk, Sascha Sauer, Silke R. Sperling

This paper is published on Nucleic Acids Research, 2016, Vol. 44, No. 6. The authors acknowledge the published source for providing the PDF version of the paper.

Link: http://dx.doi.org/10.1093/nar/gkv1244

2.1 Synopsis

DPF3, also named BAF45c, is a member of the BAF chromatin remodeling complex. In human and mouse, DPF3 consists of two distinct isoforms, namely DPF3a (BAF45c1) and DPF3b (BAF45c2). The latter recognizes methylated and acetylated lysine residues of histone H3 and H4 via its double PHD fingers, and thereby recruits the BAF complex to target chromatin sites. In this study, we aimed to explore the function of DPF3a, which is characterized by a half PHD finger and a specific C-terminus of so far unknown function.

DPF3a and DPF3b were shown to be significantly up-regulated in hypertrophic TOF hearts in our previous study. Here, we observed that both transcripts were activated in hypertrophic hearts of patients with HCM and AS. Moreover, we analyzed the expression profile of DPF3a and DPF3b during differentiation of human-induced pluripotent stem cell-derived cardiomyocytes (hiPSC-CMs) and found that *DPF3a* is a fetal-like gene, which might play a role in pathological cardiac hypertrophy.

We first performed tandem affinity purification followed by mass spectrometry to search for DPF3a and DPF3b interacting proteins in the cytoplasm in HEK293 cells. We identified 11 and 6 proteins specifically interacting with DPF3a and DPF3b, respectively. All subunits of the CK2 were found to be exclusive interaction partners of DPF3a. This result was further confirmed by GST pulldown. We could show that DPF3a interacts with CK2α and CK2β. By performing *in vitro* kinase assays, we found that DPF3a phosphorylation *in vitro* is dependent on CK2. To analyze which residues of DPF3a are phosphorylated by CK2 *in vivo*, we carried out mass spectrometry and observed three phosphorylation sites in DPF3a. Furthermore, we showed that S348 of DPF3a was phosphorylated by CK2 both *in vitro* and *in vivo*.

Considering the activation and translocation of Ck2α upon hypertrophic stimuli, we explored the role of DPF3a in cardiac hypertrophy by inducing hypertrophic stress in mouse HL1 cells, rat H9C2 cells, and hiPSC-CMs using phenylephrine (PE) and endothelin 1 (ET-1). In response to hypertrophic stimulation, DPF3a expression and phosphorylation were significantly increased. Moreover, knockdown of DPF3 decreased ET-1 induced hypertrophy in hiPSC-CMs. In addition, cardiomyocytes transfected with WT DPF3a were much larger than cardiomyocytes transfected with S348A mutant, suggesting that S348 phosphorylation is essential for the hypertrophic response.

To identify downstream targets of DPF3a, we performed a protein binding microarray (PBM) and ChIP-seq. DPF3a did not exhibit sequence-specific binding to dsDNA in PBM. Our ChIP-seq experiments revealed approximately 800 binding sites with an enrichment

of E-box motif in these targets in C2C12 cells, suggesting DPF3a might be associated with DNA via interacting with E-box binding transcription factors. Subsequent co-immunoprecipitation showed that DPF3a specifically interacted with all three HEY transcriptional repressors. Using siRNA knockdown combined with ChIP-qPCR, we confirmed that HEY1 serves as a linker between DPF3a and DNA in C2C12 cells. Moreover, we showed that the half PHD finger mediates the interaction between DPF3a and HEY1, and S348 phosphorylation enhances this interaction. Additionally, the BAF complex core component BRG1 formed in complex with DPF3 and HEY1, and therefore was targeted to the genomic sites via this association.

Using reporter gene assays, we showed DPF3a has transactivation activity that is transmitted by its specific C-terminus. Consequently, we observed that DPF3a inhibited HEY1-mediated repression, suggesting that DPF3a might release HEY1 from DNA via a protein-protein interaction. Moreover, we found significant up-regulation of several DPF3-HEY targets in hypertrophic hearts of patients with AS and HCM.

To summarize, we found a novel pathway mediated by the BAF chromatin remodeling factor DPF3a driving cardiac hypertrophy. This pathway involves kinase activity, post-translational modification, and transcriptional regulation, and may therefore offer new directions for pharmaceutical interventions of pathological cardiac hypertrophy. The inhibition of this pathway is now a long-term therapeutic goal for the treatment of the course of heart failure.

2.2 Project contributions

For this project, I performed the majority of the experiments (approximately 70%), including *in vitro* kinase assay, co-immunoprecipitation, immunofluorescence staining, siRNA knockdown, chromatin immunoprecipitation, gene expression analysis, and reporter gene assay. Furthermore, I conceived the ideas for the project and wrote the manuscript together with SR. Sperling.

Contributions of co-authors

Concept: SR. Sperling

GST pulldown: J. Schlesinger

hiPSC-CMs differentiation: S. Schoenhals

Tandem affinity purification: M. Tönjes, I. Dunkel

Mass spectrometry analysis: D. Meierhofer, S. Sauer

Immunohistochemistry of TOF hearts: E. Cano

Site-directed mutagenesis: K. Schulz

Protein binding array: MF. Berger, ML. Bulyk

Contribution of material and reagents: T. Haack, SA. Seyfried

2538–2553 *Nucleic Acids Research, 2016, Vol. 44, No. 6* *Published online 17 November 2015*
doi: 10.1093/nar/gkv1244

Phosphorylation of the chromatin remodeling factor DPF3a induces cardiac hypertrophy through releasing HEY repressors from DNA

Huanhuan Cui[1,2,3,4], Jenny Schlesinger[1,3], Sophia Schoenhals[1,2], Martje Tönjes[3], Ilona Dunkel[3], David Meierhofer[5], Elena Cano[1], Kerstin Schulz[1], Michael F. Berger[6,7], Timm Haack[8], Salim Abdelilah-Seyfried[8,9], Martha L. Bulyk[6,7,10], Sascha Sauer[5,11] and Silke R. Sperling[1,2,3,4,*]

[1]Department of Cardiovascular Genetics, Experimental and Clinical Research Center, Charité – Universitätsmedizin Berlin and Max Delbrück Center for Molecular Medicine, 13125 Berlin, Germany, [2]Department of Biology, Chemistry and Pharmacy, Freie Universität Berlin, 14195 Berlin, Germany, [3]Group of Cardiovascular Genetics, Department of Vertebrate Genomics, Max Planck Institute for Molecular Genetics, 14195 Berlin, Germany, [4]DZHK (German Center for Cardiovascular Research), partner site Berlin, Berlin, Germany, [5]Max Planck Institute for Molecular Genetics, 14195 Berlin, Germany, [6]Division of Genetics, Department of Medicine, Brigham and Women's Hospital and Harvard Medical School, Boston, MA 02115, USA, [7]Committee on Higher Degrees in Biophysics, Harvard University, Cambridge, MA 02138, USA, [8]Hannover Medical School, Institute of Molecular Biology, Carl-Neuberg Str. 1, D-30625 Hannover, Germany, [9]Potsdam University, Institute of Biochemistry and Biology, Department of Animal Physiology, Karl-Liebknecht Str. 24-25, 14476 Potsdam-Golm, Germany, [10]Department of Pathology, Brigham and Women's Hospital and Harvard Medical School, Boston, MA 02115, USA and [11]CU Systems Medicine, University of Würzburg, 97080 Würzburg, Germany

Received August 07, 2015; Revised October 22, 2015; Accepted November 01, 2015

ABSTRACT

DPF3 (BAF45c) is a member of the BAF chromatin remodeling complex. Two isoforms have been described, namely DPF3a and DPF3b. The latter binds to acetylated and methylated lysine residues of histones. Here, we elaborate on the role of DPF3a and describe a novel pathway of cardiac gene transcription leading to pathological cardiac hypertrophy. Upon hypertrophic stimuli, casein kinase 2 phosphorylates DPF3a at serine 348. This initiates the interaction of DPF3a with the transcriptional repressors HEY, followed by the release of HEY from the DNA. Moreover, BRG1 is bound by DPF3a, and is thus recruited to HEY genomic targets upon interaction of the two components. Consequently, the transcription of downstream targets such as *NPPA* and *GATA4* is initiated and pathological cardiac hypertrophy is established. In human, DPF3a is significantly upregulated in hypertrophic hearts of patients with hypertrophic cardiomyopathy or aortic stenosis. Taken together, we show that activation of DPF3a upon hypertrophic stimuli switches cardiac fetal gene expression from being silenced by HEY to being activated by BRG1. Thus, we present a novel pathway for pathological cardiac hypertrophy, whose inhibition is a long-term therapeutic goal for the treatment of the course of heart failure.

INTRODUCTION

Cardiac hypertrophy is defined as the increase in myocardial mass in response to pressure or volume stress, or mutations of sarcomeric proteins (1). Pathological hypertrophy represents a key risk factor for heart failure and accompanies nearly all forms of cardiovascular disease, including hypertension, hypertrophic cardiomyopathy (HCM) and aortic stenosis (AS). Sustained hypertrophy, which can eventually lead to heart failure, is associated with increased interstitial fibrosis, cell death and contractile dysfunction (2–4). Therefore, the prevention of pathological hypertrophy is of great therapeutic interest for cardiovascular disease.

On the cellular level, cardiac hypertrophy is characterized by an increase in cardiomyocyte size, with enhanced protein synthesis and changes to the sarcomere organization (5). Pathological stress is mediated via several intracellular signaling pathways that eventually activate the fetal gene program. The casein kinase 2 (CK2)-mediated signaling cas-

*To whom correspondence should be addressed. Tel: +49 30450540123; Fax: +49 30450540159; Email: silke.sperling@charite.de

cades have been shown to be important for the development of cardiac hypertrophy. CK2 is a typical serine/threonine kinase consisting of two catalytic subunits (αα, αα' or α'α') as well as two regulatory β subunits and has been implicated in many cellular and developmental processes (6). CK2α', one of the catalytic subunits, is activated by the cardiac growth factor angiotensin II, which results in an imbalanced feedback loop between p27 and CK2α' that is crucial for agonist- and stress-induced cardiac hypertrophic growth (7). Knockout of the other catalytic subunit CK2α in mice leads to structural defects in the heart and somites, with mice dying in mid-gestation (8). In response to hypertrophic stimuli, CK2α translocates to the nucleus and activates histone deacetylase 2 (HDAC2) by phosphorylating HDAC2 at serine 394 (9).

Cardiac hypertrophy is accompanied by up-regulation of the fetal gene program. Fetal genes are a set of genes that are often expressed only in the developing heart and are re-expressed during cardiac hypertrophy, and include natriuretic peptides (*NPPA*, *NPPB*), structure proteins (*β-MHC*, *α-skeletal actin*) and others (5). Transcriptional reprogramming of gene expression and reactivation of fetal genes are tightly controlled by transcription factors as well as chromatin modifying and remodeling factors (10–12).

The chromatin remodeling complexes alter chromatin structure using the free energy of ATP hydrolysis to change nucleosome positions relative to the DNA. The mammalian SWI/SNF-like complex (BAF complex) consists of 9–12 components, including the core component encoded by either brahma (BRM) or brahma-related gene 1 (BRG1) (13). Depletion of myocardial BRG1 causes a thin, compact myocardium and absent interventricular septum, and leads to embryonic lethality. In embryonic cardiomyocytes, BRG1 forms a complex with poly (ADP-ribose) polymerases (PARPs) to activate the fetal gene beta-myosin heavy chain (*β-MHC*), while it represses the cardiac contractile protein alpha-myosin heavy chain (*α-MHC*) via interaction with HDACs. Normally, BRG1 is turned off in the adult heart, but when the heart is stressed by disease or pressure overload, BRG1 is reactivated and interacts with HDACs and PARPs to repress *α-MHC* and activate *β-MHC* expression (14). A recent study showed that *Mhrt*, a cardiac specific long non-coding RNA, protects the heart from pathological hypertrophy via binding to BRG1, and thereby inhibiting chromatin targeting and gene regulation (15). Another muscle-specific component of the BAF complex is BAF60c (encoded by *SMARCD3*), which is highly expressed in heart and skeletal muscle during development (16). In skeletal muscle differentiation, phosphorylation of BAF60c by the p38α kinase promotes MyoD-BAF60c binding into the BAF complex, and thereby remodels chromatin and activates transcription of myogenic genes (17,18).

In 2008, we identified DPF3 (also named BAF45c) as a novel epigenetic factor for heart and muscle development. *DPF3* is significantly up-regulated in patients with Tetralogy of Fallot (TOF), which is characterized by structural cardiac defects and right ventricular hypertrophy (19,20). Morpholino knockdown of *dpf3* in zebrafish leads to impaired skeletal and cardiac muscle development and severely reduced ventricular contractility, with disassembled muscular fibers caused by transcriptional deregulation of structural and regulatory proteins (20). DPF3 consists of two distinct isoforms, namely DPF3a and DPF3b. The latter contains two plant homeodomains (PHD) that can bind to methylated and acetylated lysine residues of histone H3 and H4 (20), enabling a regulatory switch between poised and activated chromatin stages (21).

Here, we aim to shed light on the function of DPF3a, which is characterized by a half PHD finger and a specific C-terminus of so far unknown function. We show that DPF3, in particular DPF3a, is significantly up-regulated in pathologic cardiac hypertrophy in patients with HCM as well as AS. In response to hypertrophic stimuli, the protein kinase CK2 phosphorylates DPF3a that consequently binds and releases the transcriptional repressors HEY and recruits BRG1 to respective targets. Consequently, phosphorylated DPF3a (pDPF3a) initiates transcription of fetal genes promoting cardiac hypertrophy.

MATERIALS AND METHODS

Human samples

All cardiac samples were obtained with the approval of the ethics committee of the Charité – Universitätsmedizin Berlin and written informed consent was obtained for all individuals. Excised cardiac tissue from the left ventricular outflow tract was used in the study. It was obtained from four unrelated patients with AS undergoing aortic valve replacement, and from eight unrelated patients with HCM and severe obstruction of the left ventricular outflow tract undergoing transaortic subvalvular myotomy–myectomy. Both patient groups were characterized by severe hypertrophy of the left ventricle. Tissue from normal human hearts was obtained from unmatched organ donors without cardiac disease. All samples were snap frozen in liquid nitrogen after excision and stored at −80°C. Paraffin embedded TOF and normal heart samples were obtained as previously described (22).

Human-induced pluripotent stem cell-derived cardiomyocytes (hiPSC-CMs)

The human-induced pluripotent stem cell line derived from a healthy individual was generously provided by the Stem Cell Core Facility of the Berlin Institute of Health (BIH). Cardiomyocyte differentiation was mediated by modulating Wnt-signaling, applying small molecules under fully defined conditions (23,24). Briefly, iPSCs were maintained in Essential 8 Media (Gibco) on Geltrex (Gibco) 6-well plates. iPSCs were dissociated using an EDTA-based passaging procedure (25) and 0.2–0.4 million cells were seeded in one 12-well plate containing Essential 8 media supplemented with 5 μM Pro-survival Compound, DDD00033325 (Calbiochem). After 24 h, Essential 8 media was exchanged and cells were maintained for an additional 24 h.

At day 0, differentiation was induced using RPMI/B27 without insulin supplemented with 9 μM GSK-3 inhibitor XVI (Calbiochem). Exactly 24 h later, media was changed to RPMI/B27 without insulin, and cells were subsequently cultivated for 48 h. On day 3, the differentiation media was exchanged for RPMI/B27 without insulin supplemented with 5 μM IWP2 (Calbiochem), and cells were cultivated

for an additional 48 h. The media was then changed back to RPMI/B27 without insulin on day 5 of differentiation. From day 7 onwards, cells were cultivated in RPMI/B27 and media was exchanged every 3 days.

Flow cytometry

After 15 days of differentiation, cells were washed twice with pre-warmed PBS and were singularized by applying 0.25% Trypsin/EDTA. Cells were fixed with 1% formaldehyde for 20 min at room temperature and were permealized using 90% ice-cold methanol and were subsequently stored at −20°C. For evaluation of differentiation efficiency, 10^5 cells were evaluated. Briefly, cells were washed twice in PBS with 0.5% BSA (Flow Buffer 1) and incubated with the primary antibody against cardiac Troponin T (mouse IgG1, Lab Vision; 1:500) in PBS with 0.5% BSA and 0.1% Triton-X (Flow Buffer 2) at 4°C overnight. Afterwards, cells were washed with Flow Buffer 1 and were incubated with the secondary antibody Goat anti-Mouse IgG1 conjugated to Alexa Fluor 488 (1:1000) for 30 min at room temperature. Samples were washed twice with Flow Buffer 1 and were filtered through a 50 μm filter and evaluated on a BD FACS Canto II.

Metabolic selection of hiPSC-CMs

As the analyzed population showed only an insufficient purity of 78% iPS-CMs metabolic purification applying lactate was performed as previously described (26). Briefly, cells were reseeded in lower density in RPMI supplemented with insulin, 20% Fetal Bovine Serum (FBS) and 5 μM Pro-survival Compound, DDD00033325 (Calbiochem) by applying 0.25% Trypsin/EDTA. Cells were allowed to recover for 4 days and were then cultivated in RPMI without Glucose and HEPES supplemented with 4 mM Sodium DL-lactate solution (Sigma) for 4 days. Afterwards, media was changed back to RPMI with insulin. All subsequent analyses were performed at a cell density of 37 500 cells/cm^2.

Cell culture

C2C12 myoblasts, H9C2 cardiomyocytes and HEK293T cells were cultured at 5% CO_2 and 37°C in Dulbecco's Modified Eagle's Medium (Gibco) supplemented with 1% penicillin/streptomycin (Gibco) and 10% FBS (Biochrom). HL-1 cells were cultured in Claycomb medium (Sigma) containing 10% FBS, 100 mM norepinephrine, 4 mM L-glutamine and 1% penicillin/streptomycin.

For phenylephrine (PE) or Edothelin 1 (ET-1) treatment, HL-1, H9C2 or hiPSC-CMs were incubated with 10 μM PE (Sigma) or 1 nM ET-1 for 24 h. Cells were then harvested for RNA isolation or fixed with methanol for immunofluorescence staining.

Isolation and transfection of mouse primary cardiomyocytes

Neonatal hearts were isolated from 1–3 days old mice. After removing atria and large arteries, ventricles were minced and treated with collagenase buffer for 1 h at room temperature with gently shaking. The enzyme digestion was stopped by the addition of 10% FBS containing DMEM. Fibroblasts were removed twice by 1 h pre-plating. The cardiomyocytes were counted and plated on collagen-coated culture dishes and were maintained in 10% FBS in DMEM without antibiotics. Isolated mouse primary cardiomyocytes were cultured for 3 days and then transfected with Flag-tagged DPF3a WT and S348A mutant constructs using Lipofectmine 3000 (Invitrogen).

Recombinant protein expression and purification

GST fusion proteins were expressed in *E. coli* BL21 DE3 pRARE3 and purified using Glutathione–Sepharose matrix (GE Healthcare) according to the manufacturer's instructions.

GST pull-down

GST-CK2α/α'/β fusion proteins were coupled to Glutathione–Sephharose matrix, according to the manufacturer's indication (GE Healthcare), and subsequently incubated with Flag-DPF3a/b recombinant proteins for 2 h at 4°C in binding buffer (4.2 mM Na_2HPO_4, 2 mM KH_2PO_4, 250 mM NaCl, 10 mM KCl, 0.1% NP40, 0.5% BSA, pH 7.2, complete protease inhibitor (Roche)). Matrices were washed three times in binding buffer, resuspended in 4x LDS sample buffer, denatured at 95°C for 5 min and subjected to Western blot analysis.

Phosphorylation prediction and conservation analysis of DPF3a

The multiple alignment of DPF3a in different species was generated using ClustalW2 (27). Phosphorylation site prediction was performed using NetPhos 2.0 Server (28) with standard parameters. CK2-specific phosphorylation site prediction was carried out using KinasePhos 2.0 (29) with standard parameters.

Mass spectrometry analysis

Tandem affinity purification followed by mass spectrometry was carried out as described previously (20). To study the phosphorylation of DPF3a, HEK293T cells were transfected with Flag-DPF3a. Cell extracts were immunoprecipitated with anti-Flag M2 antibody (Sigma) and immunoprecipitated complexes were digested in solution. Phosphopeptide enrichment was conducted using the Titansphere Phos-TiO kit (GL Sciences). Mass spectrometry analysis for identification of proteins and for detection of protein phosphorylation was performed as previously described (30,31).

In vitro kinase assay

In vitro phosphorylation of recombinant proteins was performed as described previously (32). Briefly, 1 μg of GST fusion proteins were incubated with recombinant active CK2 (NEB) and ATPγS (Epitomics) in the reaction buffer at 30°C for 2 h. Proteins were then alkylated with 2.5 mM p-Nitrobenzyl mesylate (PNBM, Epitomics) for 2 h at room temperature and the products were analyzed by Western

blot using an anti-Thiophosphate ester antibody (Epitomics). The CK2-specific inhibitor tetrabomocinnamic acid (TBCA, Millipore) was used to abolish CK2 activity in the *in vitro* kinase assay.

Generation of anti-pDPF3a antibody

The DPF3a antibody that can specifically recognize phosphorylated S348 (anti-pDPF3a) was generated in rabbit by Thermo Fisher Scientific. The phosphorylated peptide against the epitope CRRSGRG[pS]PTADK of DPF3a was used.

Co-immunoprecipitation (CoIP)

HEK293T cells were transiently transfected with the indicated expression vectors for Flag- or HA-tagged proteins using polyethylenimine (PEI). The cells were lysed in CoIP buffer (20 mM Tris-HCl pH 7.4, 150 nM NaCl, 1 mM EDTA, 1% Triton, 1 mM DTT, 0.1 mM PMSF, 1 mM NaVO4, protease inhibitor (Roche) and phosphatase inhibitor (Roche)). Protein concentrations were determined using the Bradford assay (Sigma). A total of 500 μg cell extracts were incubated with Flag M2 matrix (Sigma) or HA-matrix (Roche) for 2 h at 4°C. The matrix was then washed three times with ice-cold CoIP buffer and eluted for Western blot.

Western blotting and quantification

Cells and human cardiac biopsies were treated with lysis buffer (20 mM Tris-HCl pH 7.4, 150 nM NaCl, 1 mM EDTA, 1% Triton, 1 mM DTT, 0.1 mM PMSF, protease inhibitor (Roche), 1 mM $NaVO_4$) for protein extraction. Western blot was performed according to standard protocols. All antibodies, with their respective dilutions, are given in Supplementary Table S1. Image Lab 5.0 (Bio-Rad) was used to quantify the blot signals.

Immunofluorescence staining

For cell immunofluorescence analysis, the cells were fixed with methanol. Blocking was carried out in 3% normal goat serum in PBS for 1 h at room temperature. Primary and secondary antibodies were applied in the same buffer for 2 h at room temperature, each followed by three washes in PBS and a DAPI counterstaining. The cells were mounted in Mowiol 4–88 (Carl Roth) and examined on a LSM 710 confocal microscope (Carl Zeiss). The cell size of transfected cells was measured using ImageJ.

For human tissue immunofluorescence analysis, paraffin-embedded right ventricular biopsies of healthy and TOF individuals were rehydrated and subjected to heat-mediated antigen retrieval and quenching of endogenous peroxidase activity. Blocking was performed with donkey serum (10%) and BSA (2%) in PBT (0.3%) and primary antibodies were applied overnight at 4°C in the same buffer. Corresponding secondary antibodies were subsequently applied, and the tissue incubated for 1 h at room temperature; this was followed by application of Vectastain Elite ABC Kit (Vector Lab) and TSA Plus Cyanine-5 System (Perkin Elmer) according to the manufacturer's instructions. Nuclei were counterstained with DAPI and slides mounted with Fluoromount (Sigma). Omission of the first antibody served as a negative control. All images were captured using a Leica SP5 confocal microscope. Antibodies and reagents with their respective dilutions are listed in Supplementary Table S1.

RNAi knockdown

For RNAi knockdown, C2C12 cells or hiPSC-CMs were transfected with siRNAs (Supplementary Table S2) targeting *Dpf3a*, *Hey1* and *Ck2α*, respectively. As a control, the cells were transfected with an unspecific siRNA (siNon). Cells were grown to 50% confluence for at least 2 days without addition of antibiotics. A total of 1×10^5 cells were seeded into 6-well plates with 2 ml media resulting in 40% confluence after 4 h. The mixture of 4.4 μl (20 μM) siRNA in 100 μl of DMEM media and 8.8 μl Lipofectamine 3000 (Invitrogen) in 100 μl DMEM media was incubated for 15 min at room temperature and added drop-wise to the cells. The cell culture medium was changed after 24 h and cells were harvested for protein extraction or RNA preparation after 48 h.

Gene expression analysis

Total RNA of cultured cells and human cardiac biopsies was isolated using TRIzol reagent (Invitrogen) followed by DNase digest (Promega) and ethanol precipitation according to standard protocols. Reverse transcription reactions were carried out via AMV-RT (Promega) with random hexamers (Amersham Pharmacia Biotech). Quantitative real-time PCR measurements were performed using the GoTaq qPCR Master Mix (Promega) and the ABI PRISM 7900HT Sequence Detection System. Gene expression was calculated using the ΔCT method with normalization to the housekeeping gene *HPRT* or *GAPDH*. Primer sequences are given in Supplementary Table S3.

Chromatin immunoprecipitation (ChIP) and qPCR

ChIP experiments with C2C12 cells were carried out with the MAGnify™ Chromatin Immunoprecipitation System (Life Technologies) following the manufacturer's instructions with some modifications. Sonication was performed using the Bioruptor UCD300 (Diagenode) to obtain chromatin fragments of approximately 100–500 bp. For Hey1 ChIP, C2C12 cells were transiently transfected with Flag-Hey1 and empty Flag vector, which was used as a control. Anti-pDPF3a and anti-Flag M2 antibodies were used in ChIP experiments. ChIP DNA was purified using the Zymo ChIP DNA cleanup kit. ChIP results were analyzed by quantitative PCR. ChIP enrichment was normalized to the input and expressed as relative enrichment of the material precipitated by the indicated antibody on target regions. ChIP primers are listed in Supplementary Table S4.

Site-directed mutagenesis

Site-directed mutagenesis of DNA was performed using the QuikChange II site-directed mutagenesis kit (Agilent)

according to manufacturer's instructions. Oligonucleotides for mutagenesis were designed to introduce mutations of the DPF3a phosphorylation sites. Mutagenesis was confirmed by plasmid sequencing (Eurofins Genomics).

Reporter gene assay

For luciferase assays, approximately 10^4 HEK293 cells were transiently transfected with 50 ng of reporter vector, 5 ng of Renilla luciferase vector for internal normalization of transfection efficiency and 50–150 ng of the respective expression vectors. Activity was measured by Dual-Luciferase assay (Promega) after 48 h in a Centro LB960 Luminometer (Berthold, Bad Wildbad, Germany). All measurements were performed in triplicates.

RESULTS

DPF3 is significantly up-regulated in hypertrophic hearts

In mammals, *DPF3* occurs in two splice variants, namely *DPF3a* and *DPF3b*. DPF3a (BAF45c1) is characterized by a functionally unknown half PHD finger followed by a unique C-terminus, whereas DPF3b (BAF45c2) comprises a C-terminus harboring a double PHD finger previously characterized by us and others (Figure 1A) (20,21). Both variants are expressed in all four chambers of the normal human adult hearts with *DPF3a* being continuously higher expressed than *DPF3b* (Figure 1B).

Previously, we showed that both *DPF3a* and *DPF3b* are significantly up-regulated in the hypertrophic right ventricle of TOF hearts (19,20). To further investigate the role of *DPF3* in pathological cardiac hypertrophy, we studied cases of HCM and pressure overload related hypertrophy resulting from AS. The details of all human heart samples are given in Supplementary Table S5. Quantitative real-time PCR showed a significant up-regulation of *DPF3* as well as the two individual splice variants in the left ventricle of HCM and AS cases compared to normal hearts (NH) ($P < 0.05$; Figure 1, C and D). Pathological cardiac hypertrophy is regulated by re-activation of fetal gene expression. To test if *DPF3* is a fetal-like gene, we analyzed the expression of *DPF3a* and *DPF3b* during differentiation of human-induced pluripotent stem cell-derived cardiomyocytes (hiPSC-CMs). The differentiation process and purity of hiPSC-CMs was characterized by marker gene analysis and flow cytometry (Supplementary Figure S1). Interestingly, *DPF3a* shows a similar expression profile to the fetal gene *NPPA* with the highest expression at day 10, whereas *DPF3b* is expressed at a very low level during the differentiation process (Figure 1E). Taken together, all these results suggest that *DPF3a* can be considered as a fetal-like gene, which might play a role in pathological cardiac hypertrophy in general.

CK2 binds and *in vitro* phosphorylates DPF3a

To elucidate the role of DPF3 in cardiac hypertrophy, we first searched for DPF3 interacting proteins in HEK293 cells. Using the tandem affinity purification (TAP) technique followed by mass spectrometry (MS) analysis, we identified 11 and 6 proteins specifically interacting with DPF3a or DPF3b, respectively, with a Mascot score >40 and a minimum number of two matching spectra (Table 1). All subunits of the tetrameric casein kinase 2 complex, CK2α, CK2α' and CK2β were found as exclusive interaction partners of DPF3a (Table 1). None of the CK2 subunits was identified when DPF3b was used as the bait protein.

This observation led us to investigate whether DPF3a could directly associate with CK2α/α'/β *in vitro*. Thus, we performed *in vitro* interaction studies with purified proteins, using GST-tagged purified CK2α/α'/β in combination with Flag-tagged DPF3a/b. Pull-down assays showed that DPF3a strongly interacts with CK2β and weakly binds to CK2α (Figure 2A). This is in line with the fact that CK2α is the catalytic subunit, whereas CK2β is the regulatory subunit of CK2 and responsible for substrate recognition (6). Again, we observed no interactions between CK2 subunits and DPF3b (Figure 2A). CK2 is a well-known ubiquitously expressed and evolutionarily conserved serine/threonine protein kinase (6). To investigate whether DPF3a is phosphorylated by CK2, we applied *in vitro* kinase assays using purified GST-fusion protein of DPF3a, with GST-DPF3b and GST-NEP serving as negative and positive control, respectively (33). Both DPF3a and NEP, but not DPF3b, were *in vitro* phosphorylated by CK2 and DPF3a phosphorylation became saturated when 500U CK2 was applied in the kinase assay (Figure 2B). Moreover, DPF3a phosphorylation is reduced upon treatment with increasing amounts of the CK2 specific inhibitor TBCA (Figure 2C), indicating that DPF3a phosphorylation *in vitro* is largely dependent on CK2 activity.

S348 of DPF3a is phosphorylated by CK2 *in vivo*

In order to analyze which residues of DPF3a are phosphorylated by CK2, we used the prediction tools Netphos 2.0 (28) and KinasePhos 2.0 (29). We found potential phosphorylation sites for the full DPF3a sequence and revealed several sites in the DPF3a-specific C-terminus. Here, multiple minimal CK2 consensus motifs (S/T-X-X-E/D) were predicted between aa293 and aa357 (T309, T310, S316, S318 and S348) (Supplementary Figure S2). The DPF3a specific C-terminus is highly conserved across vertebrate and mammalian species (Supplementary Figure S3). To confirm potential phosphorylation sites, we analyzed the phosphorylation of DPF3a in HEK293 cells using immunoprecipitation followed by mass spectrometry analysis. In total, we identified three phosphorylation sites in DPF3a, namely S138, S348 and T350 (Table 2). Of these, in particular S348 is conserved in human, mouse and chicken (Figure 2D), which suggests a potential functional role of this site. Therefore, we studied the CK2 dependent phosphorylation of DPF3a S348 using an *in vitro* kinase assay on purified GST-fusion protein in which serine 348 was mutated to alanine (S348A). We found that phosphorylation of DPF3a by CK2 is significantly reduced by the mutation of S348A compared to the wild-type (WT) DPF3a (Figure 2E). We also mutated all five predicted CK2 mediated phosphorylation sites (5xAla) and observed a further reduction of DPF3a phosphorylation (Figure 2E), suggesting additional functional phosphorylation sites *in vitro*.

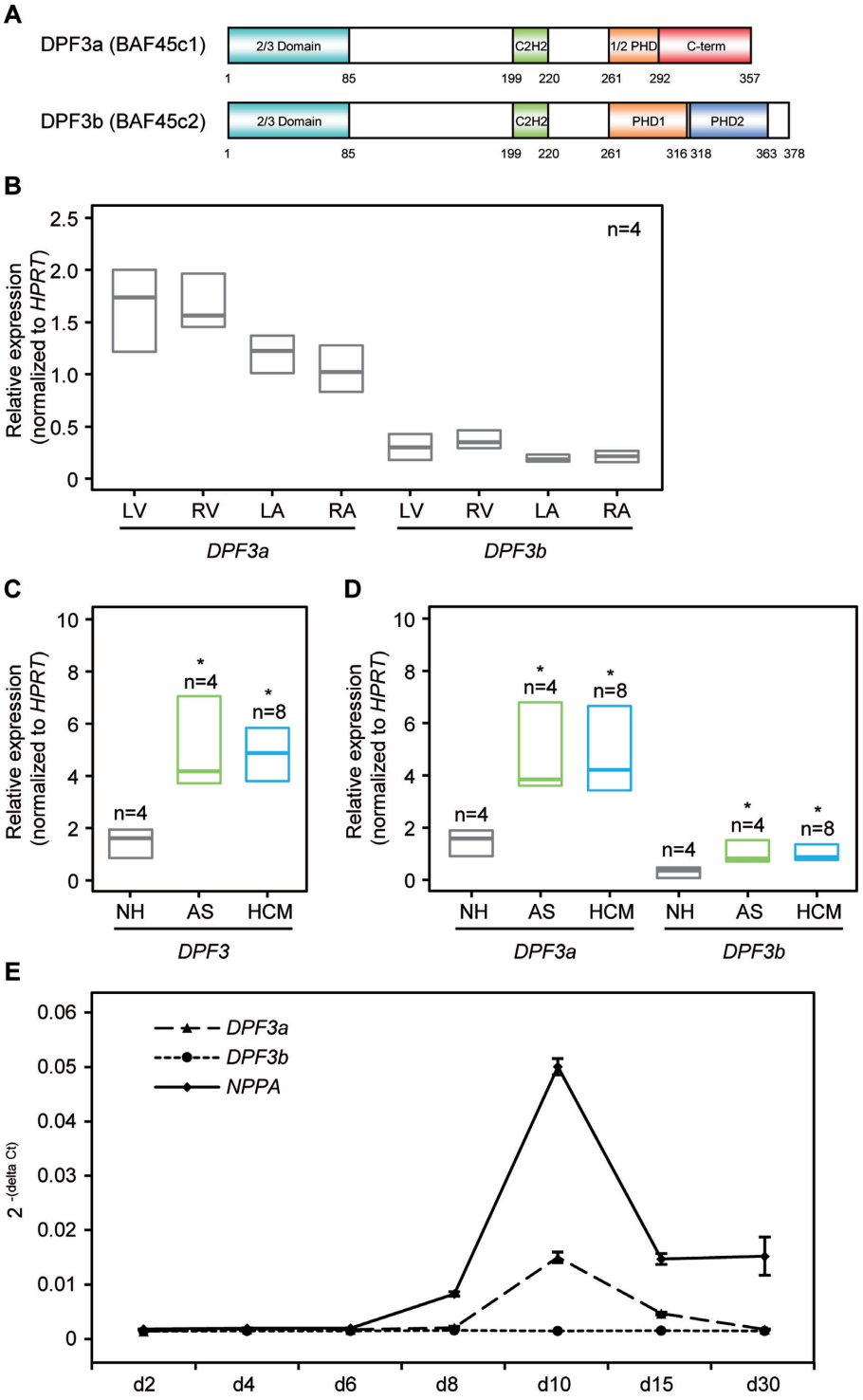

Figure 1. Up-regulation of *DPF3* in hypertrophic hearts. (**A**) Schematic representation of the DPF3 isoforms. The isoform DPF3a contains a half PHD finger and a specific C-terminus, whereas DPF3b contains a double PHD finger. Amino acid positions are depicted. Teal: 2/3 domain; green: C2H2-Krüppel-like zinc finger; orange: first plant homeodomain; blue: second plant homeodomain; red: DPF3a specific C-terminus. (**B**) Expression analysis of *DPF3a* and *DPF3b* splice variants in normal human heart tissues (n = 4) of left ventricle (LV), right ventricle (RV), left atrium (LA) and right atrium (RA) using qPCR. Results represent median expression levels with 25% and 75% quartile; assays were performed in triplicates. (**C**) Expression of *DPF3* mRNA in hypertrophic and healthy hearts. qPCR analysis of *DPF3* mRNA levels in myocardial, left ventricular tissue from patients with aortic stenosis (AS), hypertrophic cardiomyopathy (HCM) and normal hearts (NH). (**D**) Analysis of splice variants expression of *DPF3a* and *DPF3b* in AS, HCM and NH. Statistically significant differences were analyzed using a two-sided Student *t*-test (*$P < 0.05$). (**E**) Temporal expression profiles of *DPF3a*, *DPF3b* and *NPPA* during differentiation of human-induced pluripotent stem cell-derived cardiomyocytes (hiPSC-CMs). qPCR was performed on samples obtained from different days during cardiac differentiation. Expression values were normalized to the housekeeping gene *GAPDH*.

Table 1. DPF3a and DPF3b specific interaction partners in cytoplasm

Bait protein	Hugo ID	Accession number	MW (Da)	Mascot score	Matching spectra	Protein name
DPF3a	CSNK2A1	P68400	45 229	459	13	Casein kinase II subunit alpha
	CSNK2A2	P19784	41 358	251	10	Casein kinase II subunit alpha'
	CSNK2B	P67870	25 268	54	5	Casein kinase II subunit beta
	ASCC3L1	O75643	246 006	56	3	activating signal cointegrator 1 complex subunit 3-like 1
	UBR4	Q5T4S7	580 547	49	8	Zinc finger UBR1-type protein 1, ubiquitin protein ligase E3 component n-recognin 4
	UBR5	O95071	312 352	49	5	E3 ubiquitin-protein ligase EDD1
	HDGFRP3	Q9Y3E1	22 663	101	3	Hepatoma-derived growth factor-related protein 3
	HSPA1L	P34931	70 730	71	6	Heat shock 70 kDa protein 1L
	AIFM1	O95831	67 144	41	4	Apoptosis-inducing factor 1, mitochondrial precursor
	IGKC	P01834	11 773	61	2	Ig kappa chain C region
	GPSN2	Q9NZ01	36 410	51	4	Synaptic glycoprotein SC2
DPF3b	TUBA8	Q9NY65	50 746	75	9	Tubulin alpha-8 chain
	XPOT	O43592	111 148	41	5	Exportin-T
	TUBA3E	Q6PEY2	50 626	444	13	Tubulin alpha-3E chain
	EEF1A2	Q05639	50 780	51	3	Elongation factor 1-alpha 2
	TIMM50	Q3ZCQ8	39 850	143	3	Import inner membrane translocase subunit TIM50, mitochondrial precursor
	AHSA1	O95433	38 421	48	2	Activator of 90 kDa heat shock protein ATPase homolog 1

Protein specifically associated with DPF3a or DPF3b in the cytoplasm identified by tandem affinity purification followed by mass spectrometry. Da: Dalton, MW: molecular weight.

Table 2. Phosphorylated sites in DPF3a

Peptide	Mascot score	PEP	Position
EEES(ph)IQEIQR	171.99	2.08E-05	138
GS(ph)PTADKK	108.43	2.05E-06	348
GSPT(ph)ADKK	130.66	1.83E-11	350

Phosphorylated sites within DPF3a identified by mass spectrometric analysis. PEP: posterior error probabilities.

Furthermore, we generated a DPF3a antibody that can specifically recognize phosphorylated S348 (anti-pDPF3a). The specificity of the anti-pDPF3a antibody was confirmed by Western blot and immunofluorescence with peptide control assays (Supplementary Figure S4). In immunofluorescence staining, we found that pDpf3a is exclusively present in the nucleus in HL1 and C2C12 cells (Supplementary Figure S4, Figure 2I). Further, we could verify the *in vitro* phosphorylation of Dpf3a S348 by Ck2 using the anti-pDPF3a antibody (Figure 2F). In order to investigate phosphorylation of S348 *in vivo*, we knocked down Ck2 using RNA interference in C2C12 myoblasts. Treatment with siCk2α significantly reduced Ck2α mRNA and protein expression (Figure 2, G and H). Elimination of Ck2α function did not affect the expression of Dpf3a (Figure 2G). Notably, the phosphorylation of DPF3a at S348 was abolished in Ck2α knockdown (Figure 2, H and I), suggesting that S348 is *in vivo* phosphorylated by Ck2.

Phosphorylation of S348 is essential for cardiac hypertrophy

Considering a previous report showing activation and translocation of Ck2α upon hypertrophic stimuli (9), we investigated this pathway with respect to Dpf3a and examined whether hypertrophic stimuli induce phosphorylation of DPF3a mediated by Ck2α. We induced hypertrophic stress in mouse HL1, rat H9C2 cells as well as hiPSC-CMs using 10 μM phenylephrine (PE). The expression of *Nppa*, a marker of hypertrophy, increased in HL1 and H9C2 cells upon PE treatment (Supplementary Figure S5A). PE stimulation significantly increased the mRNA expression (Supplementary Figure S5A) and the phosphorylation of Dpf3a in both HL1 and H9C2 cells (Supplementary Figure S5B). During differentiation of hiPSC-CMs, the protein level of pDPF3a increased on day 5 and remained stable thereafter (Supplementary Figure S5C). In line with another publication (34), hiPSC-CMs did not respond to PE with unchanged *NPPA* expression (Figure 3A). However, endothelin 1 (ET-1) treatment successfully increased *NPPA* and *DPF3a* expression in hiPSC-CMs (Figure 3A). DPF3a phosphorylation was significantly increased upon ET-1 stimulation (Figure 3B). Moreover, we observed much higher levels of DPF3a phosphorylation in hypertrophic left ventricle of patients with HCM and AS compared to NH hearts (Figure 3C). In addition, many more pDPF3a positive cells were found in the hypertrophic right ventricle of TOF hearts compared to NH hearts (Figure 3D). Furthermore, knockdown of DPF3 in hiPSC-CMs decreased the increment of *NPPA* expression in the ET-1 situation (Figure 3E), suggesting that ET-1 induced hypertrophy can be buffered by the abolition of DPF3. To further investigate whether S348 phosphorylation is required for hypertrophy, mouse primary cardiomyocytes were transfected with Flag-tagged WT DPF3a or S348A mutant constructs (Figure 3F). Non-transfected cells were used as controls and stained for cell size measurements. Overexpression of DPF3a WT increased cell size and *Nppa* expression, whereas cell size changes and *Nppa* expression alterations could not be observed in those transfected with the S348A mutant constructs (Figure 3, G and H), indicating that the phosphorylation of S348 is required for the hypertrophic response.

DPF3a interacts with the transcription repressors HEY

To identify downstream targets of DPF3a, we performed protein binding microarray (PBM) and ChIP-seq analysis. In the PBM experiments, a purified GST-tagged DPF3a or DPF3b protein was applied to a 'universal' PBM representing all 10 bp double-stranded DNA (dsDNA) sequences (35). Neither DPF3a nor DPF3b exhib-

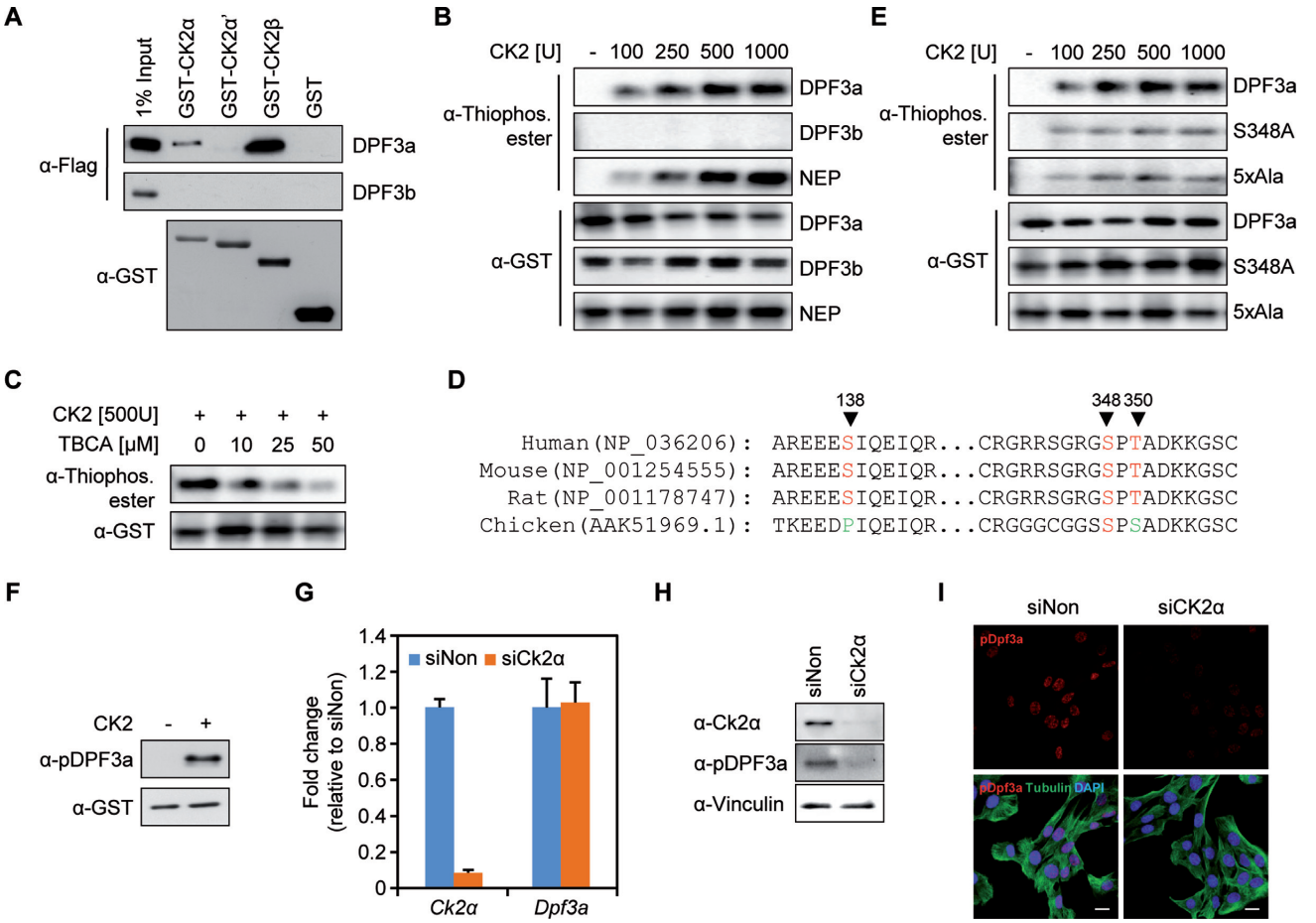

Figure 2. CK2 binds and phosphorylates DPF3a at S348. (**A**) GST pull-down with GST-CK2 subunits and Flag-DPF3a/b. Similar expression of GST levels could be shown for the CK2 subunits and the control GST vector. GST pull-down results show an interaction of the CK2α and β subunit with full-length DPF3a. (**B**) *In vitro* CK2 kinase assay with recombinant CK2 and purified GST fusion DPF3a. Increasing amount of CK2 was incubated with GST-DPF3a and combinations of ATPγS and p-nitrobenzyl mesylate (PNBM) as indicated; reaction products were analyzed by Western blot with anti-Thiophosphate ester antibody. GST-DPF3b and GST-NEP were used as the negative and positive control, respectively. Immunoblotting against GST demonstrates that a similar amount of protein was used for each condition. (**C**) The CK2 specific inhibitor, tetrabromocinnamic acid (TBCA), was used in the kinase assay and effectively reduced DPF3 phosphorylation. (**D**) Sequence conservation of DPF3a peptides surrounding the identified phosphorylation sites in human, mouse, rat and chicken. (**E**) GST-DPF3a WT, S348A mutant or 5xAla mutant were *in vitro* phosphorylated by CK2 before blotting. (**F**) GST-DPF3a was phosphorylated by CK2 and detected using the anti-pDPF3a antibody in immunoblotting. (**G**) Knockdown of Ck2α in C2C12 cells using siRNA. Expression of *Ck2α* and *Dpf3a* after Ck2α siRNA knockdown was analyzed by qPCR. (**H**) The protein level of Ck2α and pDPF3a was was analyzed by immunoblotting in Ck2α knockdown situation. (**I**) Immunofluorescence analysis of pDPF3a in Ck2α knockdown situation in C2C12 cells. C2C12 cells were transfected with Ck2α siRNA for 48 h. The cells were then fixed with methanol and stained with antibody against pDPF3a (red) and antibody against Tubulin (green). Scale bar, 20 μm.

ited sequence-specific binding to dsDNA (data not shown). However, previously we found several hundred sites of indirect DNA binding using ChIP-chip. For DPF3b, we could show that this binding is mediated by specific histone marks (20). Focusing on pDPF3a, we now identified approximately 800 binding sites in ChIP-seq experiments using undifferentiated and differentiated C2C12 cells (data not shown). Using a pattern matching approach, we found that the E-box motif, which represents the favored binding motif of basic helix-loop-helix (bHLH) transcription factors, is highly enriched in pDPF3a target sites (Supplementary Table S6).

bHLH transcription factors, such as HAND1/2, MYOD1, HES1 and HEY1/2, are important for embryonic development with respect to cardiac and muscle development. In order to study the interaction of DPF3a with these bHLH transcription factors (MYOD1, HAND1, HES1 and HEY1), we performed CoIP analysis with lysates of transiently transfected HEK293 cells. We observed a specific interaction between DPF3a and HEY1, the hairy and enhancer of split-related family of bHLH-type transcriptional repressors (Figure 4A). HEY genes redundantly function during mouse embryonic cardiovascular development, neurogenesis and somitogenesis (36), and thus match the expression and proposed function of DPF3a. Finally, we found that all proteins of the HEY family, namely HEY1, HEY2 and HEYL, specifically interact with DPF3a (Supplementary Figure S6A). In the following study, we exclusively focus on HEY1 as an example to analyze the function of DPF3a-HEY interactions.

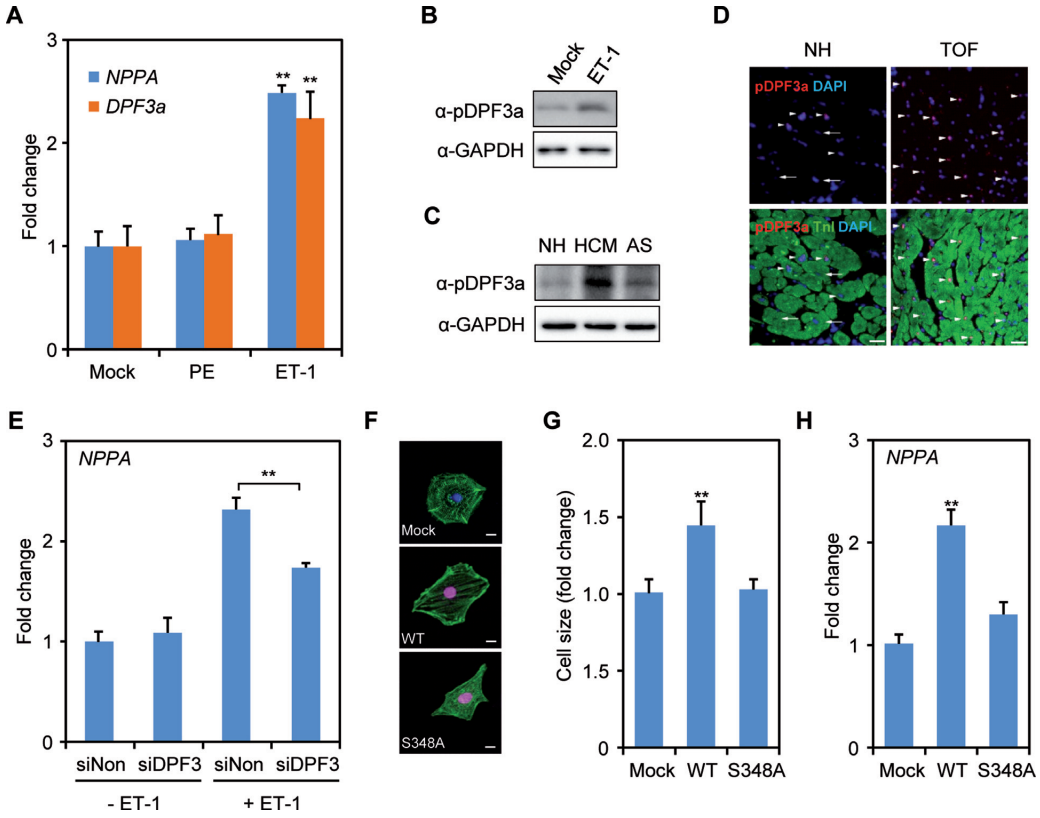

Figure 3. DPF3a S348 phosphorylation is important for cardiac hypertrophy. (**A**) *NPPA* and *DPF3a* mRNA expression was analyzed in human-induced pluripotent stem cell-derived cardiomyocytes (hiPSC-CMs) after phenylephrine (PE) or endothelin 1 (ET-1) treatment for 24 h. (**B**) Immunoblotting analysis of the pDPF3a protein level with anti-pDPF3a antibody in ET-1 induced hypertrophic hiPSC-CMs. (**C**) The protein level of pDPF3a was analyzed in the hearts of patients with hypertrophic cardiomyopathy (HCM) and aortic stenosis (AS). (**D**) Immunofluorescence of paraffin-embedded right ventricular biopsies of normal hearts (NH) and Tetralogy of Fallot (TOF) individuals. Red: pDPF3a; green: Troponin I (TnI); arrow: pDPF3a positive cardiomyocytes; arrow with tail: pDPF3a negative cardiomyocytes. Scale bar, 25 μm. (**E**) siRNA knockdown of DPF3 followed by ET-1 treatment in hiPCS-CMs. Expression of *NPPA* after DPF3 siRNA knockdown and ET-1 treatment was analyzed by qPCR. (**F**) Mouse primary cardiomyocytes were transfected with either Flag-tagged DPF3a WT or S348A constructs. Cells were then stained with antibody against Flag (red), and antibody against Actinin (green). Scale bar, 10 μm. (**G**) The surface areas of transfected cells were measured using ImageJ ($n = 20$, $^{**}P < 0.01$, *t*-test). (**H**) The mRNA expression of the hypertrophic marker Nppa *was analyzed* by qPCR in the transfected mouse primary cardiomyocytes.

We further identified common targets of Dpf3a and Hey1 using ChIP-qPCR experiments in C2C12 cells (Supplementary Figure S7A), in which *Hey1* is highly expressed in contrast to almost no expression of *Hey2* and *Heyl* (Supplementary Figure S7B). These results indicate that Dpf3a might indirectly bind DNA via its interaction with the DNA-binding transcriptional repressor Hey1 in C2C12 cells. To confirm this hypothesis, we performed siRNA knockdown of *Hey1* in C2C12 cells, which resulted in a notable reduction of Hey1 expression on mRNA and protein level (Figure 4B). Inhibition of *Hey1* did not cause expression alterations of *Hey2* or *Heyl* (Supplementary Figure S6B). We checked Dpf3a binding in the Hey1 knockdown situation and found a striking reduction of Dpf3a enrichment at selected targets (Figure 4, C and D). In line with this, we also analyzed Hey1 enrichment at these targets in a Dpf3a knockdown (Supplementary Figure S7C) situation in C2C12 cells and observed no significant changes of Hey1-DNA binding (Supplementary Figure S7D and E). These results underline that Hey1 indeed serves as a linker between Dpf3a and DNA.

Since posttranslational modifications like phosphorylation can modulate the nature and strength of protein–protein interactions, we aimed to elucidate the protein domain of DPF3a required for the interaction with HEY1 and investigated whether this interaction depends on the phosphorylation state of DPF3a. We assumed that the DPF3a-HEY1 interaction is mediated by the DPF3a specific half PHD and/or C-terminus, as we did not observe an interaction between DPF3b and HEY1 (Supplementary Figure S6, B and C). Using CoIP analysis, we found that lacking the half PHD finger prevents the interaction of DPF3a with HEY1, confirming this hypothesis (Figure 4E).

Furthermore, we analyzed whether DPF3a phosphorylation affects its interaction with HEY1. We performed CoIP analysis of HEY1 with DPF3a followed by *in vitro* de-phosphorylation of the CoIP pellet using FastAP alkaline phosphatase. Immunoblotting analysis showed that dephosphorylation of the DPF3a-HEY1 complex abolished their interaction (Figure 4F). Finally, we co-transfected HA-tagged HEY1 with Flag-tagged WT DPF3a, S348A or 5xAla mutant into HEK293 cells. Similar expression of WT,

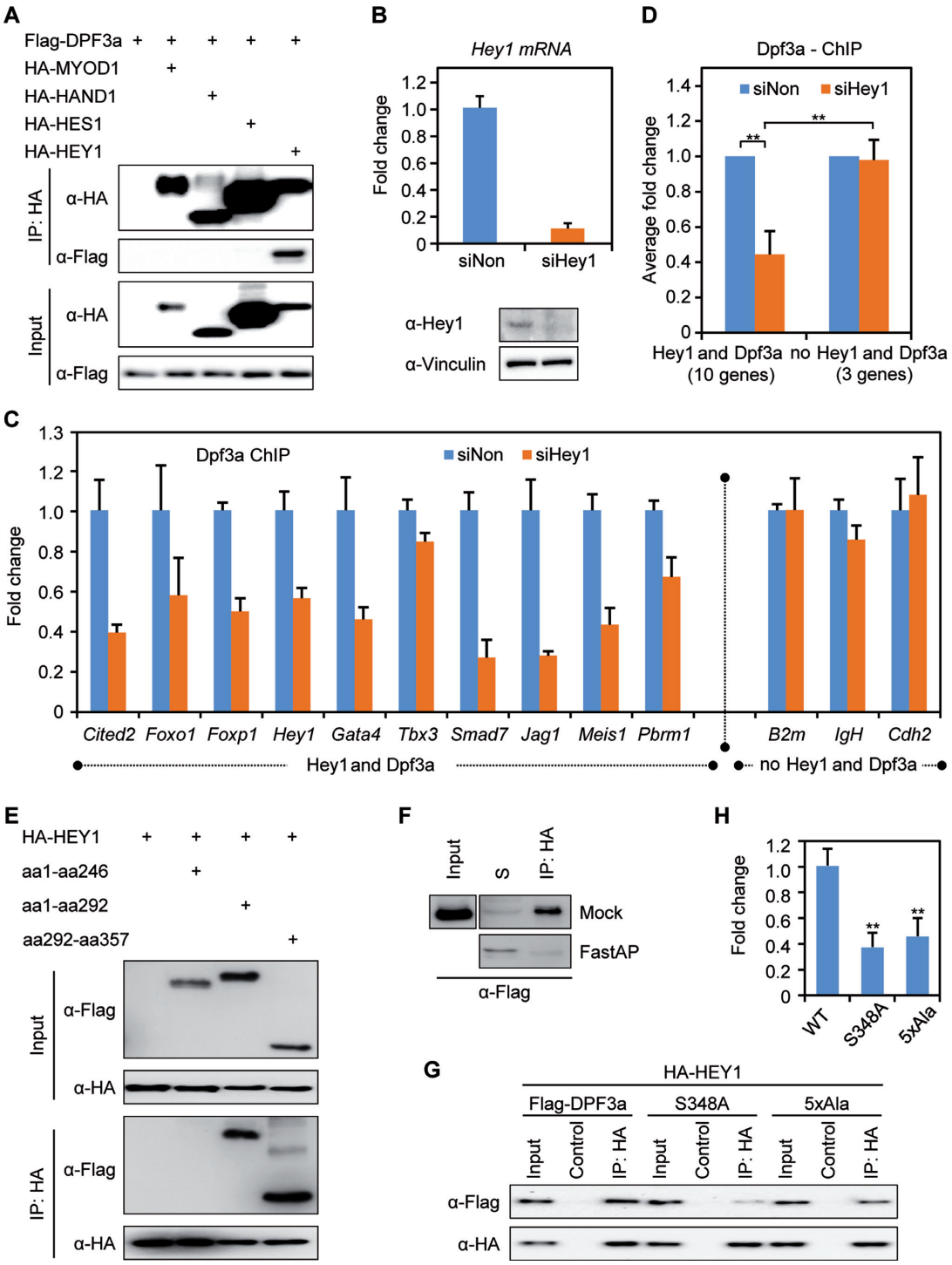

Figure 4. HEY protein links DPF3a to DNA. (**A**) DPF3a specifically interacts with HEY1. HEK293 cells were transiently transfected with Flag-tagged DPF3a and with HA-tagged MYOD1, HAND1, HES1 or HEY1. Cell lysates were incubated with an anti-HA matrix or anti-Flag matrix to pull down HA-tagged or Flag-tagged protein together with interacting proteins, which were further probed with anti-Flag or anti-HA antibody in immunoblots. (**B**) C2C12 cells were transfected with Hey1 siRNA for 48 h and knockdown efficiency of *Hey1* in C2C12 cells was analyzed by qPCR and immunoblotting. (**C** and **D**) Dpf3a ChIP experiments were performed and Dpf3a enrichment at selected promoters in siHey1 knockdown was compared to siNon control. Binding of Dpf3a was quantified by qPCR (triplicate experiments, $^{**}P < 0.01$, *t*-test). (**E**) The interaction of DPF3a and HEY1 is mediated via the half PHD finger. Co-immunoprecipitation (CoIP) of HA-tagged HEY1 with different Flag-tagged DPF3a constructs (WT, aa1–246, aa1–292 and aa292–357) from lysates of transiently transfected HEK293 cells. (**F**) CoIP of Flag-tagged DPF3a and HA-tagged HEY1 followed by de-phosphorylation assay using FastAP Alkaline phosphatase. S: supernatant. (**G**) Phosphorylation of serine 348 of DPF3a is critical for the interaction with HEY1. CoIP of HA-tagged HEY1 with Flag-tagged DPF3a mutants (WT, S348A, 5xAla). (**H**) Quantification of the DPF3a and HEY1 interaction using Image Lab 5.0 (triplicate experiments, $^{**}P < 0.01$, *t*-test).

S348A and 5xAla DPF3a protein levels were detected (Figure 4G, lane 1, 4, 7). We found that WT DPF3a efficiently interacted with HEY1 (Figure 4G, lane 3), but the S348A and 5xAla mutants showed a strikingly decreased interaction (Figure 4G, lane 6, 9, Figure 4H). These results suggest that the S348 phosphorylation is critical for the DPF3a-HEY1 interaction mediated by the half PHD finger.

DPF3a recruits BRG1 to genomic targets

Previous work has shown that both DPF3a and DPF3b are in a complex with the BAF chromatin remodeling complex and interact with other BAF components like BRG1 and BAF60c (20,37). To determine whether HEY1 interacts with any other BAF components or whether its interaction with DPF3a is independent of the BAF complex, we performed CoIP assays. We did not find any interaction between HEY1 and BRG1 or BAF60c (Figure 5A, lane 2, 4). However, HEY1, DPF3a and BRG1 formed a complex in the CoIP assay (Figure 5A, lane 3). Thus, our results suggest that HEY1 is associated with the BAF complex via DPF3a and the interaction between DPF3a and HEY1 is independent of the BAF complex.

To confirm this hypothesis, we performed ChIP-qPCR in order to identify common Brg1-Dpf3a-Hey1 targets in WT C2C12 and after Hey1 knockdown and found a complementary reduction of Brg1 binding to Dpf3a-Hey1 target sites (Figure 5, B and C). Moreover, we observed a reduction of Brg1 binding at respective targets sites in the Dpf3a knockdown condition (Figure 5, D and E). Taken together, these results indicate that the Dpf3a-Hey1 complex directs the BAF chromatin remodeling complex to specific genomic target sites.

DPF3a releases HEY from the genomic targets

To examine the role of DPF3a in transcriptional activation, HEK293 cells were co-transfected with an expression vector encoding DPF3 protein fragments fused to the GAL4 binding domain and a reporter vector containing the GAL4 promoter linked to the firefly luciferase gene. Only DPF3a, but not DPF3b, showed transactivation activity, which is transmitted by the DPF3a specific C-terminus (aa291–357) (Figure 6A). This underlines a role of DPF3a in the transcriptional activation.

Previous studies showed that HEY proteins function as direct transcriptional repressors and a number of HEY target genes involved in cardiac hypertrophy have been identified previously (38–41). In our reporter gene assays, HEY1 significantly repressed the promoter activity of its target genes like *NPPA*, *GATA4*, *HEY1* and *JAG1* (Figure 6B). DPF3a alone had no impact on the promoter activity of these target genes. Subsequently, co-transfection of reporter constructs with HEY1 and DPF3a expression vectors revealed no suppression of transcriptional activities of these targets. DPF3a notably reduced the repression of HEY1 targets (Figure 6B), suggesting that DPF3a might release HEY1 from DNA via a protein–protein interaction. In addition to this, mutation of the HEY1 binding E-box element (gggCACGGGtca to gggCAtca) in the *JAG1* promoter abolished the repression by HEY1.

Furthermore, we analyzed the expression of *HEY1* and *HEY2* genes in hypertrophic hearts of patients with AS and HCM, in which *DPF3a* was found to be up-regulated. We did not observe any obvious alteration of the expression of the HEY genes (Supplementary Figure S8). However, DPF3a-HEY1 targets, including the hypertrophic marker *NPPA* as well as *FOXO1* (forkhead box O1), *GATA4* (GATA binding protein 4), *TBX3* (T-box 3) and *SMAD7* (SMAD family member 7), were found to be significantly up-regulated (Figure 6C).

Model of the CK2-DPF3a-HEY-BRG1 pathway

Finally, we developed a model summarizing our findings (Figure 7). Upon hypertrophic stimuli, the protein kinase CK2 phosphorylates DPF3a at the highly conserved amino acid S348 at its C-terminus. pDPF3a binds and releases the transcriptional repressors HEY and recruits BRG1 to respective targets. Consequently, DPF3a initiates transcription of fetal genes and promotes pathological cardiac hypertrophy.

DISCUSSION

We present a novel pathway driving pathological cardiac hypertrophy in response to hypertrophic stimuli. This pathway is triggered by kinase activation leading to phosphorylation of a BAF chromatin remodeling factor and consequently triggering the release of DNA-binding transcriptional repressors. In the past, reports have demonstrated the impact of individual components, namely CK2, BRG1 and HEY, involved in the process of cardiac hypertrophy. However, their connection through the chromatin remodeler DPF3a had not yet been elucidated.

The SWI/SNF chromatin remodeling complexes are recruited to numerous genomic target sites by sequence-specific transcription factors and histone-binding epigenetic regulators (42). Each SWI/SNF complex utilizes either BRG1 or BRM as alternative subunits with DNA-dependent ATPase activity. The non-catalytic subunits of SWI/SNF are often referred to as BAFs (BRG1 or BRM associated factors). With respect to cardiac diseases, several BAFs (BAF60c, BAF45c2/DPF3b) have been identified to play a role in the development of congenital structural heart diseases. BAF60c mediates its function by the interaction with DNA-binding transcription factors such as TBX5, GATA4, MYOD or SIX4, which are essential for cardiac and muscle development (16,18,43). Another mode of functional transition is the binding to specific histone modifications, as in case of DPF3b (20). Either way, these BAFs promote gene transcription through their association with BRG1, which is highly expressed in the developing heart. In contrast, in the adult heart BRM represents the prominent catalytic unit; however, upon hypertrophic stimuli cardiomyocytes switch to a fetal-like state and BRG1 is reactivated as the catalytic unit (14,44). It had been shown that BRG1 is up-regulated in patients with hypertrophic cardiomyopathy and, moreover, forms a complex with PARPs and several HDACs to induce the fetal gene program in transverse aortic constriction-banded mice (14). In line with this, Brg1 null mice show significantly reduced hypertrophic response upon TAC-binding compared

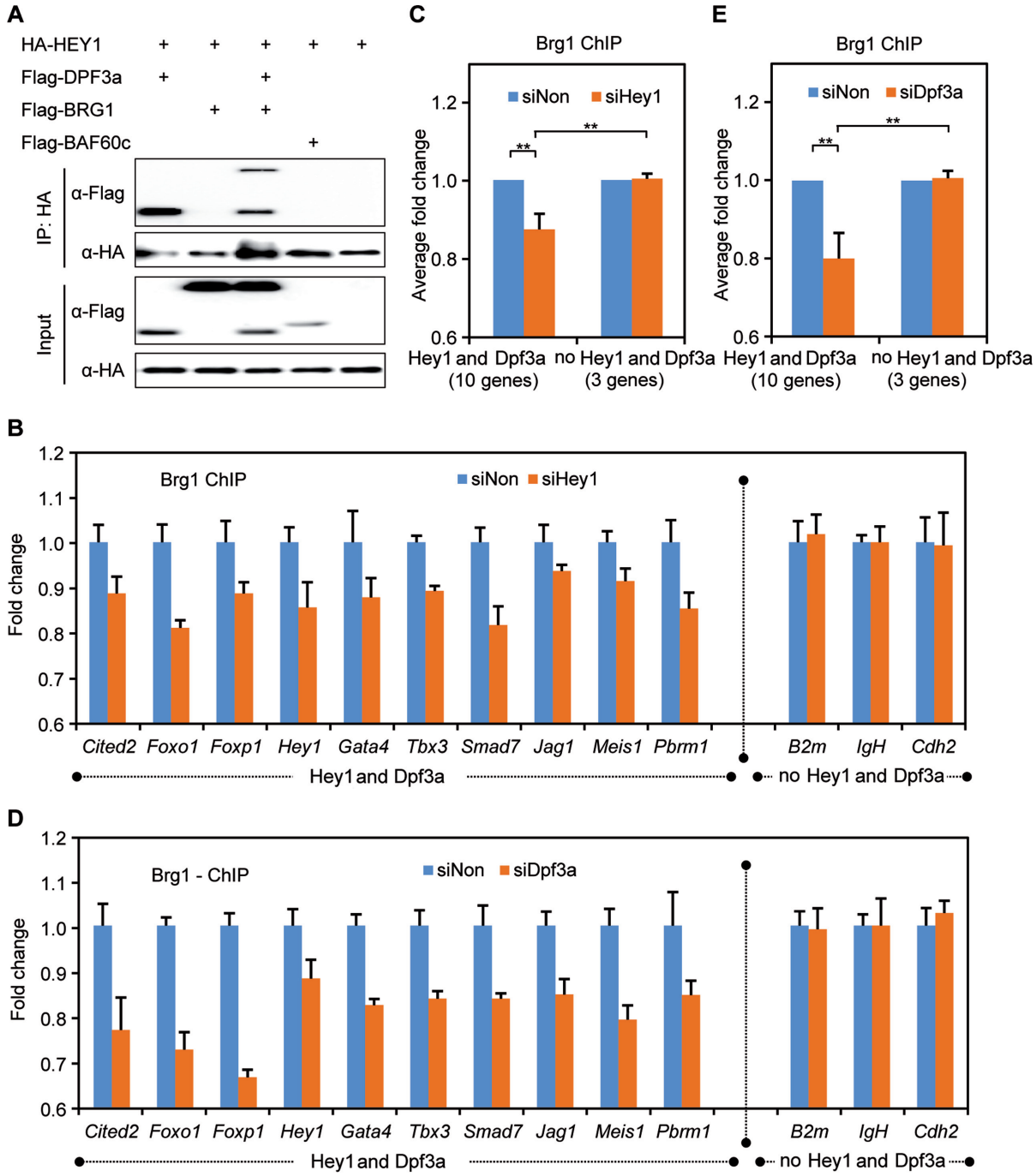

Figure 5. DPF3a recruits BRG1 to DNA via interaction with HEY. (**A**) HEY1 specifically interacts with DPF3a and associates with the BAF complex via this interaction. CoIP of HA-tagged HEY1 with Flag-tagged DPF3a, BAF60c and BRG1 constructs from lysates of transiently transfected HEK293 cells. (**B** and **C**) Brg1 ChIP experiments were performed and Brg1 enrichment at selected promoters in siHey1 knockdown was compared to siNon control. Binding of Brg1 was quantified by qPCR (triplicate experiments, $^{**}P < 0.01$, *t*-test). (**D** and E) Brg1 enrichment at selected promoters in siHey1 knockdown was compared to siNon control. Binding of Brg1 was quantified by ChIP and real-time PCR (triplicate experiments, $^{**}P < 0.01$, *t*-test).

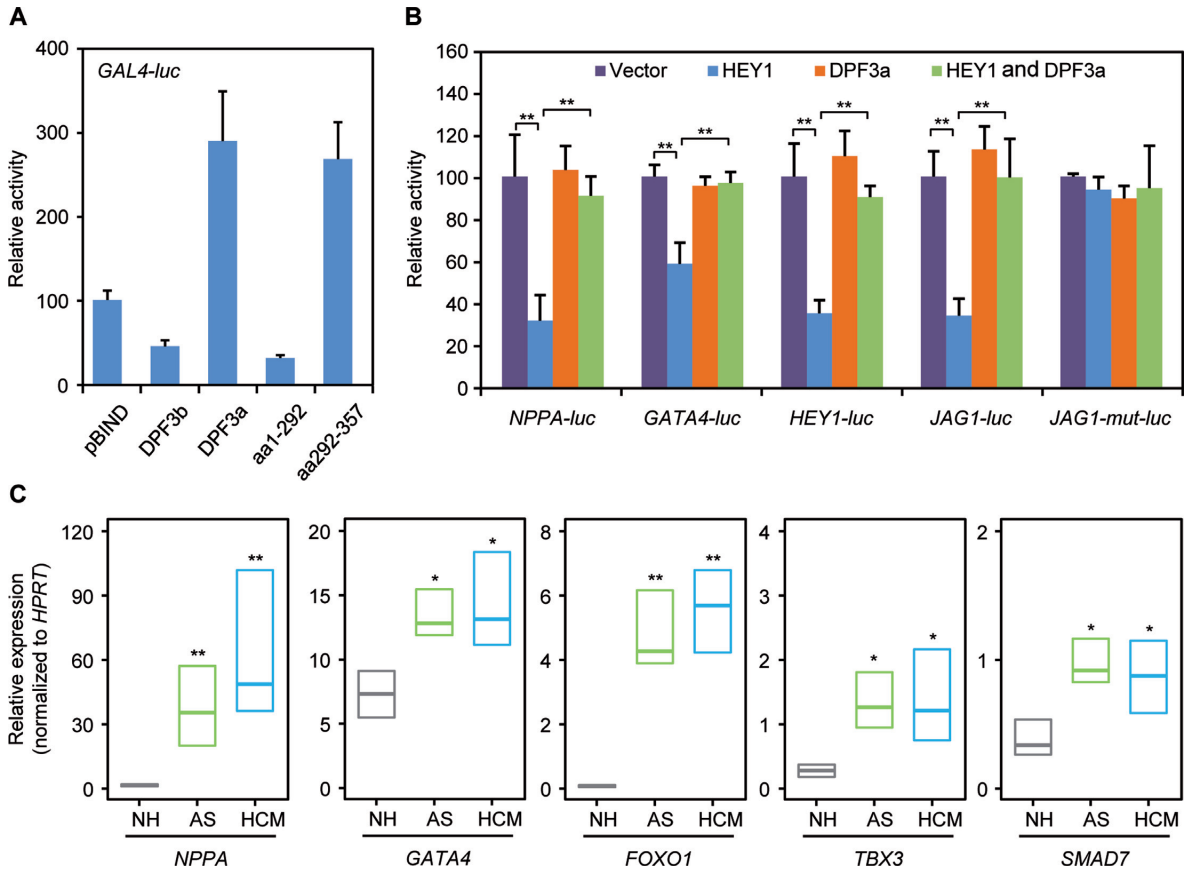

Figure 6. DPF3a releases HEY from the targets. (**A**) GAL4 trans-activation assays. HEK293 cells were co-transfected with an expression vector encoding DPF3 protein fragments fused to the GAL4 binding domain and a reporter vector containing the GAL4 promoter linked to the firefly luciferase gene. Luciferase activity was normalized to renilla luciferase activity. One representative experiment performed in triplicates is shown. (**B**) DPF3a significantly reduces HEY1 mediated repression. HEK293 cells were transiently transfected with *NPPA*, *GATA4*, *HEY1*, *JAG1* and *JAG1-mut* reporter constructs in the presence of empty control vector alone, *HEY1* expression vector, *DPF3a* expression vector or *HEY1* and *DPF3a* in combination. The results represent the average of three independent experiments (**$P < 0.01$, *t*-test). (**C**) Expression analysis of *FOXO1*, *GATA4*, *TBX3* and *SMAD7* in AS, HCM and NH using qPCR. Results represent median expression levels with 25% and 75% quartiles. Statistically significant differences were analyzed using a two-sided Student *t*-test (*$P < 0.05$, **$P < 0.01$).

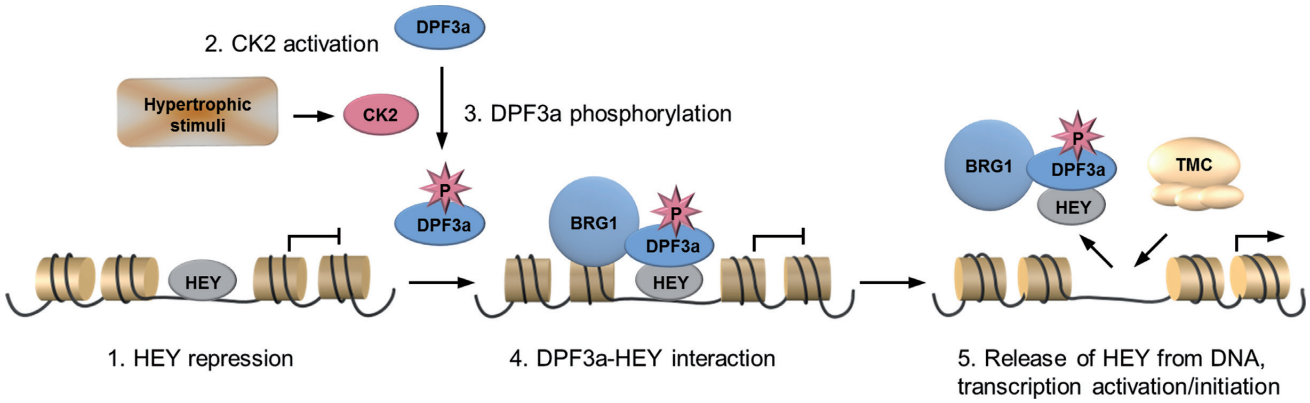

Figure 7. Illustration of pDPF3a mediated regulation of HEY-target genes. Hypertrophic signals stimulate CK2, which phosphorylates DPF3a at S348. Phosphorylation of DPF3a enhances its ability to bind the transcription repressors HEY. Subsequently, DPF3a releases HEY from the genomic targets and the transcription is then activated by the transcriptional machinery complex (TMC).

to WT mice (14). However, it was unclear how BRG1 is targeted to genes of the fetal gene program in this setting. Our data suggest that DPF3a functions as the mediator to direct BRG1 to fetal genes that are repressed by HEY proteins in a WT adult stage but are re-expressed upon hypertrophic stimuli. Moreover, we show that the binding of DPF3a to HEY proteins is significantly enhanced by phosphorylation of S348, located in an evolutionary conserved and DPF3a-specific C-terminal domain. The phosphorylation level of DPF3a is significantly higher in hypertrophic states (e.g. ET-1 treated hiPSC-CMs or hypertrophic TOF hearts). This phosphorylation of DPF3a is mediated by CK2. Previously it had been shown that signaling of hypertrophic stimuli (e.g. PE) can be mediated by CK2, involving its two catalytic subunits CK2α and CK2α'. CK2α was shown to phosphorylate and thereby activate HDAC2, which results in the repression of anti-hypertrophic genes (9). CK2α' was shown to induce cardiac hypertrophy via interacting with the anti-hypertrophic cell cycle regulator p27 (7). Insights into the down-stream mediators, namely chromatin or transcription factors, and a potential role of DPF3a await elucidation.

In general, protein phosphorylation is a key event in regulating protein localization, activity and protein–protein interactions (45,46). We found that pDPF3a is predominately located in the nucleus. It had previously been shown that CK2α translocates from the cytoplasm to the nucleus (9), where it is suggested to phosphorylate DPF3a. However, this needs further investigation, as a non-pDPF3a specific antibody is currently lacking. Moreover, the conformational change of DPF3a upon phosphorylation awaits further analysis. Frequently, phosphorylation occurs within an interaction domain and thereby directly affects the binding energy (45). However, the interaction of DPF3a with HEY proteins is mediated by its half PHD finger, whereas S348 phosphorylation is located in the structurally unsolved neighboring C-terminus. It is very likely that a conformational change through allosteric mechanisms affects the DPF3a-HEY interaction.

In patients with pathological cardiac hypertrophy suffering from aortic stenosis or hypertrophic cardiomyopathy, we observed a significant up-regulation of common DPF3a and HEY targets, such as *GATA4*, *FOXO1*, *SMAD7* and *TBX3*. These genes play well-known roles in cardiac development and disease (47–50). For instance, GATA4 regulates cardiac fetal genes (51) and stress-induced cardiac hypertrophy *in vivo* (52). Activation of FOXO1 is an important mediator of cardiac hypertrophy (53).

In the future, it will be of interest to study the development of pathological hypertrophy in a respective mouse model. So far, we have generated a $Dpf3^{tm1sper}$ knockout mouse, which is viable and fertile (data not shown), and can undergo TAC-banding in order to study its hypertrophic response. In this study, we observed that knockdown of DPF3 buffered the ET-1 induced hypertrophy in hiPSC-CMs. It might be that a reduction of hypertrophy in the knockout compared to the WT mouse will be observed. An essential aspect for these experiments is that, within the D4 protein family, the protein domains of Dpf3a involved in the novel pathway described here are unique for Dpf3a. In contrast, all Dpf3b domains are highly conserved within the D4 family, consisting of neural expressed Dpf1 and ubiquitously expressed Dpf2. Thus, other D4 family members most likely balance the physiological role of Dpf3 during development.

A number of HEY mouse models have been established (40,54). Interestingly, *HEY2* knockout mice on a mixed genetic background develop cardiomyopathy with cardiac hypertrophy (55). Moreover, overexpression of *HEY2* in the myocardium prevents PE-induced cardiac hypertrophy *in vivo* and *in vitro* (56). The anti-hypertrophic function of HEY2 is most likely mediated by the inhibition of fetal genes like *Nppa* and *Gata4*. Our model suggests that DPF3a induces pathological cardiac hypertrophy by the release of HEY from these genes. It had been shown that members of the HEY protein family (HEY1, HEY2, HEYL) share genomic targets and perform similar functions (41). Moreover, we show that all three HEY proteins physically bind to DPF3a. Thus, DPF3a can be considered as a cofactor of HEY proteins in order to regulate cardiac gene expression.

Taken together, we provide evidence for a novel pathway involved in the development of pathological cardiac hypertrophy. The latter can occur primarily in cases of hypertrophic cardiomyopathy or Tetralogy of Fallot or secondary, due to pressure overload like in cases of aortic stenosis or hypertension. Pathological cardiac hypertrophy leads to remodeling of the ventricular chambers and eventually heart failure. Thus, pharmacological inhibition of hypertrophic cardiomyocyte growth has been a long-term therapeutic goal for the treatment of heart failure. Future studies are needed to explore the potential of the pathway presented to be targeted for pharmaceutical interventions.

SUPPLEMENTARY DATA

Supplementary Data are available at NAR Online.

ACKNOWLEDGEMENT

We are deeply grateful to the patients and their families for their cooperation. We thank Dr Manfred Gessler for providing the reporter vectors, Dr Jochen Walter for the Nep construct, Dr Sebastian Diecke for the control hiPSCs and Dr David Allis for useful comments on DPF3. We also thank Andreas Perrot for cardiac sample contribution, Vikas Bansal and Dr Marcel Grunert for bioinformatics support, Uwe Eising for assistance in graphic assistant, and the confocal microscopy team at the Max-Delbrück-Center for Molecular Medicine for helpful assistance and discussions. We further thank Dr Cornelia Dorn and Dr Marcel Grunert for discussion and review of the manuscript.

FUNDING

Deutsch Forschungsgemeinschaft [DFG 85421021 to S.R.S.]; European Community's Seventh Framework Programme ['CardioNet' People-2011-ITN-289600 to S.R.S.]; German Research Foundation [Heisenberg professorship 574157 to S.R.S.]; German Ministry for Research and Education [BMBF, 0315082, 01EA1303 to S.S]; REBIRTH cluster of excellence to (T.H. and S.A.S.); Berlin Institute of Health (BIH-CRG2-ConDi); PhD scholarship of the China Scholarship Council (to H.C.) and Research grant from European Society of Cardiology (to E.C.).

Conflict of interest statement. None declared.

REFERENCES

1. Lips,D.J., deWindt,L.J., van Kraaij,D.J. and Doevendans,P.A. (2003) Molecular determinants of myocardial hypertrophy and failure: alternative pathways for beneficial and maladaptive hypertrophy. *Eur. Heart J.*, **24**, 883–896.
2. Levy,D., Garrison,R.J., Savage,D.D., Kannel,W.B. and Castelli,W.P. (1990) Prognostic implications of echocardiographically determined left ventricular mass in the Framingham Heart Study. *N. Engl. J. Med.*, **322**, 1561–1566.
3. Barry,S.P., Davidson,S.M. and Townsend,P.A. (2008) Molecular regulation of cardiac hypertrophy. *Int. J. Biochem. Cell Biol.*, **40**, 2023–2039.
4. Bernardo,B.C., Weeks,K.L., Pretorius,L. and McMullen,J.R. (2010) Molecular distinction between physiological and pathological cardiac hypertrophy: experimental findings and therapeutic strategies. *Pharmacol. Ther.*, **128**, 191–227.
5. Frey,N., Katus,H.A., Olson,E.N. and Hill,J.A. (2004) Hypertrophy of the heart: a new therapeutic target? *Circulation*, **109**, 1580–1589.
6. Litchfield,D.W. (2003) Protein kinase CK2: structure, regulation and role in cellular decisions of life and death. *Biochem. J.*, **369**, 1–15.
7. Hauck,L., Harms,C., An,J., Rohne,J., Gertz,K., Dietz,R., Endres,M. and von Harsdorf,R. (2008) Protein kinase CK2 links extracellular growth factor signaling with the control of p27(Kip1) stability in the heart. *Nat. Med.*, **14**, 315–324.
8. Seldin,D.C., Lou,D.Y., Toselli,P., Landesman-Bollag,E. and Dominguez,I. (2008) Gene targeting of CK2 catalytic subunits. *Mol. Cell. Biochem.*, **316**, 141–147.
9. Eom,G.H., Cho,Y.K., Ko,J.H., Shin,S., Choe,N., Kim,Y., Joung,H., Kim,H.S., Nam,K.I., Kee,H.J. *et al.* (2011) Casein kinase-2alpha1 induces hypertrophic response by phosphorylation of histone deacetylase 2 S394 and its activation in the heart. *Circulation*, **123**, 2392–2403.
10. Akazawa,H. and Komuro,I. (2003) Roles of cardiac transcription factors in cardiac hypertrophy. *Circ. Res.*, **92**, 1079–1088.
11. Bruneau,B.G. (2010) Chromatin remodeling in heart development. *Curr. Opin. Genet. Dev.*, **20**, 505–511.
12. Mathiyalagan,P., Keating,S.T., Du,X.J. and El-Osta,A. (2014) Chromatin modifications remodel cardiac gene expression. *Cardiovasc. Res.*, **103**, 7–16.
13. Ho,L. and Crabtree,G.R. (2010) Chromatin remodelling during development. *Nature*, **463**, 474–484.
14. Hang,C.T., Yang,J., Han,P., Cheng,H.L., Shang,C., Ashley,E., Zhou,B. and Chang,C.P. (2010) Chromatin regulation by Brg1 underlies heart muscle development and disease. *Nature*, **466**, 62–67.
15. Han,P., Li,W., Lin,C.H., Yang,J., Shang,C., Nurnberg,S.T., Jin,K.K., Xu,W., Lin,C.Y., Lin,C.J. *et al.* (2014) A long noncoding RNA protects the heart from pathological hypertrophy. *Nature*, **514**, 102–106.
16. Lickert,H., Takeuchi,J.K., Von Both,I., Walls,J.R., McAuliffe,F., Adamson,S.L., Henkelman,R.M., Wrana,J.L., Rossant,J. and Bruneau,B.G. (2004) Baf60c is essential for function of BAF chromatin remodelling complexes in heart development. *Nature*, **432**, 107–112.
17. Simone,C., Forcales,S.V., Hill,D.A., Imbalzano,A.N., Latella,L. and Puri,P.L. (2004) p38 pathway targets SWI-SNF chromatin-remodeling complex to muscle-specific loci. *Nat. Genet.*, **36**, 738–743.
18. Forcales,S.V., Albini,S., Giordani,L., Malecova,B., Cignolo,L., Chernov,A., Coutinho,P., Saccone,V., Consalvi,S., Williams,R. *et al.* (2012) Signal-dependent incorporation of MyoD-BAF60c into Brg1-based SWI/SNF chromatin-remodelling complex. *EMBO J.*, **31**, 301–316.
19. Kaynak,B., von Heydebreck,A., Mebus,S., Seelow,D., Hennig,S., Vogel,J., Sperling,H.P., Pregla,R., Alexi-Meskishvili,V., Hetzer,R. *et al.* (2003) Genome-wide array analysis of normal and malformed human hearts. *Circulation*, **107**, 2467–2474.
20. Lange,M., Kaynak,B., Forster,U.B., Tonjes,M., Fischer,J.J., Grimm,C., Schlesinger,J., Just,S., Dunkel,I., Krueger,T. *et al.* (2008) Regulation of muscle development by DPF3, a novel histone acetylation and methylation reader of the BAF chromatin remodeling complex. *Genes Dev.*, **22**, 2370–2384.
21. Zeng,L., Zhang,Q., Li,S., Plotnikov,A.N., Walsh,M.J. and Zhou,M.M. (2010) Mechanism and regulation of acetylated histone binding by the tandem PHD finger of DPF3b. *Nature*, **466**, 258–262.
22. Grunert,M., Dorn,C., Schueler,M., Dunkel,I., Schlesinger,J., Mebus,S., Alexi-Meskishvili,V., Perrot,A., Wassilew,K., Timmermann,B. *et al.* (2014) Rare and private variations in neural crest, apoptosis and sarcomere genes define the polygenic background of isolated Tetralogy of Fallot. *Hum. Mol. Genet.*, **23**, 3115–3128.
23. Lian,X., Hsiao,C., Wilson,G., Zhu,K., Hazeltine,L.B., Azarin,S.M., Raval,K.K., Zhang,J., Kamp,T.J. and Palecek,S.P. (2012) Robust cardiomyocyte differentiation from human pluripotent stem cells via temporal modulation of canonical Wnt signaling. *Proc. Natl. Acad. Sci. U.S.A.*, **109**, E1848–E1857.
24. Lian,X., Zhang,J., Azarin,S.M., Zhu,K., Hazeltine,L.B., Bao,X., Hsiao,C., Kamp,T.J. and Palecek,S.P. (2013) Directed cardiomyocyte differentiation from human pluripotent stem cells by modulating Wnt/beta-catenin signaling under fully defined conditions. *Nat. Protoc.*, **8**, 162–175.
25. Burridge,P.W., Matsa,E., Shukla,P., Lin,Z.C., Churko,J.M., Ebert,A.D., Lan,F., Diecke,S., Huber,B., Mordwinkin,N.M. *et al.* (2014) Chemically defined generation of human cardiomyocytes. *Nat. Methods*, **11**, 855–860.
26. Tohyama,S., Hattori,F., Sano,M., Hishiki,T., Nagahata,Y., Matsuura,T., Hashimoto,H., Suzuki,T., Yamashita,H., Satoh,Y. *et al.* (2013) Distinct metabolic flow enables large-scale purification of mouse and human pluripotent stem cell-derived cardiomyocytes. *Cell Stem Cell*, **12**, 127–137.
27. McWilliam,H., Li,W., Uludag,M., Squizzato,S., Park,Y.M., Buso,N., Cowley,A.P. and Lopez,R. (2013) Analysis Tool Web Services from the EMBL-EBI. *Nucleic Acids Res.*, **41**, W597–W600.
28. Blom,N., Gammeltoft,S. and Brunak,S. (1999) Sequence and structure-based prediction of eukaryotic protein phosphorylation sites. *J. Mol. Biol.*, **294**, 1351–1362.
29. Wong,Y.H., Lee,T.Y., Liang,H.K., Huang,C.M., Wang,T.Y., Yang,Y.H., Chu,C.H., Huang,H.D., Ko,M.T. and Hwang,J.K. (2007) KinasePhos 2.0: a web server for identifying protein kinase-specific phosphorylation sites based on sequences and coupling patterns. *Nucleic Acids Res.*, **35**, W588–W594.
30. Freiwald,A., Weidner,C., Witzke,A., Huang,S.Y., Meierhofer,D. and Sauer,S. (2013) Comprehensive proteomic data sets for studying adipocyte-macrophage cell-cell communication. *Proteomics*, **13**, 3424–3428.
31. Meierhofer,D., Weidner,C., Hartmann,L., Mayr,J.A., Han,C.T., Schroeder,F.C. and Sauer,S. (2013) Protein sets define disease states and predict in vivo effects of drug treatment. *Mol. Cell. Proteomics*, **12**, 1965–1979.
32. Allen,J.J., Li,M., Brinkworth,C.S., Paulson,J.L., Wang,D., Hubner,A., Chou,W.H., Davis,R.J., Burlingame,A.L., Messing,R.O. *et al.* (2007) A semisynthetic epitope for kinase substrates. *Nat. Methods*, **4**, 511–516.
33. Siepmann,M., Kumar,S., Mayer,G. and Walter,J. (2010) Casein kinase 2 dependent phosphorylation of neprilysin regulates receptor tyrosine kinase signaling to Akt. *PLoS One*, **5**, e13134.
34. Foldes,G., Matsa,E., Kriston-Vizi,J., Leja,T., Amisten,S., Kolker,L., Kodagoda,T., Dolatshad,N.F., Mioulane,M., Vauchez,K. *et al.* (2014) Aberrant alpha-adrenergic hypertrophic response in cardiomyocytes from human induced pluripotent cells. *Stem Cell Rep.*, **3**, 905–914.
35. Berger,M.F., Philippakis,A.A., Qureshi,A.M., He,F.S., Estep,P.W. 3rd and Bulyk,M.L. (2006) Compact, universal DNA microarrays to comprehensively determine transcription-factor binding site specificities. *Nat. Biotechnol.*, **24**, 1429–1435.
36. Weber,D., Wiese,C. and Gessler,M. (2014) Hey bHLH Transcription Factors. *Curr. Top. Dev. Biol.*, **110**, 285–315.
37. Ishizaka,A., Mizutani,T., Kobayashi,K., Tando,T., Sakurai,K., Fujiwara,T. and Iba,H. (2012) Double plant homeodomain (PHD) finger proteins DPF3a and -3b are required as transcriptional co-activators in SWI/SNF complex-dependent activation of NF-kappaB RelA/p50 heterodimer. *J. Biol. Chem.*, **287**, 11924–11933.
38. Kathiriya,I.S., King,I.N., Murakami,M., Nakagawa,M., Astle,J.M., Gardner,K.A., Gerard,R.D., Olson,E.N., Srivastava,D. and Nakagawa,O. (2004) Hairy-related transcription factors inhibit GATA-dependent cardiac gene expression through a signal-responsive mechanism. *J. Biol. Chem.*, **279**, 54937–54943.

39. Fischer,A., Klattig,J., Kneitz,B., Diez,H., Maier,M., Holtmann,B., Englert,C. and Gessler,M. (2005) Hey basic helix-loop-helix transcription factors are repressors of GATA4 and GATA6 and restrict expression of the GATA target gene ANF in fetal hearts. *Mol. Cell. Biol.*, **25**, 8960–8970.
40. Fischer,A., Steidl,C., Wagner,T.U., Lang,E., Jakob,P.M., Friedl,P., Knobeloch,K.P. and Gessler,M. (2007) Combined loss of Hey1 and HeyL causes congenital heart defects because of impaired epithelial to mesenchymal transition. *Circ. Res.*, **100**, 856–863.
41. Heisig,J., Weber,D., Englberger,E., Winkler,A., Kneitz,S., Sung,W.K., Wolf,E., Eilers,M., Wei,C.L. and Gessler,M. (2012) Target gene analysis by microarrays and chromatin immunoprecipitation identifies HEY proteins as highly redundant bHLH repressors. *PLoS Genet*, **8**, e1002728.
42. Peterson,C.L. and Workman,J.L. (2000) Promoter targeting and chromatin remodeling by the SWI/SNF complex. *Curr. Opin. Genet. Dev.*, **10**, 187–192.
43. Meng,Z.X., Li,S., Wang,L., Ko,H.J., Lee,Y., Jung,D.Y., Okutsu,M., Yan,Z., Kim,J.K. and Lin,J.D. (2013) Baf60c drives glycolytic metabolism in the muscle and improves systemic glucose homeostasis through Deptor-mediated Akt activation. *Nat. Med.*, **19**, 640–645.
44. Mehrotra,A., Joe,B. and de la Serna,I.L. (2013) SWI/SNF chromatin remodeling enzymes are associated with cardiac hypertrophy in a genetic rat model of hypertension. *J. Cell. Physiol.*, **228**, 2337–2342.
45. Nishi,H., Hashimoto,K. and Panchenko,A.R. (2011) Phosphorylation in protein-protein binding: effect on stability and function. *Structure*, **19**, 1807–1815.
46. Olsen,J.V., Blagoev,B., Gnad,F., Macek,B., Kumar,C., Mortensen,P. and Mann,M. (2006) Global, in vivo, and site-specific phosphorylation dynamics in signaling networks. *Cell*, **127**, 635–648.
47. Chen,Q., Chen,H., Zheng,D., Kuang,C., Fang,H., Zou,B., Zhu,W., Bu,G., Jin,T., Wang,Z. *et al.* (2009) Smad7 is required for the development and function of the heart. *J. Biol. Chem.*, **284**, 292–300.
48. Evans-Anderson,H.J., Alfieri,C.M. and Yutzey,K.E. (2008) Regulation of cardiomyocyte proliferation and myocardial growth during development by FOXO transcription factors. *Circ. Res.*, **102**, 686–694.
49. Zhou,P., He,A. and Pu,W.T. (2012) Regulation of GATA4 transcriptional activity in cardiovascular development and disease. *Curr. Top. Dev. Biol.*, **100**, 143–169.
50. Greulich,F., Rudat,C. and Kispert,A. (2011) Mechanisms of T-box gene function in the developing heart. *Cardiovasc. Res.*, **91**, 212–222.
51. Liang,Q., De Windt,L.J., Witt,S.A., Kimball,T.R., Markham,B.E. and Molkentin,J.D. (2001) The transcription factors GATA4 and GATA6 regulate cardiomyocyte hypertrophy in vitro and in vivo. *J. Biol. Chem.*, **276**, 30245–30253.
52. van Berlo,J.H., Elrod,J.W., Aronow,B.J., Pu,W.T. and Molkentin,J.D. (2011) Serine 105 phosphorylation of transcription factor GATA4 is necessary for stress-induced cardiac hypertrophy in vivo. *Proc. Natl. Acad. Sci. U.S.A.*, **108**, 12331–12336.
53. Battiprolu,P.K., Hojayev,B., Jiang,N., Wang,Z.V., Luo,X., Iglewski,M., Shelton,J.M., Gerard,R.D., Rothermel,B.A., Gillette,T.G. *et al.* (2012) Metabolic stress-induced activation of FoxO1 triggers diabetic cardiomyopathy in mice. *J. Clin. Invest.*, **122**, 1109–1118.
54. Gessler,M., Knobeloch,K.P., Helisch,A., Amann,K., Schumacher,N., Rohde,E., Fischer,A. and Leimeister,C. (2002) Mouse gridlock: no aortic coarctation or deficiency, but fatal cardiac defects in Hey2 -/- mice. *Curr. Biol.*, **12**, 1601–1604.
55. Sakata,Y., Kamei,C.N., Nakagami,H., Bronson,R., Liao,J.K. and Chin,M.T. (2002) Ventricular septal defect and cardiomyopathy in mice lacking the transcription factor CHF1/Hey2. *Proc. Natl. Acad. Sci. U.S.A.*, **99**, 16197–16202.
56. Xiang,F., Sakata,Y., Cui,L., Youngblood,J.M., Nakagami,H., Liao,J.K., Liao,R. and Chin,M.T. (2006) Transcription factor CHF1/Hey2 suppresses cardiac hypertrophy through an inhibitory interaction with GATA4. *Am. J. Physiol. Heart Circ. Physiol.*, **290**, H1997–H2006.

Supplementary Data to:

Phosphorylation of the chromatin remodeling factor DPF3a induces cardiac hypertrophy through releasing HEY repressors from DNA

Huanhuan Cui[1,2,3], Jenny Schlesinger[1,3], Sophia Schoenhals[1,2], Martje Tönjes[3], Ilona Dunkel[3], David Meierhofer[4], Elena Cano[1], Kerstin Schulz[1], Michael F. Berger[5,6], Timm Haack[7], Salim Abdelilah-Seyfried[7,8], Martha L. Bulyk[5,6,9], Sascha Sauer[4,10], Silke R. Sperling[1,2,3,11*]

[1] Department of Cardiovascular Genetics, Experimental and Clinical Research Center, Charité - Universitätsmedizin Berlin and Max Delbrück Center for Molecular Medicine, 13125 Berlin, Germany

[2] Department of Biology, Chemistry, and Pharmacy, Freie Universität Berlin, 14195 Berlin, Germany

[3] Group of Cardiovascular Genetics, Department of Vertebrate Genomics, Max Planck Institute for Molecular Genetics, 14195 Berlin, Germany

[4] Max Planck Institute for Molecular Genetics, 14195 Berlin, Germany

[5] Division of Genetics, Department of Medicine, Brigham and Women's Hospital and Harvard Medical School, Boston, MA 02115, USA

[6] Committee on Higher Degrees in Biophysics, Harvard University, Cambridge, MA 02138, USA

[7]Hannover Medical School, Institute of Molecular Biology, Carl-Neuberg Str. 1, D-30625 Hannover, Germany

[8]Potsdam University, Institute of Biochemistry and Biology, Department of Animal Physiology, Karl-Liebknecht Str. 24-25, 14476 Potsdam-Golm, Germany

[9] Department of Pathology, Brigham and Women's Hospital and Harvard Medical School, Boston, MA 02115, USA

[10] CU Systems Medicine, University of Würzburg, 97080 Würzburg, Germany

[11] DZHK (German Center for Cardiovascular Research), partner site Berlin, Berlin, Germany

* To whom correspondence should be addressed. Tel: +4930450540123; Fax: +4930450540159; Email: silke.sperling@charite.de

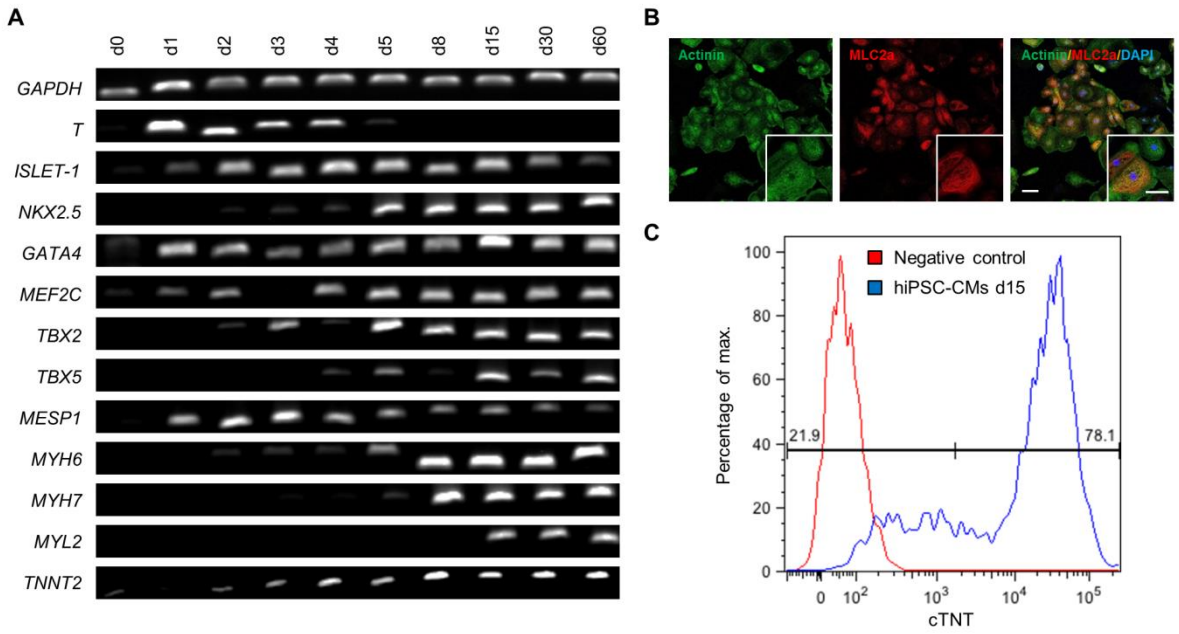

Supplementary Figure S1. Characterization of successful differentiation of human-induced pluripotent stem cells to cardiomyocytes.

(A) Analysis of mesodermal and cardiac gene expression during differentiation from day 0 to day 60.

(B) Immunostaining for characteristic cardiac markers. Scale bars indicate 50 and 20 µM, respectively.

(C) Cardiac Troponin T expression was analyzed at day 15 by flow cytometry.

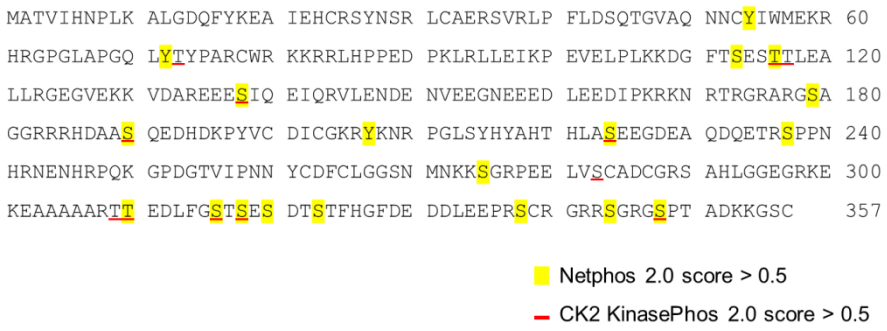

Supplementary Figure S2. Phosphorylation prediction of DPF3a.

Prediction of phosphorylation sites within the human DPF3a sequence (NP_036206) using the prediction tools Netphos 2.0 and KinasePhos 2.0.

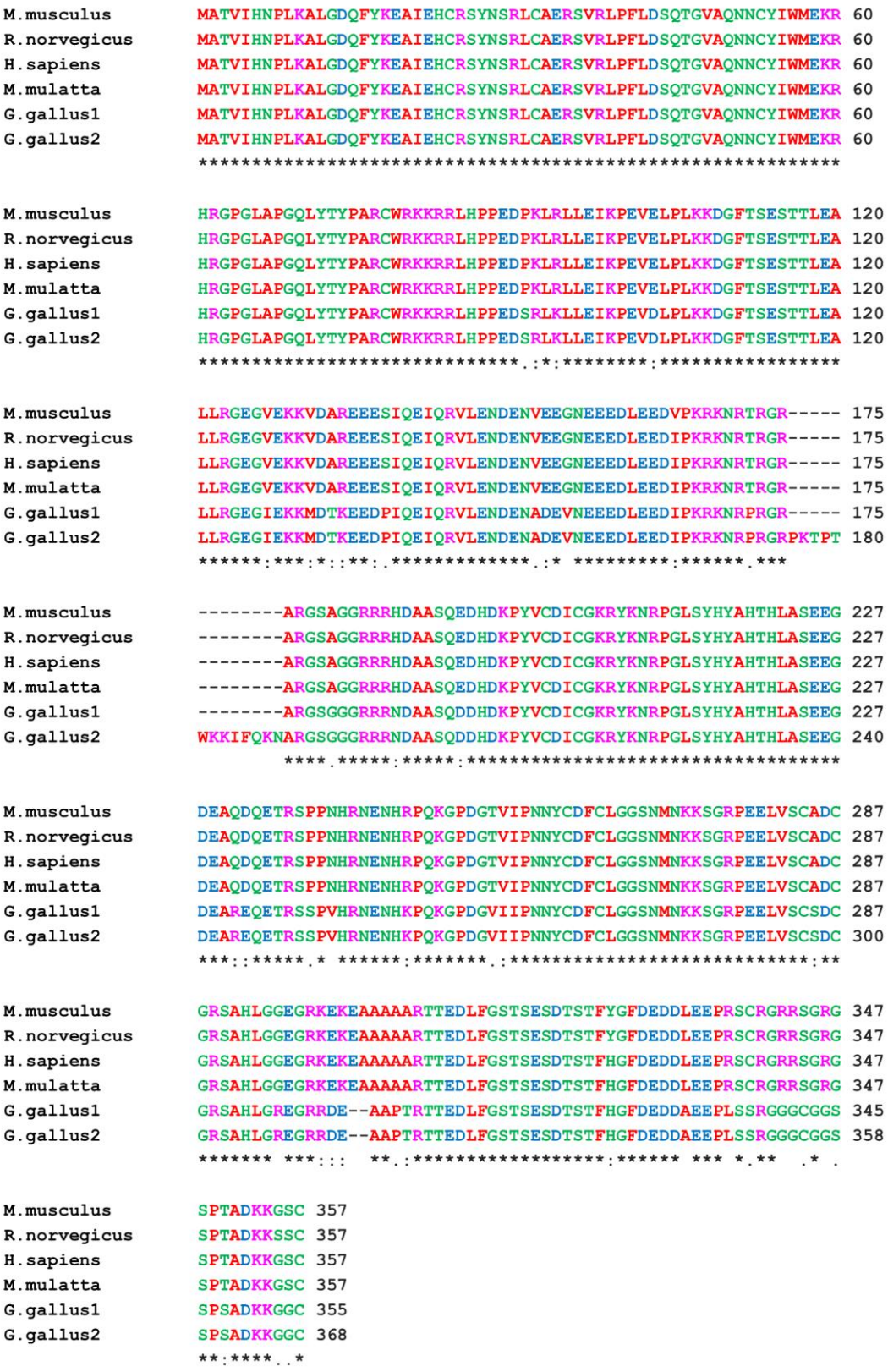

Supplementary Figure S3. Conservation analysis of DPF3a.

Protein sequence conservation analysis of DPF3a using ClustalW2 in *H. sapiens* (NP_036206), *M. mulatta* (AFE80282), *M. musculus* (NP_001254555), *R. norvegicus* (NP_001178747) and *G. gallus* (AAK51969.1 and AAK51970).

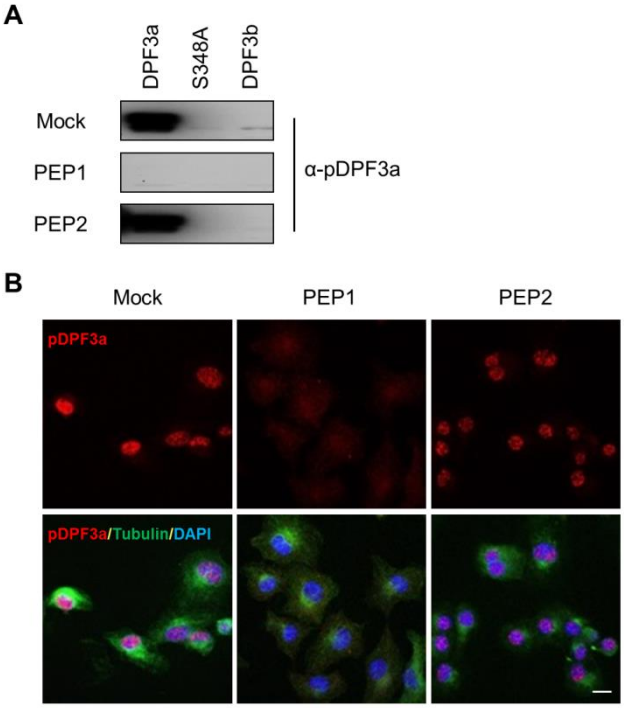

Supplementary Figure S4. Specificity of anti-pDPF3a.

(A) Flag-tagged DPF3a WT, S348A, and DPF3b from lysates of transiently transfected HEK293 cells were electrophoresed on a SDS-polyacrylamide gel and probed using the anti-pDPF3a antibody, pre-incubated with either PEP1 or PEP2 control peptide. PEP1: GRRSGRGS$^{(P)}$PTADKKGS; PEP2: GRRSGRGSPTADKKGS.

(B) HL1 cells were fixed and stained with antibody against pDPF3a (red) and antibody against Tubulin (green). Anti-pDPF3a antibody was pre-incubated with either PEP1 or PEP2 control peptide. Scale bar, 20 μm.

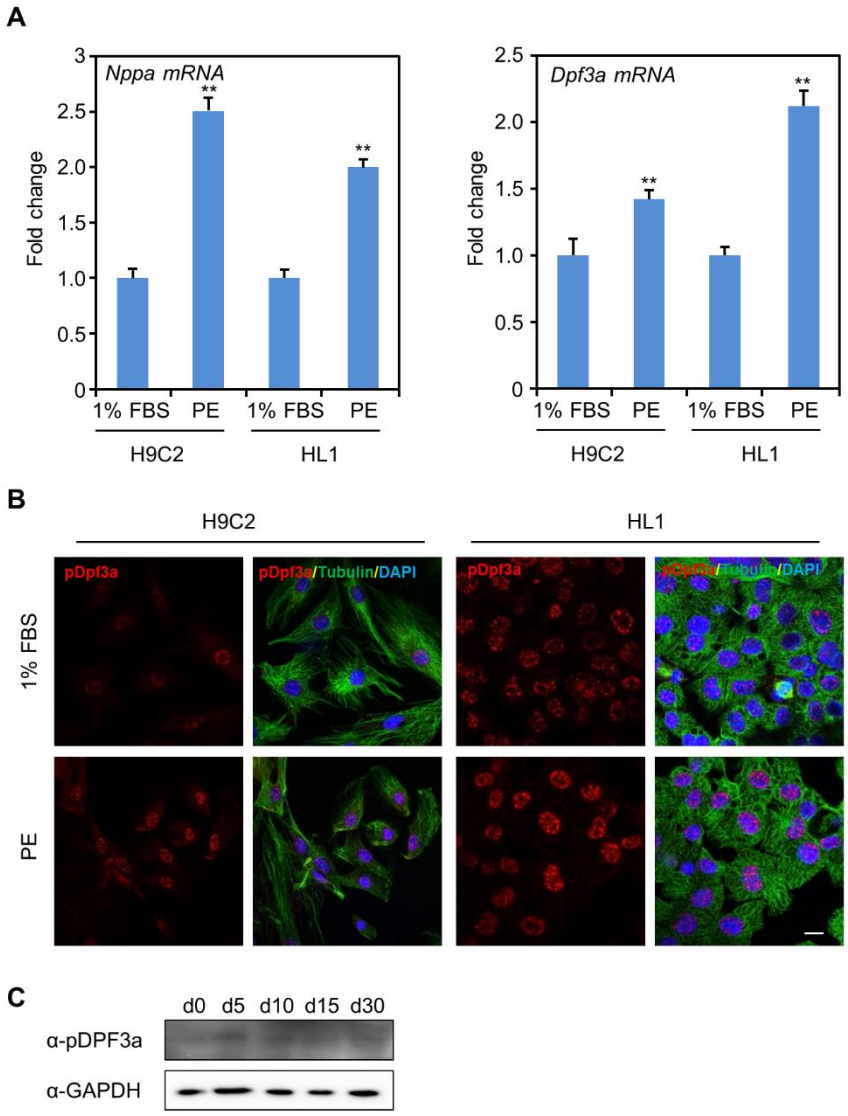

Supplementary Figure S5. DPF3a expression and phosphorylation in cardiac cells.

(A) *Nppa* and *Dpf3a* mRNA expression were analyzed in HL1 and H9C2 cardiomyocytes after phenylephrine (PE) treatment for 24 hours. 1% FBS was used as control.

(B) Nuclear localization of pDPF3a was increased by phenylephrine (PE) in HL1 and H9C2 cardiomyocytes. Red: pDPF3a; green: Tubulin. Scale bar, 20 μm.

(C) The protein level of phosphorylated DPF3a during differentiation of human-induced pluripotent stem cells to cardiomyocytes. Immunoblotting were performed on samples obtained from different day during cardiac differentiation.

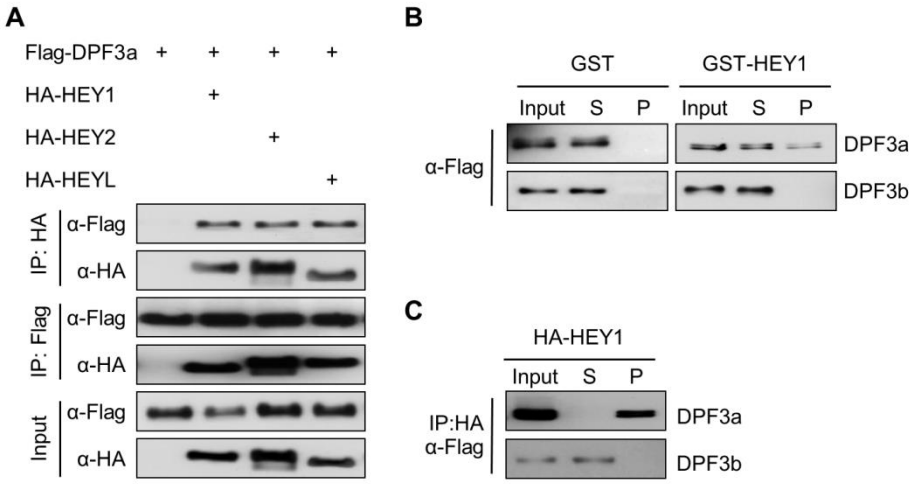

Supplementary Figure S6. Interactions between DPF3a/b and HEY proteins.

(A) DPF3a interacts with all HEY proteins. HEK293 cells were transiently transfected with Flag-tagged DPF3a and with HA-tagged HEY1, HEY2 or HEYL. Cell lysates were incubated with an anti-HA matrix to pull down HA-tagged protein together with interacting proteins, which were further probed with anti-Flag antibody in immunoblotting.

(B) GST pull-down with GST-HEY1 and Flag-DPF3a and DPF3b. GST vector was used as a negative control. S: supernatant, P: immunoprecipitation pellet.

(C) Co-immunoprecipitation of HA-tagged HEY1 with Flag-tagged DPF3a and DPF3b from lysates of transiently transfected HEK293 cells.

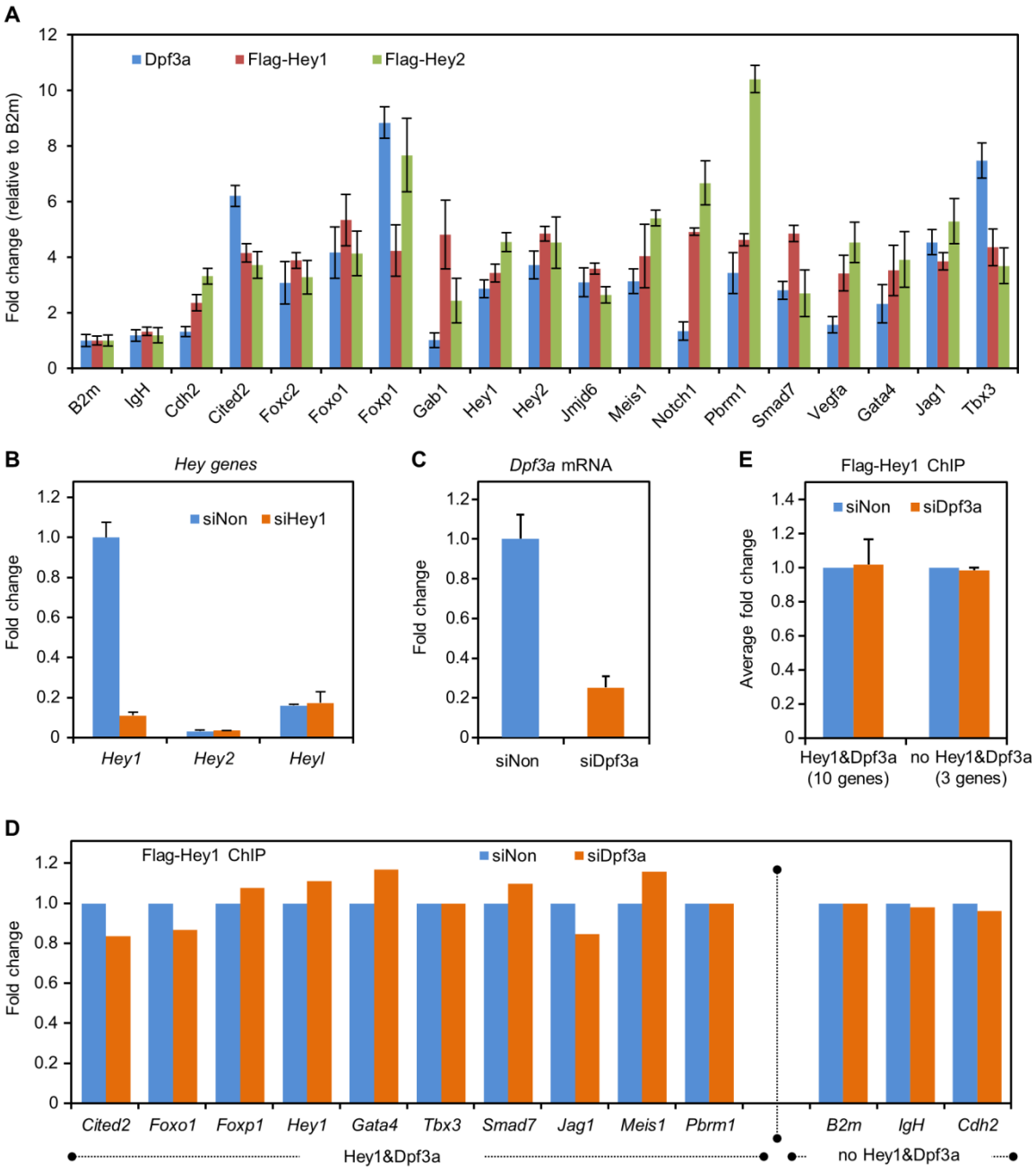

Supplementary Figure S7. ChIP-qPCR and siRNA knockdown in C2C12 cells

(A) Co-occurrence of Dpf3a, Hey1 and Hey2 binding. Dpf3a, Hey1 and Hey2 enrichment at selected promoters was analyzed using ChIP and qPCR.

(B) Expression levels of *Hey1*, *Hey2* and *Heyl* genes before and after siHey1 knockdown.

(C) Knockdown efficiency of *Dpf3a* in C2C12 cells was analyzed by qPCR.

(D-E) Hey1 enrichment at selected promoters in siDpf3a knockdown was compared to siNon control. Binding of Hey1 was quantified by ChIP and qPCR (triplicate experiments).

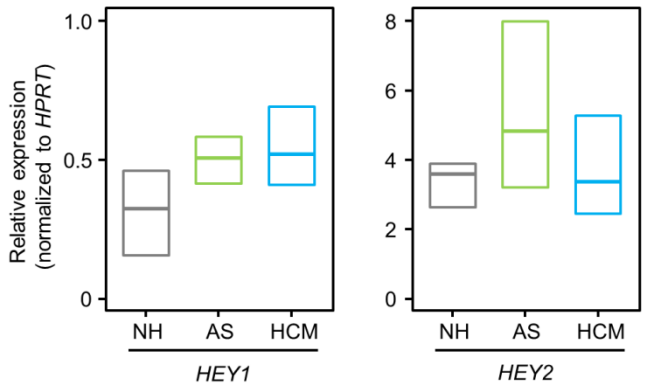

Supplementary Figure S8. *HEY1* and *HEY2* expression in human hearts.

Expression of *HEY1* and *HEY2* in aortic stenosis (AS), hypertrophic cardiomyopathy (HCM) and normal heart (NH) was analyzed using qPCR. Results represent median expression levels with 25% and 75% quartiles. Expression levels were analyzed by a two-sided Wilcoxon test and resulted in no significant findings between the analyzed groups.

Supplementary Table S1. Antibodies used in different experiments.

Antibodies used in chromatin immunoprecipitation (ChIP), Immunofluorescence (IF), Western blot (WB) and fluorescence-activated cell sorting (FACS), and their respective amounts/dilutions applied in the experiments are given.

Primary antibodies	**Company**	**Used amount/dilution**
Anti-SNF2β/BRG1, rabbit antiserum	Upstate (07-478)	ChIP: 5 µg
Anti-CK2 alpha, rabbit polyclonal	Abcam (ab10466)	WB: 1:500
Anti-Gapdh, mouse monoclonal	Ambion (AM4300)	WB: 1:5000
Anti-Flag, rabbit polyclonal	AnaSpec (29674)	IF: 1:500
Anti-Flag M2, mouse monoclonal	Sigma (F3165)	WB: 1:1000, IF: 1:400, ChIP: 2 µg
Anti-GST, rabbit polyclonal	Invitrogen (71-7500)	WB: 1:500
Anti-HA, rat monoclonal	Roche (11867423001)	WB: 1:2000
Anti-Hey1, rabbit polyclonal	Abcam (ab22614)	WB: 1:100
Anti-His HRP, mouse monoclonal	Macs Molecular (130-092-785)	WB: 1:5000
Anti-pDPF3a, rabbit polyclonal	Self-made	WB: 1:500, IF: 1:100, ChIP: 5 µg
Anti-Thiophosphate Ester, rabbit monoclonal	Epitomics (2686-1)	WB: 1:5000
Anti-Troponin I, goat polyclonal	HyTest (4T21/2)	IF: 1:200
Anti- Troponin T, mouse monoclonal	Lab Vision (MS-295)	FACS: 1:500
Anti- Mlc2a, mouse monoclonal	Synaptic Systems (311011)	IF: 1:200
Anti-Tubulin, mouse monoclonal	Sigma (T9026)	IF: 1:800
Anti-Actinin, mouse monoclonal	Sigma (A7811)	IF: 1:400
Anti-Vinculin, mouse monoclonal	Sigma (V9131)	WB: 1:25000
Normal Mouse IgG preimmuneserum	Santa Cruz Biotech (sc-2027)	ChIP: 5 µg
Normal Rabbit IgG preimmuneserum	Santa Cruz Biotech (sc-1237)	ChIP: 5 µg
Secondary antibodies		
Anti-mouse IgG (HRP)	Sigma(A0168)	WB: 1:10000
Anti-mouse IgG (Alexa Flour 488)	Invitrogen (A11029)	IF: 1:2000
Anti-rabbit IgG (Alexa Flour 568)	Invitrogen (A11036)	IF: 1:2000
Anti-rabbit IgG(Biotin)	Jackson lab(711-065-152)	IF: 1:500
Anti-goat IgG (Alexa Flour 568)	Invitrogen (A11057)	IF: 1:500
Anti-rabbit IgG (HRP)	Sigma (A2074)	WB: 1:10000
Anti-rat IgG (HRP)	Sigma (A9542)	WB: 1:20000

Supplementary Table S2. siRNAs used for knockdown experiments.

Sequences of siRNAs used in knockdown experiments.

Name	Target	Species	Company	Accession NO.	Target sequence
siDpf3a	Dpf3a	mouse	Invitrogen	NM_058212	TGACTCTGGTCATTGTTCTAGTTCT
siHey1	Hey1	mouse	Invitrogen	NM_010423	CGACGAGACCGAATCAATATT
siCk2a1	Ck2a1	mouse	Invitrogen	NM_007788	GATTATAGTTTGGATATGTTT
siNon	Synthetic	mouse	Invitrogen	Synthetic	Not provided
siFITC	Synthetic	mouse	Invitrogen	Synthetic	Not provided
siDPF3	DPF3	human	Qiagen	NM_012074	AAGGGAAATCAAAGAATCGA
					AAGAGGATATTCCCAAGCGAA
					AACAGACTCTCTGGGCAATTA
					AAGAAACGTATCAATACCCAT
siNON	Synthetic	human	Qingen	Synthetic	Not provided

Supplementary Table S3. Sequences of qPCR expression primers

Gene	Species	Accession Number	Forward Sequence (5' - 3')	Reverse Sequence (5' - 3')
Dpf3a	mouse	NM_058212	CAGACGGGACAGTCATTCCTAAT	CTCCCAAATGAGCAGAGCGT
Dpf3	mouse	NM_058212/NM_001267625	ACAACTGCTACATCTGGATGG	GTCGTAGTTTTGGGTCCTCTG
Hey1	mouse	NM_010423	TGAGCTGAGAAGGCTGGTAC	ACCCCAAACTCCGATAGTCC
Hey2	mouse	NM_013904	TGAGAAGACTAGTGCCAACAGC	TGGGCATCAAAGTAGCCTTTA
HeyL	mouse	NM_013905	CGTGGATCACTTGAAGATGC	CATTCCCGAAACCCAATACT
Ck2a1	mouse	NM_007788	GATAGCCAAGGTTCTGGGAA	CATCGCTTACGGGAGTGTC
Hprt	mouse	NM_013556	AAACAATGCAAACTTTGCTTTCC	GGTCCTTTTCACCAGCAAGCT
Dpf3a	rat	NM_001191818	AAGGCAGGAAGGAGAAGGAG	AGGCTCTTCCAAATCGTCCT
Nppa	rat	NM_012612	AGGGCTTCTTCCTCTTCCTG	TGTTGGACACCGCACTGTAT
Hprt	rat	NM_012583	TGCTGGTGAAAAGGACCTCTC	CCACTTTCGCTGATGACACAA
DPF3	human	NM_012074/NM_001280542	GGCTGCTGGAGATAAAACCTGA	TTCCTGGATGCTTTCCTCCTC
DPF3a	human	NM_012074	GACGATTTGGAAGAGCCTCG	GAGTCTGTTCCGTGGGTTTAGC
DPF3b	human	NM_001280542	CGAGGCTGTCAAGACCTACAAG	CGCAGAAGAGTAGCTGGTCATC
HEY1	human	NM_012258	ACGGGATGACCGTGGATCACCTGAAA	GCGTGCGCGTCAAAGTAAC
HEY2	human	NM_012259	ACGGGTTGAAGATGCTTCAGGCAACA	TCAGGTACCGCGCAACTTCT
NPPA	human	NM_006172	ACGGGTACAATGCCGTGTCCAACG	TTCTTCCAAATGGTCCAGCAA
TBX3	human	NM_005996	AAGGAGAATGGGACCTCTGA	CCTCGCTGGGACATAAATCT
FOXO1	human	NM_002015	CTGGCTCTCACAGCAATGAT	CACCATAGAATGCACATCCC
SMAD7	human	NM_001190821	CAGATTCCCAACTTCTTCTGG	CCCACTCTCGTCTTCTCCTC
HPRT	human	NM_000194	GGTGGAGATGATCTCTCAACTTTAA	AGGAAAGCAAAGTCTGCATTGTT
GAPDH	human	NM_002046.5	ACCCACTCCTCCACCTTTGA	TTGCTGTAGCCAAATTCGTTG
OCT4	human	NM_002701	AGTTTGTGCCAGGGTTTTTG	ACTTCACCTTCCCTCCAACC
NANOG	human	NM_024865	TTTGGAAGCTGCTGGGGAAG	GATGGGAGGAGGGGAGAGGA
T	human	NM_003181	CTCACCAATGAGATGATCGTGAC	AGGAAGGAGTACATGGCGTTG
ISLET-1	human	NM_002202	AGCAGCCCAATGACAAAACTAA	CGTGTCTCTCTGGACTGGCA
NKX2.5	human	NM_001166175	CACCTCAACAGCTCCCTGACT	ATCGCCGCCACAAACTCT
GATA4	human	NM_002052	ATCTCACTACGGGCACAGCA	TTTGAGGAGGGAAGAGGGAAG
TBX2	human	NM_005994	ACCCTGAGATGCCCAAAC	CAGTGACGGCGATGAAGT
MEF2C	human	NM_002397	TCAGGGACGAGAGAGAGAAGAAA	ACAGTCACACAGCACGCTCA
TBX5	human	NM_000192	CAGAAACTCAAGCTCACCAACAA	TGCTATAAACGCAGTCTCAGGAA
MYH6	human	NM_002471	GGTCATTGCTGAAACCGAGA	GCTCCTTGAGGTTGAAAAGCA
MESP1	human	NM_018670	ACGTGCTGGCTCTGTTG	GTCAGTTGTCCCTTGTCACTT
MYH7	human	NM_000257	GGATGTCTTCGTGCCTGATG	GGTCCTCCTTCACGGTCACT
MYL2	human	NM_000432	GGCGAGTGAACGTGAAAAAT	CAGCATTTCCCGAACGTAAT
MYL7	human	NM_021223	GAGGAGAATGGCCAGCAGGAA	GCGAACATCTGCTCCACCTCA
TNNT2	human	NM_000364	TTCACCAAAGATCTGCTCCTCGCT	TTATTACTGGTGTGGAGTGGGTGTGG

Supplementary Table S4. Primer sequences used for ChIP-qPCR in C2C12 cells

Gene	Accession NO.	Forward sequence (5' - 3')	Reverse sequence (5' - 3')
B2m	NM_009735	TGCCAAACCCTCTGTACTTCT	TTAGGCCTCTTTGCTTTACCA
Chd2	NM_001081345	CCGAGAAGTGTGTGTGTGTG	ACCTCCGTATCCTCCATCC
IgH	NG_005838	TGGTGGGGCTGGACAGAGTGT	GCCGATCAGAACCAGAACACC
Jag1	NM_013822	CAGCAAGCGAGCCCAGAG	TTTCAAAGTTCCCAGCAGAG
Smad7	NM_001042660	GCCAAAGGTCACCACCAT	TTGAGTTTCTTGAGCACCGA
Gata4	NM_008092	CTACCTGGCCAGCTCCAGT	CCTTGCACGTGACTCCCTTA
Gab1	NM_001301298	CCCAGAGGACGTCTCAGATT	CCGATCGAGTTCCTCTTCAG
Notch1	NM_008714	CGTTAGGCAGAGCAAGGG	GTGGTGTGCGTCAACGTC
Tbx3	NM_011535	TGACATAAACGCAGGACAGG	ACCAATTGTGTGGCTGCATA
Cited2	NM_010828	ATGGGCGAGCACATACACTA	ACCCATGAACTGGGAGTTGT
Foxc2	NM_013519	AGAAGAAGGATGTGCCCAAG	CCTCGCTCTTAACCACGACT
Foxo1	NM_019739	GTCGTACGCCGACCTCAT	GACAGGGTGAGCCTCTTCTC
Foxp1	NM_001197321	CAGGCGAGAAACGGAGAG	AGCTCTTCTCTGCGACACG
Vegfa	NM_001025250	TTGAATATCAAATCCCAGAGCA	GCAGCGACAAGGCAGACTAT
Hey1	NM_010423	GGGTGAGCTCTCTTCATGGT	GCAGTTAACTCCTCCTTGCC
Hey2	NM_013904	AGGAGGAGCAGCTACTGTCG	CAGCGTGGGAAAGAACCT
Meis1	NM_010789	AGACACTCCACAAATTCGCA	GCTGCAGCCTGTATTTGTGT
Pbrm1	NM_001081251	GCGCACACACATACACTGTC	CCCAGTGCTGCCGTAAAT

Supplementary Table S5. Demography of human subjects.

NH: normal heart, HCM: hypertrophic cardiomyopathy, AS: aortic stenosis

Clinical diagnosis	Age	Gender
NH	55	male
	43	male
	57	female
	37	female
AS	64	male
	68	male
	81	female
	68	female
HCM	50	male
	42	male
	53	female
	57	female
	51	female
	42	female
	50	female
	49	female

Supplementary Table S6. E-box motif identified within DPF3a peaks.

For ChIP-chip, C2C12 cells were transfected with Flag-DPF3a and ChIP was performed using anti-Flag antibody.

Method	Cell type	Antibody for ChIP	Total peaks	Peaks with E-box
ChIP-chip	C2C12 undifferentiated	Flag	134	88
ChIP-seq	C2C12 undifferentiated	pDPF3a	777	709
ChIP-seq	C2C12 differentiated	pDPF3a	821	782

3 Manuscript 2

DNA methylation alterations associated with gene expression changes depict congenital heart disease: Tetralogy of Fallot and ventricular septal defects

Marcel Grunert, Cornelia Dorn, **Huanhuan Cui**, Ilona Dunkel, Kerstin Schulz, Sophia Schoenhals, Wei Sun, Felix Berger, Wei Chen, Silke R. Sperling

Manuscript under review

3.1 Synopsis

In this project, we aimed to examine the impact of DNA methylation alterations on two common forms of CHDs, namely TOF and VSD. We analyzed genome-wide DNA methylation levels in the right ventricle of eight TOF patients and normal hearts of three unaffected individuals (NH-rv) as well as in the right atrium of eight VSC patients and normal heart of four unaffected individuals (NH-ra). In general, we observed clear methylation differences between patients and controls.

Using a stringent filtering approach, we defined differentially methylated regions (DMRs) in TOF and VSD. 14,403 hypermethylated and 1,450 hypomethylated DMRs were identified in the TOF cases compared to NH-rv, whereas 7,152 hypermethylated and 935 hypomethylated DMRs were identified in the VSD cases compared to NH-ra.

Next, we overlapped these DMRs with different genomic features. In general, DMRs are significantly enriched over all genomic features like promoters, exons and cardiac enhancers, except for CpG islands (CGIs). However, we found four and five hypermethylated DMRs CGIs in TOF and VSD, respectively, when we checked the total overlap of hyper- and hypomethylated DMRs separately for each genomic feature. Only one DMR CGI could be observed in both TOF and VSD. This DMR CGI is located in the promoter of the *SCO2* gene.

SCO2 encodes a cytochrome C oxidase assembly protein. We found a similar DNA methylation pattern of *SCO2* in both TOF and VSD, with significant hypermethylation in the promoter and weak hypomethylation in the gene body. Using qPCR, a significant reduction of *SCO2* expression in myocardial biopsies of both patient groups was observed. Moreover, the regulatory impact of this DMR at *SCO2* promoter was further demonstrated by reporter gene assays.

For TOF, we linked DNA methylation with genome-wide expression data and found a significant overlap of hypermethylated promoters and down-regulated genes, and vice versa. Moreover, we found DNA methylation changes co-localized with novel, differential splicing events among sarcomeric genes, such as *TNNI1*, *MYL7*, *PDLIM3* and *TNNT2*. Furthermore, we validated the methylation of two selected CpGs, namely the DMR summits of *SCO2* and *TNNI1*, using PacBio sequencing. In addition, we replicated the results with a second independent cohort of nine TOF patients, and additional controls.

Finally, we constructed an interaction network for TOF, based on known mutated genes in patients with CHDs and our differentially methylated and expressed genes in TOF using the STRING database.

In summary, we presented the first genome-wide study delineating the impact of alterations in DNA methylation associated with gene expression changes on TOF and VSD. We showed clear differences in DNA methylation patterns between diseased and normal hearts, which suggests that DNA methylation can be indicative of disease state and likely contributes to the pathogenesis of CHDs.

3.2 Project contributions

For this project, I cloned the SCO2 promoter regions into the reporter vector and subsequently performed the luciferase reporter gene assay. In addition, I contributed to the analysis of the reporter gene assay and wrote this section of the manuscript.

Contributions of co-authors

Concept: M. Grunert, SR. Sperling

Bioinformatics analysis: M. Grunert

Performed experiments: C. Dorn, I. Dunkel, K. Schulz, S. Schoenhals, W. Sun

Contributed reagents/analysis tools: W. Chen

Collected and provided phenotypic data: F. Berger, SR. Sperling

Wrote the manuscript: M. Grunert, C. Dorn, SR. Sperling

DNA Methylation Alterations Associated with Gene Expression Changes Depict Congenital Heart Disease: Tetralogy of Fallot and Ventricular Septal Defect

Short title: DNA Methylation in Congenital Heart Diseases

Marcel Grunert[1,2], Cornelia Dorn[1,2,3], Huanhuan Cui[1,3], Ilona Dunkel[2], Kerstin Schulz[1], Sophia Schoenhals[1,3], Wei Sun[4], Felix Berger[5], Wei Chen[4], Silke R. Sperling[1,2,3]*

[1] Department of Cardiovascular Genetics, Experimental and Clinical Research Center, Charité - Universitätsmedizin Berlin and Max Delbrück Center for Molecular Medicine, Berlin, Germany

[2] Group of Cardiovascular Genetics, Department of Vertebrate Genomics, Max Planck Institute for Molecular Genetics, Berlin, Germany

[3] Department of Biology, Chemistry and Pharmacy, Freie Universität Berlin, Berlin, Germany

[4] Laboratory for Functional and Medical Genomics, Berlin Institute for Medical Systems Biology, Max Delbrück Center for Molecular Medicine, Berlin, Germany

[5] Department of Pediatric Cardiology, German Heart Institute Berlin and Department of Pediatric Cardiology, Charité - Universitätsmedizin Berlin, Berlin, Germany

* Corresponding author
Email: silke.sperling@charite.de

GEO reviewer link for raw and processed MBD-seq data:

http://www.ncbi.nlm.nih.gov/geo/query/acc.cgi?token=chctowaahtitfur&acc=GSE62629

Abstract

Ventricular septal defect (VSD) and Tetralogy of Fallot (TOF) represent two common congenital heart disease (CHD). For these and the majority of CHDs, the causative molecular network still needs to be explored in its full complexity driven by genetic, epigenetic and environmental factors. In particular, TOF is prone to long-term clinical problems like heart failure and arrhythmias. DNA methylation is a widely studied epigenetic modification and cardiac regulatory elements have been shown to be differentially methylated in CHD. We present the first analysis of genome-wide DNA methylation data obtained from myocardial biopsies of TOF and VSD patients. We found clear methylation differences between patients and controls. We defined stringent sets of differentially methylated regions, which are significantly enriched for genomic features like promoters, exons and cardiac enhancers. For TOF, we linked DNA methylation with genome-wide expression data and found a significant overlap for hypermethylated promoters and down-regulated genes, and vice versa. We validated and replicated the methylation of selected CpGs using PacBio sequencing. The regulatory impact of one validated region, namely the SCO2 promoter, was further demonstrated by reporter assay. Moreover, we found examples of methylation changes co-localized with novel, differential splicing events among sarcomeric genes. Finally, we demonstrate the interaction of differentially methylated and expressed genes in TOF with mutated CHD genes in a molecular network. Our data suggest that epigenetic insults impact on the clinical phenotype of TOF and VSD. Studying them might offer novel therapeutic perspectives, which is the clinical imperative.

Introduction

Congenital heart defects (CHDs) are the most common birth defects in humans with an incidence of approximately 1% [1]. There are numerous different phenotypes ranging from a single septal defect up to a univentricular heart, the most common being the ventricular septal defect (VSD) with a prevalence of 20-30 per 10,000 live births [2]. VSD can occur isolated or as part of complex CHD phenotypes like Tetralogy of Fallot (TOF). The latter is the most common form of cyanotic CHD, affecting three per 10,000 live births [2]. In addition to VSD, TOF is characterized by an overriding aorta, pulmonary stenosis and right ventricular hypertrophy. Approximately one third of CHDs are associated with syndromes such as trisomy 21 (Down syndrome). The majority of CHDs occur sporadically (80%) and do not follow Mendelian inheritance. Already in 1968, James Nora suggested a multifactorial inheritance with genetic-environmental interactions [3]. Since then, many genes have been identified harboring functional mutations in patients

with CHDs and were shown to be important for heart development and potentially causative for the developmental defect. However, the underlying causes for the majority of patients remain unclear and the identification of non-genetic risk factors will be crucial for our understanding of CHD etiology and the differences in the clinical long-term outcome.

Environmental influences are known to impact on the phenotype of cardiac malformations and could possibly be transmitted by epigenetic mechanisms. A widely studied epigenetic modification is DNA methylation, which is a covalent modification of the DNA molecule and plays a role in the regulation of gene expression and genomic stability [4]. DNA methylation was found to be substantially altered in various diseases [5-7]. Studies on DNA methylation patterns in end-stage heart failure showed hypomethylation of gene promoters associated with differentially up-regulated genes [8,9]. For VSD, a number of promoters were shown to harbor DNA hyper- or hypomethylation, including genes involved in embryonic development, cell signaling, apoptosis and proliferation [10,11]. Candidate approaches revealed for example, that DNA methylation of the cardiac regulators *NKX2.5* and *HAND1* was elevated in TOF patients, whereas *TBX20* showed lower methylation levels [12,13]. TBX20 levels are elevated in TOF and expression of NKX2.5 and HAND1 is reduced, implying that DNA methylation is playing a role in CHD [14,15]. Moreover, even maternal methylation status was found to correlate with CHD [16,17].

This study aims to shift the focus of CHD research from epigenetic single-loci studies to comprehensive and unbiased epigenome analysis. Thus, we present the first genome-wide DNA methylation study on myocardial biopsies of TOF and VSD. We applied affinity-based enrichment of methylated DNA sequences with methyl-CpG-binding domain (MBD) proteins followed by next-generation sequencing (MBD-seq) [18]. Moreover, we validated the methylation levels of selected CpGs using PacBio sequencing of bisulfite treated genomic DNA and replicated these results in a second, independent cohort of TOF patients. Furthermore, we correlated DNA methylation with genome-wide expression data (RNA-seq) in TOF patients. In summary, we show clear methylation differences between CHD and normal hearts, which suggests that DNA methylation can be indicative of disease state and likely contributes to the pathogenesis of CHD.

Results

Sample selection

The cardiac samples studied have been selected to enable the study of aberrant DNA methylation/gene expression that (A) might be causative for development of TOF and VSD and (B) present the state of the postnatal TOF. Both are prone to be related to

the long-term clinical outcome. To obtain a molecular portrait that is not influenced by the biomechanical adaptation processes, we studied right atrial (ra) samples of patients with VSD, intact tricuspid valve, and normal right atrial pressure, for which we had found unexplained significant expression differences previously [19]. In contrast to these, the observed alterations in the right ventricular (rv) samples of TOF cases reveal the molecular signature of the malformation in addition to the hemodynamic adaptation portrait. The majority of TOF hearts develop heart failure and arrhythmia even after perfect surgical reconstruction and it is highly suggestive that epigenetic alterations are in part causative for this long-term clinical problem. Recently, we showed the multigenic background of these sporadic TOF cases, explaining in part the phenotypic features [20]. In the present study, we analyzed genome-wide DNA methylation levels in the right ventricle of eight TOF patients and normal hearts of three unaffected individuals (NH-rv) as well as in the right atrium of eight VSD patients and normal hearts of four unaffected individuals (NH-ra). In addition, we replicated the methylation levels of selected CpGs on a second cohort of nine TOF patients, two additional normal heart samples and moreover two right ventricular samples of cases with isolated pulmonary stenosis (PS) and hypertrophic right ventricle comparable to the studied TOF cases. The later was added to gain insights as to whether the observed alterations are related to the secondary adaptation process or potentially to the malformation themselves. All patients were clinically studied, and their hemodynamic status was worked up by cardiac catheterization and echocardiography before surgery (S1 Fig.).

Genome-wide DNA methylation levels

DNA methylation profiles were generated using MBD-seq (S1 Table). Tiling of the genome revealed that 44.6% of the autosomal 1-kilobase tiles showed a minimum difference of 10% in the mean methylation level for TOF patients compared to NH-rv controls. We found much more hypermethylated (88.3%) than hypomethylated tiling regions (11.7%) in TOF. In the VSD patients compared to NH-ra controls, we found a lower number of the autosomal tiles with a difference ≥ 10% in the mean methylation level (33.4%). However, again more hypermethylated (76.2%) than hypomethylated tiling regions (23.8%) could be observed. The genome-wide mean methylation levels for each sample are given in S2 Fig. In general, principle component analysis based on the mean methylation levels shows a clear distinction between TOF and VSD cases (Fig. 1A). This finding is not only attributable to the tissue type, as there is a clear overlap between all samples from the right ventricle and all samples from the right atrium (Fig. 1B). We did not analyze the differences between normal right ventricle and right atrium; however, our publicly available dataset provides a valuable resource for further studies.

Differentially methylated regions

We searched for autosomal regions comprising continuous CpG sites (at least one CpG) with changes in the same direction (i.e. either hyper- or hypomethylation) and with an absolute minimum difference of 10% in the mean methylation level between cases and controls. In total, we found ~3.35 million regions in TOF versus NH-rv and ~3.33 million regions in VSD versus NH-ra (Table 1). For statistical assessment, we used a one-sided t-test to compare the methylation levels of single CpGs between patient and control groups. P-values of all single CpGs in a given region were combined using the generalization of Fisher's method. Regions with an adjusted p-value (q-value) of 0.01 using the Bonferroni method were defined as differentially methylated regions (DMRs). To detect biologically significant changes in the methylation levels, we finally defined a stringent set of DMRs with at least ten continuous CpG sites and an absolute difference of ≥ 30% in the mean methylation level between the sample groups. Using this stringent filtering, we identified 14,403 hypermethylated DMRs (with an average length of 1,678 bp and an average CpG number of 16) and 1,450 hypomethylated DMRs (with an average length of 479 bp and an average CpG number of 17) in the TOF cases compared to NH-rv (Table 1 and S2 and S3 Tables). For the VSD cases, 7,152 hypermethylated DMRs (with an average length of 1,161 bp and an average CpG number of 15) and 935 hypomethylated DMRs (with an average length of 541 bp and an average CpG number of 16) were observed in comparison to NH-ra (Table 1 and S4 and S5 Tables).

Overlap of DMRs with genomic features

We examined the overlap of hyper- and hypomethylated DMRs with different genomic features, including promoter regions, exons and introns, CpG islands (CGIs) and shores, transcription factor binding sites (TFBS) and cardiac enhancers.

First, we evaluated the enrichment of the overlapping DMRs (stringent set) compared to all initially identified regions (~3.35 million for TOF and ~3.33 million for VSD) for each genomic feature. In general, DMRs are significantly enriched over all genomic features, except for CGIs (Fig. 2A,C). The highest enrichment was found in exons and predicted TFBS as well as in cardiac enhancers, which were obtained from p300 ChIP-seq data of fetal and adult human hearts [21]. Comparison of hyper- and hypomethylated DMRs indicated that hypomethylated DMRs tend to be much more enriched over all genomic features. Most strikingly, cardiac enhancers were 8.0-fold enriched for hypomethylated DMRs in TOF vs. NH-rv (Fig. 2A; p-value = 8.5×10^{-57}) and 12.1-fold enriched for VSD vs. NH-ra (Fig. 2C; p-value = 7.9×10^{-74}). Moreover, the first exons of

genes, which overlap with the promoter regions, were 4- to 6-fold enriched for hypomethylated DMRs compared to all initially identified hypomethylated regions.

Next, we looked at three classes of promoters separately, namely high-CpG promoters (HCPs), intermediate-CpG promoters (ICPs) and low-CpG promoters (LCPs) [22]. ICP regions contain many promoters that are close to CGIs and thus, they are often referred to as weak CGIs [22]. We found the ICP regions significantly enriched for hypomethylated DMRs in both patient groups (2.4-fold with p-value = 6.9×10^{-4} in TOF vs. NH-rv and 3.2-fold with p-value = 2.2×10^{-5} in VSD vs. NH-ra). Looking at the CGIs, the hypomethylated DMRs were again significantly enriched in both patient groups (Fig. 2A; 4.8-fold with p-value = 1.1×10^{-17} in TOF vs. NH-rv and Fig. 2C; 2.7-fold with p-value = 5.1×10^{-4} in VSD vs. NH-ra). Notably, in VSD vs. NH-ra there was no significant enrichment for all DMRs as well as for the hypermethylated DMRs only in the CGIs. This holds true for all DMRs in TOF vs. NH-rv. However, when analyzing the hypermethylated DMRs separately, they show a significant depletion for the CGIs compared to all initially identified hypermethylated regions in TOF (Fig. 2A; 0.4-fold with p-value = 0.04). Taken together, the enrichment for hypomethylated DMRs in ICPs tends to be similar to CGIs in both patient groups.

We next checked the total overlap of hyper- and hypomethylated DMRs separately for each genomic feature. Up to 30% of the DMRs do not overlap with any feature. The highest overlap is observed with introns (48-62%) and TFBS (30-46%), while only a very low number of DMRs is associated with CGIs (Fig. 2B,D). We found only four hypermethylated CGI DMRs in TOF vs. NH-rv (Fig. 2B) and five hypermethylated CGI DMRs in VSD vs. NH-ra (Fig. 2D). Out of the four hypermethylated DMRs in the TOF patients, three are located in promoter CGIs. In the VSD patients, only one hypermethylated promoter CGI could be observed. Nevertheless, this hypermethylated DMR overlaps with one of the regions found in the TOF patients and is located in the promoter of the *SCO2* gene, coding for the SCO2 cytochrome C oxidase assembly protein, a gene recently shown to be essential for cardiac function in *Drosophila* [23].

Methylation and expression of SCO2

In general, the DNA methylation pattern of *SCO2* is similar in both TOF and VSD patients, with a significant hypermethylation in the promoter and a weak hypomethylation in the gene body (Fig. 3A). To validate the methylation results, we analyzed four selected CpGs from the DMR summit using PacBio sequencing of bisulfite treated genomic DNA in all TOF and VSD cases as well as related controls. In addition, we included a replication cohort of nine TOF samples. For both TOF and VSD we detected a significantly higher methylation level (on average 95% in TOF versus 91% in NH-rv and 95% in VSD versus

87% in NH-ra). Moreover, we were able to replicate our results using the second cohort of TOF cases, two additional controls and two cases of PS (on average 96% in TOF versus 91% in NH-rv) (Fig. 3B). A principle component analysis demonstrates a clear separation of the controls as well as the PS cases from the TOF cases, while the two TOF cohorts are grouped together (S3 Fig.).

Quantitative real-time PCR showed a significant reduction of SCO2 expression in myocardial biopsies of both patient groups (p-value = 0.0029 for TOF and p-value = 0.0044 for VSD; Fig. 3C). Finally, we tested the regulatory impact of the DMR by luciferase assay and could show that it significantly reduces expression compared to the promoter construct without this region (Fig. 3A,D). Thus, we conclude that this CGI DMR is located in a novel regulatory element impacting in *SCO2* transcription.

Genes associated with DMRs

For further analysis of DMRs, we considered autosomal, protein-coding genes with either hyper- or hypomethylated DMRs in their promoters or exons as well as genes near hyper- or hypomethylated cardiac enhancers. Since DNA methylation is known to be age-dependent and for sample availability reasons our genome-wide study was performed on controls with a mean age of 21 years compared to cases of mean age of 1.5 years, we excluded genes known to play a role in aging based on two studies that also applied enrichment-based determination of DNA methylation [24,25]. The two studies identified 74 genes associated with aging. However, their overlap with our DMR-associated genes is very low. In total, we excluded 7 out of 1889 (0.4%) DMR-associated genes in TOF vs. NH-rv and 10 out of 956 (1.1%) genes in VSD vs. NH-ra. Of note, our replication was performed with controls having a mean age comparable to cases. Overall, for promoter and exonic regions we found almost 2-fold more genes associated with DMRs in TOF vs. NH-rv compared to VSD vs. NH-ra. However, the number of genes near differentially methylated cardiac enhancers was slightly higher for VSD cases (S6 Table). The overlap between genes associated with DMRs in TOF cases compared to VSD cases is relatively low (reciprocal overlap between 3-17%).

For genes with DMRs in their promoters and exons, we observed significant enrichment in several gene ontology (GO) terms and KEGG/Reactome pathways for both patients groups. No significant enrichment was found for genes near hyper-/hypomethylated cardiac enhancers. In TOF, we found several GO terms for sarcomeric function and one term for anatomical development associated in particular with hypomethylated exons (S4 Fig.). Moreover, we found the Reactome pathway ‘striated muscle contraction’ for hypomethylated exons. In VSD, we identified a number of GO terms for anatomical structure and especially for cardiovascular system development for

both hyper-/hypomethylated promoters and exons (S5 Fig.). We also observed more specific ontologies such as 'cardiac ventricle morphogenesis' for hypomethylated promoters and 'heart trabecula formation' for hypomethylated exons. In addition, KEGG pathways for hypertrophic and dilated cardiomyopathy (with the five genes *CACNB2*, *DES*, *MYH6*, *MYH7*, *MYBPC3*) as well as Reactome pathways for muscle contraction were found for hypomethylated exons in VSD vs. NH-ra.

DNA methylation and gene expression changes in TOF patients

To correlate DNA methylation with gene expression changes, we re-analyzed our previously published mRNA-seq data [20], which comprise TOF cases and NH-rv controls used for MBD-seq (S7 Table). Overall, we found 978 autosomal, protein-coding genes to be significantly differentially expressed (adjusted p-value < 0.05) between TOF cases and normal hearts. Out of these genes, 375 (~38%) are up-regulated and 603 (~62%) are down-regulated in TOF (S8 Table). Overrepresentation analysis for these genes revealed several significant GO terms and KEGG/Reactome pathways (S6 Fig.). Most strikingly, for up-regulated genes we determined GO terms for anatomical structure development and the KEGG 'Wnt signaling pathway', which plays a role in cardiac development and tissue remodeling in the mature heart [26].

Fig. 4 shows the overlap between autosomal, protein-coding genes that contain hyper- or hypomethylated DMRs in their promoters with genes differentially expressed in TOF. Hyper- and hypomethylated promoters are significantly associated with down-regulated (p-value = 0.01) and up-regulated (p-value = 7.2×10^{-5}) gene expression, respectively. In contrast, the overlap between hypermethylated promoters and up-regulated or hypomethylated promoters and down-regulated gene expression is not significant. Investigating DNA methylation in gene bodies (without first exons), we only found a significant overlap between up-regulated genes with hypomethylated exons (S7 Fig.; p-value = 0.02). This holds true for up-regulated genes near hypomethylated cardiac enhancers (S8 Fig p-value = 0.008).

Except for cardiac enhancers, significant GO terms and KEGG/Reactome pathways could be identified for up- or down-regulated genes with hyper- or hypomethylated promoters (Fig. 4A) and/or exons (S7 Fig.). Most interestingly, one of the down-regulated genes that shows a hypermethylated promoter is the *ECE2* gene coding for endothelin converting enzyme 2, which is known to play a role in heart development (Fig. 4B) [27]. Moreover, up-regulated genes with hypomethylated promoters are enriched for GO terms involved in developmental processes such as 'muscle tissue development' (Fig. 4A). Two examples are the receptor gene *TDGF1* (Fig. 4C) and the troponin gene *TNNI1*. *TDGF1* encodes the teratocarcinoma-derived growth factor 1, which is a co-

receptor in NODAL signaling [28]. The slow, skeletal troponin I type 1 protein is encoded by *TNNI1* and is the inhibitory subunit of the troponin complex, blocking actin-myosin interactions.

DNA methylation and differential splicing in TOF patients

DNA methylation was recently shown to impact on alternative splicing [1,29,30], which in turn has been identified in different cardiac disorders [2,31]. However, a link between DNA methylation and alternative splicing has not been demonstrated in cardiac diseases so far. Thus, we further focused on splicing changes found in the TOF cohort. From our mRNA-seq data, we identified novel alternative splicing events in the TOF patients by considering those junctions that are supported by at least ten mapped reads on average over all samples in TOF and/or NH-rv. In total, we found 214 novel splice junctions in 163 autosomal, protein-coding genes (S9 Table). Of these genes, 18% (27/163) show a significantly differential expression of the novel splice site. Among them, we could identify several sarcomeric genes, such as *TNNI1,* myosin light chain 7 (*MYL7*), PDZ and LIM domain 3 (*PDLIM3*) and cardiac troponin T (*TNNT2*). Moreover, 33% (54/163) harbor DMRs in their gene bodies. We did not identify rare, damaging local variations in genes with novel, differential splice sites [2,20]. Searching for similar gene expression data using ExpressionBlast [3,32] revealed alternative splicing of sarcomere genes associated with heart failure [4,31] to be among the most similar datasets.

In *TNNI1*, a DMR was identified that is located over the novel splice junction (Fig. 5A), which leads to a premature termination of translation due to a frameshift and could be validated by reverse transcription PCR and sequencing (Fig. 5C). Again, we validated and replicated the methylation level of the DMR summit by PacBio sequencing and identified a significantly lower methylation level in both TOF cohorts compared to the controls (on average 67% in the first TOF cohort and 62% in the second TOF cohort versus 88% in NH-rv) (Fig. 5B).

Since splicing of sarcomeric genes is altered in patients with different cardiovascular diseases [5,6,31,33], we assessed the methylation patterns of further sarcomeric genes with significantly differentially expressed novel splice sites to identify differentially methylated regions with less CpGs as defined in our stringent set of DMRs. For *MYL7*, we could identify a region of four CpGs, which is located within the novel splice site and shows a significant hypermethylation in TOF patients (34% mean methylation in TOF vs. 11% in NH-rv; p-value < 0.009). The splice site leads to a frameshift in the second EF-hand domain and a premature termination of the protein (S9A Fig.). In *PDLIM3*, we found a peak comprising three CpGs over the novel splice site, which also shows a significant hypermethylation in TOF patients (88% mean methylation in TOF vs.

28% in NH-rv; p-value < 2.8 x 10^{-5}). The splice site leads to an in-frame deletion of the ZASP domain (S9B Fig.). Finally, *TNNT2* shows a hypomethylated region of five CpGs within one of the novel splice sites, which leads to the deletion of 15 amino acids (44% mean methylation in TOF vs. 87% in NH-rv; p-value < 2.1 x 10^{-8}; S9C Fig.).

Interaction of genes with DMRs in TOF patients and genes mutated in CHD patients

Based on 52 mutated genes in CHD patients [8,9,34] and our up- or down regulated genes with hypo- or hypermethylated promoters (34 genes), respectively, as well as differentially expressed genes with differentially methylated exons/enhancers (77 genes and 15 genes, respectively), we constructed a network for TOF based on known and predicted protein-protein interactions using the STRING database [10,11,35]. All overlapping genes between differentially methylated exons or enhancers and differential expression were included in the input because the function of DNA methylation is not yet well explored for both genomic features [4,12,13]. Fig. 6 shows the resulting network with 50 (96%) connected mutated CHD genes, 8 (24%) connected genes with promoter DMRs, 4 (27%) connected genes near enhancer DMRs and 27 (35%) connected genes with gene body DMRs. In contrast to the mutated CHD genes, which comprise a higher number of transcriptional regulators (transcription factors and histone modifications), the connected genes with DMRs consist mainly of downstream targets and components of signaling cascades. This is also reflected by the location of these genes within the network and their connections to mutated CHD genes of different functional classes.

Interestingly, only three out of the genes mutated in CHD patients are significantly differentially expressed in TOF (*TDGF1*, *GATA6*, *PDGFRA*), while 13 of the genes are significantly differentially methylated in their promoters, gene bodies or enhancers. Two of the mutated genes (*PDGFRA* and *TDGF1*) are both significantly differentially methylated and expressed. In general, we found significantly more mutated CHD genes with DMRs in TOF patients compared to all autosomal, protein-coding genes (p-value = 0.001). Note that for VSD, this overlap (4/52 mutated CHD genes) is not significant (p-value = 0.26).

Discussion

We analyzed genome-wide DNA methylation levels in myocardial biopsies of TOF and VSD patients. Compared to respective normal heart samples, we identified much more hypermethylated than hypomethylated regions for both patient groups, consistent with previous findings for TOF [13-15]. Moreover, we found differences in the DNA

methylation pattern between TOF and VSD that are not only based on the tissue type (Fig. 1). Both diseases have already been shown to be associated with distinct gene expression patterns [16,17,19], which is known to be influenced by DNA methylation.

To determine biologically relevant changes in the methylation levels, we defined a stringent set of differentially methylated regions for each patient group. We identified approximately 2-fold more DMRs in TOF vs. NH-rv compared to VSD vs. NH-ra (Table 1), which might be caused by secondary adaptions to changed hemodynamics in the right ventricle of the TOF heart. This is again reflected by previously obtained array-based expression data, which show 1.5-fold more differentially expressed genes in TOF vs. NH-rv than in VSD vs. NH-ra [18,19]. DMRs are significantly enriched for most analyzed genomic features, with hypomethylated DMRs tending to be much higher enriched than hypermethylated DMRs (Fig. 2). Interestingly, hypomethylated DMRs have a much higher CpG density (e.g. on average 17 CpGs in 497 bp compared to 16 CpGs in 1,678 bp for hypermethylated DMRs in TOF), which might be a reason for the higher enrichment especially in CpG islands. In general, a very low number of CGIs is associated with DMRs. However, we found much more CGI shores overlapping with DMRs, consistent with the occurrence of most tissue-specific DNA methylation in CGI shores [21,36].

When comparing CGIs overlapping DMRs in TOF and VSD, we found a hypermethylated DMR in the promoter of the *SCO2* gene (Fig. 3A and 3B). The expression of SCO2 was significantly reduced in both patient groups (Fig. 3C), indicating a role of promoter methylation in the gene's regulation. Moreover, we could demonstrate the region's regulatory impact by luciferase assay (Fig. 3D). *SCO2* encodes a cytochrome C oxidase assembly protein and thus plays a role in the aerobic production of ATP across the inner mitochondrial membrane [22,37]. Moreover, it is a downstream mediator of p53, which modulates the balance between respiratory and glycolytic pathways. The disruption of *SCO2* in human cancer cells causes a metabolic switch toward glycolysis that is also seen in p53-deficient cells [22,38]. In the developing heart, a glycolytic metabolism maintains the cardiomyocytes in a more proliferative state, while mitochondrial oxidation results in a switch to terminal differentiation [23,39]. Interestingly, a similar metabolic switch to a more fetal phenotype is known to occur in adult hearts that are subject to hypertrophic stress [24,25,40], as also seen in our patients. Thus, the strong reduction of SCO2 expression could hint to a similar metabolic shift in the patient hearts. The functional relevance of *SCO2* in the heart is demonstrated by a recent study, which identified a severe cardiac phenotype, namely a dilated cardiomyopathy and reduced life span, in cardiac-specific knockdown of the *Drosophila SCO1* and *SCO2* homolog *scox* [20,23]. In addition, human mutations in *SCO2* have been identified in patients with fatal infantile encephalocardiomyopathy, which is characterized by hypertrophic

cardiomyopathy, lactic acidosis, and gliosis. Remarkably, the strongest reduction in COX activity was found in the heart and skeletal muscle of these patients [26,41].

To correlate DNA methylation with gene expression changes in the TOF patients, we overlapped genes with DMRs in their promoters, exons or cardiac enhancers with significantly differentially expressed genes (Fig. 4A and S7 and S8 Figs.). In general, genome-wide DNA methylation studies revealed only a weak correlation between DNA methylation changes and differential gene expression [27,42-45]. When looking at our stringent set of DMRs and the significantly expressed genes, we found a significant overlap for hypermethylated promoters and down-regulated genes as well as for hypomethylated promoters and up-regulated genes. However, the opposite comparison revealed no significant overlap. This finding is in line with previous studies showing a negative correlation of promoter methylation and gene expression [4,28,46]. In contrast, DNA methylation in gene bodies and cardiac enhancers only show a significant overlap between up-regulated genes and DNA hypomethylation. The biological relevance of this finding is unclear so far, since the role of DNA methylation is currently less well understood for both genomic features [4].

One example for a significantly down-regulated gene with a hypermethylated promoter is *ECE2* (Fig. 4B), encoding endothelin converting enzyme 2. Disruption of the gene in mice causes severe disturbance of cardiac development; for example, resulting in abnormal heart valve morphology, double outlet right ventricle and VSD [27]. The ECE2 substrate endothelin is a paracrine factor thought to be important in patterning cardiac neural crest cell derivatives [47] and regulates the expression of the transcription factor HAND2 [48]. Its important role in development is demonstrated by a complex phenotype resembling DiGeorge syndrome in knockout mice [49]. Among the significantly up-regulated genes with a hypomethylated promoter, we found *TDGF1* (Fig. 4C) and *TNNI1* (Fig. 5A). The co-receptor TDGF1 is involved in NODAL signaling and thus, plays a role in a variety of developmental processes [28]. Its expression is regulated by the cardiac transcription factor NKX2.5 [50]. Knockout of *Tdgf1* in mice disrupts the formation of the precardiac mesoderm and prevents the formation of functional cardiomyocytes [51-53]. Finally, *TDGF1* had been found to be affected by missense variations in TOF and VSD patients [54,55].

TNNI1 encodes the slow skeletal inhibitory subunit of the troponin complex. Besides reduced expression of the gene, we found a differentially expressed novel splice junction that overlaps with the identified DMR in the promoter of *TNNI1* (Fig. 5A). In addition, we identified further novel, differential alternative splicing events in several other sarcomeric genes. Assessment of these genes revealed smaller differentially methylated regions, which were located over the novel splice junctions of *MYL7*, *PDLIM3* and *TNNT2*,

in addition to our stringent set of DMRs (S9 Fig.). Splicing of sarcomeric genes has already been shown to be significantly altered in patients with ischemic cardiomyopathy, dilated cardiomyopathy and aortic stenosis [31]. In a large study of patients with dilated cardiomyopathy, a significant number of splice site and truncating mutations were found in the sarcomere gene *TTN* encoding titin [56]. Moreover, several RNA-binding proteins playing a role in mRNA or microRNA biogenesis have been linked with syndromes characterized by CHDs [57]. In CHD patients, cardiac troponin T isoform expression is modulated by heart failure and is increased in hearts that are more hemodynamically stressed [58]. Alternative splicing has recently been shown to be regulated by DNA methylation, which can affect exon recognition [29,30]. Recent studies showed that DNA methylation can either enhance or suppress the recognition of alternative exons in a context-specific manner and seems to play a more subtle fine-tuning role [59,60]. In general, two main mechanisms could transmit the information of the DNA methylation level to the splicing of the transcribed RNA, namely the alteration of the Pol II elongation rate (by the CTCF and MeCP2 proteins) and the recruitment of splicing factors from the DNA to the mRNA precursor (by the HP1 protein) [61]. Taken together, our results for *TNNI1* and other sarcomeric genes indicate that aberrant splicing might be associated with methylation changes in the TOF patients, presenting a first link between alternative splicing and DNA methylation in cardiac disease.

To validate the results obtained by genome-wide MBD-seq, we performed targeted PacBio sequencing of bisulfite converted genomic DNA for two selected regions, namely the DMR summits of *SCO2* and *TNNI1*. *SCO2* was chosen for validation due to its hypermethylated DMR in the gene promoter (located in a CpG island) in both TOF and VSD cases and the significant down-regulation of gene expression (qPCR). *TNNI1*, on the other hand, shows a hypomethylated DMR in the gene promoter as well as body (located over a novel splice site) in the TOF cases and was found to be significantly up-regulated (RNA-seq). In addition, both genes are of potential functional interest in CHD, as they play a role in cardiac energy metabolism and the sarcomere, respectively. For both regions, we could validate the significant DNA methylation difference between cases and controls. Moreover, we were able to replicate the results with a second independent cohort of nine TOF patients, and additional two controls and PS cases. To our knowledge, this is the first application of PacBio sequencing for the targeted analysis of bisulfite converted DNA, providing a fast and efficient method for the identification of DNA methylation. In general, methylation levels measured from bisulfite converted DNA tended to be higher than those obtained from MBD-seq. While proteins containing the methyl-CpG binding domain do not bind to 5-hydroxymethylcytosine, techniques based on the bisulfite conversion of DNA cannot distinguish between the two modifications [62]. Although the heart contains a

relatively low level of 5-hmC compared to other tissues [63], this additional detection of 5-hmC could partly explain the higher methylation level measured in bisulfite converted DNA. As 5-hydroxymethylation has also been recognized as a regulator of gene expression, future studies should separately capture both modifications to understand their individual impact and possible interplay.

Finally, we constructed an interaction network for TOF based on known mutated genes in CHD patients and our differentially methylated and expressed genes (Fig. 6). In this network, a high number of our genes of interest could be linked to the mutated CHD genes, which suggests that the genes are involved in similar molecular pathways. Overall, the mutated CHD genes comprise a high number of transcriptional regulators, which is also underlined by the marked excess of *de novo* mutations found in histone-modifying enzymes in a large study of CHD patients [64]. In contrast, the differentially expressed genes with differentially methylated regions consist mainly of downstream targets and signaling molecules. This supports the hypothesis that CHD is caused by genomic variations that lead to disturbances of downstream molecular networks [20]. Moreover, the mutated CHD genes themselves also show a significant association with DMRs. This illustrates that these genes, besides their genomic variations, also show remarkable changes in their DNA methylation.

In general, we used a very stringent filtering approach (with at least 10 CpGs and 30% methylation change) for DMRs to identify the most biologically relevant changes. The methylation of single CpGs can, for example, influence the binding of transcription factors or other regulatory proteins, but larger differentially methylated regions containing several CpGs might lead to more biologically significant changes. However, this stringent filtering can also lead to the loss of potentially interesting regions, which contain a smaller number of CpGs or show smaller methylation differences between patients and controls (for example for novel splice sites in sarcomeric genes). The detection of methylation changes in cardiac myocytes can, in addition, be impeded by the mixed population of cell types present in myocardial biopsies; however, we analyzed well-defined, previously characterized and homogeneous samples [19,65]. To account for age differences, we excluded DMR-associated genes whose methylation is changed during aging using the information from two enrichment-based DNA methylation studies [24,25] and added age-matched controls in the replication face of which only reduced material was available. However, the overlap of our DMR-associated and the age-related genes was very low, indicating that we have identified a functionally different group of genes. Bases on our results, the next step are functional studies evaluating the impact of observed DMRs as well as possible pathological effects of alternative splicing events. As shown for SCO2,

the identified DMRs could represent so far unknown regulatory regions, which have an effect on gene expression.

In summary, we examined DNA methylation in myocardial biopsies of TOF and VSD patients. We found clear methylation differences in comparison to respective normal heart samples and moreover, between both patients groups. In contrast to previous methylation studies in CHD tissue [10-13], we searched in a genome-wide manner for differentially methylated regions using stringent statistics. We were further able to correlate DNA methylation with gene expression in the TOF patients. Most interestingly, we also identified examples of novel, differential splicing events co-localized with methylation changes and a novel cardiac element in promoter CGI. Finally, we created an interaction network linking genes affected by DNA methylation and expression changes in TOF as well as genes affected by genomic variations in CHD patients. Taken together, our data suggest that DNA methylation can be indicative of disease state. A high number of mutated CHD genes constitute transcriptional regulators, which might result in the disturbance of molecular networks demonstrated by differential expression/splicing and also methylation of downstream targets and signaling molecules. Moreover, epigenetic mechanisms such as DNA methylation constitute a possible pathway through which environmental influences (e.g. folic acid insufficiency) could impact on heart development and thus modulate the phenotype of cardiac malformations. As epigenetic modifications represent potential drug targets that could be used to change the patient's profile to a more favorable status, understanding these changes will hopefully guide the development of novel preventive and therapeutic strategies such that differences in long-term clinical outcome of patients could be addressed, which is the clinical imperative.

Materials and Methods

Ethics statement

Studies on patients were performed according to the institutional guidelines of the German Heart Institute in Berlin, with approval of the ethics committee of the Charité - Universitätsmedizin Berlin and written informed consent of patients and/or parents, kin, caretakers, or guardians on behalf of the minor/children participants involved in our study.

Samples

MBD-seq was performed for eight patients with TOF and eight patients with VSD as well as for seven healthy controls. For selected CpGs, the DNA methylation was validated using PacBio sequencing of bisulfite treated genomic DNA in cases and controls. In addition, a second cohort of nine TOF patients, two controls and two PS cases

were used for replication (S1 Fig.). Homogeneous cohorts of sporadic patients without any additional cardiovascular or other abnormalities were selected based on our previous gene expression analysis and phenotypic evaluations [19,66]. Myocardial biopsies were taken from the right ventricle of TOF and PS patients and from the right atrium of VSD patients during the first corrective surgery as well as from normal human hearts during cardiac surgery after short-term cardioplegia. Tissue from normal human hearts was obtained from unmatched organ donors without cardiac diseases, where the hearts could not be transplanted because of organizational difficulties. Samples were collected in collaboration with the German Heart Institute in Berlin and directly snap-frozen in liquid nitrogen after excision and stored at -80°C. Genomic DNA from cardiac samples was extracted using phenol:chloroform:isoamyl alcohol (25:24:1) and treated with RNase A (Invitrogen, Carlsbad, California, USA) according to manufacturer's instructions. 500 ng of genomic DNA were applied for MBD-seq.

MBD-seq, read alignment and quality control

DNA fragmentation was performed on a Covaris S3 to obtain fragments with an average length of 200 bp. The fragment distribution was examined on a high sensitivity DNA chip. Methylated DNA was captured using the MethylCap kit (Diagenode AF-100-0048, Seraing (Ougrée), Belgium). The concentrations of the fragmented and captured DNA were determined on a Fluostar Optima plate reader (BMG Labtech, Offenburg, Germany) with the Quant-iTTN Picogreen dsDNA assay kit (Invitrogen P7589, Merelbeke, Belgium). Library preparation and amplification were performed according to the 'multiplexed paired-end ChIP protocol' (with modifications) including the indexes from the 'Multiplexing Sample Preparation Oligo Kit' (Illumina, San Diego, California, USA). The libraries (n=23) were 2 x 51 bp paired-end sequenced on an Illumina HiSeq 2000 platform. Base calling was performed with the Illumina Casava pipeline version 1.8.0. Initial sequencing quality assessment was based on data passing the Illumina Chastity filter. Subsequently, sequence reads containing adaptors and/or Phix control signals were removed. The second quality assessment was based on the remaining reads using the FASTQC quality control tool version 0.10.0 [67], which indicated a high per base quality bias to the 3' end of the reverse reads of the sample TOF-09. The quality plots demonstrated a low number of duplicated reads, with on average 83.8% of reads remaining after deduplication and a low variance of 3.2 between the samples (without the outlier TOF-09). Moreover, the majority of duplicated sequences corresponds to less or equal than three reads. Thus, we decided against removing duplicated reads for further analyses. DNA fragmentation, library preparation, sequencing and initial quality assessment were performed by NXT-DX (Gent, Belgium).

On average, sequencing of methylated DNA libraries resulted in 32.5 million read pairs per sample (S1 Table). The sequence reads were mapped to the human reference genome (GRCh37/hg19) using Bowtie version 0.12.9 [68]. The Bowtie parameters were set to zero mismatches in the seed (first 28 nucleotides). Only unique paired reads were retained and both fragments must be located within 400 bp of each other on the reference genome. On average, 61% of the reads per samples could be mapped to unique genomic locations (S1 Table). The number of CpGs in the mapped paired-end sequence reads per sample was analyzed to access the quality of the enrichment. This revealed a much higher CpG count for the sample TOF-09 in comparison to all other samples (S10 Fig.).

Genome-wide CpG methylation levels

Given the exact location of 26,752,702 autosomal CpGs in the human reference genome, a methylation score for each CpG site in each sample was calculated using BALM v1.0.1, which is based on the bi-asymmetric-Laplace model [69]. A threshold enrichment level of 0.99 was used.

As a global measurement, the reference genome was divided into 2,881,044 autosomal, non-overlapping consecutive 1-kb tiling regions and the mean CpG methylation level was calculated for all tiles in each sample (S2 Fig.). For outlier detection, a principle component analysis (PCA) was performed based on the mean methylation levels of autosomal 1-kb tiles over all samples (Fig. 1 and S11 Fig.). Based on this PCA, we identified the sample TOF-09 as an outlier clearly separated from the other samples and thus, it was excluded from further analysis (S11 Fig.).

Identification of differentially methylated regions (DMRs)

We compared the DNA methylation levels of each individual autosomal CpG between the two sample groups, i.e. TOF vs. NH-rv and VSD vs. NH-ra. Significantly higher DNA methylation levels at single CpGs in the cases or in the controls, respectively, were assessed by an unpaired one-sided t-test. To identify differentially methylated regions (DMRs), CpGs with a minimum mean methylation difference ≥ 10% were extended up- and downstream comprising all CpGs with changes in the same direction (i.e. either hyper- or hypomethylation) and with an absolute minimum difference of 10% in the mean methylation level between cases and controls.

Statistical significance for each DMR was assessed using a generalization of Fisher's method [70], which combines the one-sided p-values of all single CpGs in a region while accounting for linear correlations between neighboring CpGs [71]. P-values were corrected for multiple testing according to the Bonferroni method. We defined a

stringent set of DMRs with at least 10 CpGs and an adjusted p-value < 0.01 as well as an absolute difference in mean methylation ≥ 30% between the sample groups. The number of DMRs with ≥ 10 CpGs and ≥ 30% difference in the mean methylation corresponds to the 90% quantile over all DMRs for both TOF and VSD.

Overlap with genomic features

We obtained transcriptional start site (TSS), exon and intron coordinates for autosomal, protein-coding RefSeq genes as well as coordinates for autosomal CpG islands and transcription factor binding sites (TFBS) from the UCSC genome browser (hg19). Promoters were defined as 2 kb upstream and 500 bp downstream of the TSS [72]. Based on their relative CpG content, promoters were classified into three main groups: High-CpG promoters (HCP) contain a 500 bp window with a CpG observed vs. expected ratio > 0.75 and a GC content > 55%. Low-CpG promoters (LCP) do not contain a 500 bp window with a CpG observed vs. expected ratio > 0.48 and intermediate CpG promoters (ICPs) are neither HCPs nor LCPs [22]. CpG islands (CGIs) contain a minimum GC content of 0.5, a minimum length of 200 bp and a minimum CpG observed vs. expected ratio of 0.6 [73]. CGI shores were defined as 2 kb up- and downstream of a CpG island. TFBS (with 12.4% cardiac transcription factors based on different sources [20,74-76]) were predicted by the Transfac Matrix Database (v7.0) and conserved in the multiple alignment of human, mouse and rat. Cardiac enhancer regions were obtained from p300 ChIP-seq data of human adult and fetal hearts [21]. We calculated the fold enrichment of at least one bp overlapping DMRs (stringent set) compared to all initially identified regions for each genomic feature. Statistical significance was assessed using Fisher's exact test.

Gene expression analysis

For gene expression in TOF cases, we re-analyzed previously published mRNA-seq data gathered from right ventricles of 22 TOF cases as well as from right ventricles of four healthy individuals [20], including cases and controls also used for MBD-seq. Illumina sequencing (Genome Analyzer) of mRNA libraries on average produced 19 million single-end reads (36 bp) per sample [20] The reads were mapped to the human reference genome (hg19) using Tophat v2.0.11 [77,78] with Bowtie v2-2.2.1 [79], allowing at most 10 equally best hits and two mismatches per read. On average, 16 million reads per sample (83% of the total reads) were mapped to the reference genome (S7 Table). Approximately 13% of the mapped reads matched to multiple regions, i.e. 2-10 genomic locations. For transcript assembly and abundance estimation, Cufflinks v2.2.0 [77,78] was used with gene/transcript annotations from the UCSC genome browser (hg19, Illumina

iGenomes). Cufflinks measures gene/transcript abundances in fragments per kilobase of exon per million fragments mapped (FPKM) and revealed 21,282 genes and 38,810 transcripts with FPKM>0 in at least one sample. Based on the FPKM values of genes and transcripts, we performed a PCA over all samples (S12 Fig.). Based on this PCA, we identified the sample TOF-18 as clearly separated from the other samples in the second component and thus, it was excluded from further differential expression analysis. To identify differentially expressed genes in TOF cases versus controls (right ventricle), we used Cuffdiff v2.2.0 [77,78]. Genes with an adjusted p-value < 0.05 using the Benjamini-Hochberg method for controlling the false discovery rate were defined as significantly differentially expressed (S13 Fig. and S8 Table).

Novel splice junction detection is based on our previous analysis of the RNA-seq data (reference genome and gene annotations based on hg18). It is based on mapping of all unmapped reads to known exons or splice junctions to a set of candidate novel splice junctions, which correspond to all hypothetical additional 5' to 3' pairings in the same set of genes. Searching for novel splice junctions with more than 10 mapped reads on average over all samples in TOF, NH-rv or both resulted in 214 genes with 163 novel alternative splice junctions (S9 Table).

Definition of genes with DMRs

For further analysis of DMRs, we considered autosomal, protein-coding genes with either hyper- or hypomethylated DMRs in their promoters or exons as well as genes near hyper- or hypomethylated cardiac enhancers (based on a nearest gene approach). Since DNA methylation is known to be age-dependent, we excluded DMR-associated genes whose methylation is changed during aging using the information from two studies that also applied enrichment-based determination of DNA methylation (MBD-seq and MeDIP, respectively) [24,25].

Overlap of genes with DMRs and differentially expressed genes in TOF

Statistical significance of the overlap between genes that contain either hyper- or hypomethylated DMRs in their promoters (with first exon), exons (without first exon) or cardiac enhancers with genes that are significantly differentially expressed was assessed using a hypergeometric test. Since DNA methylation of the first exon is also associated with transcriptional silencing [80], first exons were included in promoter regions. The background genes are all autosomal, protein-coding genes without genes known to play a role in aging [24,25] (n=18,815). For the overlap, differentially expressed genes in TOF

were also reduced to genes that are not known to play a role in aging, resulting in 373 up-regulated and 599 down-regulated genes in TOF vs. NH-rv.

Validation and replication of DNA methylation by targeted PacBio sequencing

500 ng of genomic DNA were bisulfite converted using the EZ DNA Methylation Startup Kit (Zymo Research, Irvine, California, USA). In a next step, regions of interest were amplified by PCR using barcoded primers specific to bisulfite treated DNA and the Zymo Taq PreMix (Zymo Research). The primers were designed using MethPrimer [81] to amplify the summit of the region of interest, covering four (*SCO2*) and three (*TNNI1*) CpG positions, respectively. The following primers were used: hSCO2_BC1_biDNA_f: AG-barcode-CCTTTTGGGTTTAAGGGATTTGTTT; hSCO2_BC1_biDNA_r: GT-barcode-GGAAAAACACTAATCAAAATTACTCATAAATCAC; hTNNI1 _BC1_biDNA_f: AG-barcode-CCTTAAGATAGAGATATTTTAAATATTATTTATTT; hTNNI1_BC1_biDNA_r: GT-barcode-GG ACTCACTATTATCACTAACCCCCTC. After pooling and cleanup with ChIP DNA Clean & Concentrator columns (Zymo Research), libraries for PacBio sequencing were prepared using a standard 250 bp template prep protocol, and sequenced using C2/P4 DNA preparation kit (Pacific Biosciences, USA). PacBio sequencing for PCR products was performed on PacBio RS system similar as described previously [82]. The reads of insert (ROI) were obtained by RS_ReadsOfInsert.1 protocol (SMRT Portal v2.3) (parameters: ‘Minimum Full Pass’ = 5 and ‘Minimum Predicted Accuracy’ = 99), and used for further analysis. Next, the 36 samples were demultiplexed using an in-house Perl script, which resulted in 67% of the total reads with an exact 5’ and 3’ barcode combination. The reads were then mapped to the regions of interest (C to T converted FASTA file) using RazerS v3.4 [83] with 90% identity and allowing unique matches only. On average, 98.6% of the reads could be uniquely mapped resulting in a minimum read coverage of 101x (on average 386x) over the seven CpGs over all 36 samples. T to C SNPs at the CpG positions were called using VarScan v2.3.7 [84] and the methylation level was identified on the proportion of C to T conversion. For statistical significance testing, a one-sided Wilcoxon test was performed between the cases and corresponding controls for each CpG in the two regions of interest.

Overrepresentation of gene ontologies and pathways

We used ConsensusPathDB-human (release 28), a meta-database of 32 public resources of biological interaction data comprising protein-protein, genetic, metabolic, signaling, gene regulatory and drug-target interactions in human [85,86]. For enrichment

analysis, a hypergeometric test was used to calculate the statistical significance of the overlap between the genes from our input lists (based on MBD-seq and/or mRNA-seq data) and the genes present in each reference gene ontology or KEGG/Reactome pathway target list. For genes with DMRs in their promoters and/or exons as well as for their overlap to differentially expressed genes, the background genes are all autosomal, protein-coding genes without those known to play a role in aging [24,25] (n=18,815). For genes with DMRs near cardiac enhancers as well as for their overlap to differentially expressed genes, the background genes are all autosomal, protein-coding genes near cardiac enhancers without those known to play a role in aging (n=3,235). For mRNA-seq data only, the background genes are all autosomal, protein-coding genes (n=18,877).

Network construction for TOF patients

The network of genes with DMRs in TOF patients and mutated genes in CHD patients was constructed using the STRING database v9.1 with default thresholds. STRING is based on known and predicted protein-protein interactions, which include direct (physical) and indirect (functional) associations from different sources such as genomic context, high-throughput experiments, (conserved) co-expression and previous knowledge (e.g. PubMed) [35]. As input we used 52 genes that are known to be mutated in CHD patients [34], up-regulated genes with hypomethylated promoters (8 genes), down-regulated genes with hypermethylated promoters (26 genes), differentially expressed genes with differentially methylated cardiac enhancers (15 genes) and differentially expressed genes with differentially methylated exons (77 genes) in TOF patients. Disconnected genes were removed from the network.

Reverse transcription PCR and quantitative real-time PCR

Total RNA from myocardial biopsies was isolated using TRIzol reagent (Invitrogen, Carlsbad, California, USA) followed by DNase digest (Promega, Fitchburg, Wisconsin, USA or Ambion, Carlsbad, California, USA) and ethanol precipitation according to standard protocols. Reverse transcription reactions were carried out using AMV-RT (Promega, Fitchburg, Wisconsin, USA) with random hexamers (Amersham Pharmacia Biotech, Amersham, UK). For detection of novel splice sites, PCR was performed with HotStar Taq Polymerase (Qiagen, Hilden, Germany) and analyzed by gel electrophoresis. Fragments were sent for Sanger sequencing at MWG Eurofins (Ebersberg, Germany). Quantitative real-time PCR measurements were performed using SYBR Green Master Mix (Thermo Scientific, Waltham, Massachusetts, USA) and the Light Cycler 480 II (Roche, Mannheim, Germany). Gene expression was calculated using the delta-CT

method with normalization to the housekeeping gene HPRT. Primer sequences are available on request.

Reporter gene assay

The *SCO2* promoter was cloned into the pGL3 basic reporter vector (Promega). For luciferase assays, approximately 10^4 HEK293 cells were transiently transfected with 50 ng of reporter vector and 5 ng of Renilla luciferase vector for internal normalization of transfection efficiency using Transfast (Promega). Activity was measured by Dual-Luciferase assay (Promega) after 48 hours in a Centro LB960 Luminometer (Berthold, Bad Wildbad, Germany). All measurements were performed in triplicates.

Statistics

General bioinformatics and statistical analyses were conducted using R (including Bioconductor packages) and Perl.

Data access

All MBD-seq data are available from the Gene Expression Omnibus (GEO) repository at NCBI (accession number GSE62629). RNA-seq data of TOF and NH-rv samples are also available from the GEO repository (accession number GSE36761).

Acknowledgments

We are deeply grateful to the patients and families for their cooperation. We thank Katharina Wassilew for providing age-matched control samples. We further thank Andreas Perrot for discussion and review of the manuscript. We also thank NXT-DX (Gent, Belgium) for MBD-based genome-wide methylation sequencing.

References

1. Marelli AJ, Ionescu-Ittu R, Mackie AS, Guo L, Dendukuri N, Kaouache M. Lifetime prevalence of congenital heart disease in the general population from 2000 to 2010. Circulation 2014;130:749–56.
2. Ferencz C, Rubin JD, McCarter RJ, Brenner JI, Neill CA, Perry LW, et al. Congenital heart disease: prevalence at livebirth. The Baltimore-Washington Infant Study. Am. J. Epidemiol. 1985;121:31–6.
3. Nora JJ. Multifactorial inheritance hypothesis for the etiology of congenital heart diseases. The genetic-environmental interaction. Circulation 1968;38:604–17.
4. Jones PA. Functions of DNA methylation: islands, start sites, gene bodies and beyond. Nat. Rev. Genet. 2012;13:484–92.

5. Robertson KD. DNA methylation and human disease. Nat. Rev. Genet. 2005;6:597–610.

6. Heyn H, Esteller M. DNA methylation profiling in the clinic: applications and challenges. Nat. Rev. Genet. 2012;13:679–92.

7. Zaina S, Heyn H, Carmona FJ, Varol N, Sayols S, Condom E, et al. DNA methylation map of human atherosclerosis. Circ Cardiovasc Genet 2014;7:692–700.

8. Movassagh M, Choy M-K, Knowles DA, Cordeddu L, Haider S, Down T, et al. Distinct epigenomic features in end-stage failing human hearts. Circulation 2011;124:2411–22.

9. Movassagh M, Choy M-K, Goddard M, Bennett MR, Down TA, Foo RS-Y. Differential DNA methylation correlates with differential expression of angiogenic factors in human heart failure. PLoS ONE 2010;5:e8564.

10. Zhu C, Yu Z-B, Chen X-H, Pan Y, Dong X-Y, Qian L-M, et al. Screening for differential methylation status in fetal myocardial tissue samples with ventricular septal defects by promoter methylation microarrays. Mol Med Rep 2011;4:137–43.

11. Zhu C, Yu Z-B, Chen X-H, Ji C-B, Qian L-M, Han S-P. DNA hypermethylation of the NOX5 gene in fetal ventricular septal defect. Exp Ther Med 2011;2:1011–5.

12. Sheng W, Wang H, Ma X, Qian Y, Zhang P, Wu Y, et al. LINE-1 methylation status and its association with tetralogy of fallot in infants. BMC Med Genomics 2012;5:20.

13. Sheng W, Qian Y, Zhang P, Wu Y, Wang H, Ma X, et al. Association of promoter methylation statuses of congenital heart defect candidate genes with Tetralogy of Fallot. J Transl Med 2014;12:31.

14. Hammer S, Toenjes M, Lange M, Fischer JJ, Dunkel I, Mebus S, et al. Characterization of TBX20 in human hearts and its regulation by TFAP2. J. Cell. Biochem. 2008;104:1022–33.

15. Bittel DC, Butler MG, Kibiryeva N, Marshall JA, Chen J, Lofland GK, et al. Gene expression in cardiac tissues from infants with idiopathic conotruncal defects. BMC Med Genomics 2011;4:1.

16. Chowdhury S, Erickson SW, MacLeod SL, Cleves MA, Hu P, Karim MA, et al. Maternal genome-wide DNA methylation patterns and congenital heart defects. PLoS ONE 2011;6:e16506.

17. Chowdhury S, Cleves MA, MacLeod SL, James SJ, Zhao W, Hobbs CA. Maternal DNA hypomethylation and congenital heart defects. Birth Defects Res. Part A Clin. Mol. Teratol. 2011;91:69–76.

18. Serre D, Lee BH, Ting AH. MBD-isolated Genome Sequencing provides a high-throughput and comprehensive survey of DNA methylation in the human genome. Nucleic Acids Res. 2010;38:391–9.

19. Kaynak B, Heydebreck von A, Mebus S, Seelow D, Hennig S, Vogel J, et al. Genome-wide array analysis of normal and malformed human hearts. Circulation 2003;107:2467–74.

20. Grunert M, Dorn C, Schueler M, Dunkel I, Schlesinger J, Mebus S, et al. Rare and private variations in neural crest, apoptosis and sarcomere genes define the polygenic background of isolated Tetralogy of Fallot. Hum. Mol. Genet. 2014;23:3115–28.

21. May D, Blow MJ, Kaplan T, McCulley DJ, Jensen BC, Akiyama JA, et al. Large-scale discovery of enhancers from human heart tissue. Nat. Genet. 2012;44:89–93.

22. Weber M, Hellmann I, Stadler MB, Ramos L, Pääbo S, Rebhan M, et al. Distribution, silencing potential and evolutionary impact of promoter DNA methylation in the human genome. Nat. Genet. 2007;39:457–66.

23. Martínez-Morentin L, Martínez L, Piloto S, Yang H, Schon EA, Garesse R, et al. Cardiac deficiency of single cytochrome oxidase assembly factor scox induces p53-dependent apoptosis in a Drosophila cardiomyopathy model. Hum. Mol. Genet. 2015;

24. McClay JL, Aberg KA, Clark SL, Nerella S, Kumar G, Xie LY, et al. A methylome-wide study of aging using massively parallel sequencing of the methyl-CpG-enriched genomic fraction from blood in over 700 subjects. Hum. Mol. Genet. 2014;23:1175–85.

25. Salpea P, Russanova VR, Hirai TH, Sourlingas TG, Sekeri-Pataryas KE, Romero R, et al. Postnatal development- and age-related changes in DNA-methylation patterns in the human genome. Nucleic Acids Res. 2012;40:6477–94.

26. Brade T, Männer J, Kühl M. The role of Wnt signalling in cardiac development and tissue remodelling in the mature heart. Cardiovasc. Res. 2006;72:198–209.

27. Yanagisawa H, Hammer RE, Richardson JA, Emoto N, Williams SC, Takeda SI, et al. Disruption of ECE-1 and ECE-2 reveals a role for endothelin-converting enzyme-2 in murine cardiac development. J. Clin. Invest. 2000;105:1373–82.

28. la Cruz de JM, Bamford RN, Burdine RD, Roessler E, Barkovich AJ, Donnai D, et al. A loss-of-function mutation in the CFC domain of TDGF1 is associated with human forebrain defects. Hum. Genet. 2002;110:422–8.

29. Wan J, Oliver VF, Zhu H, Zack DJ, Qian J, Merbs SL. Integrative analysis of tissue-specific methylation and alternative splicing identifies conserved transcription factor binding motifs. Nucleic Acids Res. 2013;41:8503–14.

30. Gelfman S, Cohen N, Yearim A, Ast G. DNA-methylation effect on cotranscriptional splicing is dependent on GC architecture of the exon-intron structure. Genome Res 2013;23:789–99.

31. Kong SW, Hu YW, Ho JWK, Ikeda S, Polster S, John R, et al. Heart failure-associated changes in RNA splicing of sarcomere genes. Circ Cardiovasc Genet 2010;3:138–46.

32. Zinman GE, Naiman S, Kanfi Y, Cohen H, Bar-Joseph Z. ExpressionBlast: mining large, unstructured expression databases. Nat. Methods 2013;10:925–6.

33. Zaina S, Heyn H, Carmona FJ, Varol N, Sayols S, Condom E, et al. A DNA Methylation Map of Human Atherosclerosis. Circ Cardiovasc Genet 2014;

34. Andersen TA, Troelsen K de LL, Larsen LA. Of mice and men: molecular genetics of congenital heart disease. Cell. Mol. Life Sci. 2014;71:1327–52.

35. Franceschini A, Szklarczyk D, Frankild S, Kuhn M, Simonovic M, Roth A, et al. STRING v9.1: protein-protein interaction networks, with increased coverage and integration. Nucleic Acids Res. 2013;41:D808–15.

36. Irizarry RA, Ladd-Acosta C, Wen B, Wu Z, Montano C, Onyango P, et al. The human colon cancer methylome shows similar hypo- and hypermethylation at conserved tissue-specific CpG island shores. Nat. Genet. 2009;41:178–86.

37. Stiburek L, Vesela K, Hansikova H, Pecina P, Tesarova M, Cerna L, et al. Tissue-specific cytochrome c oxidase assembly defects due to mutations in SCO2 and SURF1. Biochem. J. 2005;392:625–32.

38. Matoba S, Kang J-G, Patino WD, Wragg A, Boehm M, Gavrilova O, et al. p53

regulates mitochondrial respiration. Science 2006;312:1650–3.

39. Lopaschuk GD, Jaswal JS. Energy metabolic phenotype of the cardiomyocyte during development, differentiation, and postnatal maturation. J. Cardiovasc. Pharmacol. 2010;56:130–40.

40. Kolwicz SC, Tian R. Glucose metabolism and cardiac hypertrophy. Cardiovasc. Res. 2011;90:194–201.

41. Papadopoulou LC, Sue CM, Davidson MM, Tanji K, Nishino I, Sadlock JE, et al. Fatal infantile cardioencephalomyopathy with COX deficiency and mutations in SCO2, a COX assembly gene. Nat. Genet. 1999;23:333–7.

42. Koch CM, Wagner W. Epigenetic-aging-signature to determine age in different tissues. Aging (Albany NY) 2011;3:1018–27.

43. Xie L, Weichel B, Ohm JE, Zhang K. An integrative analysis of DNA methylation and RNA-Seq data for human heart, kidney and liver. BMC Syst Biol 2011;5 Suppl 3:S4.

44. Zykovich A, Hubbard A, Flynn JM, Tarnopolsky M, Fraga MF, Kerksick C, et al. Genome-wide DNA methylation changes with age in disease-free human skeletal muscle. Aging Cell 2014;13:360–6.

45. Fan S, Zhang X. CpG island methylation pattern in different human tissues and its correlation with gene expression. Biochem. Biophys. Res. Commun. 2009;383:421–5.

46. Schultz MD, He Y, Whitaker JW, Hariharan M, Mukamel EA, Leung D, et al. Human body epigenome maps reveal noncanonical DNA methylation variation. Nature 2015;523:212–6.

47. Hutson MR, Kirby ML. Neural crest and cardiovascular development: a 20-year perspective. Birth Defects Res. C Embryo Today 2003;69:2–13.

48. Thomas T, Kurihara H, Yamagishi H, Kurihara Y, Yazaki Y, Olson EN, et al. A signaling cascade involving endothelin-1, dHAND and msx1 regulates development of neural-crest-derived branchial arch mesenchyme. Development 1998;125:3005–14.

49. Kurihara Y, Kurihara H, Oda H, Maemura K, Nagai R, Ishikawa T, et al. Aortic arch malformations and ventricular septal defect in mice deficient in endothelin-1. J. Clin. Invest. 1995;96:293–300.

50. Behrens AN, Ren Y, Ferdous A, Garry DJ, Martin CM. Nkx2-5 Regulates Tdgf1 (Cripto) Early During Cardiac Development. J Clin Exp Cardiolog 2012;Suppl 11:1–4.

51. Xu C, Liguori G, Persico MG, Adamson ED. Abrogation of the Cripto gene in mouse leads to failure of postgastrulation morphogenesis and lack of differentiation of cardiomyocytes. Development 1999;126:483–94.

52. Ding J, Yang L, Yan YT, Chen A, Desai N, Wynshaw-Boris A, et al. Cripto is required for correct orientation of the anterior-posterior axis in the mouse embryo. Nature 1998;395:702–7.

53. D'Andrea D, Liguori GL, Le Good JA, Lonardo E, Andersson O, Constam DB, et al. Cripto promotes A-P axis specification independently of its stimulatory effect on Nodal autoinduction. J. Cell Biol. 2008;180:597–605.

54. Roessler E, Ouspenskaia MV, Karkera JD, Vélez JI, Kantipong A, Lacbawan F, et al. Reduced NODAL signaling strength via mutation of several pathway members including FOXH1 is linked to human heart defects and holoprosencephaly. Am. J.

Hum. Genet. 2008;83:18–29.

55. Wang B, Yan J, Peng Z, Wang J, Liu S, Xie X, et al. Teratocarcinoma-derived growth factor 1 (TDGF1) sequence variants in patients with congenital heart defect. Int. J. Cardiol. 2011;146:225–7.

56. Herman DS, Lam L, Taylor MRG, Wang L, Teekakirikul P, Christodoulou D, et al. Truncations of titin causing dilated cardiomyopathy. N. Engl. J. Med. 2012;366:619–28.

57. Blech-Hermoni Y, Ladd AN. RNA binding proteins in the regulation of heart development. Int. J. Biochem. Cell Biol. 2013;45:2467–78.

58. Saba Z, Nassar R, Ungerleider RM, Oakeley AE, Anderson PA. Cardiac troponin T isoform expression correlates with pathophysiological descriptors in patients who underwent corrective surgery for congenital heart disease. Circulation 1996;94:472–6.

59. Lev Maor G, Yearim A, Ast G. The alternative role of DNA methylation in splicing regulation. Trends Genet. 2015;

60. Yearim A, Gelfman S, Shayevitch R, Melcer S, Glaich O, Mallm J-P, et al. HP1 is involved in regulating the global impact of DNA methylation on alternative splicing. Cell Rep 2015;10:1122–34.

61. Lev Maor G, Yearim A, Ast G. The alternative role of DNA methylation in splicing regulation. Trends Genet. 2015;31:274–80.

62. Jin S-G, Kadam S, Pfeifer GP. Examination of the specificity of DNA methylation profiling techniques towards 5-methylcytosine and 5-hydroxymethylcytosine. Nucleic Acids Res. 2010;38:e125.

63. Li W, Liu M. Distribution of 5-hydroxymethylcytosine in different human tissues. J Nucleic Acids 2011;2011:870726.

64. Zaidi S, Choi M, Wakimoto H, Ma L, Jiang J, Overton JD, et al. De novo mutations in histone-modifying genes in congenital heart disease. Nature 2013;498:220–3.

65. Grunert M, Dorn C, Schueler M, Dunkel I, Schlesinger J, Mebus S, et al. Rare and private variations in neural crest, apoptosis and sacromere genes define the polygenic background of isolated Tetralogy of Fallot. Hum. Mol. Genet. 2013;:inpress.

66. Toenjes M, Schueler M, Hammer S, Pape UJ, Fischer JJ, Berger F, et al. Prediction of cardiac transcription networks based on molecular data and complex clinical phenotypes. Mol Biosyst 2008;4:589–98.

67. Andrews S. FASTQC: http://www.bioinformatics.babraham.ac.uk/projects/fastqc/

68. Langmead B, Trapnell C, Pop M, Salzberg SL. Ultrafast and memory-efficient alignment of short DNA sequences to the human genome. Genome Biol. 2009;10:R25.

69. Lan X, Adams C, Landers M, Dudas M, Krissinger D, Marnellos G, et al. High resolution detection and analysis of CpG dinucleotides methylation using MBD-Seq technology. PLoS ONE 2011;6:e22226.

70. Brown MB. 400: A method for combining non-independent, one-sided tests of significance. Biometrics 1975;

71. Bock C. Analysing and interpreting DNA methylation data. Nat. Rev. Genet. 2012;13:705–19.

72. Ziller MJ, Gu H, Müller F, Donaghey J, Tsai LT-Y, Kohlbacher O, et al. Charting a

dynamic DNA methylation landscape of the human genome. Nature 2013;500:477–81.

73. Gardiner-Garden M, Frommer M. CpG islands in vertebrate genomes. J. Mol. Biol. 1987;

74. Barriot R, Breckpot J, Thienpont B, Brohée S, Van Vooren S, Coessens B, et al. Collaboratively charting the gene-to-phenotype network of human congenital heart defects. Genome Med 2010;2:16.

75. Fahed AC, Gelb BD, Seidman JG, Seidman CE. Genetics of congenital heart disease: the glass half empty. Circ. Res. 2013;112:707–20.

76. McCulley DJ, Black BL. Transcription factor pathways and congenital heart disease. Curr. Top. Dev. Biol. 2012;100:253–77.

77. Trapnell C, Williams BA, Pertea G, Mortazavi A, Kwan G, van Baren MJ, et al. Transcript assembly and quantification by RNA-Seq reveals unannotated transcripts and isoform switching during cell differentiation. Nat. Biotechnol. 2010;28:511–5.

78. Trapnell C, Roberts A, Goff L, Pertea G, Kim D, Kelley DR, et al. Differential gene and transcript expression analysis of RNA-seq experiments with TopHat and Cufflinks. Nat Protoc 2012;7:562–78.

79. Ben Langmead, Salzberg SL. Fast gapped-read alignment with Bowtie 2. Nat. Methods 2012;9:357–9.

80. Brenet F, Moh M, Funk P, Feierstein E, Viale AJ, Socci ND, et al. DNA methylation of the first exon is tightly linked to transcriptional silencing. PLoS ONE 2011;6:e14524.

81. Li L-C, Dahiya R. MethPrimer: designing primers for methylation PCRs. Bioinformatics 2002;18:1427–31.

82. Sun W, You X, Gogol-Döring A, He H, Kise Y, Sohn M, et al. Ultra-deep profiling of alternatively spliced Drosophila Dscam isoforms by circularization-assisted multi-segment sequencing. EMBO J. 2013;32:2029–38.

83. Weese D, Holtgrewe M, Reinert K. RazerS 3: faster, fully sensitive read mapping. Bioinformatics 2012;28:2592–9.

84. Koboldt DC, Zhang Q, Larson DE, Shen D, McLellan MD, Lin L, et al. VarScan 2: somatic mutation and copy number alteration discovery in cancer by exome sequencing. Genome Res 2012;22:568–76.

85. Kamburov A, Pentchev K, Galicka H, Wierling C, Lehrach H, Herwig R. ConsensusPathDB: toward a more complete picture of cell biology. Nucleic Acids Res. 2011;39:D712–7.

86. Kamburov A, Stelzl U, Lehrach H, Herwig R. The ConsensusPathDB interaction database: 2013 update. Nucleic Acids Res. 2012;41:D793–D800.

Table

Table 1. Differentially methylation regions (DMRs). Mean diff: mean difference in the methylation levels; NH: normal heart; ra: right atrium; rv: right ventricle; TOF: Tetralogy of Fallot; VSD: ventriuclar septal defect.

		TOF vs. NH-rv		VSD vs. NH-ra	
	Number of regions	3.351.123		3.330.027	
Hypermethylated DMRs in cases versus controls	p<0.05	1.267.386	37,8%	1.082.493	32,5%
	q<0.05	72.860	2,2%	50.703	1,5%
	q<0.01 & 10% mean diff	57.124	1,7%	39.695	1,2%
	q<0.01 & 10% mean diff & >= 3 CpGs	57.116	1,7%	39.693	1,2%
	q<0.01 & 10% mean diff & >= 10 CpGs	46.105	1,4%	30.668	0,9%
	q<0.01 & 30% mean diff	21.187	0,6%	12.303	0,4%
	q<0.01 & 30% mean diff & >= 3 CpGs	21.181	0,6%	12.301	0,4%
	q<0.01 & 30% mean diff & >= 10 CpGs (stringent set)	***14.403***	***0,4%***	***7.152***	***0,2%***
Hypomethylated DMRs in cases versus controls	p<0.05	348.913	10,4%	356.940	10,7%
	q<0.05	27.527	0,8%	19.281	0,6%
	q<0.01 & 10% mean diff	23.214	0,7%	16.109	0,5%
	q<0.01 & 10% mean diff & >= 3 CpGs	23.202	0,7%	16.103	0,5%
	q<0.01 & 10% mean diff & >= 10 CpGs	20.406	0,6%	14.518	0,4%
	q<0.01 & 30% mean diff	2.239	0,1%	1.323	0,0%
	q<0.01 & 30% mean diff & >= 3 CpGs	2.236	0,1%	1.318	0,0%
	q<0.01 & 30% mean diff & >= 10 CpGs (stringent set)	***1.450***	***0,0%***	***935***	***0,0%***

Figure legends

Fig. 1. Principle component analysis for MBD-seq samples based on the mean methylation levels of human autosomal 1-kb tiles. (A) PCA with colored area indicating the different groups of samples except the outlier TOF-09. (B) PCA with colored area indicating the different tissue groups of samples except TOF-09. NH: normal heart; PCA: principle component analysis; ra: right atrium; rv: right ventricle; TOF: Tetralogy of Fallot; VSD: ventricular septal defect.

Fig. 2. Overlap of differentially methylated regions with genomic features. (A and C) The x-axis shows the proportion of genomic features (y-axis) overlapping with the stringent set of DMRs. Three groups of points are plotted: red circles correspond to all DMRs (15,853 in TOF vs. NH-rv and 8,087 in VSD vs. NH-ra), blue squares to hypermethylated DMRs (14,403 in TOF vs. NH-rv and 7,152 in VSD vs. NH-ra) and green triangles to hypomethylated DMRs (1,450 in TOF vs. NH-rv and 935 in VSD vs. NH-ra). Filled points show significant (p-value<0.05) enrichment compared to the genome-wide

average. (B and D) Percentage of differentially hyper- and hypomethylated regions (stringent set) overlapping genomic features with the absolute numbers of DMRs on top of the bars. An individual DMR can overlap with more than one genomic feature. CGI: CpG island; DMRs: differentially methylated regions; HCP: high-CpG promoter; ICP: intermediate-CpG promoter, LCP: low-CpG promoter; NH: normal heart; ra: right atrium; rv: right ventricle; TFBS: transcription factor binding site; TOF: Tetralogy of Fallot; VSD: ventricular septal defect.

Fig. 3. Methylation and expression of *SCO2*. (A) Methylation of *SCO2* gene body and promoter region in TOF, VSD and respective normal hearts. Each dot indicates a single CpG. All protein-coding transcripts are given with their transcription start site marked by grey arrows. Expressed transcripts in TOF and/or NH (RNA-seq) are marked by '#'. (B) Methylation level over the four CpG sites marking the DMR summit measured by PacBio sequencing of bisulfite converted DNA in both TOF cohorts and NH-rv as well as in VSD and NH-ra. CpG positions on chr22 are 50966685 (CpG 1), 50966723 (CpG 2), 50966730 (CpG 3) and 50966798 (CpG 4). Significance was tested by a one-sided Wilcoxon test. (C) Expression of SCO2 mRNA in TOF and VSD measured by quantitative real-time PCR. Expression was measured in triplicates and normalized to HPRT. TOF-18 and VSD-03 had to be removed from the analysis due to outlying results and insufficient RNA yield, respectively. Significance was tested by a two-sided t-test. (D) Luciferase assay for different *SCO2* promoter constructs, which are depicted in A. Luciferase signal was normalized to the Renilla signal. Significance was tested by a two-sided t-test. CGI: CpG island; DMR: differentially methylated region; NH: normal heart; ra: right atrium; rv: right ventricle; TOF: Tetralogy of Fallot; VSD: ventricular septal defect; w/o; without. * p-value < 0.05, ** p-value < 0.01.

Fig. 4. Overlap of genes with DMRs in promoters and differentially expressed genes in TOF. (A) Given is the overlap between autosomal, protein-coding genes that contain hyper- or hypomethylated DMRs in their promoters with genes that are up- or downregulated in TOF vs. NH-rv. A significant overlap (p-value < 0.05 based on hypergeometric test) is indicated by an asterisk. GO term and KEGG/Reactome enrichment analysis was performed for up-regulated genes with hypomethylated promoters and down-regulated genes with hypermethylated promoters. Significant GO terms and KEGG/Reactome pathways (p-value < 0.05 based on hypergeometric test) as well as related genes are given for biologically relevant overlaps. (B-C) Methylation in the gene body and promoter region of (B) ECE2 and (C) TDGF1. Each dot indicates a single CpG. Protein-coding transcripts are given with their transcription start site marked by grey arrows. DMRs: differentially methylated regions; BP: biological process (GO term); CC:

cellular component (GO term); CGI: CpG island; GO: gene ontology; MF: molecular function (GO term); NH: normal heart; rv: right ventricle; TOF: Tetralogy of Fallot.

Fig. 5. Novel splicing event and methylation in the gene body and promoter region of the sarcomeric gene TNNI1. (A) Mean methylation level over the gene body and promoter region measured by MBD-seq in the first TOF cohort and in NH-rv. Each dot indicates a single CpG. The protein-coding transcript is given with its transcription start site marked by a grey arrow. (B) Methylation level over the three CpG sites marking the DMR summit measured by PacBio sequencing of bisulfite converted DNA in both TOF cohorts and NH-rv. CpG positions on chr1 are 201386246 (CpG 1), 201386273 (CpG 2) and 201386328 (CpG 3). Significance was tested by a one-sided Wilcoxon test. (C) Indicated is the schematic representation of the transcript, the resulting protein and expression analysis for the splice junction (RT-PCR for representative samples and RNA-seq for all samples). Significance was tested by a two-sided t-test. CGI: CpG island; DMR: differentially methylated region; NH: normal heart; rv: right ventricle; TOF: Tetralogy of Fallot. ** p-value ≤ 0.01; *** p-value ≤ 0.001.

Fig. 6. Interconnection network based on genes with DMRs in TOF patients and CHD disease genes. The network is based on known and predicted protein-protein interactions using the STRING database. The input was based on 52 mutated CHD genes, up-regulated genes with hypomethylated promoters (n=8), down-regulated genes with hypermethylated promoters (n=26), differentially expressed genes with differentially methylated cardiac enhancers (n=15) and differentially expressed genes with differentially methylated exons (n=77). Disconnected genes were removed from the network. DMR: differentially methylated region (stringent set); CHD: congenital heart disease.

Figure 1

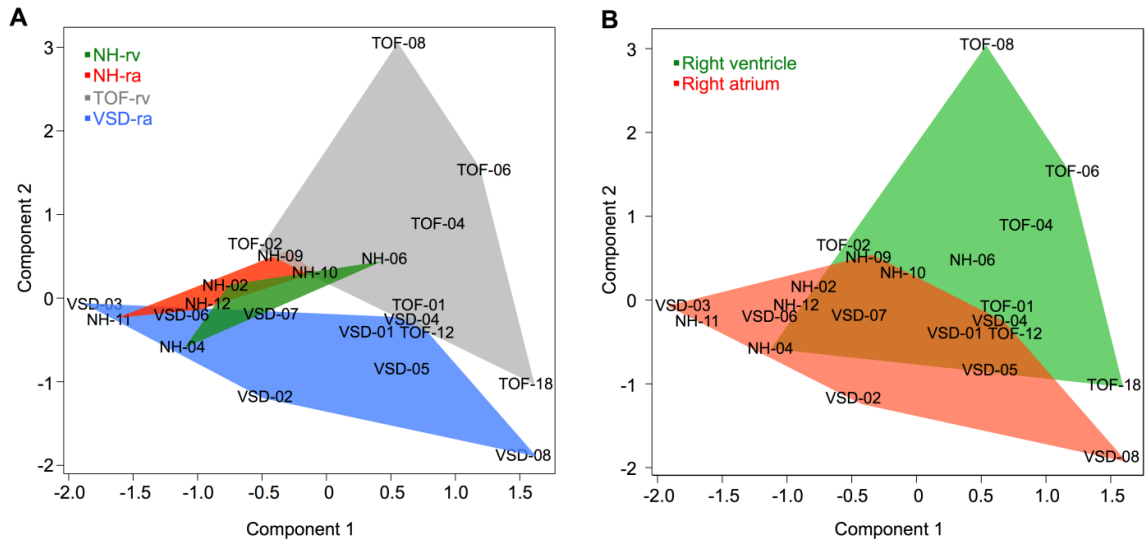

Figure 2

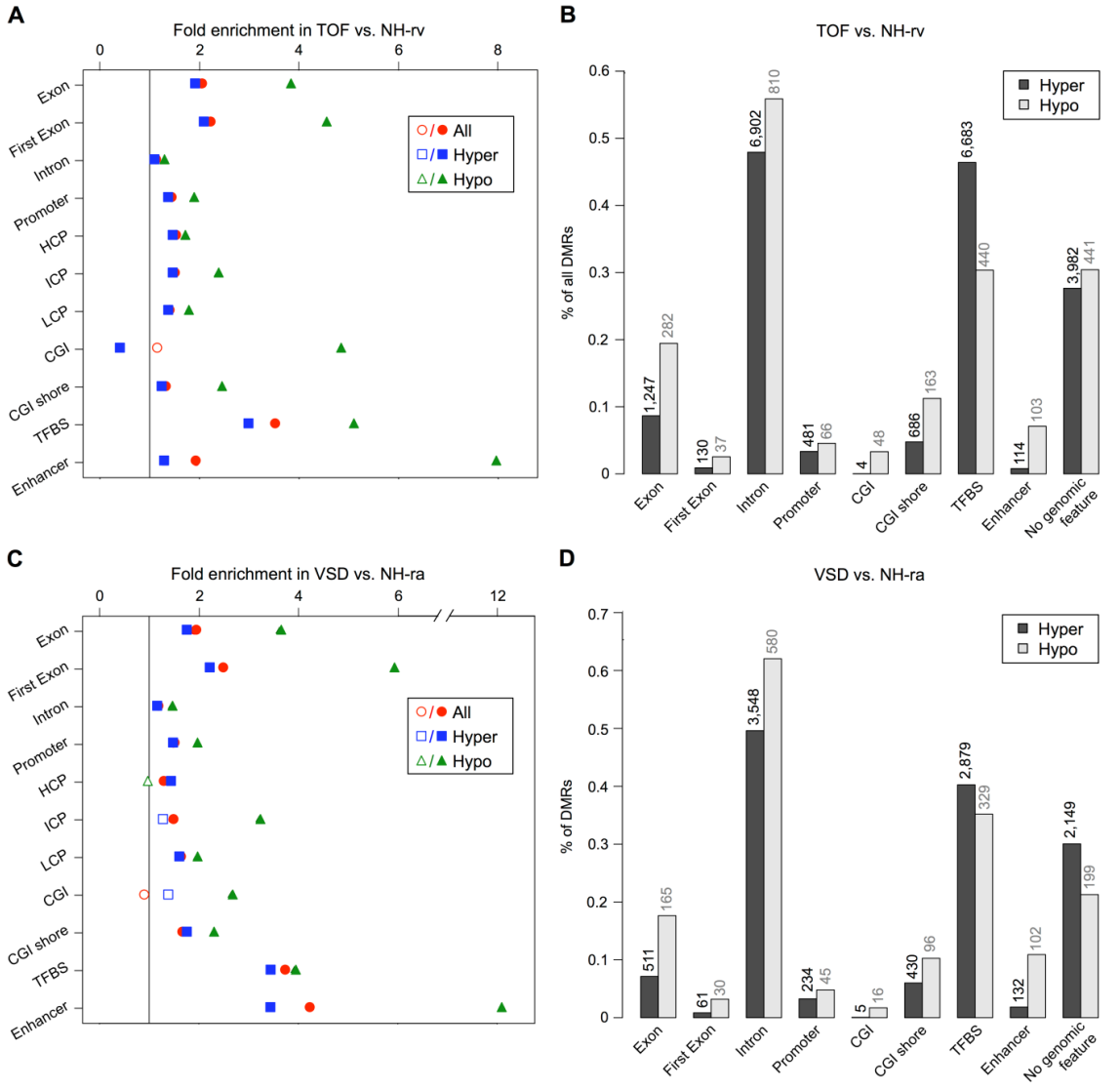

Figure 3

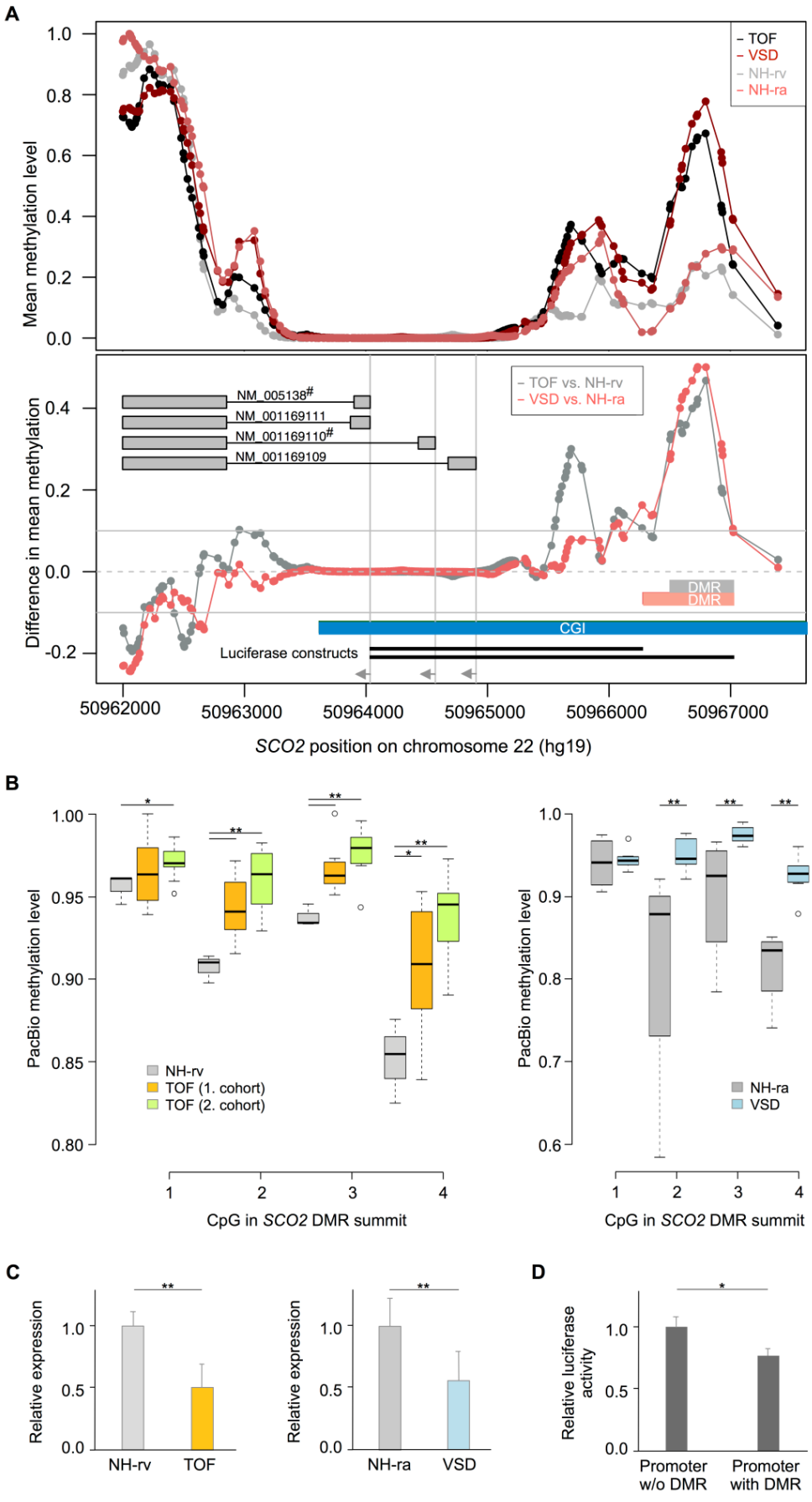
A
Mean methylation level
TOF
VSD
NH-rv
NH-ra
Difference in mean methylation
TOF vs. NH-rv
VSD vs. NH-ra
NM_005138#
NM_001169111
NM_001169110#
NM_001169109
DMR
DMR
CGI
Luciferase constructs
50962000
50963000
50964000
50965000
50966000
50967000
SCO2 position on chromosome 22 (hg19)
B
PacBio methylation level
NH-rv
TOF (1. cohort)
TOF (2. cohort)
CpG in SCO2 DMR summit
NH-ra
VSD
C
Relative expression
NH-rv
TOF
NH-ra
VSD
D
Relative luciferase activity
Promoter w/o DMR
Promoter with DMR

Figure 4

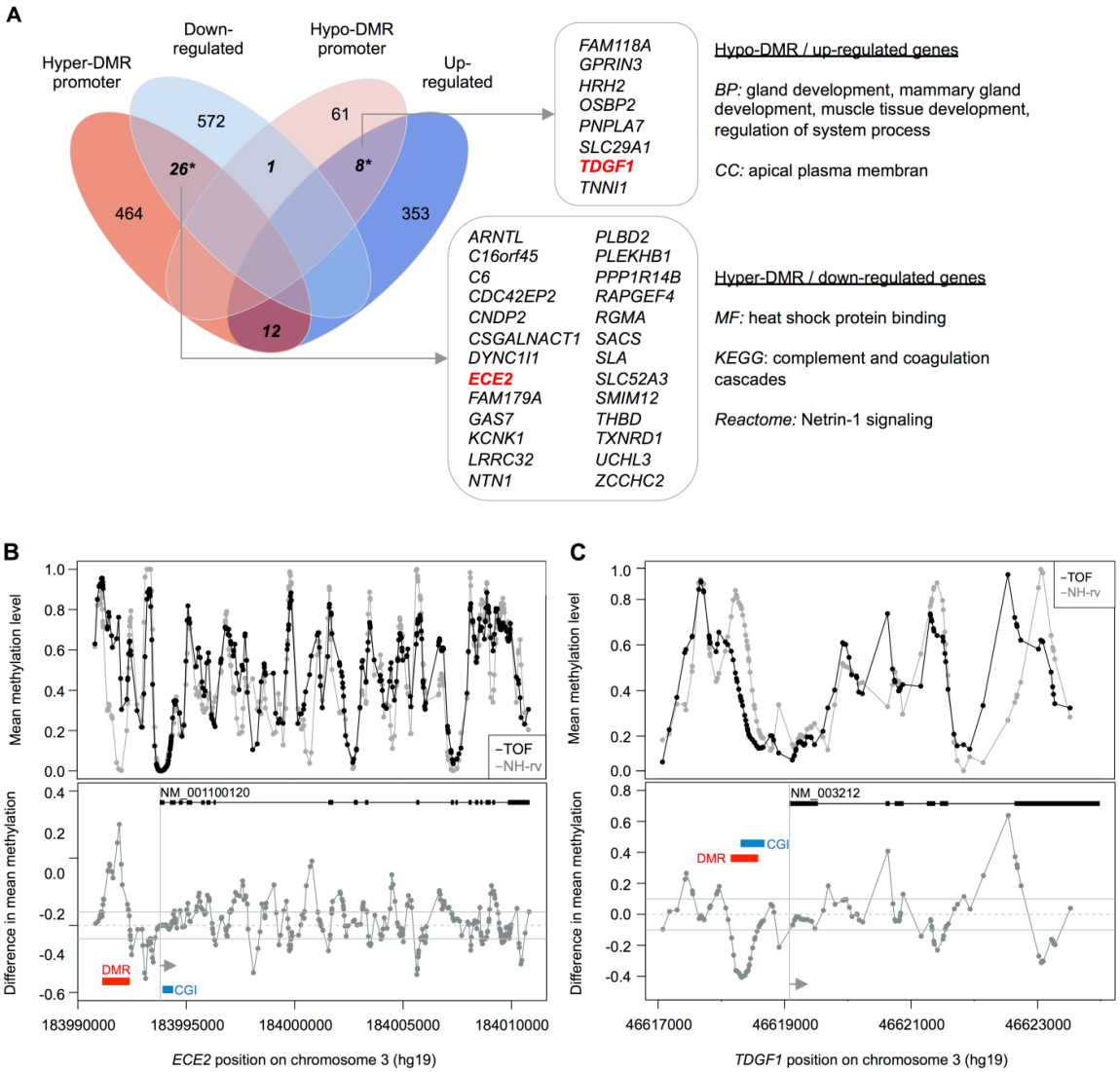
A
Hyper-DMR promoter
Down-regulated
Hypo-DMR promoter
Up-regulated
572
61
464
353
26*
1
8*
12
FAM118A
GPRIN3
HRH2
OSBP2
PNPLA7
SLC29A1
TDGF1
TNNI1
Hypo-DMR / up-regulated genes
BP: gland development, mammary gland development, muscle tissue development, regulation of system process
CC: apical plasma membran
ARNTL
C16orf45
C6
CDC42EP2
CNDP2
CSGALNACT1
DYNC1I1
ECE2
FAM179A
GAS7
KCNK1
LRRC32
NTN1
PLBD2
PLEKHB1
PPP1R14B
RAPGEF4
RGMA
SACS
SLA
SLC52A3
SMIM12
THBD
TXNRD1
UCHL3
ZCCHC2
Hyper-DMR / down-regulated genes
MF: heat shock protein binding
KEGG: complement and coagulation cascades
Reactome: Netrin-1 signaling
B
Mean methylation level
−TOF
−NH-rv
Difference in mean methylation
NM_001100120
DMR
CGI
183990000
183995000
184000000
184005000
184010000
ECE2 position on chromosome 3 (hg19)
C
Mean methylation level
−TOF
−NH-rv
Difference in mean methylation
NM_003212
DMR
CGI
46617000
46619000
46621000
46623000
TDGF1 position on chromosome 3 (hg19)

Figure 5

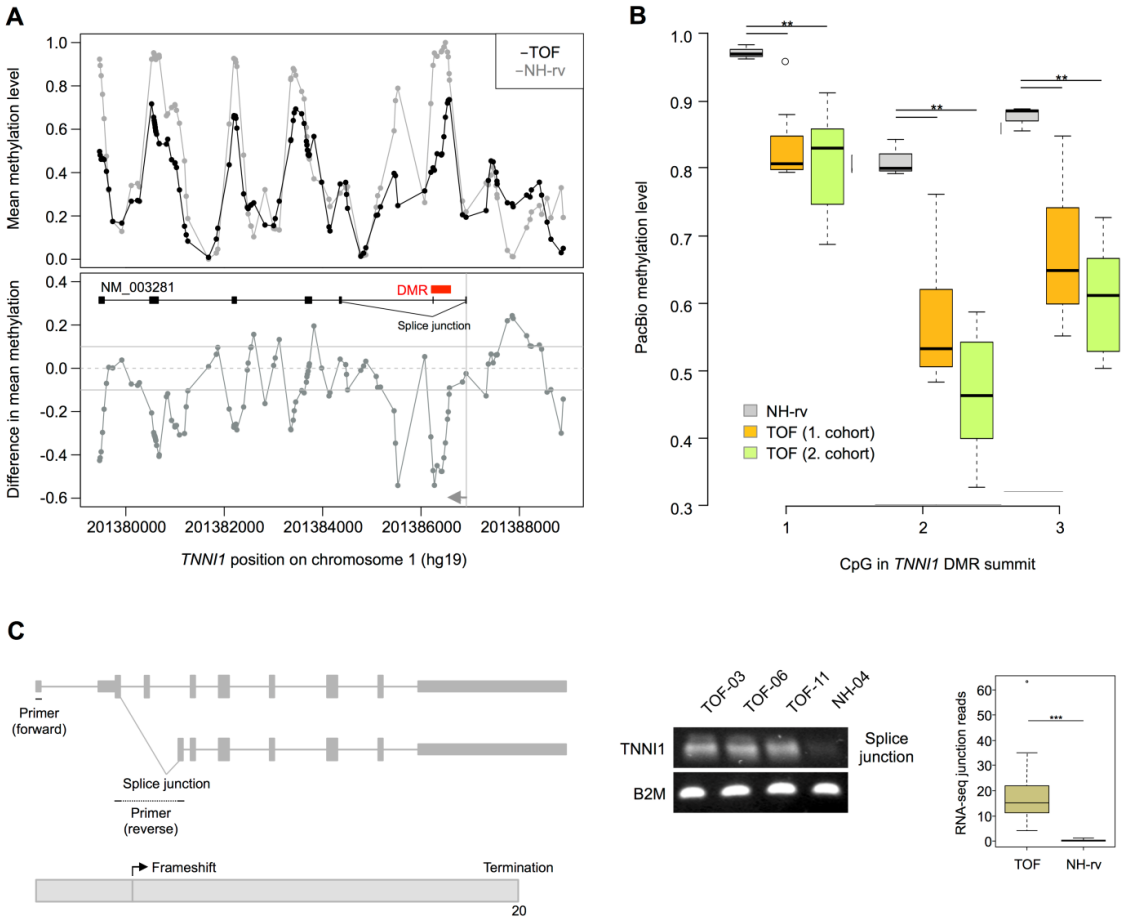
A
Mean methylation level
−TOF
−NH-rv
Difference in mean methylation
NM_003281
DMR
Splice junction
201380000
201382000
201384000
201386000
201388000
TNNI1 position on chromosome 1 (hg19)
B
PacBio methylation level
NH-rv
TOF (1. cohort)
TOF (2. cohort)
CpG in TNNI1 DMR summit
C
Primer (forward)
Splice junction
Primer (reverse)
Frameshift
Termination
20
TOF-03
TOF-06
TOF-11
NH-04
TNNI1
B2M
Splice junction
RNA-seq junction reads
TOF
NH-rv

Figure 6

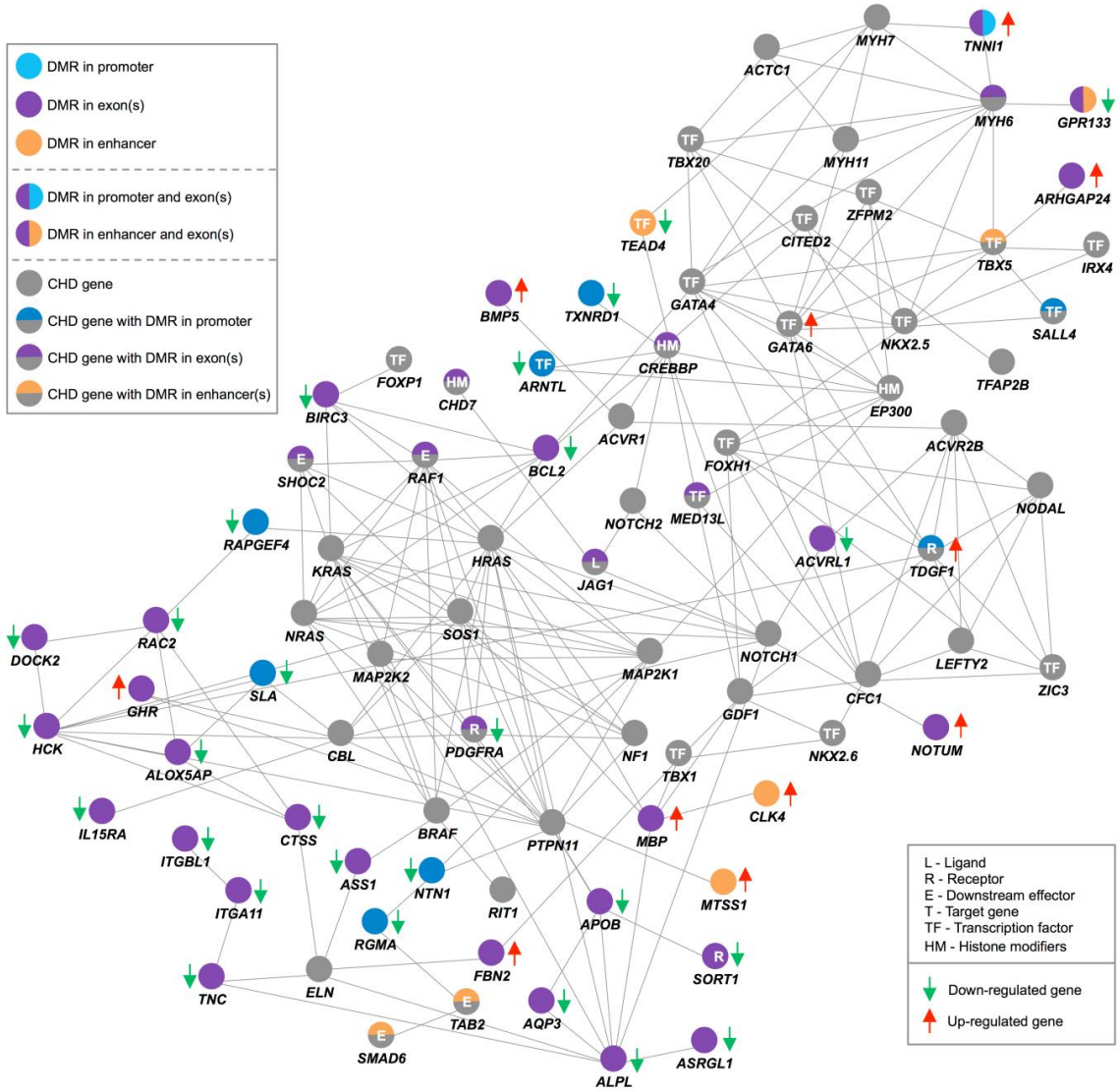
DMR in promoter
DMR in exon(s)
DMR in enhancer
DMR in promoter and exon(s)
DMR in enhancer and exon(s)
CHD gene
CHD gene with DMR in promoter
CHD gene with DMR in exon(s)
CHD gene with DMR in enhancer(s)
MYH7
TNNI1
ACTC1
MYH6
GPR133
TBX20
MYH11
ARHGAP24
ZFPM2
TEAD4
CITED2
TBX5
IRX4
GATA4
BMP5
TXNRD1
GATA6
NKX2.5
SALL4
FOXP1
CREBBP
ARNTL
TFAP2B
CHD7
BIRC3
EP300
ACVR1
ACVR2B
FOXH1
SHOC2
RAF1
BCL2
NODAL
NOTCH2
MED13L
RAPGEF4
KRAS
HRAS
JAG1
ACVRL1
TDGF1
NRAS
SOS1
DOCK2
RAC2
NOTCH1
LEFTY2
ZIC3
MAP2K2
MAP2K1
SLA
GHR
GDF1
CFC1
HCK
CBL
PDGFRA
NF1
NKX2.6
NOTUM
ALOX5AP
TBX1
CLK4
IL15RA
CTSS
BRAF
PTPN11
MBP
ITGBL1
ASS1
NTN1
MTSS1
ITGA11
RIT1
APOB
RGMA
FBN2
SORT1
TNC
ELN
TAB2
AQP3
SMAD6
ASRGL1
ALPL
L - Ligand
R - Receptor
E - Downstream effector
T - Target gene
TF - Transcription factor
HM - Histone modifiers
Down-regulated gene
Up-regulated gene

Supplementary Information

Supplemental Figure 1

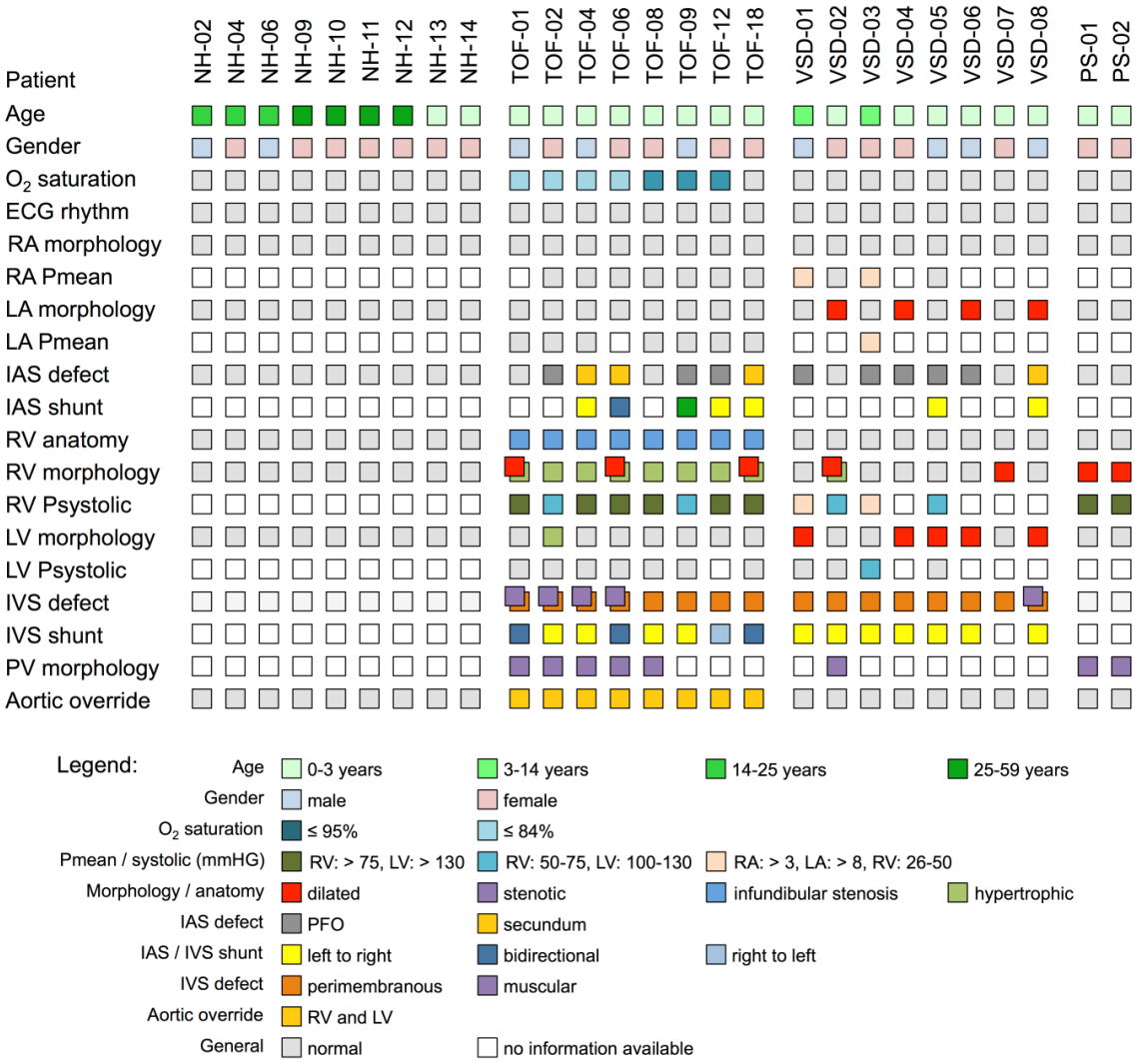

S1 Fig. Phenotype matrix for patients and healthy controls. Each individual is represented by one column. In addition to general information, all pathological features are indicated. Double boxes are used for more than one information per row. See legend for color-code information. ECG: electrocardiogram; IAS: intra-atrial septum; IVS: intra-ventricular septum; LA: left atrium; LV: left ventricle; NH: normal heart; PFO: patent foramen ovale; Pmean: mean pressure; Psystolic: systolic pressure; PV: pulmonary valve; PS: pulmonary valve stenosis, RA: right atrium; RV: right ventricle; TOF: Tetralogy of Fallot; VSD: ventricular septal defect.

Supplemental Figure 2

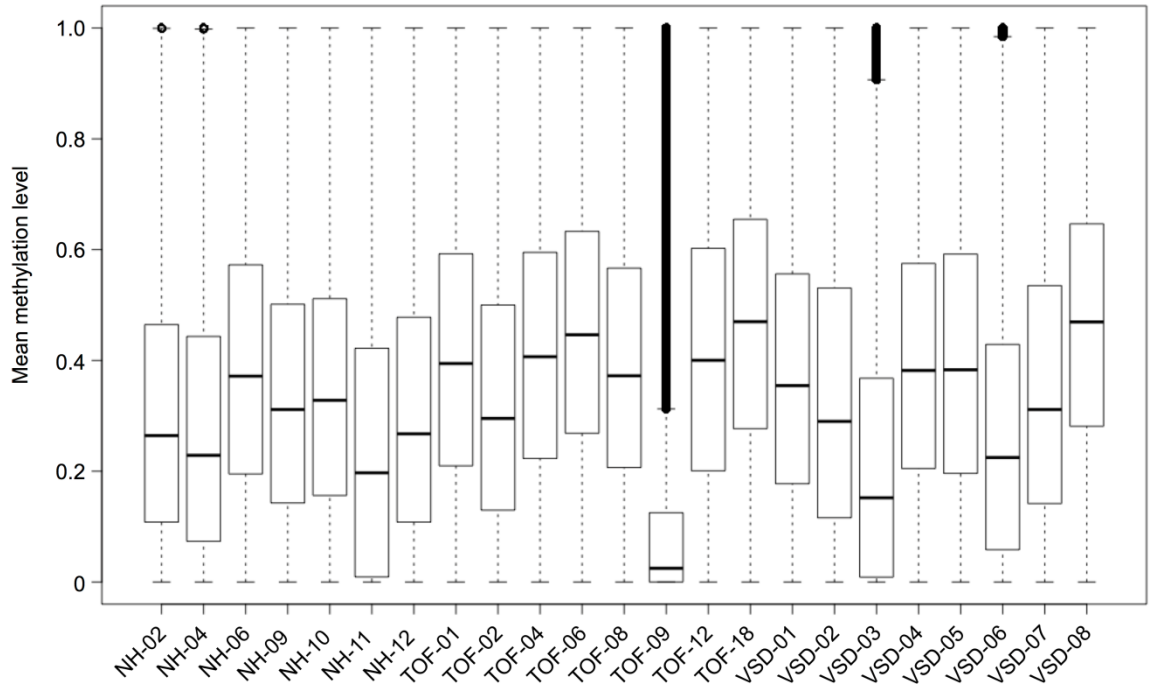

S2 Fig. Mean methylation level for each sample. The human reference genome (hg19) was divided into ~2,8 million non-overlapping consecutive 1-kb tiling regions (based on autosomes) and the mean CpG methylation level for all tiles in each sample was calculated. Normal heart samples from right ventricle are NH-02, NH-04 and NH-06. The sample TOF-09 represents an outlier as it is clearly separated from the other samples. Normal heart samples from right atrium are NH-09, NH-10, NH-11 and NH-12. NH: normal heart; TOF: Tetralogy of Fallot; VSD: ventricular septal defect.

Supplemental Figure 3

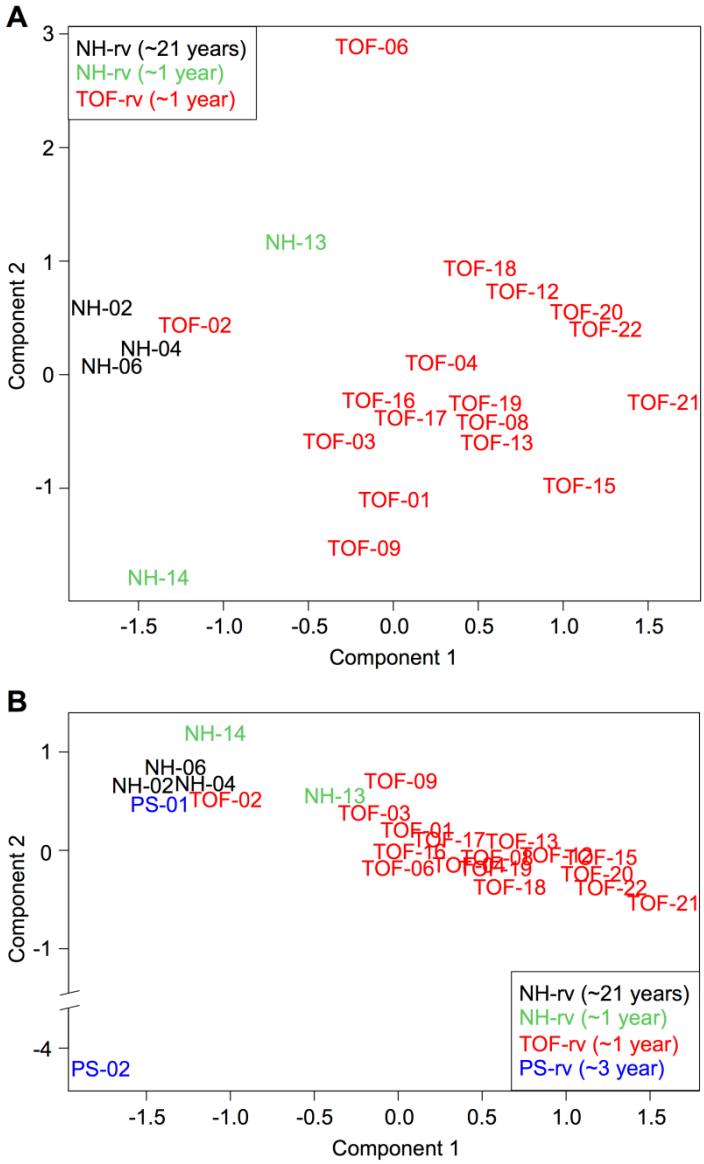

S3 Fig. Principle component analysis for PacBio methylation levels. The analysis is based on the DNA methylation level of seven CpGs in the DMR summits of SCO2 (4 CpGs) and TNNI1 (3 CpGs) measured by PacBio sequencing of bisulfite converted DNA. For each group, the average age over the related individuals is given in brackets. (A) PCA based on TOF samples (1. and 2.cohort) and normal heart samples obtained from the right ventricle. (B) PCA based on normal heart samples as well as from TOF (1.cohort and 2.cohort) and PS samples all obtained from the right ventricle. NH: normal heart; PCA: principle component analysis; PS: pulmonary valve stenosis; rv: right ventricle; TOF: Tetralogy of Fallot.

Supplemental Figure 4

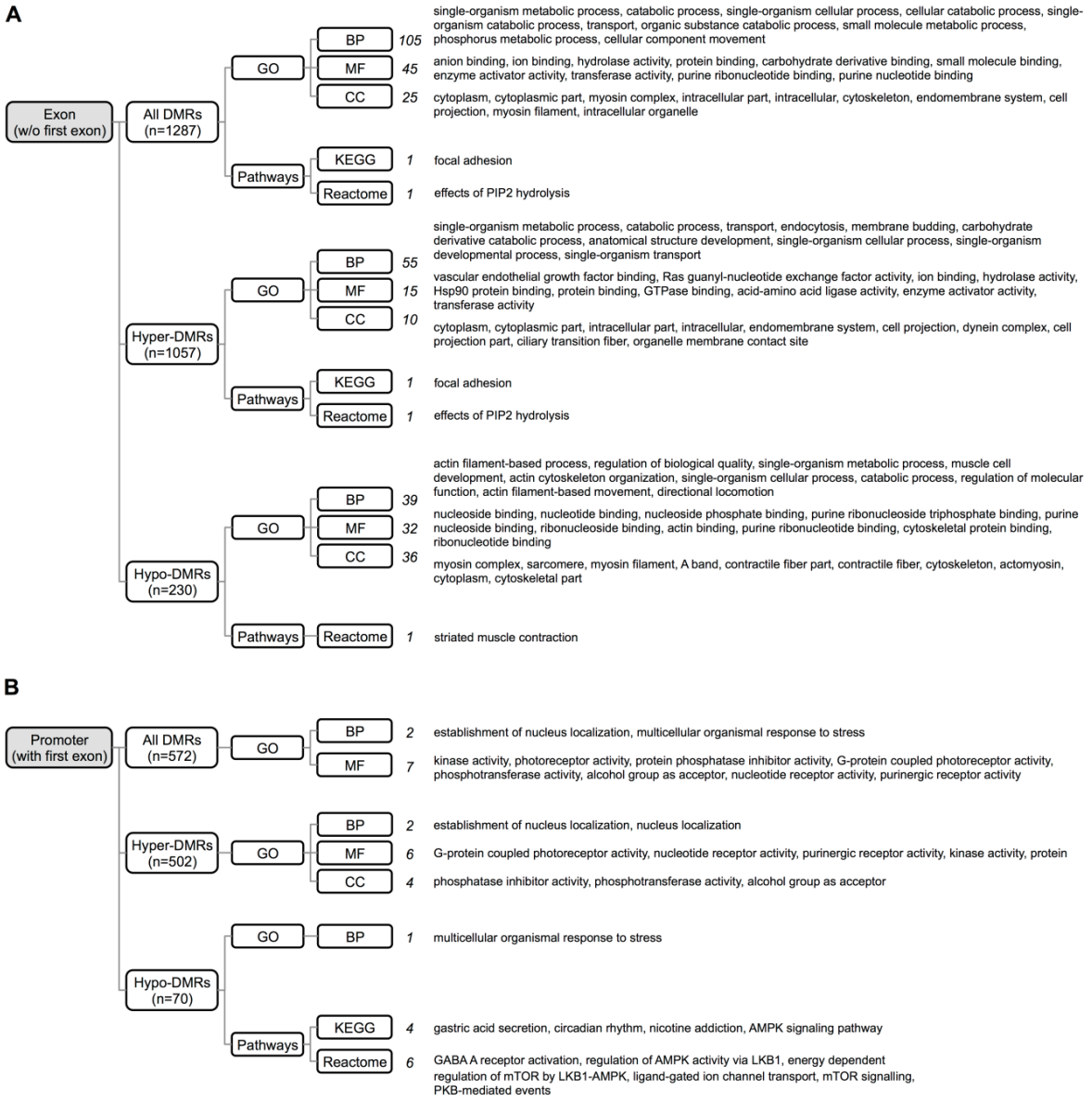

S4 Fig. Enrichment analysis for genes with DMRs in TOF vs. NH-rv. GO term and KEGG/Reactome enrichment analysis was performed for autosomal, protein-coding genes with (A) exons and (B) promoters with hypo- and hypermethylated DMRs in TOF vs. NH-rv. Only significant GO terms and KEGG/Reactome pathways (p-value < 0.05 based on hypergeometric test) are given. The total number of significant GO terms and pathways is indicated in front of the written terms/names. If there are more than 10 significant GO terms or pathways, only the top 10 of the terms/names are given. DMRs: differentially methylated regions; BP: biological process (GO term); CC: cellular component (GO term); MF: molecular function (GO term); GO: gene ontology; NH: normal heart; rv: right ventricle; TOF: Tetralogy of Fallot.

Supplemental Figure 5

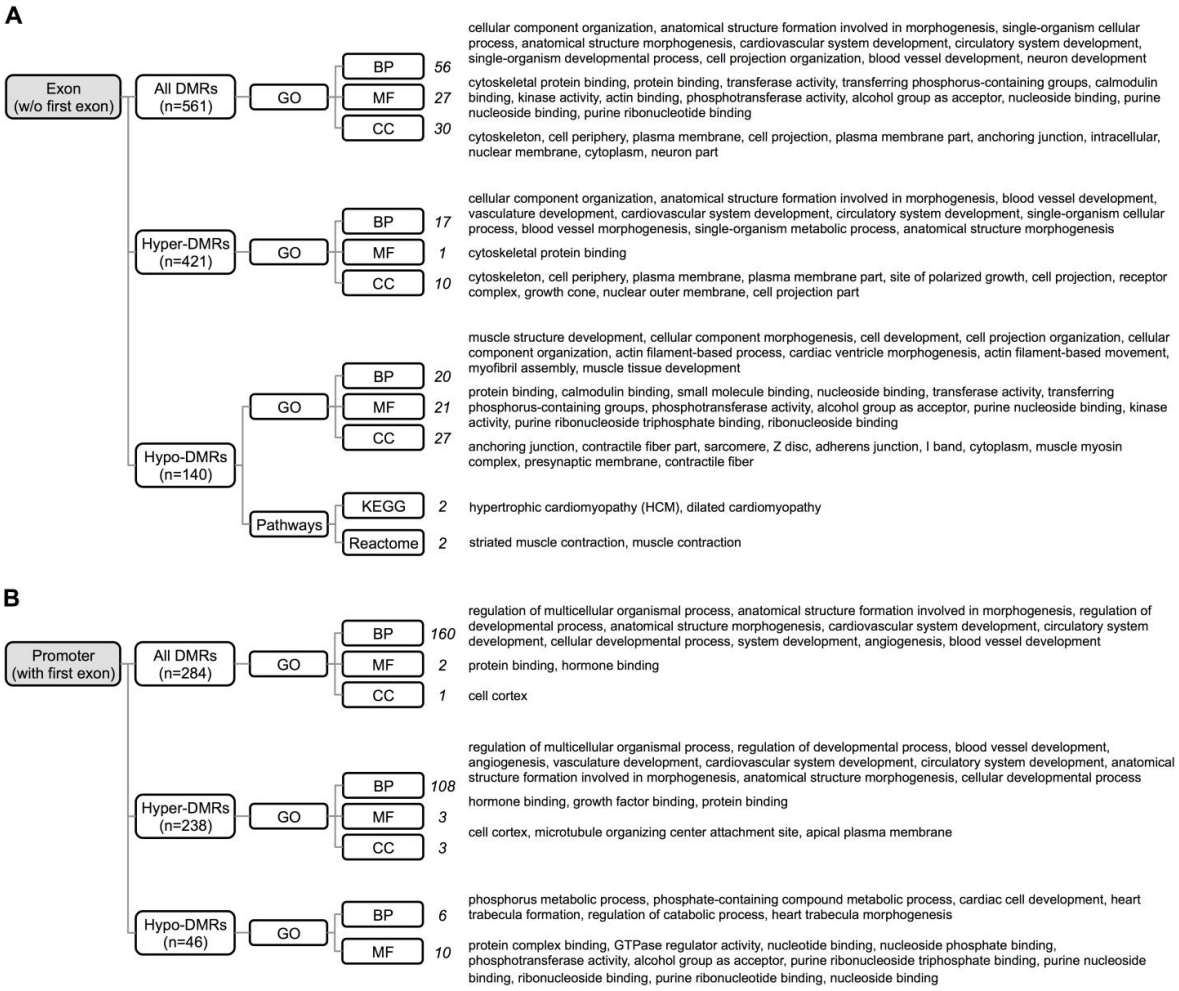

S5 Fig. Enrichment analysis for genes with DMRs in VSD vs. NH-ra. GO term and KEGG/Reactome enrichment analysis was performed for autosomal, protein-coding genes with (A) exons and (B) promoters with hypo- and hypermethylated DMRs in VSD vs. NH-ra. Only significant GO terms and KEGG/Reactome pathways (p-value < 0.05 based on hypergeometric test) are given. The total number of significant GO terms and pathways is indicated in front of the written terms/names. If there are more than 10 significant GO terms or pathways, only the top 10 of the terms/names are given. DMRs: differentially methylated regions; BP: biological process (GO term); CC: cellular component (GO term); MF: molecular function (GO term); GO: gene ontology; NH: normal heart; ra: right atrium; VSD: ventricular septal defect.

Supplemental Figure 6

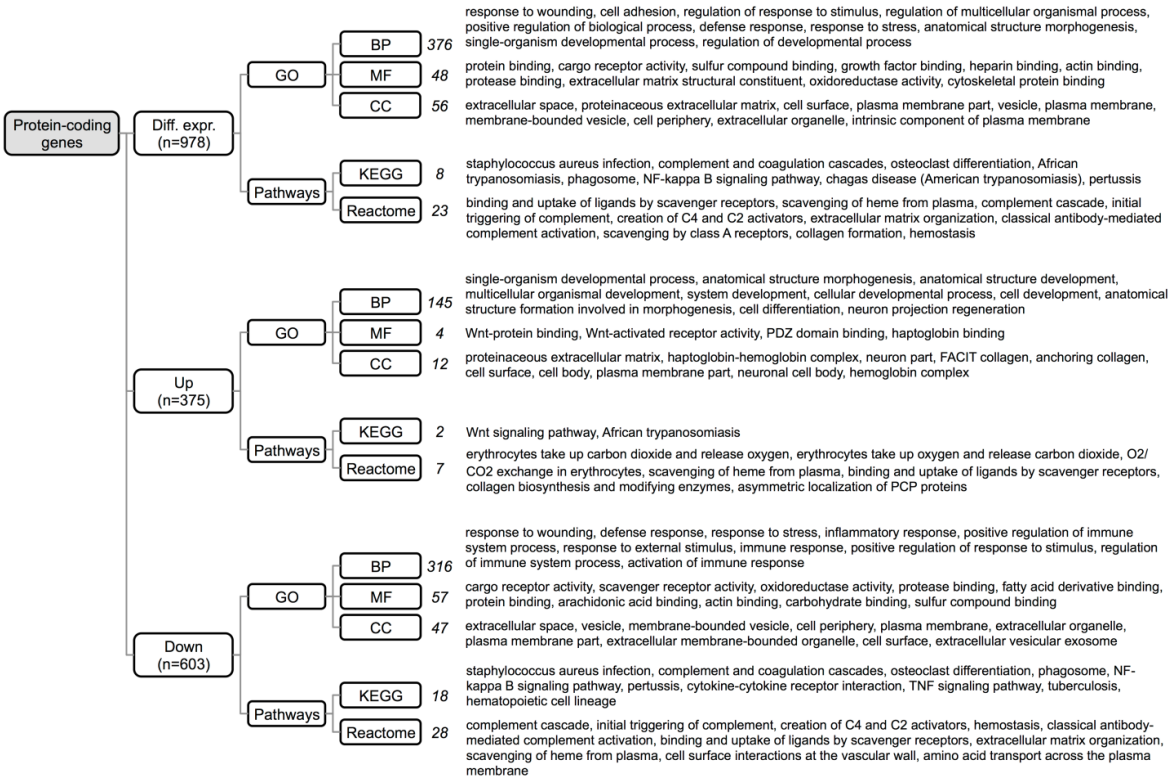

S6 Fig. Enrichment analysis for differentially expressed genes in TOF vs. NH-rv. GO term and KEGG/Reactome enrichment analysis was performed for autosomal, protein-coding differentially expressed genes (RNA-seq) in TOF vs. NH-rv. Only significant GO terms and KEGG/Reactome pathways (p-value < 0.05 based on hypergeometric test) are given. The total number of significant GO terms and pathways is indicated in front of the written terms/names. If there are more than 10 significant GO terms or pathways, only the top 10 of the terms/names are given. BP: biological process (GO term); CC: cellular component (GO term); MF: molecular function (GO term); GO: gene ontology; NH: normal heart; rv: right ventricle; TOF: Tetralogy of Fallot.

Supplemental Figure 7

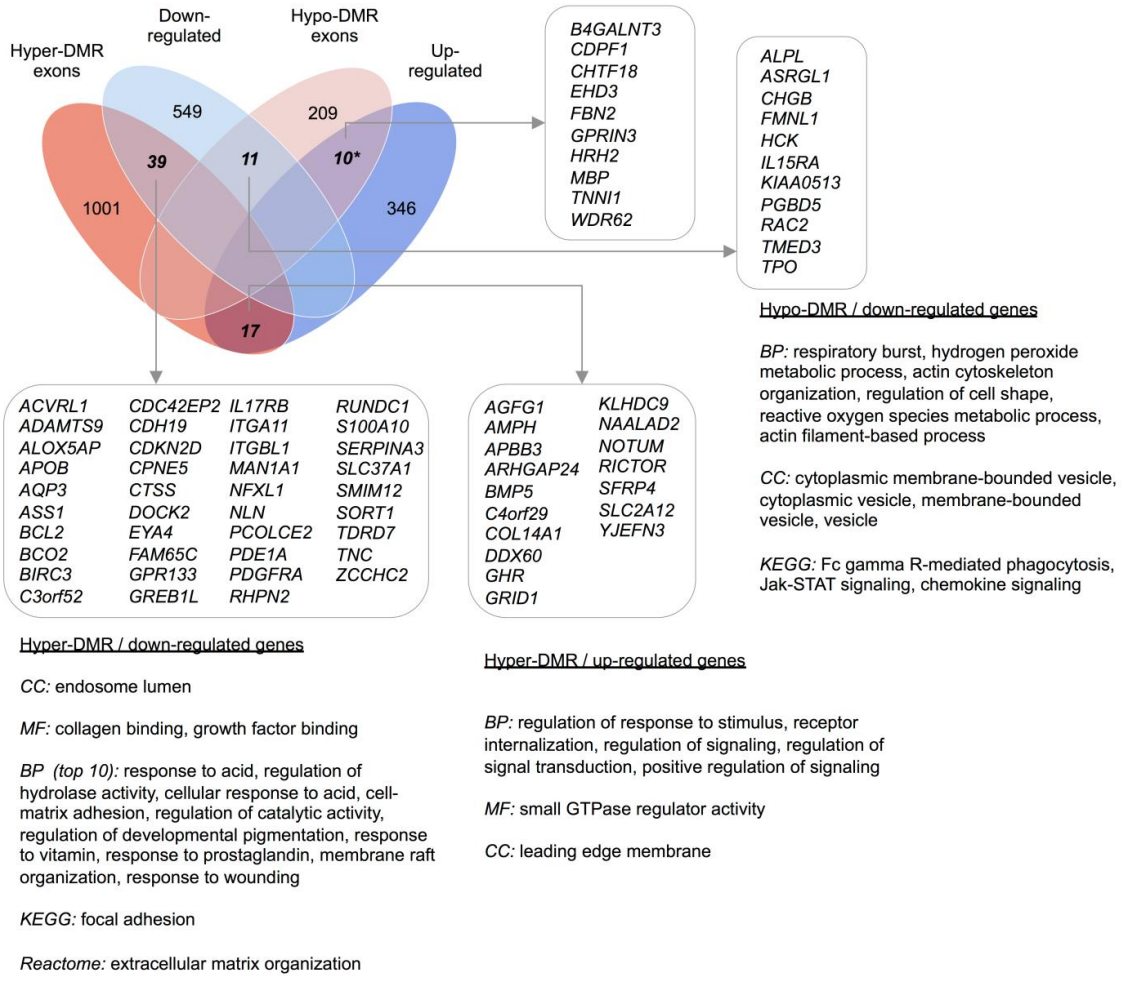

S7 Fig. Overlap of genes with DMRs in gene body and differentially expressed genes in TOF. Given is the overlap between autosomal, protein-coding genes that contain either hyper- or hypomethylated DMRs in their exons with genes that are either up- or down-regulated in TOF vs. NH-rv. A significant overlap (p-value < 0.05 based on hypergeometric test) is indicated by an asterisk. GO term and KEGG/Reactome enrichment analysis was performed for up- or down-regulated genes with hypo- or hypermethylated exons. Significant GO terms and KEGG/Reactome pathways (p-value < 0.05 based on hypergeometric test) as well as related genes are given for biologically relevant overlaps. DMRs: differentially methylated regions; BP: biological process (GO term); CC: cellular component (GO term); GO: gene ontology; MF: molecular function (GO term); NH: normal heart; rv: right ventricle; TOF: Tetralogy of Fallot.

Supplemental Figure 8

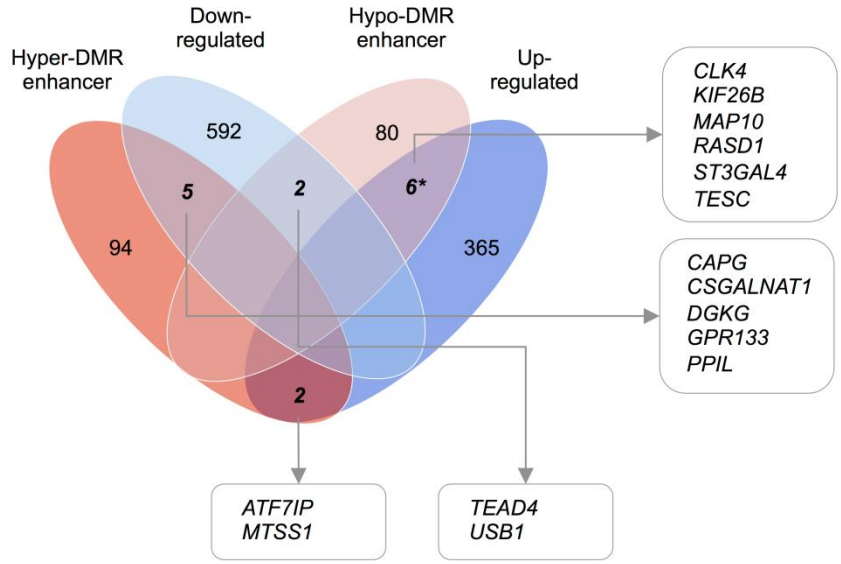

S8 Fig. Overlap of genes with DMRs in cardiac enhancers and differentially expressed genes in TOF. Given is the overlap between autosomal, protein-coding genes that contain either hyper- or hypomethylated DMRs near cardiac enhancers with their expression either up- or down-regulated in TOF vs. NH-rv. A significant overlap (p-value < 0.05 based on hypergeometric test) is indicated by an asterisk. GO term and KEGG/Reactome enrichment analysis was performed for up- and down-regulated genes near hypo- or hypermethylated enhancers. No significant GO terms and KEGG/Reactome pathways (p-value < 0.05 based on hypergeometric test) were found. DMRs: differentially methylated regions; BP: biological process (GO term); CC: cellular component (GO term); MF: molecular function (GO term); GO: gene ontology; NH: normal heart; rv: right ventricle; TOF: Tetralogy of Fallot.

Supplemental Figure 9

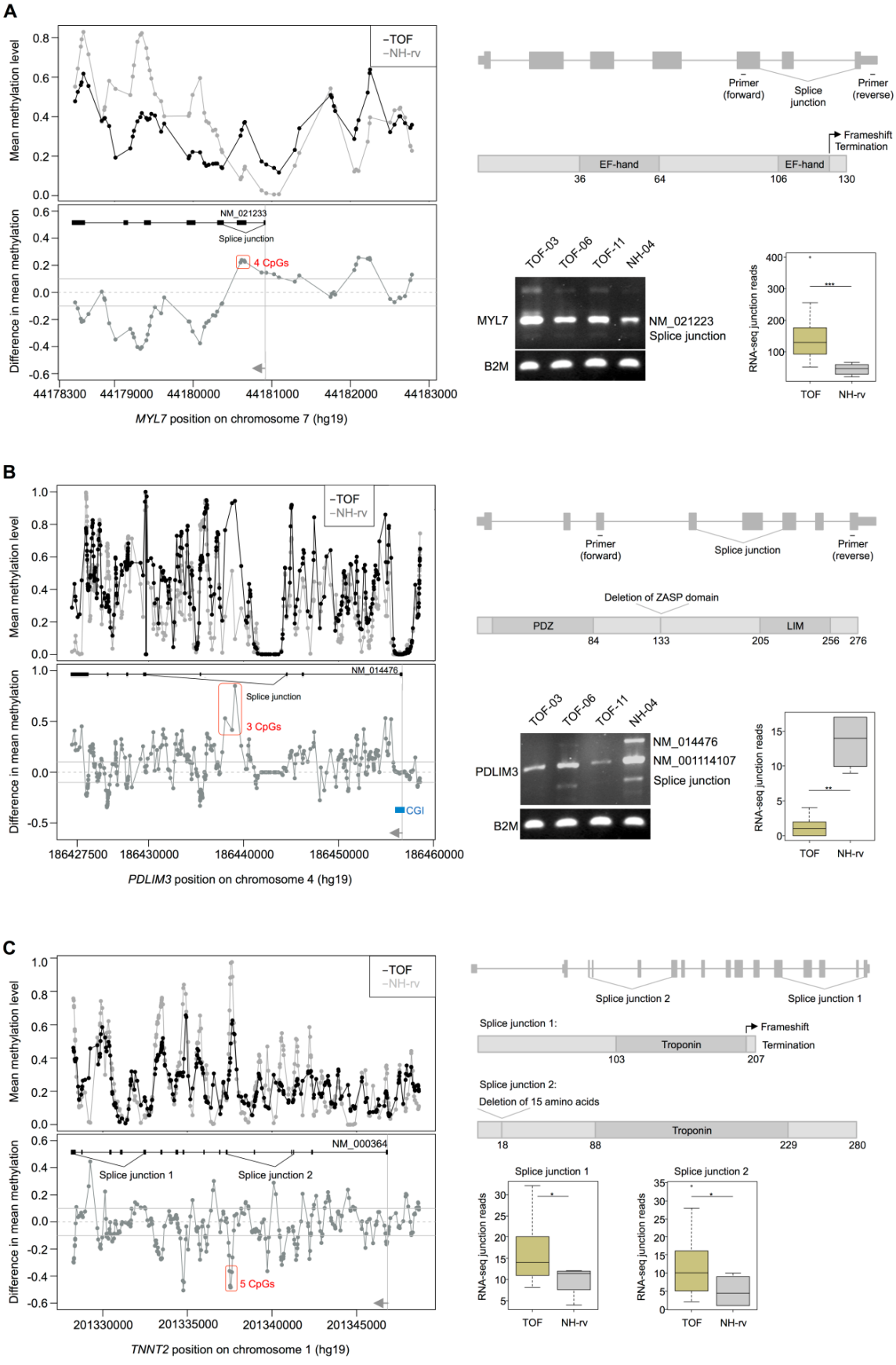

S9 Fig. Novel splicing events and methylation in the gene bodies and promoter regions of sarcomeric genes. Left panels show the methylation over the gene bodies and promoter regions. Each dot indicates a single CpG. Protein-coding transcripts are given with their transcription start site marked by grey arrows. Right panels indicate schematic representations of transcripts, resulting proteins (with functional domains indicated in dark grey) and expression analysis for the splice junctions (RT-PCR for representative samples and RNA-seq for all samples). For (A) *MYL7*, **(**B) *PDLIM3* and **(**C) *TNNT2*, smaller regions with significant methylation changes were identified. CGI: CpG island; NH: normal heart; rv: right ventricle; TOF: Tetralogy of Fallot. * p-value ≤ 0.05; ** p-value ≤ 0.01; *** p-value ≤ 0.001.

Supplemental Figure 10

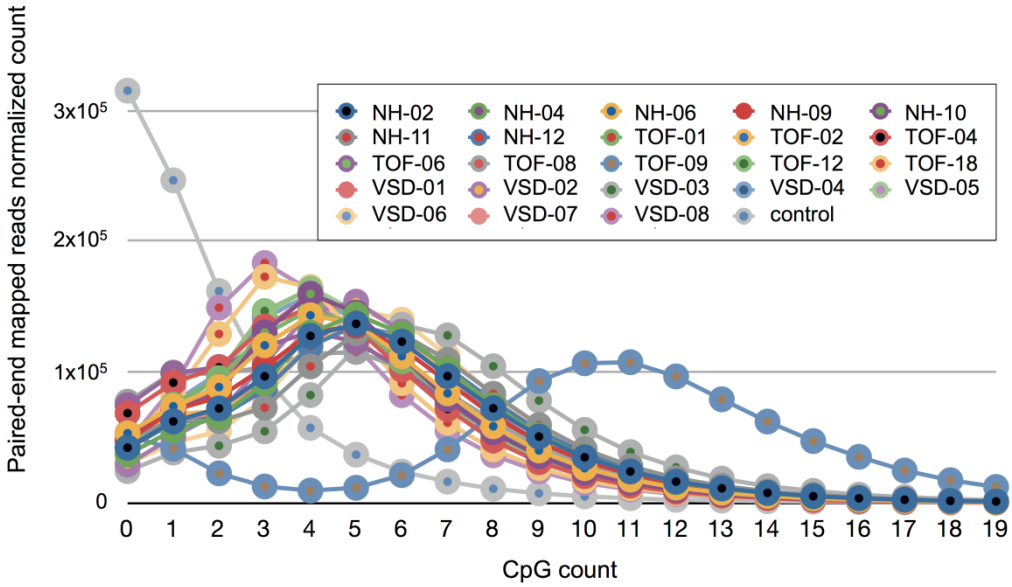

S10 Fig. CpG enrichment. Amount of paired-end mapped reads versus the number of CpGs in the sequence for each sample. The sample TOF-09 represents an outlier as it is clearly separated from the other samples.

Supplemental Figure 11

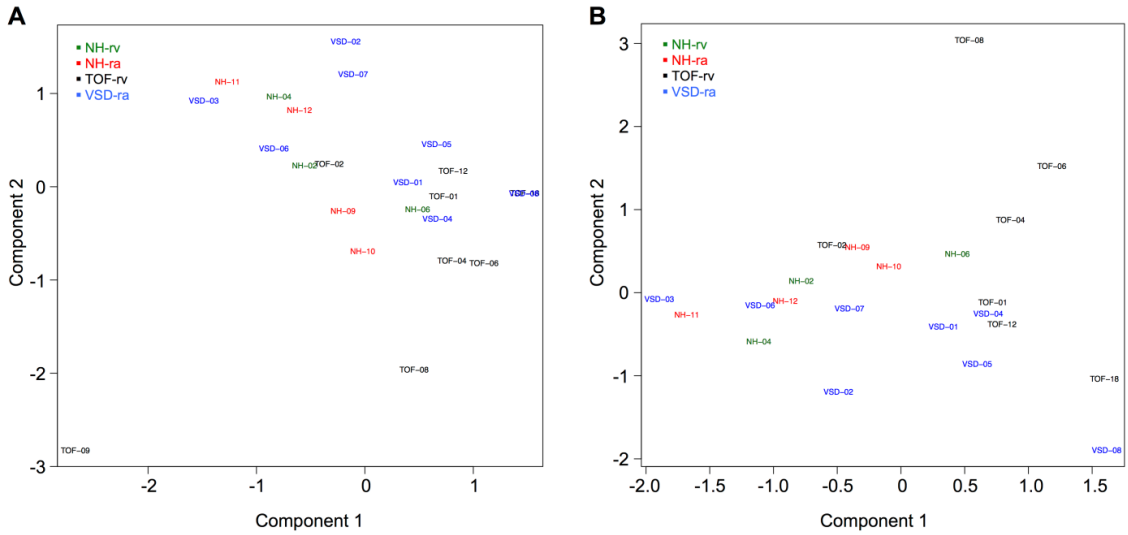

S11 Fig. Principle component analysis for MBD-seq samples based on the mean methylation levels of human autosomal 1-kb tiles. (A) PCA based on all samples. (B) PCA based on all samples except TOF-09 (read quality problem). NH: normal heart; PCA: principle component analysis; ra: right atrium; rv: right ventricle; TOF: Tetralogy of Fallot; VSD: ventricular septal defect.

Supplemental Figure 12

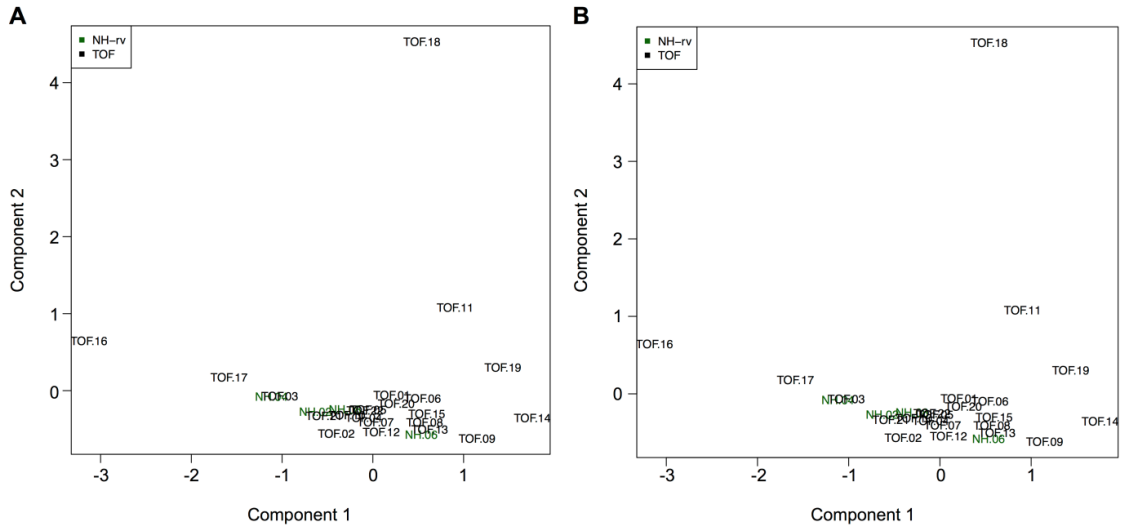

S12 Fig. Principle component analysis for mRNA-seq samples based on FPKM values. (A**)** PCA based on FPKM values of genes over all samples. (B) PCA based on FPKM values of transcripts over all samples. FPKM: fragments per kilobase of exon per million fragments mapped; NH: normal heart; PCA: principle component analysis; rv: right ventricle; TOF: Tetralogy of Fallot.

Supplemental Figure 13

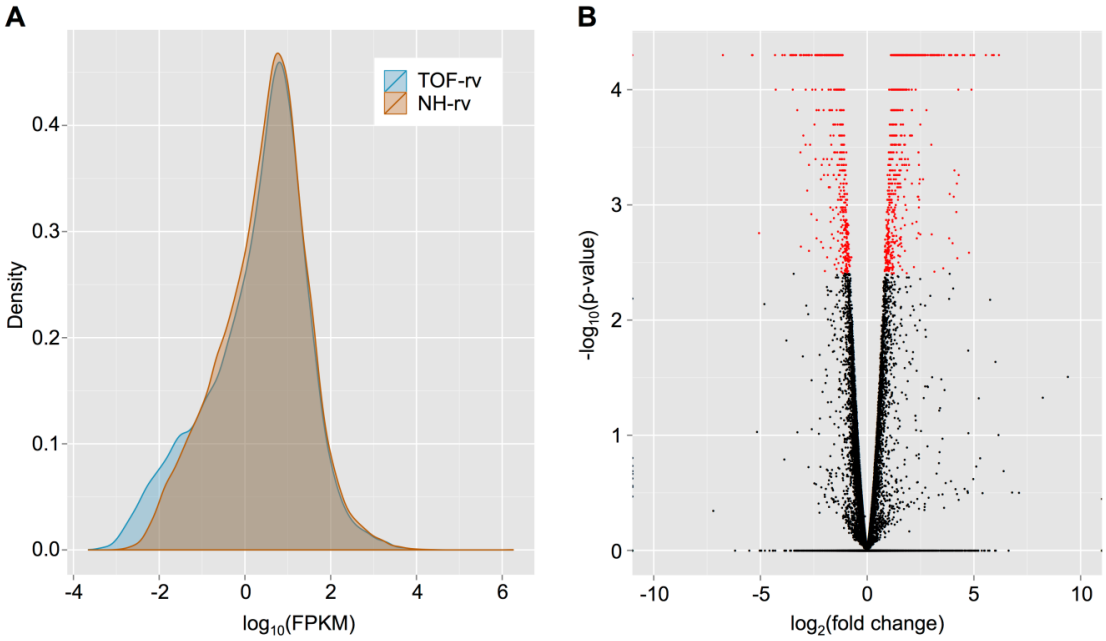

S13 Fig. Differential gene expression in TOF versus normal heart. (A) Expression level distribution for genes in TOF cases and controls. (B) Volcano plot with significantly differentially expressed genes (adjusted p-value < 0.05) marked in red (fold change NH/TOF). FPKM: fragments per kilobase of exon per million fragments mapped; NH: normal heart; rv: right ventricle; TOF: Tetralogy of Fallot.

Supplemental Table 1. Overview of total reads and mapped reads per sample in MBD-seq. Sequence reads were mapped to the human reference genome (GRCh37/hg19). NH: normal heart; ra: right atrium; rv: right ventricle; TOF: Tetralogy of Fallot; VSD: ventricular septal defect.

Sample	Group	Age of individual in years	Total number of reads	Paired-end reads	Mapping percentage	Mapped paired-end reads
NH-02	NH-rv	24	47569658	23786525	65	15374514
NH-04	NH-rv	18	53075730	26538387	62	16437554
NH-06	NH-rv	20	66004770	33001206	61	20144656
NH-09	NH-ra	59	54962084	27481835	62	16999773
NH-10	NH-ra	37	44677966	22340363	65	14529275
NH-11	NH-ra	51	55880944	27942201	63	17669555
NH-12	NH-ra	54	59290144	29645547	62	18468880
TOF-01	TOF-rv	1,3	70761234	35380120	61	21493725
TOF-02	TOF-rv	1,9	59111830	29553846	64	18906919
TOF-04	TOF-rv	0,9	67622110	33813236	60	20367780
TOF-06	TOF-rv	1,3	85584608	42794928	61	26017721
TOF-08	TOF-rv	0,6	59031550	29515151	62	18373570
TOF-09	TOF-rv	1,0	57064252	28532033	55	15575688
TOF-12	TOF-rv	0,6	74542936	37270268	62	22921953
TOF-18	TOF-rv	1,0	87731536	43867904	62	27398559
VSD-01	VSD-ra	11,8	60436516	30217546	61	18360614
VSD-02	VSD-ra	0,4	68282984	34142109	65	22034919
VSD-03	VSD-ra	3,3	74487372	37245684	58	21467261
VSD-04	VSD-ra	1,0	67133638	33564773	58	19451972
VSD-05	VSD-ra	0,5	71607848	35801781	60	21328398
VSD-06	VSD-ra	0,2	52015926	26010078	57	14931172
VSD-07	VSD-ra	0,7	83129874	41567106	61	25408646
VSD-08	VSD-ra	0,3	76454034	38229049	65	24874320

Supplemental Table 2. Significantly hypermethylated regions (stringent set) in TOF versus NH-rv. Positions based on human reference genome hg19. NH: normal heart; rv: right ventricle; TOF: Tetralogy of Fallot (data not shown).

Supplemental Table 3. Significantly hypomethylated regions (stringent set) in TOF versus NH-rv. Positions based on human reference genome hg19. NH: normal heart; rv: right ventricle; TOF: Tetralogy of Fallot (data not shown).

Supplemental Table 4 Table. Significantly hypermethylated regions (stringent set) in VSD versus NH-ra. Positions based on human reference genome hg19. NH: normal heart; ra: right atrium; VSD: ventricular septal defect (data not shown).

Supplemental Table 5 Table. Significantly hypomethylated regions (stringent set) in VSD versus NH-ra. Positions based on human reference genome hg19. NH: normal heart; ra: right atrium; VSD: ventricular septal defect (data not shown).

Supplemental Table 6. Number of autosomal, protein-coding genes associated with DMRs in their promoters, exons or cardiac enhancers. DMR: differentially methylated region; NH: normal heart; ra: right atrium; rv: right ventricle; TOF: Tetralogy of Fallot; VSD: ventricular septal defect.

	TOF vs. NH-rv	VSD vs. NH-ra	Overlap between TOF/NH-rv and VSD/NH-ra
Number of genes with hypermethylated promoters including fist exons	502	238	17
Number of genes with hypermethylated exons without first exons	1057	421	65
Number of genes near hypermethylated cardiac enhancers	101	116	7
Number of genes with hypomethylated promoters including fist exons	70	46	5
Number of genes with hypomethylated exons without first exons	230	140	17
Number of genes near hypomethylated cardiac enhancers	88	90	15

Supplemental Table 7. Overview of total reads and mapped reads per sample in mRNA-seq. Sequence reads were mapped to the human reference genome (hg19). NH: normal heart; TOF: Tetralogy of Fallot.

Sample ID	MBD-seq	PacBio-seq	Total number of reads	Mapping percentage	Mapped reads	Multimapped reads
NH-02	yes	yes	20106950	59	11841986	1861252
NH-04	yes	yes	12961101	85	10970315	1597894
NH-06	yes	yes	20296818	86	17432503	2155818
NH-08	-	-	23597799	85	20074450	2350982
TOF-01	yes	yes	10888508	87	9485446	1234887
TOF-02	yes	yes	19907118	79	15782560	1935776
TOF-03	-	yes	21882581	82	17970343	2320303
TOF-04	yes	yes	23167354	83	19295750	2647551
TOF-05	-	-	14570039	85	12392143	1582325
TOF-06	yes	yes	21750958	84	18336537	2563080
TOF-07	-	-	18392413	83	15212629	1746339
TOF-08	yes	yes	15106033	81	12196546	1602174
TOF-09	yes	yes	23512940	86	20119361	2858289
TOF-10	-	-	23026631	78	17864520	2422450
TOF-11	-	-	17430948	88	15315848	1766597
TOF-12	yes	yes	13437909	87	11729860	1268000
TOF-13	-	yes	21026718	87	18290926	2242734
TOF-14	-	-	16936456	86	14489696	2064661
TOF-15	-	yes	21409551	84	17879043	2241085
TOF-16	-	yes	16813107	85	14222455	2099424
TOF-17	-	yes	24364507	83	20278905	2693307
TOF-18	yes	yes	20193649	86	17369967	2237840
TOF-19	-	yes	15564794	83	12981546	2441457
TOF-20	-	yes	21553557	87	18784326	2299320
TOF-21	-	yes	17564630	87	15243228	1905361
TOF-22	-	yes	24353916	83	20325596	2729431

Supplemental Table 8 Table. Significantly differentially expressed autosomal, protein-coding genes in TOF versus NH-rv. Positions based on human reference genome hg19. FPKM: fragments per kilobase of million fragments mapped; NH: normal heart; rv: right ventricle; TOF: Tetralogy of Fallot (data not shown).

Supplemental Table 9 Table. Novel splice junctions identified in normal heart and/or TOF samples. DMR in gene body is indicated by 1 (present) or 0 (absent). NH: normal heart; rv: right ventricle; TOF: Tetralogy of Fallot (data not shown).

4 Discussion

Epigenetic mechanisms and modifications such as chromatin remodeling and DNA methylation play an important role in the regulation of gene expression in many biological processes. In cardiac development and differentiation, gene expression is tightly controlled by epigenetic regulators and modifiers. Dysregulation of these factors causes alterations of epigenetic and expression patterns, and thus leads to cardiac diseases and heart failure. In the first part of this study, the function of the chromatin remodeling factor DPF3a was characterized by applying biochemical and molecular assays *in vitro* and *in vivo*. We described a novel pathway of cardiac hypertrophy mediated by DPF3a. In the second part of this study, we investigated the alterations of genome-wide DNA methylation on myocardial biopsies of patients with TOF and VSD, two common CHDs.

4.1 Regulation of cardiac hypertrophy by DPF3a

4.1.1 Phosphorylation of DPF3a

Using tandem affinity purification followed by mass spectrometry analysis, all three subunits of CK2 in the cytoplasm of HEK239 cells were found to be potential interaction partners for DPF3a but not DPF3b. A stringent threshold set with a Mascot score of >40 and a minimum number of two matching spectra was used for the identification of interaction partners in MS analysis to exclude unspecific binding proteins (Gingras et al., 2005). Only a few other proteins were identified in addition to the CK2 subunits, suggesting the high specificity of DPF3a and CK2 interactions. A pulldown assay using GST-tagged CK2 subunits and Flag-tagged DPF3a/b confirmed the specific interaction of DPF3a with CK2α and CK2β. These results indicate the specific C-terminus and the half PHD finger of DPF3a are likely the interaction domains. The strong and weak interaction of DPF3a with CK2β and CK2α, respectively, can be explained by the fact that CK2β is the regulatory subunit of CK2, which is responsible for substrate recognition, whereas CK2α is the catalytic subunit, which is responsible for the kinase activity (Litchfield, 2003). Moreover, *in vitro* kinase assays showed that the phosphorylation of DPF3a is dependent on CK2. Subsequent mass spectrometry analysis identified three phosphorylation sites in DPF3a *in vivo*: S138, S348 and T350. S138 is located at the N-terminus, which is critical for BRG1 binding (unpublished data). The phosphorylation of S138 might be involved in regulating the interaction of DPF3a and BRG1. S348 and T350 are located at the DPF3a-specific C-terminus, the structure and function of which are as yet unclear. Interestingly,

S348 is the only conserved residue in human, mouse and chicken, suggesting this site has a potential functional role. In particular, S348 is in the amino acid sequence SGRG that is identical to the first four amino acids of histone H4, known to be phosphorylated by CK2 at S1 (Cheung et al., 2005). In the present study, we were able to confirm that S348 is indeed phosphorylated by CK2 both *in vitro* and *in vivo*.

Protein phosphorylation is a key post-translational modification that can modulate a protein's role in physiological processes such as localization, activity, and protein-protein interactions (Nishi et al., 2011; Olsen et al., 2006). Phosphorylated DPF3a (pDPF3a) is predominately located in the nucleus in cardiomyocytes (e.g. cardiac tissue, hiPSC-CMs, HL1 and H9C2 cells) and skeletal muscle cells (e.g. C2C12 cells). There is an increase of pDPF3a in the nucleus due to hypertrophic stimulation. Possible explanations for this include: 1) DPF3a is only expressed in the nucleus and hypertrophic signals activate the nuclear expression and phosphorylation of DPF3a; 2) DPF3a is located in the nucleus as well as the cytoplasm, and upon hypertrophic stimuli, DPF3a translocates from the cytoplasm to the nucleus where it is suggested to be phosphorylated by CK2. In addition, we observed slightly more S348A mutant than WT in the cytoplasm, suggesting that S348 phosphorylation might play a role in DPF3a translocation; however, this needs further investigation – a non-pDPF3a-specific antibody would be helpful to understand the role of S348 phosphorylation in DPF3a translocation. DPF3a also interacts with HEY proteins via its half PHD finger and S348 phosphorylation impacts on this interaction. Frequently, phosphorylation occurs within an interaction domain and thereby directly affects the binding energy (Nishi et al., 2011). However, S348 is located in the structurally unsolved C-terminus of DPF3a. It is very likely that S348 phosphorylation causes long-range conformational changes of DPF3a through allosteric mechanisms and affects the DPF3a-HEY1 interaction. More recently, DPF3a (but not DPF3b) was identified as an RNA binding protein in a PAR-CLIP experiment (unpublished data). It is probable that the DPF3a-RNA interaction is mediated by the specific C-terminus where S348 is located. Thus it would be interesting to examine if the phosphorylation of S348 affects the binding of DPF3a to its RNA targets.

4.1.2 DPF3a in cardiac hypertrophy

DPF3 first drew our attention in a screen for marker genes of diseased and normal human myocardium (Kaynak et al., 2003). *DPF3* transcripts (*DPF3a* and *DPF3b*) were found to be up-regulated in patients with TOF (Lange et al., 2008). We analyzed the expression of *DPF3a* and *DPF3b* in the hypertrophic left ventricle of patients with HCM and AS and

found both splice variants were activated in HCM and AS. During hiPSC-CM differentiation, the expression of *DPF3a* was continuously higher than *DPF3b* from day 6 to 60. This is in line with the expression pattern of *Dpf3a* and *Dpf3b* transcripts in heart during mouse embryogenesis (Lange et al., 2008). Interestingly, only *DPF3a* showed the same expression pattern as the fetal gene *NPPA*, which is a molecular marker of pathological cardiac hypertrophy (Gardner, 2003). These findings suggest DPF3a is a fetal-like gene that is expressed during cardiomyocyte differentiation and is re-expressed upon hypertrophic stimuli (Duygu et al., 2013). However, the specific role of DPF3a in cardiac hypertrophy is yet to be elucidated.

In mammals, both DPF3a and DPF3b belong to the BAF chromatin remodeling complexes. These complexes utilize either BRG1 or BRM as alternative catalytic subunits, which have DNA-stimulated ATPase activity (Ho and Crabtree, 2010). Usually, the BAF complexes are recruited to genomic targets by DNA-binding transcription factors and/or histone-binding epigenetic regulators (Peterson and Workman, 2000). The non-catalytic subunits of BAF complexes, such as BAF60c and DPF3b, have been identified to be involved in gene transcription during cardiac development and disease (Bruneau, 2010). BAF60c promotes cardiac gene transcription by interacting with the cardiac-specific transcription factors TBX5, GATA4 and NKX2-5 (Lickert et al., 2004). DPF3b functions as a histone reader to target cardiac and muscle specific chromatin sites (Lange et al., 2008). Either way, BRG1 is recruited to the genomic target sites by associating with these BAF subunits. Usually, BRG1 is highly expressed in the developing heart and is turned off in the adult heart; however, in cardiomyocytes, upon hypertrophic stimuli or pressure overload, BRG1 is reactivated and induces the fetal gene program (Hang et al., 2010; Mehrotra et al., 2013). It has been shown that Brg1 forms a complex with PARPs and several HDACs to regulate the switch of *α-MHC* and *β-MHC* expression in transverse aortic constriction (TAC)-banded mice. As a result, Brg1-null hearts showed significantly reduced hypertrophic response upon TAC-binding compared to control mice. Moreover, *BRG1* was activated in patients with HCM and its expression level was correlated with the severity of HCM in the human heart (Hang et al., 2010). At this time, the exact mechanism by which BRG1 was targeted to fetal genes in this setting was still unknown. Our data suggest that DPF3a mediates and recruits BRG1 to fetal genes that are repressed by HEY proteins in a wild type (WT) stage cells. We have shown that upon exposure to hypertrophic stimuli, DPF3a is activated with enhanced expression and phosphorylation at S348 (e.g. ET-1 treated hiPSC-CMs or hypertrophic TOF hearts). Phosphorylation of S348 thus enhances the binding of DPF3a to HEY proteins; consequently, HEY proteins are released from the DNA and the fetal gene program is activated. S348 phosphorylation

is mediated by CK2, which has been shown to activate the signaling of hypertrophic stimuli. The catalytic subunit CK2α was shown to phosphorylate and thereby activate HDAC2, resulting the repression of anti-hypertrophic genes (Eom et al., 2011). The other catalytic subunit CK2α' was shown to induce cardiac hypertrophy via interaction with the anti-hypertrophic cell cycle regulator p27 (Hauck et al., 2008). However, neither study clearly identified how the CK2 signals change the chromatin structure and the fetal gene transcription that eventually leads to cardiac hypertrophy. Insights into the down-stream mediators such as chromatin or transcription factors await further elucidation; therefore, at present we can only speculate as to the potential role of DPF3a as mediator in these pathways.

In this study, we found that overexpression of DPF3a results in larger cardiomyocytes and knockdown of DPF3 buffers ET-1 induced hypertrophy in hiPSC-CMs. To further study the function of Dpf3a in the development of cardiac hypertrophy in an *in vivo* animal model, we recently generated a Dpf3 knockout mouse line, $Dpf3^{tm1sper}$. So far, we have established that the $Dpf3^{tm1sper}$ mice are viable and fertile (unpublished data). As all Dpf3b domains are highly conserved within the d4 protein family, it is likely that other d4 family members, Dpf1 and Dpf2, balance the physiological role of Dpf3 during development. However, it is important to note that the protein domains (half PHD and C-terminus) of Dpf3a involved in the novel hypertrophic pathway are unique to Dpf3a. In the future, the $Dpf3^{tm1sper}$ mice will be exposed to stress using TAC-binding to study the hypertrophic response. It is possible that a reduction of hypertrophy will be observed in the knockout but not the WT.

We have demonstrated that DPF3a physically interacts with HEY proteins. It has been reported that all three HEY transcription factors function similarly and share genomic targets (Heisig et al., 2012). Therefore, DPF3a can be considered to be a cofactor of HEY proteins that together regulate respective target genes. Moreover, Hey transcription factors contribute to cardiac development. During embryonic development, Hey1 and Hey2 are expressed in the heart, with Hey1 being expressed in the atrium and Hey2 being expressed in the ventricle (Wiese et al., 2010). Dpf3a is expressed in all four chambers of the developing and adult heart, which suggests that Hey1 and Hey2 represent the interaction partners of Dpf3a in atrial and ventricular cardiomyocytes during cardiac development, respectively. Furthermore, animal studies have highlighted the role of Hey in development and disease. Knockout of Hey1 or HeyL does not lead to obvious cardiac defects, whereas Hey2 depleted and Hey1/HeyL double knockout mice develop CHDs, including VSD, dysplastic atrioventricular and cardiomyopathy with cardiac hypertrophy (Fischer et al., 2007; Sakata et al., 2002). Interestingly, Hey2 cardiac-specific

overexpressing mice prevent PE-induced cardiac hypertrophy *in vivo* and *in vitro* (Xiang et al., 2006). In our model, we suggest that Dpf3a induces hypertrophy by interacting and subsequently releasing Hey repressors from the fetal genes *Nppa* and *Gata4*. It is likely that the amount of Dpf3a is not enough to titrate Hey2 in PE-treated Hey2 overexpressing mice; thus, Hey2 overexpressing mice show an anti-hypertrophic phenotype because the fetal gene program is not activated.

Pathological cardiac hypertrophy primarily occurs in cases of HCM, with the second most common cause being pressure overload, as is the case with AS. We observed a significant up-regulation of common DPF3a-HEY target genes in HCM and AS cardiac biopsies. These genes, which include *GATA4*, *FOXO1*, *TBX3* and *SMAD7*, are known to play important roles in cardiac development and disease. The cardiac transcription factor GATA4 directly regulates cardiac fetal genes such as *NPPA* and *NPPB* (Liang et al., 2001a). Phosphorylation of GATA4 at S105 is necessary for stress-induced cardiac hypertrophy *in vivo* (van Berlo et al., 2011). Moreover, GATA4-bound cardiac-specific enhancers are restored in pathological hypertrophy (He et al., 2014). FOXO1 is an important mediator of cardiac hypertrophy and its activity is essential in Akt-mediated cardiac hypertrophy (Battiprolu et al., 2012). TBX3 is required for conduction tissue identity and plays a critical role in the functional development, maturation, and homeostasis of the conduction system (Frank et al., 2012). SMAD7 belongs to the TGF-β superfamily that has been implicated in cardiac structural development and several cardiac disorders (Chen et al., 2009; Yuan and Jing, 2010).

In summary, we present a novel pathway of cardiac gene transcription that eventually leads to pathological cardiac hypertrophy. This pathway is triggered by CK2 kinase activation, leading to phosphorylation of the BAF chromatin remodeling factor DPF3a and the consequent release of DNA-binding transcriptional repressors HEY from DNA. The novel pathway provides a molecular basis for the development of pathological cardiac hypertrophy. Thus, in the future, it will be of interest to examine this pathway as a therapeutic target and explore its potential role in pharmaceutical interventions of heart failure.

4.2 DNA methylation in TOF and VSD

In Chapter 3, we presented the first genome-wide DNA methylation analysis of human congenital cardiac defects in myocardial biopsies of patients with TOF and VSD, as well as healthy controls. In general, we observed distinct methylation profiles between patients

and controls, which could contribute to the distinct gene expression patterns in TOF and VSD (Kaynak et al., 2003). Moreover, we found more hypermethylated than hypomethylated regions in both TOF and VSD patients compared to normal hearts, respectively. This finding is in line with previous candidate gene studies in TOF (Sheng et al., 2014) and VSD (Zhu et al., 2011a; Zhu et al., 2011b). In addition, we identified many more differentially methylated regions (DMRs) in TOF than in VSD, which might be caused by the secondary adaptions and hemodynamic changes in TOF hearts.

We found an enrichment of DMRs in different genomic features like promoters, exons and cardiac enhancers, except for CpG islands (CGIs). When we checked the total overlap of hyper- and hypomethylated DMRs separately for each genomic feature, we found four and five hypermethylated DMRs associated with CGIs in TOF and VSD, respectively. It has been shown that the hypermethylation of the CGIs is a common feature of human diseases (Bock et al., 2006; Issa, 2004). With respect to TOF and VSD, only one CGI overlapping DMR has been found in both cases. This hypermethylated DMR is located at the promoter of *SCO2*, a gene coding for the cytochrome c oxidase (COX) assembly protein that is important for maintaining cellular copper homeostasis and redox regulation (Leary et al., 2007). In both TOF and VSD, *SCO2* is significantly down-regulated. The newly-discovered regulatory region at the *SCO2* promoter may influence chromatin structure and thus contribute to the regulation of gene activity. *SCO2* expression has been reported to be regulated by the transcription factor p53 (Matoba et al., 2006), which can be activated in response to stress (Zhuang et al., 2012). The hypertrophic stress presented in TOF may modulate this pathway to switch the metabolic state from adult-like mitochondrial oxidation to fetal-like glycolytic metabolism (Lopaschuk and Jaswal, 2010). Moreover, cardiac-specific knockdown of the *Drosophila SCO1* and *SCO2* homolog *scox* results in severe dilated cardiomyopathy and reduced life span because of the reduction of COX activity and the metabolic switch (Martinez-Morentin et al., 2015). In addition, mutations in the *SCO2* gene cause hypertrophic cardiomyopathy in humans, which is probably due to reduced COX activity in these patients (Gurgel-Giannetti et al., 2013).

When we overlapped genes containing DMRs in their promoters, exons or cardiac enhancers with significantly differentially expressed genes in TOF, we found a significant overlap for hypermethylated promoters and down-regulated genes as well as for hypomethylated promoters and up-regulated genes. Moreover, we identified a number of novel, differential alternative splicing events overlapped with promoter DMRs in four sarcomeric genes, namely *TNNT1, TNNT2, MYL7* and *PDLIM3*. Splicing of key sarcomeric genes has been suggested to play a causal role in pathological heart failure (Kong et al., 2010). In patients with ischemic cardiomyopathy, dilated cardiomyopathy and

AS, alternative splicing of *TNNT2*, *MYH7* and *TTN* have been found to be significantly altered (Herman et al., 2012). In addition, splicing of sarcomeric genes, in case of *TTN*, regulated by cardiac splicing factor RBM20, is associated with heart failure (Guo et al., 2012). Recent studies demonstrated alternative splicing was regulated by DNA methylation, an epigenetic modification that can affect the recognition of alternative exons in a context-specific manner (Maunakea et al., 2013; Yearim et al., 2015). So far, at least three factors, namely CTCF, MeCP2 and HP1, are known to transmit information from DNA methylation to splicing regulation either via altering the Pol II elongation rate or recruiting splicing factors from the DNA to the mRNA precursor (Lev Maor et al., 2015). Our results for sarcomeric genes in TOF presented the first link between alternative splicing and DNA methylation in CHDs.

Taken together, we investigated DNA methylation in TOF and VSD and showed that the alterations of DNA methylation likely impact on the clinical phenotype of TOF and VSD. Our results provide the first insights into the epigenetic alterations underlying CHDs. These findings will be helpful to develop novel therapeutic perspectives for CHDs by targeting epigenetic modifications.

5 References

Abu-Farha, M., Elisma, F., and Figeys, D. (2008). Identification of protein-protein interactions by mass spectrometry coupled techniques. Adv. Biochem. Eng. Biotechnol. *110*, 67-80.

Apitz, C., Webb, G.D., and Redington, A.N. (2009). Tetralogy of Fallot. Lancet *374*, 1462-1471.

Arrowsmith, C.H., Bountra, C., Fish, P.V., Lee, K., and Schapira, M. (2012). Epigenetic protein families: a new frontier for drug discovery. Nat. Rev. Drug Discov. *11*, 384-400.

Ballestar, E., and Wolffe, A.P. (2001). Methyl-CpG-binding proteins. Targeting specific gene repression. Eur. J. Biochem. *268*, 1-6.

Barry, S.P., Davidson, S.M., and Townsend, P.A. (2008). Molecular regulation of cardiac hypertrophy. Int. J. Biochem. Cell Biol. *40*, 2023-2039.

Battiprolu, P.K., Hojayev, B., Jiang, N., Wang, Z.V., Luo, X., Iglewski, M., Shelton, J.M., Gerard, R.D., Rothermel, B.A., Gillette, T.G.*, et al.* (2012). Metabolic stress-induced activation of FoxO1 triggers diabetic cardiomyopathy in mice. J. Clin. Invest. *122*, 1109-1118.

Bella, J.N., Tang, W., Kraja, A., Rao, D.C., Hunt, S.C., Miller, M.B., Palmieri, V., Roman, M.J., Kitzman, D.W., Oberman, A.*, et al.* (2007). Genome-wide linkage mapping for valve calcification susceptibility loci in hypertensive sibships: the Hypertension Genetic Epidemiology Network Study. Hypertension *49*, 453-460.

Bernardo, B.C., Weeks, K.L., Pretorius, L., and McMullen, J.R. (2010). Molecular distinction between physiological and pathological cardiac hypertrophy: experimental findings and therapeutic strategies. Pharmacol. Ther. *128*, 191-227.

Bier, E., and Bodmer, R. (2004). Drosophila, an emerging model for cardiac disease. Gene *342*, 1-11.

Blecher-Gonen, R., Barnett-Itzhaki, Z., Jaitin, D., Amann-Zalcenstein, D., Lara-Astiaso, D., and Amit, I. (2013). High-throughput chromatin immunoprecipitation for genome-wide mapping of in vivo protein-DNA interactions and epigenomic states. Nat. Protoc. *8*, 539-554.

Block, H., Maertens, B., Spriestersbach, A., Brinker, N., Kubicek, J., Fabis, R., Labahn, J., and Schafer, F. (2009). Immobilized-metal affinity chromatography (IMAC): a review. Methods Enzymol. *463*, 439-473.

Bock, C., Paulsen, M., Tierling, S., Mikeska, T., Lengauer, T., and Walter, J. (2006). CpG island methylation in human lymphocytes is highly correlated with DNA sequence, repeats, and predicted DNA structure. PLoS Genet. *2*, e26.

Boon, A., Cheriex, E., Lodder, J., and Kessels, F. (1997). Cardiac valve calcification: characteristics of patients with calcification of the mitral annulus or aortic valve. Heart *78*, 472-474.

Branco, M.R., Ficz, G., and Reik, W. (2012). Uncovering the role of 5-hydroxymethylcytosine in the epigenome. Nat. Rev. Genet. *13*, 7-13.

Bruneau, B.G. (2008). The developmental genetics of congenital heart disease. Nature *451*, 943-948.

Bruneau, B.G. (2010). Chromatin remodeling in heart development. Curr. Opin. Genet. Dev. *20*, 505-511.

Buck-Koehntop, B.A., and Defossez, P.A. (2013). On how mammalian transcription factors recognize methylated DNA. Epigenetics *8*, 131-137.

Bueno, O.F., De Windt, L.J., Tymitz, K.M., Witt, S.A., Kimball, T.R., Klevitsky, R., Hewett, T.E., Jones, S.P., Lefer, D.J., Peng, C.F.*, et al.* (2000). The MEK1-ERK1/2 signaling pathway promotes compensated cardiac hypertrophy in transgenic mice. EMBO J. *19*, 6341-6350.

Bueno, O.F., and Molkentin, J.D. (2002). Involvement of extracellular signal-regulated kinases 1/2 in cardiac hypertrophy and cell death. Circ. Res. *91*, 776-781.

Bultman, S., Gebuhr, T., Yee, D., La Mantia, C., Nicholson, J., Gilliam, A., Randazzo, F., Metzger, D., Chambon, P., Crabtree, G.*, et al.* (2000). A Brg1 null mutation in the mouse reveals functional differences among mammalian SWI/SNF complexes. Mol. Cell *6*, 1287-1295.

Campos, E.I., and Reinberg, D. (2009). Histones: annotating chromatin. Annu. Rev. Genet. *43*, 559-599.

Canagarajah, B.J., Khokhlatchev, A., Cobb, M.H., and Goldsmith, E.J. (1997). Activation mechanism of the MAP kinase ERK2 by dual phosphorylation. Cell *90*, 859-869.

Cantin, G.T., Shock, T.R., Park, S.K., Madhani, H.D., and Yates, J.R., 3rd (2007). Optimizing TiO2-based phosphopeptide enrichment for automated multidimensional liquid chromatography coupled to tandem mass spectrometry. Anal. Chem. *79*, 4666-4673.

Chang, C.P., and Bruneau, B.G. (2012). Epigenetics and cardiovascular development. Annu. Rev. Physiol. *74*, 41-68.

Chen, Q., Chen, H., Zheng, D., Kuang, C., Fang, H., Zou, B., Zhu, W., Bu, G., Jin, T., Wang, Z.*, et al.* (2009). Smad7 is required for the development and function of the heart. J. Biol. Chem. *284*, 292-300.

Chestkov, A.V., Baka, I.D., Kost, M.V., Georgiev, G.P., and Buchman, V.L. (1996). The d4 gene family in the human genome. Genomics *36*, 174-177.

Cheung, W.L., Turner, F.B., Krishnamoorthy, T., Wolner, B., Ahn, S.H., Foley, M., Dorsey, J.A., Peterson, C.L., Berger, S.L., and Allis, C.D. (2005). Phosphorylation of histone H4 serine 1 during DNA damage requires casein kinase II in S. cerevisiae. Curr. Biol. *15*, 656-660.

Christoffels, V.M., Habets, P.E., Franco, D., Campione, M., de Jong, F., Lamers, W.H., Bao, Z.Z., Palmer, S., Biben, C., Harvey, R.P.*, et al.* (2000). Chamber formation and morphogenesis in the developing mammalian heart. Dev. Biol. *223*, 266-278.

Clapier, C.R., and Cairns, B.R. (2009). The biology of chromatin remodeling complexes. Annu. Rev. Biochem. *78*, 273-304.

Claycomb, W.C., Lanson, N.A., Jr., Stallworth, B.S., Egeland, D.B., Delcarpio, J.B., Bahinski, A., and Izzo, N.J., Jr. (1998). HL-1 cells: a cardiac muscle cell line that contracts and retains phenotypic characteristics of the adult cardiomyocyte. Proc. Natl. Acad. Sci. USA *95*, 2979-2984.

Dambrot, C., Passier, R., Atsma, D., and Mummery, C.L. (2011). Cardiomyocyte differentiation of pluripotent stem cells and their use as cardiac disease models. Biochem. J. *434*, 25-35.

Davlouros, P.A., Niwa, K., Webb, G., and Gatzoulis, M.A. (2006). The right ventricle in congenital heart disease. Heart *92 Suppl 1*, i27-38.

De Luca, A., Sarkozy, A., Ferese, R., Consoli, F., Lepri, F., Dentici, M.L., Vergara, P., De Zorzi, A., Versacci, P., Digilio, M.C.*, et al.* (2011). New mutations in ZFPM2/FOG2 gene in tetralogy of Fallot and double outlet right ventricle. Clin. Genet. *80*, 184-190.

Delgado-Olguin, P., Huang, Y., Li, X., Christodoulou, D., Seidman, C.E., Seidman, J.G., Tarakhovsky, A., and Bruneau, B.G. (2012). Epigenetic repression of cardiac progenitor gene expression by Ezh2 is required for postnatal cardiac homeostasis. Nat. Genet. *44*, 343-347.

Down, T.A., Rakyan, V.K., Turner, D.J., Flicek, P., Li, H., Kulesha, E., Graf, S., Johnson, N., Herrero, J., Tomazou, E.M.*, et al.* (2008). A Bayesian deconvolution strategy for immunoprecipitation-based DNA methylome analysis. Nat. Biotechnol. *26*, 779-785.

Duygu, B., Poels, E.M., and da Costa Martins, P.A. (2013). Genetics and epigenetics of arrhythmia and heart failure. Front Genet *4*, 219.

Efthimiadis, G.K., Pagourelias, E.D., Gossios, T., and Zegkos, T. (2014). Hypertrophic cardiomyopathy in 2013: Current speculations and future perspectives. World J. Cardiol. *6*, 26-37.

Enriquez, A.D., and Goldman, M.E. (2014). Management of hypertrophic cardiomyopathy. Ann Glob Health *80*, 35-45.

Eom, G.H., Cho, Y.K., Ko, J.H., Shin, S., Choe, N., Kim, Y., Joung, H., Kim, H.S., Nam, K.I., Kee, H.J.*, et al.* (2011). Casein kinase-2alpha1 induces hypertrophic response by phosphorylation of histone deacetylase 2 S394 and its activation in the heart. Circulation *123*, 2392-2403.

Evans, S.M., Yelon, D., Conlon, F.L., and Kirby, M.L. (2010). Myocardial lineage development. Circ. Res. *107*, 1428-1444.

Fedorova, E., and Zink, D. (2008). Nuclear architecture and gene regulation. Biochim. Biophys. Acta *1783*, 2174-2184.

Fila, J., and Honys, D. (2012). Enrichment techniques employed in phosphoproteomics. Amino Acids *43*, 1025-1047.

Fischer, A., Klattig, J., Kneitz, B., Diez, H., Maier, M., Holtmann, B., Englert, C., and Gessler, M. (2005). Hey basic helix-loop-helix transcription factors are repressors of GATA4 and GATA6 and restrict expression of the GATA target gene ANF in fetal hearts. Mol. Cell. Biol. *25*, 8960-8970.

Fischer, A., Steidl, C., Wagner, T.U., Lang, E., Jakob, P.M., Friedl, P., Knobeloch, K.P., and Gessler, M. (2007). Combined loss of Hey1 and HeyL causes congenital heart defects because of impaired epithelial to mesenchymal transition. Circ. Res. *100*, 856-863.

Forcales, S.V., Albini, S., Giordani, L., Malecova, B., Cignolo, L., Chernov, A., Coutinho, P., Saccone, V., Consalvi, S., Williams, R.*, et al.* (2012). Signal-dependent incorporation of MyoD-BAF60c into Brg1-based SWI/SNF chromatin-remodelling complex. EMBO J. *31*, 301-316.

Force, T., Bonow, R.O., Houser, S.R., Solaro, R.J., Hershberger, R.E., Adhikari, B., Anderson, M.E., Boineau, R., Byrne, B.J., Cappola, T.P.*, et al.* (2010). Research priorities in hypertrophic cardiomyopathy: report of a Working Group of the National Heart, Lung, and Blood Institute. Circulation *122*, 1130-1133.

Frank, D.U., Carter, K.L., Thomas, K.R., Burr, R.M., Bakker, M.L., Coetzee, W.A., Tristani-Firouzi, M., Bamshad, M.J., Christoffels, V.M., and Moon, A.M. (2012). Lethal arrhythmias in Tbx3-deficient mice reveal extreme dosage sensitivity of cardiac conduction system function and homeostasis. Proc. Natl. Acad. Sci. USA *109*, E154-163.

Frey, N., Katus, H.A., Olson, E.N., and Hill, J.A. (2004). Hypertrophy of the heart: a new therapeutic target? Circulation *109*, 1580-1589.

Frey, N., and Olson, E.N. (2003). Cardiac hypertrophy: the good, the bad, and the ugly. Annu. Rev. Physiol. *65*, 45-79.

Gabig, T.G., Mantel, P.L., Rosli, R., and Crean, C.D. (1994). Requiem: a novel zinc finger gene essential for apoptosis in myeloid cells. J. Biol. Chem. *269*, 29515-29519.

Gardner, D.G. (2003). Natriuretic peptides: markers or modulators of cardiac hypertrophy? Trends Endocrinol. Metab. *14*, 411-416.

Gardner, D.G., Chen, S., Glenn, D.J., and Grigsby, C.L. (2007). Molecular biology of the natriuretic peptide system: implications for physiology and hypertension. Hypertension *49*, 419-426.

Garg, V., Kathiriya, I.S., Barnes, R., Schluterman, M.K., King, I.N., Butler, C.A., Rothrock, C.R., Eapen, R.S., Hirayama-Yamada, K., Joo, K.*, et al.* (2003). GATA4 mutations cause human congenital heart defects and reveal an interaction with TBX5. Nature *424*, 443-447.

Gill, T.J., 3rd, Smith, G.J., Wissler, R.W., and Kunz, H.W. (1989). The rat as an experimental animal. Science *245*, 269-276.

Gilsbach, R., Preissl, S., Gruning, B.A., Schnick, T., Burger, L., Benes, V., Wurch, A., Bonisch, U., Gunther, S., Backofen, R.*, et al.* (2014). Dynamic DNA methylation orchestrates cardiomyocyte development, maturation and disease. Nat Commun *5*, 5288.

Gingras, A.C., Aebersold, R., and Raught, B. (2005). Advances in protein complex analysis using mass spectrometry. J. Physiol. *563*, 11-21.

Glaeser, C., Kotzot, D., Caliebe, A., Kottke, R., Schulz, S., Schweigmann, U., and Hansmann, I. (2006). Gene symbol: JAG1. Disease: tetralogy of Fallot. Hum. Genet. *119*, 674.

Goldmuntz, E., Clark, B.J., Mitchell, L.E., Jawad, A.F., Cuneo, B.F., Reed, L., McDonald-McGinn, D., Chien, P., Feuer, J., Zackai, E.H.*, et al.* (1998). Frequency of 22q11 deletions in patients with conotruncal defects. J. Am. Coll. Cardiol. *32*, 492-498.

Goldmuntz, E., Geiger, E., and Benson, D.W. (2001). NKX2.5 mutations in patients with tetralogy of fallot. Circulation *104*, 2565-2568.

Griffin, C.T., Brennan, J., and Magnuson, T. (2008). The chromatin-remodeling enzyme BRG1 plays an essential role in primitive erythropoiesis and vascular development. Development *135*, 493-500.

Grunert, M., Dorn, C., Schueler, M., Dunkel, I., Schlesinger, J., Mebus, S., Alexi-Meskishvili, V., Perrot, A., Wassilew, K., Timmermann, B.*, et al.* (2014). Rare and private variations in neural crest, apoptosis and sarcomere genes define the polygenic background of isolated Tetralogy of Fallot. Hum. Mol. Genet. *23*, 3115-3128.

Guo, W., Schafer, S., Greaser, M.L., Radke, M.H., Liss, M., Govindarajan, T., Maatz, H., Schulz, H., Li, S., Parrish, A.M.*, et al.* (2012). RBM20, a gene for hereditary cardiomyopathy, regulates titin splicing. Nat. Med. *18*, 766-773.

Gurgel-Giannetti, J., Oliveira, G., Brasileiro Filho, G., Martins, P., Vainzof, M., and Hirano, M. (2013). Mitochondrial cardioencephalomyopathy due to a novel SCO2 mutation in a Brazilian patient: case report and literature review. JAMA Neurol *70*, 258-261.

Haas, J., Frese, K.S., Park, Y.J., Keller, A., Vogel, B., Lindroth, A.M., Weichenhan, D., Franke, J., Fischer, S., Bauer, A.*, et al.* (2013). Alterations in cardiac DNA methylation in human dilated cardiomyopathy. EMBO Mol. Med. *5*, 413-429.

Han, P., Hang, C.T., Yang, J., and Chang, C.P. (2011). Chromatin remodeling in cardiovascular development and physiology. Circ. Res. *108*, 378-396.

Han, P., Li, W., Lin, C.H., Yang, J., Shang, C., Nurnberg, S.T., Jin, K.K., Xu, W., Lin, C.Y., Lin, C.J.*, et al.* (2014). A long noncoding RNA protects the heart from pathological hypertrophy. Nature *514*, 102-106.

Hang, C.T., Yang, J., Han, P., Cheng, H.L., Shang, C., Ashley, E., Zhou, B., and Chang, C.P. (2010). Chromatin regulation by Brg1 underlies heart muscle development and disease. Nature *466*, 62-67.

Harvey, R.P. (2002). Patterning the vertebrate heart. Nat. Rev. Genet. *3*, 544-556.

Hauck, L., Harms, C., An, J., Rohne, J., Gertz, K., Dietz, R., Endres, M., and von Harsdorf, R. (2008). Protein kinase CK2 links extracellular growth factor signaling with the control of p27(Kip1) stability in the heart. Nat. Med. *14*, 315-324.

He, A., Gu, F., Hu, Y., Ma, Q., Ye, L.Y., Akiyama, J.A., Visel, A., Pennacchio, L.A., and Pu, W.T. (2014). Dynamic GATA4 enhancers shape the chromatin landscape central to heart development and disease. Nat Commun *5*, 4907.

Heisig, J., Weber, D., Englberger, E., Winkler, A., Kneitz, S., Sung, W.K., Wolf, E., Eilers, M., Wei, C.L., and Gessler, M. (2012). Target gene analysis by microarrays and chromatin immunoprecipitation identifies HEY proteins as highly redundant bHLH repressors. PLoS Genet. *8*, e1002728.

Herman, D.S., Lam, L., Taylor, M.R., Wang, L., Teekakirikul, P., Christodoulou, D., Conner, L., DePalma, S.R., McDonough, B., Sparks, E.*, et al.* (2012). Truncations of titin causing dilated cardiomyopathy. N. Engl. J. Med. *366*, 619-628.

Ho, L., and Crabtree, G.R. (2010). Chromatin remodelling during development. Nature *463*, 474-484.

Hoffman, J.I., and Kaplan, S. (2002). The incidence of congenital heart disease. J. Am. Coll. Cardiol. *39*, 1890-1900.

Hon, G.C., Rajagopal, N., Shen, Y., McCleary, D.F., Yue, F., Dang, M.D., and Ren, B. (2013). Epigenetic memory at embryonic enhancers identified in DNA methylation maps from adult mouse tissues. Nat. Genet. *45*, 1198-1206.

Hoyal, C.R., Kammerer, S., Roth, R.B., Reneland, R., Marnellos, G., Kiechle, M., Schwarz-Boeger, U., Griffiths, L.R., Ebner, F., Rehbock, J.*, et al.* (2005). Genetic polymorphisms in DPF3 associated with risk of breast cancer and lymph node metastases. J. Carcinog. *4*, 13.

Ishizaka, A., Mizutani, T., Kobayashi, K., Tando, T., Sakurai, K., Fujiwara, T., and Iba, H. (2012). Double plant homeodomain (PHD) finger proteins DPF3a and -3b are required as transcriptional co-activators in SWI/SNF complex-dependent activation of NF-kappaB RelA/p50 heterodimer. J. Biol. Chem. *287*, 11924-11933.

Issa, J.P. (2004). CpG island methylator phenotype in cancer. Nat. Rev. Cancer *4*, 988-993.

Jenkins, K.J., Correa, A., Feinstein, J.A., Botto, L., Britt, A.E., Daniels, S.R., Elixson, M., Warnes, C.A., Webb, C.L., and American Heart Association Council on Cardiovascular Disease in the, Y. (2007). Noninherited risk factors and congenital cardiovascular defects: current knowledge: a scientific statement from the American Heart Association Council on Cardiovascular Disease in the Young: endorsed by the American Academy of Pediatrics. Circulation *115*, 2995-3014.

Johnson, D.S., Mortazavi, A., Myers, R.M., and Wold, B. (2007). Genome-wide mapping of in vivo protein-DNA interactions. Science *316*, 1497-1502.

Jones, P.A. (2012). Functions of DNA methylation: islands, start sites, gene bodies and beyond. Nat. Rev. Genet. *13*, 484-492.

Kaiser, P., Meierhofer, D., Wang, X., and Huang, L. (2008). Tandem affinity purification combined with mass spectrometry to identify components of protein complexes. Methods Mol. Biol. *439*, 309-326.

Kang, H., Jung, J.W., Kim, M.K., and Chung, J.H. (2009). CK2 is the regulator of SIRT1 substrate-binding affinity, deacetylase activity and cellular response to DNA-damage. PLoS One *4*, e6611.

Karkera, J.D., Lee, J.S., Roessler, E., Banerjee-Basu, S., Ouspenskaia, M.V., Mez, J., Goldmuntz, E., Bowers, P., Towbin, J., Belmont, J.W.*, et al.* (2007). Loss-of-function mutations in growth differentiation factor-1 (GDF1) are associated with congenital heart defects in humans. Am. J. Hum. Genet. *81*, 987-994.

Kathiriya, I.S., King, I.N., Murakami, M., Nakagawa, M., Astle, J.M., Gardner, K.A., Gerard, R.D., Olson, E.N., Srivastava, D., and Nakagawa, O. (2004). Hairy-related transcription factors inhibit GATA-dependent cardiac gene expression through a signal-responsive mechanism. J. Biol. Chem. *279*, 54937-54943.

Kaynak, B., von Heydebreck, A., Mebus, S., Seelow, D., Hennig, S., Vogel, J., Sperling, H.P., Pregla, R., Alexi-Meskishvili, V., Hetzer, R.*, et al.* (2003). Genome-wide array analysis of normal and malformed human hearts. Circulation *107*, 2467-2474.

Kelly, R.G. (2007). Building the right ventricle. Circ. Res. *100*, 943-945.

Kelly, R.G., Brown, N.A., and Buckingham, M.E. (2001). The arterial pole of the mouse heart forms from Fgf10-expressing cells in pharyngeal mesoderm. Dev. Cell *1*, 435-440.

Khositseth, A., Tocharoentanaphol, C., Khowsathit, P., and Ruangdaraganon, N. (2005). Chromosome 22q11 deletions in patients with conotruncal heart defects. Pediatr. Cardiol. *26*, 570-573.

Kimes, B.W., and Brandt, B.L. (1976). Properties of a clonal muscle cell line from rat heart. Exp. Cell Res. *98*, 367-381.

Kirchner, M., and Selbach, M. (2012). In vivo quantitative proteome profiling: planning and evaluation of SILAC experiments. Methods Mol. Biol. *893*, 175-199.

Kong, S.W., Hu, Y.W., Ho, J.W., Ikeda, S., Polster, S., John, R., Hall, J.L., Bisping, E., Pieske, B., dos Remedios, C.G.*, et al.* (2010). Heart failure-associated changes in RNA splicing of sarcomere genes. Circ. Cardiovasc. Genet. *3*, 138-146.

Kosova, G., Hotaling, J.M., Ohlander, S., Niederberger, C., Prins, G.S., and Ober, C. (2014). Variants in DPF3 and DSCAML1 are associated with sperm morphology. J. Assist. Reprod. Genet. *31*, 131-137.

Krueger, F., Kreck, B., Franke, A., and Andrews, S.R. (2012). DNA methylome analysis using short bisulfite sequencing data. Nat. Methods *9*, 145-151.

Laird, P.W. (2010). Principles and challenges of genomewide DNA methylation analysis. Nat. Rev. Genet. *11*, 191-203.

Lan, F., Lee, A.S., Liang, P., Sanchez-Freire, V., Nguyen, P.K., Wang, L., Han, L., Yen, M., Wang, Y., Sun, N.*, et al.* (2013). Abnormal calcium handling properties underlie familial hypertrophic cardiomyopathy pathology in patient-specific induced pluripotent stem cells. Cell Stem Cell *12*, 101-113.

Lange, M., Kaynak, B., Forster, U.B., Tonjes, M., Fischer, J.J., Grimm, C., Schlesinger, J., Just, S., Dunkel, I., Krueger, T.*, et al.* (2008). Regulation of muscle development by DPF3, a novel histone acetylation and methylation reader of the BAF chromatin remodeling complex. Genes Dev. *22*, 2370-2384.

Leary, S.C., Cobine, P.A., Kaufman, B.A., Guercin, G.H., Mattman, A., Palaty, J., Lockitch, G., Winge, D.R., Rustin, P., Horvath, R.*, et al.* (2007). The human cytochrome c oxidase assembly factors SCO1 and SCO2 have regulatory roles in the maintenance of cellular copper homeostasis. Cell Metab *5*, 9-20.

Lessard, J., Wu, J.I., Ranish, J.A., Wan, M., Winslow, M.M., Staahl, B.T., Wu, H., Aebersold, R., Graef, I.A., and Crabtree, G.R. (2007). An essential switch in subunit composition of a chromatin remodeling complex during neural development. Neuron *55*, 201-215.

Leu, M., Ehler, E., and Perriard, J.C. (2001). Characterisation of postnatal growth of the murine heart. Anat. Embryol. (Berl.) *204*, 217-224.

Lev Maor, G., Yearim, A., and Ast, G. (2015). The alternative role of DNA methylation in splicing regulation. Trends Genet. *31*, 274-280.

Levy, D., Garrison, R.J., Savage, D.D., Kannel, W.B., and Castelli, W.P. (1990). Prognostic implications of echocardiographically determined left ventricular mass in the Framingham Heart Study. N. Engl. J. Med. *322*, 1561-1566.

LeWinter, M.M. (2005). Functional consequences of sarcomeric protein abnormalities in failing myocardium. Heart Fail. Rev. *10*, 249-257.

Liang, P., Song, F., Ghosh, S., Morien, E., Qin, M., Mahmood, S., Fujiwara, K., Igarashi, J., Nagase, H., and Held, W.A. (2011). Genome-wide survey reveals dynamic widespread tissue-specific changes in DNA methylation during development. BMC Genomics *12*, 231.

Liang, Q., De Windt, L.J., Witt, S.A., Kimball, T.R., Markham, B.E., and Molkentin, J.D. (2001a). The transcription factors GATA4 and GATA6 regulate cardiomyocyte hypertrophy in vitro and in vivo. J. Biol. Chem. *276*, 30245-30253.

Liang, Q., Wiese, R.J., Bueno, O.F., Dai, Y.S., Markham, B.E., and Molkentin, J.D. (2001b). The transcription factor GATA4 is activated by extracellular signal-regulated kinase 1- and 2-mediated phosphorylation of serine 105 in cardiomyocytes. Mol. Cell. Biol. *21*, 7460-7469.

Lickert, H., Takeuchi, J.K., Von Both, I., Walls, J.R., McAuliffe, F., Adamson, S.L., Henkelman, R.M., Wrana, J.L., Rossant, J., and Bruneau, B.G. (2004). Baf60c is essential for function of BAF chromatin remodelling complexes in heart development. Nature *432*, 107-112.

Lin, X., Huo, Z., Liu, X., Zhang, Y., Li, L., Zhao, H., Yan, B., Liu, Y., Yang, Y., and Chen, Y.H. (2010). A novel GATA6 mutation in patients with tetralogy of Fallot or atrial septal defect. J. Hum. Genet. *55*, 662-667.

Lips, D.J., deWindt, L.J., van Kraaij, D.J., and Doevendans, P.A. (2003). Molecular determinants of myocardial hypertrophy and failure: alternative pathways for beneficial and maladaptive hypertrophy. Eur. Heart J. *24*, 883-896.

Litchfield, D.W. (2003). Protein kinase CK2: structure, regulation and role in cellular decisions of life and death. Biochem. J. *369*, 1-15.

Liu, C.X., Shen, A.D., Li, X.F., Jiao, W.W., Bai, S., Yuan, F., Guan, X.L., Zhang, X.G., Zhang, G.R., and Li, Z.Z. (2009). Association of TBX5 gene polymorphism with ventricular septal defect in the Chinese Han population. Chin. Med. J. (Engl.) *122*, 30-34.

Lopaschuk, G.D., and Jaswal, J.S. (2010). Energy metabolic phenotype of the cardiomyocyte during development, differentiation, and postnatal maturation. J. Cardiovasc. Pharmacol. *56*, 130-140.

Lowes, B.D., Minobe, W., Abraham, W.T., Rizeq, M.N., Bohlmeyer, T.J., Quaife, R.A., Roden, R.L., Dutcher, D.L., Robertson, A.D., Voelkel, N.F.*, et al.* (1997). Changes in gene expression in the intact human heart. Downregulation of alpha-myosin heavy chain in hypertrophied, failing ventricular myocardium. J. Clin. Invest. *100*, 2315-2324.

Luger, K., Mader, A.W., Richmond, R.K., Sargent, D.F., and Richmond, T.J. (1997). Crystal structure of the nucleosome core particle at 2.8 A resolution. Nature *389*, 251-260.

Maeda, J., Yamagishi, H., Matsuoka, R., Ishihara, J., Tokumura, M., Fukushima, H., Ueda, H., Takahashi, E., Yoshiba, S., and Kojima, Y. (2000). Frequent association of 22q11.2 deletion with tetralogy of Fallot. Am. J. Med. Genet. *92*, 269-272.

Major, R.J., and Poss, K.D. (2007). Zebrafish Heart Regeneration as a Model for Cardiac Tissue Repair. Drug Discov. Today Dis. Models *4*, 219-225.

Marian, A.J., Mares, A., Jr., Kelly, D.P., Yu, Q.T., Abchee, A.B., Hill, R., and Roberts, R. (1995). Sudden cardiac death in hypertrophic cardiomyopathy. Variability in phenotypic expression of beta-myosin heavy chain mutations. Eur. Heart J. *16*, 368-376.

Marston, S., Copeland, O., Jacques, A., Livesey, K., Tsang, V., McKenna, W.J., Jalilzadeh, S., Carballo, S., Redwood, C., and Watkins, H. (2009). Evidence from human myectomy samples that MYBPC3 mutations cause hypertrophic cardiomyopathy through haploinsufficiency. Circ. Res. *105*, 219-222.

Martinez-Morentin, L., Martinez, L., Piloto, S., Yang, H., Schon, E.A., Garesse, R., Bodmer, R., Ocorr, K., Cervera, M., and Arredondo, J.J. (2015). Cardiac deficiency of single cytochrome oxidase assembly factor scox induces p53-dependent apoptosis in a Drosophila cardiomyopathy model. Hum. Mol. Genet. *24*, 3608-3622.

Matoba, S., Kang, J.G., Patino, W.D., Wragg, A., Boehm, M., Gavrilova, O., Hurley, P.J., Bunz, F., and Hwang, P.M. (2006). p53 regulates mitochondrial respiration. Science *312*, 1650-1653.

Maunakea, A.K., Chepelev, I., Cui, K., and Zhao, K. (2013). Intragenic DNA methylation modulates alternative splicing by recruiting MeCP2 to promote exon recognition. Cell Res. *23*, 1256-1269.

McBurney, M.W., Jones-Villeneuve, E.M., Edwards, M.K., and Anderson, P.J. (1982). Control of muscle and neuronal differentiation in a cultured embryonal carcinoma cell line. Nature *299*, 165-167.

Mehrotra, A., Joe, B., and de la Serna, I.L. (2013). SWI/SNF chromatin remodeling enzymes are associated with cardiac hypertrophy in a genetic rat model of hypertension. J. Cell. Physiol. *228*, 2337-2342.

Meng, Z.X., Li, S., Wang, L., Ko, H.J., Lee, Y., Jung, D.Y., Okutsu, M., Yan, Z., Kim, J.K., and Lin, J.D. (2013). Baf60c drives glycolytic metabolism in the muscle and improves systemic glucose homeostasis through Deptor-mediated Akt activation. Nat. Med. *19*, 640-645.

Merscher, S., Funke, B., Epstein, J.A., Heyer, J., Puech, A., Lu, M.M., Xavier, R.J., Demay, M.B., Russell, R.G., Factor, S.*, et al.* (2001). TBX1 is responsible for cardiovascular defects in velo-cardio-facial/DiGeorge syndrome. Cell *104*, 619-629.

Mertsalov, I.B., Kulikova, D.A., Alimova-Kost, M.V., Ninkina, N.N., Korochkin, L.I., and Buchman, V.L. (2000). Structure and expression of two members of the d4 gene family in mouse. Mamm. Genome *11*, 72-74.

Minkkila, K., and Tikanoja, T. (1996). [Increasing incidence of congenital heart diseases]. Duodecim *112*, 199-204.

Miyata, S., Minobe, W., Bristow, M.R., and Leinwand, L.A. (2000). Myosin heavy chain isoform expression in the failing and nonfailing human heart. Circ. Res. *86*, 386-390.

Moore, J.C., Spijker, R., Martens, A.C., de Boer, T., Rook, M.B., van der Heyden, M.A., Tertoolen, L.G., and Mummery, C.L. (2004). A P19Cl6 GFP reporter line to quantify cardiomyocyte differentiation of stem cells. Int. J. Dev. Biol. *48*, 47-55.

Moorman, A.F., and Christoffels, V.M. (2003). Cardiac chamber formation: development, genes, and evolution. Physiol. Rev. *83*, 1223-1267.

Moorman, A.F., de Jong, F., Denyn, M.M., and Lamers, W.H. (1998). Development of the cardiac conduction system. Circ. Res. *82*, 629-644.

Moretti, A., Bellin, M., Welling, A., Jung, C.B., Lam, J.T., Bott-Flugel, L., Dorn, T., Goedel, A., Hohnke, C., Hofmann, F.*, et al.* (2010). Patient-specific induced pluripotent stem-cell models for long-QT syndrome. N. Engl. J. Med. *363*, 1397-1409.

Movassagh, M., Vujic, A., and Foo, R. (2011). Genome-wide DNA methylation in human heart failure. Epigenomics *3*, 103-109.

Mukhopadhyay, A., Deplancke, B., Walhout, A.J., and Tissenbaum, H.A. (2008). Chromatin immunoprecipitation (ChIP) coupled to detection by quantitative real-time PCR to study transcription factor binding to DNA in Caenorhabditis elegans. Nat. Protoc. *3*, 698-709.

Muslin, A.J. (2008). MAPK signalling in cardiovascular health and disease: molecular mechanisms and therapeutic targets. Clin. Sci. (Lond.) *115*, 203-218.

Ninkina, N.N., Mertsalov, I.B., Kulikova, D.A., Alimova-Kost, M.V., Simonova, O.B., Korochkin, L.I., Kiselev, S.L., and Buchman, V.L. (2001). Cerd4, third member of the d4 gene family: expression and organization of genomic locus. Mamm. Genome *12*, 862-866.

Nishi, H., Hashimoto, K., and Panchenko, A.R. (2011). Phosphorylation in protein-protein binding: effect on stability and function. Structure *19*, 1807-1815.

Nishimura, R.A., and Ommen, S.R. (2006). Hypertrophic cardiomyopathy: the search for obstruction. Circulation *114*, 2200-2202.

Novaro, G.M., Sachar, R., Pearce, G.L., Sprecher, D.L., and Griffin, B.P. (2003). Association between apolipoprotein E alleles and calcific valvular heart disease. Circulation *108*, 1804-1808.

Olsen, J.V., Blagoev, B., Gnad, F., Macek, B., Kumar, C., Mortensen, P., and Mann, M. (2006). Global, in vivo, and site-specific phosphorylation dynamics in signaling networks. Cell *127*, 635-648.

Olson, E.N. (2006). Gene regulatory networks in the evolution and development of the heart. Science *313*, 1922-1927.

Ortlepp, J.R., Hoffmann, R., Ohme, F., Lauscher, J., Bleckmann, F., and Hanrath, P. (2001). The vitamin D receptor genotype predisposes to the development of calcific aortic valve stenosis. Heart *85*, 635-638.

Penny, D.J., and Vick, G.W., 3rd (2011). Ventricular septal defect. Lancet *377*, 1103-1112.

Peterson, C.L., and Workman, J.L. (2000). Promoter targeting and chromatin remodeling by the SWI/SNF complex. Curr. Opin. Genet. Dev. *10*, 187-192.

Reik, W., and Dean, W. (2001). DNA methylation and mammalian epigenetics. Electrophoresis *22*, 2838-2843.

Reyes, J.C., Barra, J., Muchardt, C., Camus, A., Babinet, C., and Yaniv, M. (1998). Altered control of cellular proliferation in the absence of mammalian brahma (SNF2alpha). EMBO J. *17*, 6979-6991.

Richards, A.M. (2007). Natriuretic peptides: update on Peptide release, bioactivity, and clinical use. Hypertension *50*, 25-30.

Rivera, C.M., and Ren, B. (2013). Mapping human epigenomes. Cell *155*, 39-55.

Rochais, F., Mesbah, K., and Kelly, R.G. (2009). Signaling pathways controlling second heart field development. Circ. Res. *104*, 933-942.

Roessler, E., Ouspenskaia, M.V., Karkera, J.D., Velez, J.I., Kantipong, A., Lacbawan, F., Bowers, P., Belmont, J.W., Towbin, J.A., Goldmuntz, E.*, et al.* (2008). Reduced NODAL signaling strength via mutation of several pathway members including FOXH1 is linked to human heart defects and holoprosencephaly. Am. J. Hum. Genet. *83*, 18-29.

Rose, B.A., Force, T., and Wang, Y. (2010). Mitogen-activated protein kinase signaling in the heart: angels versus demons in a heart-breaking tale. Physiol. Rev. *90*, 1507-1546.

Sadoshima, J., and Izumo, S. (1997). The cellular and molecular response of cardiac myocytes to mechanical stress. Annu. Rev. Physiol. *59*, 551-571.

Sakata, Y., Kamei, C.N., Nakagami, H., Bronson, R., Liao, J.K., and Chin, M.T. (2002). Ventricular septal defect and cardiomyopathy in mice lacking the transcription factor CHF1/Hey2. Proc. Natl. Acad. Sci. USA *99*, 16197-16202.

Sanna, B., Bueno, O.F., Dai, Y.S., Wilkins, B.J., and Molkentin, J.D. (2005). Direct and indirect interactions between calcineurin-NFAT and MEK1-extracellular signal-regulated kinase 1/2 signaling pathways regulate cardiac gene expression and cellular growth. Mol. Cell. Biol. *25*, 865-878.

Schoenebeck, J.J., and Yelon, D. (2007). Illuminating cardiac development: Advances in imaging add new dimensions to the utility of zebrafish genetics. Semin. Cell Dev. Biol. *18*, 27-35.

Seldin, D.C., Lou, D.Y., Toselli, P., Landesman-Bollag, E., and Dominguez, I. (2008). Gene targeting of CK2 catalytic subunits. Mol. Cell. Biochem. *316*, 141-147.

Serre, D., Lee, B.H., and Ting, A.H. (2010). MBD-isolated Genome Sequencing provides a high-throughput and comprehensive survey of DNA methylation in the human genome. Nucleic Acids Res. *38*, 391-399.

Shaul, Y.D., and Seger, R. (2007). The MEK/ERK cascade: from signaling specificity to diverse functions. Biochim. Biophys. Acta *1773*, 1213-1226.

Sheng, W., Qian, Y., Zhang, P., Wu, Y., Wang, H., Ma, X., Chen, L., Ma, D., and Huang, G. (2014). Association of promoter methylation statuses of congenital heart defect candidate genes with Tetralogy of Fallot. J. Transl. Med. *12*, 31.

Snider, P., and Conway, S.J. (2011). Probing human cardiovascular congenital disease using transgenic mouse models. Prog. Mol. Biol. Transl. Sci. *100*, 83-110.

Soemedi, R., Wilson, I.J., Bentham, J., Darlay, R., Topf, A., Zelenika, D., Cosgrove, C., Setchfield, K., Thornborough, C., Granados-Riveron, J.*, et al.* (2012). Contribution of global rare copy-number variants to the risk of sporadic congenital heart disease. Am. J. Hum. Genet. *91*, 489-501.

Sperling, S.R. (2011). Systems biology approaches to heart development and congenital heart disease. Cardiovasc. Res. *91*, 269-278.

Spirito, P., Autore, C., Formisano, F., Assenza, G.E., Biagini, E., Haas, T.S., Bongioanni, S., Semsarian, C., Devoto, E., Musumeci, B.*, et al.* (2014). Risk of sudden death and outcome in patients with hypertrophic cardiomyopathy with benign presentation and without risk factors. Am. J. Cardiol. *113*, 1550-1555.

Srivastava, D. (2006). Making or breaking the heart: from lineage determination to morphogenesis. Cell *126*, 1037-1048.

Stankunas, K., Hang, C.T., Tsun, Z.Y., Chen, H., Lee, N.V., Wu, J.I., Shang, C., Bayle, J.H., Shou, W., Iruela-Arispe, M.L.*, et al.* (2008). Endocardial Brg1 represses ADAMTS1 to maintain the microenvironment for myocardial morphogenesis. Dev. Cell *14*, 298-311.

Stewart, B.F., Siscovick, D., Lind, B.K., Gardin, J.M., Gottdiener, J.S., Smith, V.E., Kitzman, D.W., and Otto, C.M. (1997). Clinical factors associated with calcific aortic valve disease. Cardiovascular Health Study. J. Am. Coll. Cardiol. *29*, 630-634.

Suzuki, M.M., and Bird, A. (2008). DNA methylation landscapes: provocative insights from epigenomics. Nat. Rev. Genet. *9*, 465-476.

Thanassoulis, G., Campbell, C.Y., Owens, D.S., Smith, J.G., Smith, A.V., Peloso, G.M., Kerr, K.F., Pechlivanis, S., Budoff, M.J., Harris, T.B.*, et al.* (2013). Genetic associations with valvular calcification and aortic stenosis. N. Engl. J. Med. *368*, 503-512.

Theodorou, M., Speletas, M., Mamara, A., Papachristopoulou, G., Lazou, V., Scorilas, A., and Katsantoni, E. (2013). Identification of a STAT5 target gene, Dpf3, provides novel insights in chronic lymphocytic leukemia. PLoS One *8*, e76155.

Thum, T., Galuppo, P., Wolf, C., Fiedler, J., Kneitz, S., van Laake, L.W., Doevendans, P.A., Mummery, C.L., Borlak, J., Haverich, A.*, et al.* (2007). MicroRNAs in the human heart: a clue to fetal gene reprogramming in heart failure. Circulation *116*, 258-267.

Tirziu, D., Giordano, F.J., and Simons, M. (2010). Cell communications in the heart. Circulation *122*, 928-937.

Tomita-Mitchell, A., Mahnke, D.K., Struble, C.A., Tuffnell, M.E., Stamm, K.D., Hidestrand, M., Harris, S.E., Goetsch, M.A., Simpson, P.M., Bick, D.P.*, et al.* (2012). Human gene copy number spectra analysis in congenital heart malformations. Physiol. Genomics *44*, 518-541.

Tomita-Mitchell, A., Maslen, C.L., Morris, C.D., Garg, V., and Goldmuntz, E. (2007). GATA4 sequence variants in patients with congenital heart disease. J. Med. Genet. *44*, 779-783.

van Berlo, J.H., Elrod, J.W., Aronow, B.J., Pu, W.T., and Molkentin, J.D. (2011). Serine 105 phosphorylation of transcription factor GATA4 is necessary for stress-induced cardiac hypertrophy in vivo. Proc. Natl. Acad. Sci. USA *108*, 12331-12336.

Vieira, A.R., McHenry, T.G., Daack-Hirsch, S., Murray, J.C., and Marazita, M.L. (2008). Candidate gene/loci studies in cleft lip/palate and dental anomalies finds novel susceptibility genes for clefts. Genet. Med. *10*, 668-674.

Wade, P.A. (2001). Methyl CpG-binding proteins and transcriptional repression. Bioessays *23*, 1131-1137.

Waldo, K.L., Kumiski, D.H., Wallis, K.T., Stadt, H.A., Hutson, M.R., Platt, D.H., and Kirby, M.L. (2001). Conotruncal myocardium arises from a secondary heart field. Development *128*, 3179-3188.

Walsh, R., Rutland, C., Thomas, R., and Loughna, S. (2010). Cardiomyopathy: a systematic review of disease-causing mutations in myosin heavy chain 7 and their phenotypic manifestations. Cardiology *115*, 49-60.

Wang, L., and Proud, C.G. (2002). Ras/Erk signaling is essential for activation of protein synthesis by Gq protein-coupled receptor agonists in adult cardiomyocytes. Circ. Res. *91*, 821-829.

Wang, Z., Zhai, W., Richardson, J.A., Olson, E.N., Meneses, J.J., Firpo, M.T., Kang, C., Skarnes, W.C., and Tjian, R. (2004). Polybromo protein BAF180 functions in mammalian cardiac chamber maturation. Genes Dev. *18*, 3106-3116.

Watkins, S.J., Borthwick, G.M., and Arthur, H.M. (2011). The H9C2 cell line and primary neonatal cardiomyocyte cells show similar hypertrophic responses in vitro. In Vitro Cell. Dev. Biol. Anim. *47*, 125-131.

Wiese, C., Heisig, J., and Gessler, M. (2010). Hey bHLH factors in cardiovascular development. Pediatr. Cardiol. *31*, 363-370.

Wolf, M.J., and Rockman, H.A. (2011). Drosophila, genetic screens, and cardiac function. Circ. Res. *109*, 794-806.

Xiang, F., Sakata, Y., Cui, L., Youngblood, J.M., Nakagami, H., Liao, J.K., Liao, R., and Chin, M.T. (2006). Transcription factor CHF1/Hey2 suppresses cardiac hypertrophy through an inhibitory interaction with GATA4. Am. J. Physiol. Heart Circ. Physiol. *290*, H1997-2006.

Xie, L., Weichel, B., Ohm, J.E., and Zhang, K. (2011). An integrative analysis of DNA methylation and RNA-Seq data for human heart, kidney and liver. BMC Syst. Biol. *5 Suppl 3*, S4.

Xin, M., Olson, E.N., and Bassel-Duby, R. (2013). Mending broken hearts: cardiac development as a basis for adult heart regeneration and repair. Nat. Rev. Mol. Cell Biol. *14*, 529-541.

Yaffe, D., and Saxel, O. (1977). Serial passaging and differentiation of myogenic cells isolated from dystrophic mouse muscle. Nature *270*, 725-727.

Yang, L., Soonpaa, M.H., Adler, E.D., Roepke, T.K., Kattman, S.J., Kennedy, M., Henckaerts, E., Bonham, K., Abbott, G.W., Linden, R.M.*, et al.* (2008). Human cardiovascular progenitor cells develop from a KDR+ embryonic-stem-cell-derived population. Nature *453*, 524-528.

Yearim, A., Gelfman, S., Shayevitch, R., Melcer, S., Glaich, O., Mallm, J.P., Nissim-Rafinia, M., Cohen, A.H., Rippe, K., Meshorer, E.*, et al.* (2015). HP1 is involved in

regulating the global impact of DNA methylation on alternative splicing. Cell Rep *10*, 1122-1134.

Yuan, S.M., and Jing, H. (2010). Cardiac pathologies in relation to Smad-dependent pathways. Interact. Cardiovasc. Thorac. Surg. *11*, 455-460.

Zeng, L., Zhang, Q., Li, S., Plotnikov, A.N., Walsh, M.J., and Zhou, M.M. (2010). Mechanism and regulation of acetylated histone binding by the tandem PHD finger of DPF3b. Nature *466*, 258-262.

Zhang, G., and Neubert, T.A. (2006). Use of detergents to increase selectivity of immunoprecipitation of tyrosine phosphorylated peptides prior to identification by MALDI quadrupole-TOF MS. Proteomics *6*, 571-578.

Zhang, W., Li, X., Shen, A., Jiao, W., Guan, X., and Li, Z. (2008). GATA4 mutations in 486 Chinese patients with congenital heart disease. Eur. J. Med. Genet. *51*, 527-535.

Zhao, W., Niu, G., Shen, B., Zheng, Y., Gong, F., Wang, X., Lee, J., Mulvihill, J.J., Chen, X., and Li, S. (2013). High-resolution analysis of copy number variants in adults with simple-to-moderate congenital heart disease. Am. J. Med. Genet. A *161A*, 3087-3094.

Zhu, C., Yu, Z.B., Chen, X.H., Ji, C.B., Qian, L.M., and Han, S.P. (2011a). DNA hypermethylation of the NOX5 gene in fetal ventricular septal defect. Exp. Ther. Med. *2*, 1011-1015.

Zhu, C., Yu, Z.B., Chen, X.H., Pan, Y., Dong, X.Y., Qian, L.M., and Han, S.P. (2011b). Screening for differential methylation status in fetal myocardial tissue samples with ventricular septal defects by promoter methylation microarrays. Mol Med Rep *4*, 137-143.

Zhuang, J., Ma, W., Lago, C.U., and Hwang, P.M. (2012). Metabolic regulation of oxygen and redox homeostasis by p53: lessons from evolutionary biology? Free Radic. Biol. Med. *53*, 1279-1285.

6 Appendix

6.1 Summary

Epigenetic mechanisms, including ATP-dependent chromatin remodeling and DNA methylation, alter chromatin structure and thus modulate gene expression patterns temporally and spatially in cardiac development and disease.

Activation of the chromatin remodeling factor DPF3a in hypertrophic human hearts has raised interest in its role in pathological cardiac hypertrophy. In the present study, we identified a novel molecular pathway, mediated by DPF3a, which drives cardiac hypertrophy. We showed that CK2 binds and phosphorylates DPF3a at S348, which is located in the C-terminus. Upon hypertrophic stimuli, DPF3a accumulates in the nucleus in cultured cardiomyocytes and human cardiac biopsies. Phosphorylation of S348 initiates the interaction of DPF3a with HEY transcriptional repressors, leading to the release of HEY from DNA. Moreover, DPF3a recruits BRG1 to genomic targets via its interaction with HEY. Consequently, the transcription of fetal genes known to be involved in pathological hypertrophy is initiated. In addition, we showed that DPF3a is incapable of binding to DNA directly, instead, HEY factors act as the linker between DPF3a and DNA.

By performing MBD-seq, we presented the first genome-wide DNA methylation analysis of human congenital heart defects and depicted the impact of alterations of DNA methylation associated with gene expression changes in patients with Tetralogy of Fallot. Moreover, we provided insight into the functional role of identified alterations of DNA methylation; for example, in the case of *SCO2*, a novel regulatory element located at the *SCO2* promoter CpG island was identified. For sarcomeric genes such as *TNNT1*, *TNNT2*, *MYL7* and *PDLIM3*, we found methylation changes of these genes co-localized with novel, differential splicing events that have been shown to contribute to heart failure and cardiomyopathies.

Taken together, we characterized the detailed function of the chromatin remodeling factor DPF3a in cardiac hypertrophy, and analyzed DNA methylation in congenital heart defects. These findings provided insights into epigenetic regulation underlying cardiac defects, and hopefully will help to develop novel therapeutic perspectives for cardiac diseases by targeting epigenetic regulators or modifications.

6.2 Zusammenfassung

Epigenetische Mechanismen wie das ATP-abhängige Remodeling der Nukleosomen und DNA-Methylierung verändern die Struktur des Chromatins und beeinflussen damit die zeitliche und räumliche Expression von Genen sowohl bei der Herzentwicklung als auch bei Herzerkrankungen.

Die Aktivierung des Chromatin-Remodeling Faktors DPF3a im hypertrophen Myokard des Menschen weckte das Interesse an dessen Rolle bei der pathologischen Hypertrophie im Herzen. In der vorliegenden Studie haben wir einen neuen molekularen Stoffwechselweg gefunden, wie Hypertrophie durch DPF3a vermittelt wird. Es wurde gezeigt, dass DPF3 durch CK2 gebunden und am C-Terminus an Serin 348 (S348) phosphoryliert wird. In Proben von kultivierten Kardiomyozyten und menschlichen Herzbiopsien sammelte sich DPF3a nach hypertropher Stimulation im Zellkern an. Es konnte gezeigt werden, dass die Phosphorylierung von S348 die Interaktion von DPF3a mit HEY-Transkriptionsrepressoren initiiert, was zu deren Freisetzung von der DNA führt. Durch die Interaktion mit HEY führt DPF3a BRG1 darüber hinaus zu bestimmten genomischen Zielen. Dadurch wird die Transkription von fetalen Genen initiiert, die für ihre Rolle bei der pathologischen Hypertrophie bekannt sind. Zusätzlich wird in dieser Arbeit gezeigt, dass DPF3a nicht direkt an die DNA binden kann. Stattdessen wirken die HEY-Faktoren als Linker zwischen DPF3a und der DNA.

Mit der Durchführung von MBD-seq wird in dieser Arbeit die erste genomweite DNA-Methylierungsanalyse zu angeborenen Herzfehlern im Menschen vorgestellt. Hierbei wurde der Einfluss von DNA-Methylierungsveränderungen mit einhergehenden Veränderungen in der Genexpression bei Patienten mit Fallot‘scher Tetralogie untersucht. Darüber hinaus wird ein Einblick in die funktionelle Rolle der identifizierten Veränderungen in der DNA-Methylierung gegeben. Zum Beispiel wurde ein neues regulatives Element an der Promotor CpG Insel von *SCO2* gefunden. Für Gene des Sarkomers wie *TNNT1*, *TNNT2*, *MYL7* und *PDLIM3* wurden Methylierungsveränderungen identifiziert, die gemeinsam mit differentiellem Spleißen einhergehen. Für diese Gene wurde bereits gezeigt, dass sie eine wichtige Rolle bei der Herzschwäche und den Kardiomyopathien spielen.

Zusammenfassend wurde in dieser Arbeit die Rolle des Chromatin-Remodeling Faktors DPF3a bei der kardialen Hypertrophie sowie DNA-Methylierung in angeborenen Herzerkrankungen untersucht. Die Ergebnisse geben wichtige Einblicke in die epigenetische Regulation bei der Entstehung von Herzfehlen. Diese könnten zur Entwicklung neuer therapeutischer Perspektiven für Herzerkrankungen durch gezielte epigenetische Regulatoren und Modifikationen beitragen.

6.3 Abbreviations

ac	Acetylation
AS	Aortic stenosis
AVN	Atrio-ventricular node
BAF	Brahma-associated factor
bHLH	Basic helix-loop-helix
BS-seq	Bisulfite sequencing
CGI	CpG island
CHD	Congenital heart disease
ChIP	Chromatin immunoprecipitation
CK2	Casein kinase 2
DMR	Differentially methylated region
DNMT	DNA methyltransferase
E	Embryonic day of mouse development
ESC	Embryonic stem cell
ET-1	Endothelin 1
FHF	First heart field
GO	Gene ontology
HCM	Hypertrophic cardiomyopathy
HDAC	Histone deacetylase
IMAC	Immobilized-metal affinity chromatography
iPSC	Induced pluripotent stem cell
LA	Left atrium
lncRNA	Long non-coding RNA
LV	Left ventricle
MAPK	Mitogen-activated protein kinase
MBD	Methyl-CpG binding domain
me	Methylation
MeDIP	Methylation-dependent immunoprecipitation
MRE	Methylation-sensitive restriction enzyme digestion
MS	Mass spectropmetry
ncRNA	Non-coding RNA
NH	Normal heart
P	Phosphorylation
PARP	Ploy ADP-ribose polymerase
PE	Phenylephrine

PHD	Plant homeodomain
RA	Right atrium
RV	Right ventricle
SAN	Sino-atrial node
SHF	Second heart field
SILAC	Stable isotope labeling by amino acids in cell culture
siRNA	Small interfering RNA
TAP	Tandem affinity purification
TET	Ten-eleven translocation
TFBS	Transcription factor binding site
TOF	Tetralogy of Fallot
VSD	Ventricular septal defect
WT	Wild type

6.4 Curriculum Vitae

For reasons of data protection, the curriculum vitae is not published in the electronic version.

6.5 Acknowledgements

I want to express my deep and sincere gratitude to all people who have helped and supported me during my PhD study in Berlin.

First and foremost, I would like to thank my supervisor Prof. Dr. Silke Rickert-Sperling for giving me the opportunity to work on this project and complete my PhD thesis in her group, for her patience, encouragement, enthusiasm, and continuous support through my PhD study.

I also would like to thank Prof. Dr. Ana Pombo for being the reviewer of my thesis.

My sincere thanks goes to all present and former members of Sperling Lab for creating an open and cooperative working atmosphere. In particular, I thank Dr. Jenny Schlesinger and Ilona Dunkel for introducing me to the DPF3 project and teaching me to work in an efficient way in the lab; Vikas Bansal for cooperation and discussion on the Histone project, for helping me with all kind of bioinformatics questions; Katherina Bellmann for working together on the DPF3 knockout mice, for your kindness with explaining me German protocols; Kerstin Schulz, our “Chuck Norris”, for excellent technical assistance, and your continuous help not only in the lab but also besides lab-life; Dr. Marcel Grunert for dealing with all small and big problems of our computers, for reviewing my thesis and translating the summary into German; Ashley Cooper for patiently editing this thesis; Dr. Elena Cano, Dr. Cornelia Dorn, Dr. Markus Schüler, Andreas Perrot, Sophia Schönhals and Sandra Appelt for your warm personalities and fruitful discussions; Martina Luig and Barbara Gibas for all the administrative assistance during my study.

I am grateful to all patients and family members who generously participated in this research. I wish to thank all our collaborators and co-authors for their contributions.

I would like to thank the China Scholarship Council (CSC) for providing me with four years’ scholarship. I would like to express my further thanks to all my friends in Berlin, the Chinese Community on Campus Buch and our basketball team in Dahlem.

Finally, my special thanks goes to my parents, my sister and my wife for all their continuous and unparalleled love, understanding and encouragement. Without your support, this work would have never been possible. And my son, you give me so much happiness and motivation.

6.6 Selbständigkeitserklärung

Hiermit erkläre ich, dass ich diese Arbeit selbständig verfasst habe und keine anderen als die angegebenen Quellen und Hilfsmittel in Anspruch genommen habe. Ich versichere, dass diese Arbeit in dieser oder anderer Form keiner anderen Prüfungsbehörde vorgelegt wurde.

Huanhuan Cui Berlin, Oktober 2015